# Investigating the role of human mitochondrial matrix AAA+ proteases in proteostasis and disease

Submitted by

**Erica J. Brodie**

**BBiolScHons**

This thesis is submitted in total fulfilment of the requirements for the degree of Doctor of Philosophy

Department of Biochemistry and Genetics

School of Molecular Sciences

College of Science, Health and Engineering

La Trobe University

Victoria, Australia

May 2016

# Table of Contents

# Abbreviations

| | |
|---|---|
| 2×YT | 2× Yeast Tryptone media |
| Å | Angstrom |
| α | anti |
| Ac | acetate |
| α-casein | alpha-casein |
| AAA+ | ATPases associated with various cellular activities |
| ATP | adenosine triphosphate |
| ATPγS | adenosine 5′-O-(3-thio)triphosphate |
| bp | base pair(s) |
| BSA | bovine serum albumin |
| Ci | curie |
| C-terminus | carboxyl terminus |
| °C | degrees Celsius |
| *C. elegans* | *Caenorhabditis elegans* |
| CLPP | casein-lytic peptidase subunit P |
| CLPX | casein-lytic peptidase subunit X |
| $CO_2$ | carbon dioxide |
| BN-PAGE | blue native polyacrylamide gel electrophoresis |
| BV | bed volume(s) |
| delta psi (Δψ) | membrane potential |
| DDM | n-Dodecyl β-D-maltoside |
| DMEM | Dulbecco's Modified Eagle Medium |
| DNA | deoxyribonucleic acid |
| dNTP | deoxynucleotide triphosphate |
| DTT | dithiothreitol |
| ECL | enhanced chemiluminescence |
| *E. coli* | *Escherichia coli* |
| EDTA | ethylenediaminetetraacetic acid |
| ER | endoplasmic reticulum |
| Em | emission |
| Ex | excitation |
| FBS | fetal bovine serum |

| | |
|---|---|
| g | gram(s) |
| *g* | gravity |
| GFP | green fluorescent protein |
| h | hour(s) |
| HCl | hydrochloric acid |
| HRP | horse radish peroxidase |
| Kb | kilobase(s) |
| KCl | potassium chloride |
| kDa | kilo-dalton(s) |
| IgG | immunoglobulin G |
| IMAC | immobilised metal affinity chromatography |
| IPTG | isopropyl β-D-1-thiogalactopyranoside |
| L | litre(s) |
| LB | luria broth |
| mA | milliamp(s) |
| mg | milligram(s) |
| $MgCl_2$ | magnesium chloride |
| min | minute(s) |
| ml | millilitre(s) |
| mM | millimolar |
| MPPα | mitochondrial processing peptidase subunit alpha |
| MOPS | 3-(N-morpholino)propanesulfonic acid |
| MW | molecular weight |
| NaCl | sodium chloride |
| ng | nanogram(s) |
| nM | nanomolar |
| Ni-NTA | nickel-nitrilotriacetic acid |
| nm | nanometre |
| N-terminus | amino terminus |
| OD | optical density |
| ON | over-night |
| PAGE | polyacrylamide gel electrophoresis |
| PBS | phosphate buffered saline |
| PCR | polymerase chain reaction |

| | |
|---|---|
| pmol | picomole |
| PMSF | phenylmethanesulfonyl fluoride |
| PVDF | polyvinylidene fluorine |
| RNA | ribonucleic acid |
| rpm | revolutions per minute |
| RT | room temperature |
| *S. cerevisiae* | *Saccharomyces cerevisiae* |
| SDH5/SDHAF2 | Succinate dehydrogenase (SDH) assembly factor 2 |
| SEC | size exclusion chromatography |
| SEM | standard error of the mean |
| SEM buffer | sucrose, EDTA and MOPS |
| SDS | sodium dodecyl sulphate |
| s | second(s) |
| S | Svedberg unit, sedimentation coefficient |
| siRNA | small interfering RNA |
| SsrA | small stable RNA gene A |
| StAR | steroidogenic acute regulatory protein |
| t | time |
| TAE | tris-acetate EDTA |
| TBS-T | tris-buffered saline plus Tween-20 |
| TCEP | tris(2-carboxyethyl)phosphine |
| U | units |
| µg | microgram(s) |
| µl | microlitre(s) |
| µM | micromolar |
| V | volt(s) |
| W | watt(s) |
| WT | wild-type |

# Abstract

Mitochondria play crucial roles in energy production and the regulation of metabolic pathways and as such the correct maintenance of mitochondrial integrity is essential to the overall health of a cell. An important aspect of mitochondrial integrity is maintenance of protein homeostasis (proteostasis) within the organelle, and key to this is the regulated removal of damage or unwanted proteins in a timely fashion. This process is carried out by ATP-dependent proteases such as LONM, CLPXP and *m*-AAA protease and mutations in these components are associated with diverse human diseases. To date, however, little is known about the physiological role of these machines or the substrates they recognise. Similarly, the mechanism of action of substrate binding and specificity of these proteases also remains poorly defined.

In this study, the two matrix localised ATP-dependent proteases, LONM and CLPXP were examined. In the first part of this study the recognition motif of two known, but poorly defined, "native" substrates of LONM (StAR and SDH5) was analysed. This analysis identified a general binding motif for LONM, in which "native" protein substrates contain two elements for recognition by LONM. Mutation or deletion of these elements rendered the protein stable *in vitro*. Significantly, these findings suggest that preventing the premature clearance of some proteins may serve as a useful therapeutic option to treat disease states associated with a proteostasis imbalance.

In the second part of this study, the molecular basis of Perrault syndrome was examined through generating disease-specific point mutations in CLPP (T145P, C147S and Y229D). Interestingly, although all three mutants were successfully imported into mitochondria, they each exhibited a range of defects. While C147S exhibited relatively mild defects, Y229D exhibited a loss of interaction with the partner peptidase CLPX. In contrast T145P exhibited broad defects in oligomerisation, interaction with the partner unfoldase CLPX and surprisingly exhibited a hyper-stimulated peptidase activity. Collectively these data provide a molecular basis for the underlying cause of Perrault syndrome.

# Statement of Authorship

Except where reference is made in the text of the thesis, this thesis contains no material published elsewhere or extracted in whole or in part from a thesis accepted for the award of any other degree or diploma.

No other person's work has been used without due acknowledgment in the main text of the thesis.

This thesis has not been submitted for the award of any degree or diploma in any other tertiary institution.

Where applicable, research procedures reported in the thesis were approved by the Genetic Manipulation Supervisory Committee (GMSC), approval number: GMSC12-17 with variations 1-3.

Signed

Date: 06/05/2016

Erica Brodie

# Acknowledgements

Firstly, I would like to acknowledge La Trobe University and the Australian Government for awarding me an Australian Postgraduate Award to support my doctoral studies.

Secondly, to Dr. Kaye Truscott for allocating a position and project for me in her lab and for providing ample supervision and support during my PhD. Certainly the pursuit of knowledge and understanding of mitochondrial proteostasis has its complications, but I thank you for always being optimistic and encouraging me to persevere. To my co-supervisor Dr. David Dougan, thank you for always, somehow, finding the time for my project and for providing valuable assistance and guidance. Your dedication and tireless enthusiasm for science is highly motivating and an inspiration.

To my mentor Dr. Wendy Cook, I cannot thank you enough for your support. You went above and beyond in your role as my mentor and I truly appreciate all your time that you invested in me, my project and for all your counsel.

Thank you to Dr. Tatiana Soares da Costa and Associate Professor Matthew Perugini for your assistance in setting up and analysing the sedimentation velocity experiment data for my final chapter.

To my esteemed lab members, first of all thank you to Chew and James for training me when I started in the lab. To Ralf (Sir Ralf), I will always cherish the memories of you in the lab as your persistent and earnest quest for quality and integrity is something to be admired. Your dedication, ambition and self-motivation were highly regarded, and while you were sometimes too determined to improve the lab environment, I always appreciated your continuous support and advice. To Jess, I cannot thank you enough for being so reliable and dependable throughout my PhD, you are a genuine delight to have in the lab and I am so appreciative of your unwavering support and assistance. Your constant positively and determination makes you an exceptional scientist and loyal friend, and I hope you can unleash that confidence

buried within yourself so you can push the limits and shine like you deserve. To Adi, I can't imagine this lab without you, thank you for making every day enjoyable and for always being so sensible, responsible and honest (but sometimes too honest!). You are worthy and diligent scientist, so don't let anyone crush your spirits. To Anu and Ju Lin, thank you for being so lovely to work with and for always being positive, cheerful and helpful. No doubt there will be struggles ahead but don't let this dishearten you, keep persisting and it will be well worth it in the end. Good luck! Additionally, I am grateful to Dr. Linda Ward and Dr. Jason Paxman for offering their rational, practical and honest advice regarding my PhD and biochemistry in general.

For the people outside academia, thank you for letting me vicariously experience a normal life. To Tammy, cheers for all our coffee rendezvous, sometimes it was the only time I saw the sun! Thank you for your advice and perspectives on so many topics. To Parky, Jade and Simone thank you for your enthusiasm, support and always listening to my lab-related dramas. To my other hockey teammates, Paige, Boydi, Liz, Soph, Katie, Rach, Jay and Farky, thank you for making my time outside the lab all the more enjoyable!

To Shashi, thank you for constantly pushing me forward and having my back when it really mattered. I will always fondly remember our late-night lab encounters. Congratulations on your illustrious PhD success, you should be proud of yourself and what you have achieved so far. 'All our dreams can come true if we have the courage to pursue them.'

To my family, I am forever grateful for your unwavering support of me in the good times and the bad. To my grandparents Harold and Joan, thank you for your endless faith in me and for all your encouragement. You are both in my heart and mind every day. Lastly, to my Mum, Carolyn, who always let me follow my passion, I could not be here today without your unconditional love and support, you have been a constant inspiration and driving force behind me in everything that I do. Thank you for always being so considerate and thoughtful, you have my utmost appreciation and respect and I dedicate this work to you.

# Chapter 1: Introduction

## 1.1 Mitochondria

Mitochondria are double-membrane bound organelles essential for the function of eukaryotic organisms. They are the site of complex metabolic processes that generate and regulate the levels of critical molecules for cellular function, various signalling pathways and initiating apoptosis. The human mitochondrial proteome consists of ~1150 annotated proteins (Calvo et al., 2016) that exist in various concentrations in mitochondrial compartments depending on the metabolic requirements of the cell. Mitochondria are believed to have originated from an endosymbiotic relationship between an alpha-proteobacterium and an ancient Archaea (Andersson et al., 1998; van der Giezen, 2011). Over time, a large portion of the alpha-proteobacterial genome was transferred and incorporated into the host genome or made functionally redundant (Martin & Schnarrenberger, 1997; Timmis et al., 2004), resulting in the majority of mitochondrial proteins being encoded on nuclear DNA with a small subset remaining encoded on the DNA retained within mitochondria (mtDNA) (Anderson et al., 1981). As a consequence of the bacterial origin of the mitochondrion, almost 75% of the genes encoding mitochondrial proteins have sequence similarity to bacterial genes (Calvo & Mootha, 2010).

## 1.2 Biogenesis of mitochondrial proteins

Approximately 70% of nuclear-encoded mitochondrial proteins are directed to the organelle via a mitochondrial targeting sequence, known as a presequence, which typically consists of between 20-60 residues at the N-terminus that form an amphipathic α-helix (Emanuelsson et al., 2000; Vögtle et al., 2009). Targeting sequences can also be located internally or at the C-terminus (Chacinska et al., 2009). Precursor proteins (preproteins) gain entry into mitochondria by engaging with, and transporting through, the translocase of the outer membrane (TOM) complex. They are then sorted to the different membranes or

compartments via specialised translocation machinery (outlined in Figure 1.1).

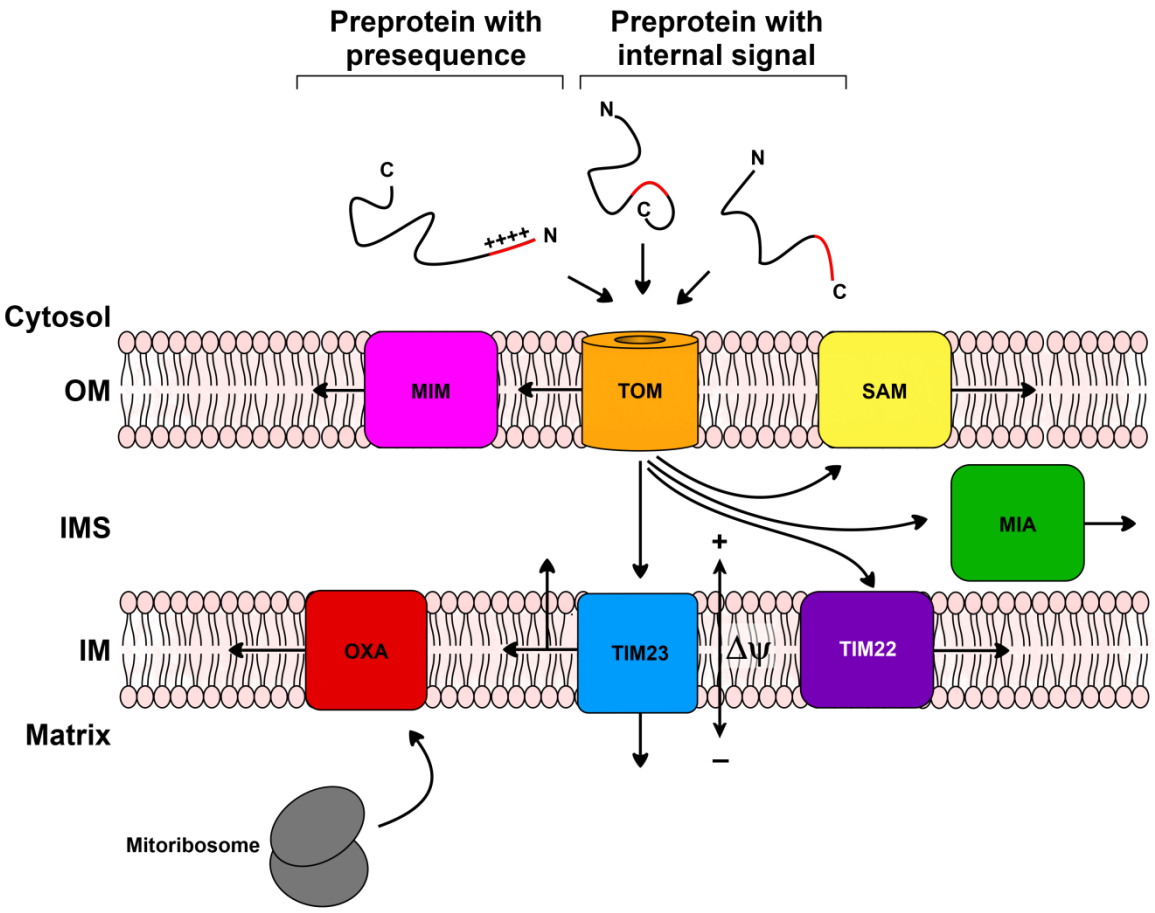


**Figure 1.1:** Import pathways of nuclear-encoded preproteins into mitochondrial membranes and compartments. Preproteins can comprise targeting signals on their N-terminus, C-terminus or internal locations. Following translocation through the outer membrane via TOM (translocase of the outer membrane), precursor proteins are directed to their specific location within the mitochondrion via the interaction with distinct protein complexes such as MIM (mitochondrial import machinery), SAM (sorting and assembly machinery), MIA (mitochondrial intermembrane space import and assembly machinery) or TIM (translocase of the inner membrane) complex 22 or 23. Proteins encoded by mitochondrial DNA are directed to the inner membrane via OXA (oxidase assembly machinery). Import into the matrix is dependent upon a membrane potential (Δψ). OM, outer membrane, IMS, intermembrane space, IM inner membrane.

Presequence containing preproteins destined for the matrix, inner membrane or intermembrane space engage with the translocase of the inner membrane (TIM) 23 complex for sorting to their respective

compartments (Figure 1.2). Matrix destined proteins are fully translocated through the aqueous channel formed by TIM23 complex driven by the membrane potential and ATP to regulate mtHSP70 function (Kang et al., 1990). Presequence containing preproteins with bipartite sorting signals transfer laterally into the inner membrane via the TIM23 complex. The vast majority of proteins targeted via TIM23 have their presequence removed in the matrix by the mitochondrial processing peptidase (MPP) (outlined in Figure 1.2) (Chacinska et al., 2009; Gakh et al., 2002).

MPP is a heterodimeric metallopeptidase composed of two subunits: MPPα and MPPβ (Gakh et al., 2002; Shimokata et al., 1998). Investigation into the cleavage specificity of MPP revealed that cleavage of most proteins follow the R-2 rule where an arginine residue is located two residues upstream of the scissile bond (Gakh et al., 2002). A subset of matrix proteins undergo a second cleavage step by intermediate processing peptidase 55 (Icp55), which removes the N-terminal residue exposed by MPP cleavage (R-3 rule), or octapeptidyl aminopeptidase 1 (Oct1), which removes the next eight residues following MPP cleavage site (R-10 rule). These steps can enhance the metabolic stability of the imported protein (Gakh et al., 2002; Inoue et al., 2015; Vögtle et al., 2011; Vögtle et al., 2009). Proteins with a bipartite sorting signal are additionally processed by the inner membrane peptidase (IMP) or other peptidases to release the protein into the intermembrane space (Gakh et al., 2002; Habib et al., 2007; Neupert & Herrmann, 2007). As mitochondrial proteins are translocated in an unfolded and extended conformation, they must fold into their native three-dimensional conformation within the organelle to reach their functional state. This may occur spontaneously or with the assistance of resident molecular chaperones such as HSP60 (Rospert et al., 1996).

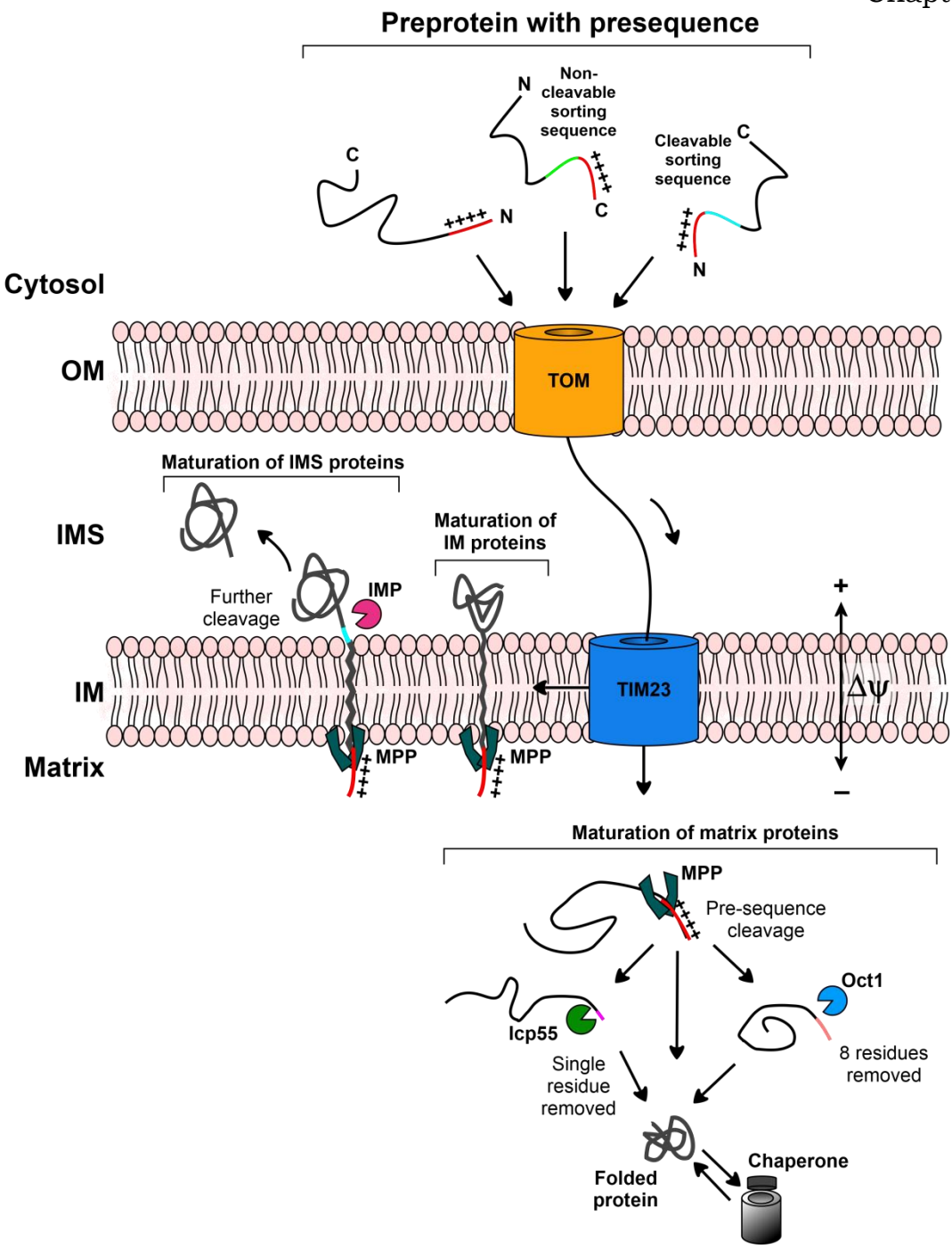


**Figure 1.2:** Import and processing pathway of mitochondrial precursor proteins via the TIM23 complex. After translocation through the outer membrane via TOM, preproteins engage with TIM23 at the inner membrane and are either imported into the matrix or are directed laterally into the inner membrane (via a hydrophobic sorting sequence). Within the matrix, presequence cleavage is mediated by MPP (mitochondrial processing peptidase) typically following the R-2 rule. Proteins may be processed further by Icp55 (intermediate cleaving peptidase 55) which removes one residue (R-3 rule) or Oct1 (octapeptidyl aminopeptidase 1) which removes eight residues (R-10 rule). Proteins can then fold into their native conformation with or without assistance from molecular chaperones. Soluble IMS proteins may undergo an additional cleavage step by IMP (inner membrane peptidase) or other peptidases to release the mature protein into the IMS.

Mitochondrial DNA (mtDNA) contains 37 genes coding for 22 tRNAs, 2 rRNAs and 13 subunits of respiratory chain complexes I, III, IV and V, which are synthesised in the matrix (Anderson et al., 1981). Multiple copies of mtDNA are packaged together in nucleoids that are composed of layers of DNA, polymerases and various other mtDNA-binding proteins (Bogenhagen et al., 2008; Lu et al., 2007; Wang & Bogenhagen, 2006). Following translation, respiratory chain subunits are inserted into the inner membrane via oxidase assembly protein 1 (OXA1) and may be processed by IMP or *m*-AAA (matrix-ATPase associated with various cellular activities) protease prior to assembly into the respiratory chain complexes (Gakh et al., 2002; Koppen & Langer, 2007). Coordinated interplay and regulation between the mitochondrion and the nucleus is essential to ensure subunits of the respiratory chain complexes are cooperatively synthesised (from both genomes) and assembled in the matrix and inner membrane. Nuclear-encoded assembly factors and chaperones also contribute to the precise formation of respiratory chain complexes (Ghezzi & Zeviani, 2012).

Mutations in the translocation, sorting or processing machinery can result in impaired import or biogenesis of mitochondrial proteins and can negatively impact metabolic pathways, activate stress responses and induce mitochondria-specific autophagy (mitophagy) (Harbauer et al., 2014; Narendra et al., 2008; Wrobel et al., 2015).

## 1.3 Maintaining mitochondrial integrity

Cellular function, metabolic requirements and energy production can influence mitochondrial dynamics, morphology and protein repertoire (Calvo et al., 2016; Justo et al., 2005; McCarron et al., 2013). The preservation of mitochondrial function is fundamental for cellular viability and longevity and as such, mitochondria possess the means to ensure their function is maintained during normal conditions and also in response to different levels of stress-induced damage (Figure 1.3). Mitochondrial dysfunction can be caused by a break-down in any of the

mitochondrial quality control mechanisms outlined in Figure 1.3. Not surprisingly, impaired mitochondrial function has been implicated in the pathogenesis of various neurodegenerative disorders, cardiovascular disease, diabetes, cancers and the aging process (Boland et al., 2013; Bratic & Larsson, 2013; Johri & Beal, 2012; Lin & Beal, 2006; Patti & Corvera, 2010).

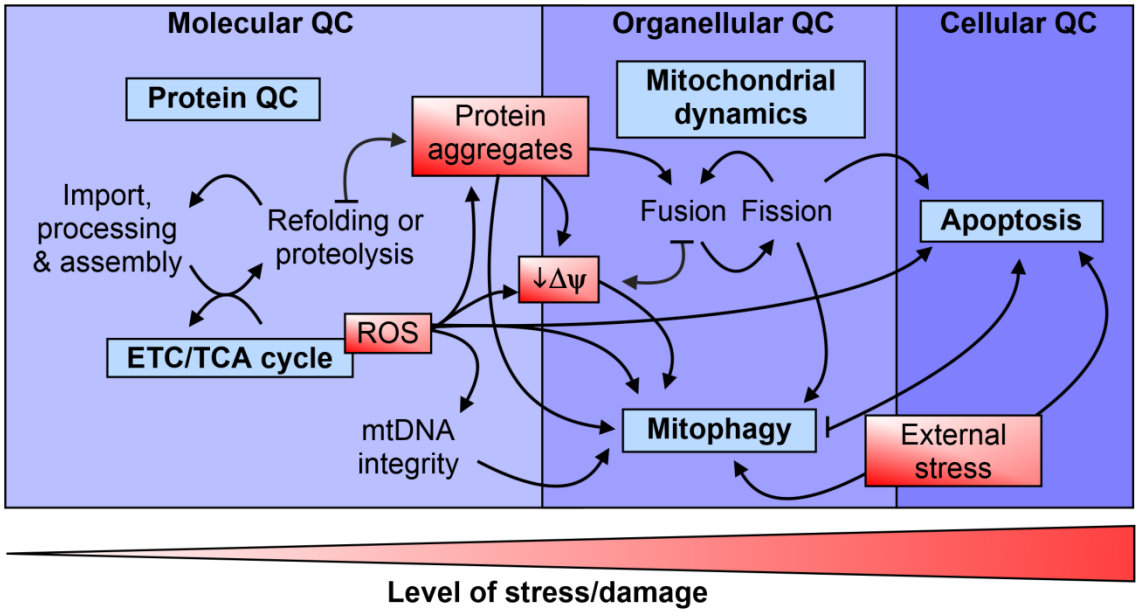


**Figure 1.3:** Mechanisms of mitochondrial quality control. Mitochondria maintain functional integrity under normal and stress conditions through different levels of quality control (QC). However, the specific molecular effectors linking these QC mechanisms are not well established. Molecular QC involves maintaining a balanced protein folding environment to ensure the continued functioning of proteins and the metabolic pathways in which they are involved. Newly imported or misfolded proteins are refolded or degraded by resident chaperones and proteases. The accumulation of protein aggregates can decrease membrane potential (Δψ) or induce mitophagy (organellular QC). Mitochondrial dynamics (cycles of fusion and fission) is also involved in organellular QC and can alleviate local stress or mitochondrial dysfunction. However, impaired dynamics can signal apoptosis (cellular QC). Mitochondrial fission is also a critical step in the activation of mitophagy. Reactive oxygen species (ROS) produced by the electron transport chain (ETC) or tricarboxylic acid (TCA) cycle can inflict oxidative damage to proteins and mtDNA if levels are not adequately regulated. Elevated levels of ROS can also activate mitophagy or apoptosis. Additionally, impaired mitochondrial function as a consequence of external stress (e.g. chemical exposure) can result in the activation of mitophagy or apoptosis.

### 1.3.1 Molecular quality control

The functional activity of a protein is dependent on its three-dimensional conformation. Following import, mitochondrial proteins must fold into their final tertiary structure from an unfolded state and, if required, assemble into their quaternary structures. Proteins may fold spontaneously or may be assisted by molecular chaperones to facilitate formation of their final conformation, largely by preventing intermolecular aggregation (Hartl et al., 2011).

Protein homeostasis (proteostasis) within the mitochondrion is maintained by a network of chaperones and proteases that monitor the protein folding environment, comprised of newly imported, unassembled, folded, misfolded or damaged proteins, and mediate the refolding or regulated degradation of these proteins as required (Anand et al., 2013; Voos et al., 2013). A proteostasis imbalance can lead to a decrease in mitochondrial membrane potential ($\Delta\psi$) (Panov et al., 2002) or the activation of mitophagy without mitochondrial depolarisation (Jin & Youle, 2013)

#### 1.3.1.1 Regulating mitochondrial respiration

Due to the location of the electron transport chain (ETC), mitochondrial proteins are frequently exposed to reactive oxygen species (ROS). Mitochondrial-derived ROS, most often in the form of superoxide ($O_2^{\bullet -}$), are a by-product of the ETC and tricarboxylic acid (TCA) cycle (Figure 1.4). In the absence of ROS scavengers or antioxidant enzymes such as superoxide dismutase (SOD), ROS can cause oxidative damage to proteins and mtDNA (Bulua et al., 2011; Li et al., 2013; Stowe & Camara, 2009). SOD family antioxidants catalyse the dismutation of $O_2^{\bullet -}$ to $H_2O_2$ which is then reduced to $H_2O$ by other enzymes such as catalase, glutathione peroxidase and peroxiredoxin (Stowe & Camara, 2009).

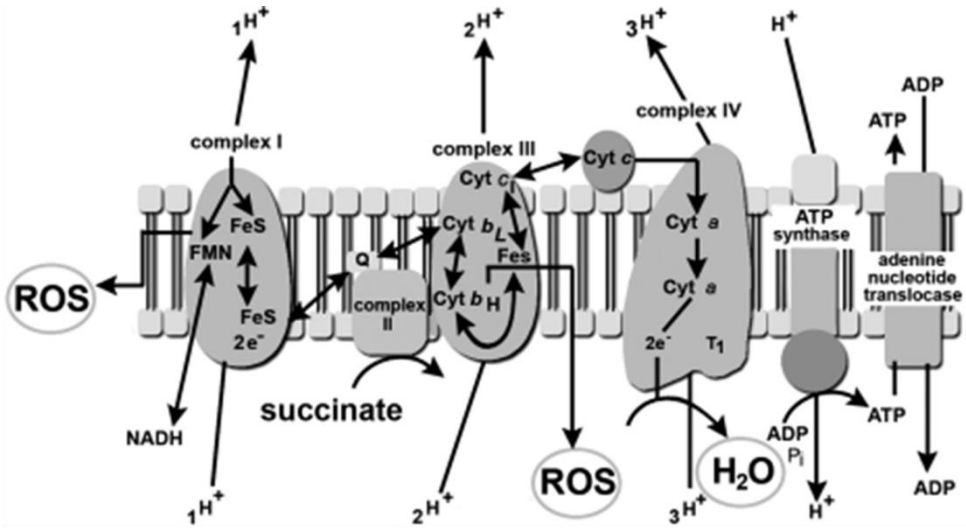


| Complex | I | II | III | IV | V |
|---|---|---|---|---|---|
| nDNA-encoded subunits | 37 | 4 | 10 | 10 | 24 |
| mtDNA-encoded subunits | 7 | 0 | 1 | 3 | 2 |
| Known assembly factors | 13 | 4 | 11 | 20 | 10 |

**Figure 1.4:** Proteins directly associated with mitochondrial respiration (oxidative phosphorylation). Respiratory chain complexes are composed of individual subunits encoded from nuclear or mitochondrial genomes. Their association or incorporation into the inner membrane (IM) is mediated by specific nuclear-encoded assembly factors. During oxidative phosphorylation, electrons ($e^-$) are transferred through each complex and protons ($H^+$) are pumped from the matrix (M) to the intermembrane space (IMS) which creates a membrane potential ($\Delta\psi$) to drive ATP production via complex V (ATP synthase). Complex II is also involved in the TCA cycle where succinate is oxidised to fumarate. The sites of reactive oxygen species (ROS) production generated by the respiratory chain and the tricarboxylic acid cycle are indicated. Figure adapted from Stowe and Camara (2009).
[Respiratory chain subunits and assembly factors derived from: *http://www.genenames.org/cgi-bin/genefamilies/set/645,* Ghezzi & Zeviani, 2012; Jonckheere et al., 2012: Kadenbach & Hüttemann, 2015; Sánchez-Caballero et al., 2016).

ROS production can also be influenced by cellular oxygen levels, mitochondrial membrane potential ($\Delta\psi$) and mitochondrial stress (e.g. hypoxia) (Li et al., 2013). ROS production is essential for cellular inflammatory responses, activating apoptosis and for adapting mitochondria to low oxygen conditions through the regulation of the hypoxia-inducible factor 1 alpha subunit (HIF-1α) (Dröge, 2002; Finkel,

2012). However, excessive ROS production can alter the redox state of mitochondria which prevents mitochondrial protein import (Wright et al., 2001) and can contribute to mitochondrial dysfunction and cellular aging (Bratic & Larsson, 2013; Payne & Chinnery, 2015).

In order to prevent proteotoxic stress caused by ROS or other factors and to reduce the accumulation of partially folded protein intermediates, chaperones and proteases with distinct roles in protein quality control (PQC) exist in each mitochondrial compartment and contribute to proteostasis (Voos, 2013). This includes a vast network of chaperones (e.g. Hsp78, mtHsp70, and co-chaperones mtGrpE and DnaJ, HSP60 and its co-chaperone HSP10) that contribute to the folding of newly imported proteins and also refolding of misfolded proteins under both normal and stress-induced conditions (Voos, 2013). When protein folding or refolding fails, several ATP-dependent proteases facilitate the removal of unwanted proteins within mitochondria (see below).

#### 1.3.1.2 PQC proteases

Misfolded proteins that are unable to be refolded by chaperones in a timely fashion are degraded by proteases. Degradation of large proteins generally involves the ATP-dependent unfolding and cleavage of the polypeptide chain into smaller fragments that are then cleared by oligopeptidases (Koppen & Langer, 2007).

Non-imported mitochondrial proteins and proteins of the mitochondrial outer membrane are tagged with ubiquitin and degraded by the cytosolic 26S proteasome (Cohen et al., 2008; Karbowski & Youle, 2011; Wrobel et al., 2015). Similarly, the 26S proteasome also contributes to the degradation of proteins within the inner membrane and the intermembrane space whereby misfolded proteins are retro-translocated across the outer membrane into the cytosol (Bragoszewski et al., 2015; Clarke et al., 2012; Radke et al., 2008). Additionally, the 26S proteasome was implicated in the proteostasis of the matrix as matrix-localised

proteins have also been found to be ubiquitinated (Jeon et al., 2007; Lau et al., 2012). However, the precise mechanism regulating the export of ubiquitinated proteins from the matrix has not been well established.

Other proteases contributing to protein homeostasis of the intermembrane space include HtrA2 (High temperature requirement A) which is an ATP-independent serine peptidase (Savopoulos et al., 2000) and *i*-AAA protease which is an inner membrane-bound AAA+ protease comprised of six subunits of YME1L (Yme1-like) (Leonhard et al., 1996). Matrix proteases associated with PQC include inner membrane bound *m*-AAA protease (Leonhard et al., 1996), the soluble proteases hCLPXP (composed of CLPX and CLPP subunits) and LONM (Koppen & Langer, 2007).

In the event that proteostasis becomes impaired or over-burdened, the accumulation of specific proteins can activate signalling pathways that results in the upregulation of PQC-specific chaperones and proteases. Specifically, this includes the mitochondrial unfolded protein response ($UPR^{mt}$) and the StAR overload response (SOR) (Bahat et al., 2014; Yoneda et al., 2004; Zhao et al., 2002).

### 1.3.2 Organellular quality control

Mitochondria are highly dynamic organelles that exist as a network of interconnected compartments that constantly fuse and divide in processes termed fusion and fission, respectively (Westermann, 2010). Mitochondrial fusion promotes complementation and homogeneity within the mitochondrial population by mixing mitochondrial contents such as mtDNA. It also maintains membrane potential, thereby reducing the number of dysfunctional mitochondria within a cell (Chen et al., 2005; Chen et al., 2003). Conversely, mitochondrial fission is required to increase the mitochondrial population within a cell and is essential for apoptosis and mitophagy (Lee et al., 2004a; Twig et al., 2008; Youle & van der Bliek, 2012). The correct balance of mitochondrial fusion and

fission cycles (mitochondrial dynamics) regulates mitochondrial morphology, cellular energy requirements and maintains functional integrity across the mitochondrial population (Detmer & Chan, 2007; Youle & van der Bliek, 2012). Impairment of the mitochondrial fusion or fission machinery can result in apoptosis and is associated with physiological disorders such as Dominant Optic Atrophy (DOA) and Charcot-Marie-Tooth disease (CMT2A) as well as cellular aging (Alexander et al., 2000; Chen et al., 2005; Chen et al., 2003; Delettre et al., 2000; Figge et al., 2012; Lee et al., 2004a; Nunnari & Suomalainen, 2012; Olichon et al., 2003; Zuchner et al., 2004).

Mitophagy is a quality control mechanism that involves the selective degradation of defective or superfluous mitochondria by lysosomes (Kim et al., 2007). Mitophagy is vital for the reduction of mitochondria in certain cells (e.g. reticulocytes and adipocytes) but can also be induced in response to excessive ROS, mtDNA mutations, membrane depolarisation, nutrient starvation or the accumulation of misfolded proteins (Elmore et al., 2001; Jin & Youle, 2013; Kundu et al., 2008; Lemasters et al., 1998; Rodriguez-Enriquez et al., 2009; Scherz-Shouval et al., 2007; Suen et al., 2010; Zhang et al., 2008; Zhang et al., 2009).

### 1.3.3 Cellular quality control

As mitochondrial morphology and physiology are associated with cellular health, the accumulation of defective mitochondria can be deleterious to cellular function (Wang & Youle, 2009). Impaired mitochondrial dynamics or mitochondrial stress induced by chemical exposure, hypoxia, excessive ROS, dramatic loss of membrane potential, or mtDNA mutations can initiate apoptosis via the intrinsic pathway (Adam et al., 2015; Gu et al., 2014; Harrison et al., 2005; Raimundo et al., 2012; Suzuki et al., 2011; Takahashi et al., 2004; Wang et al., 2008). In addition, mitochondria also induce apoptosis in response to other stimuli such as viral infections, heat shock, serum starvation and radiation damage (Castelli et al., 1997; Díaz-Guerra et al., 1997; Li et al., 1999;

Mercille & Massie, 1994; Watters, 1999). In this regard, mitochondria have become appealing targets for cancer therapies (Boland et al., 2013; Indran et al., 2011).

### 1.3.4 Genetic contribution to mitochondrial dysfunction

Mutations in mitochondrial genes (located on either nDNA or mtDNA) can result in a variety of disorders with differing phenotypes, progression and severity of symptoms (Szklarczyk et al., 2014; Tuppen et al., 2010). These mutations can be inherited or derived from exogenous factors. Most 'mitochondrial disorders' are commonly associated with mutations in respiratory chain subunits or assembly factors (outlined in Figure 1.4) and result in impaired oxidative phosphorylation (OXPHOS) activity (Bird et al., 2014; Chinnery, 2014; Ghezzi & Zeviani, 2012). Mutations in genes encoding other mitochondrial proteins can affect protein targeting, import or biogenesis (MacKenzie & Payne, 2007; Rötig, 2011), mtDNA replication (Morino et al., 2014), mitochondrial dynamics (Detmer & Chan, 2007), homeostatic functions (Lutsenko & Cooper, 1998; Rotig et al., 1997) or proteostasis (Baker & Haynes, 2011; Bezawork-Geleta et al., 2014) can also cause mitochondrial dysfunction.

## 1.4 Protein quality control of the mitochondrial matrix: a role for AAA+ proteases

Within each compartment of the mitochondrion, a distinct PQC network of chaperones and proteases operates to maintain proteostasis. Specifically, the mitochondrial matrix represents an isolated environment where proteostasis must be tightly regulated as resident proteins are not readily retro-translocated across the double membrane for degradation by the 26S proteasome in the cytosol. Thus, essential proteins and metabolic functions occurring in the mitochondrial matrix are protected from proteotoxic stress by matrix proteases LONM, CLPXP

and *m*-AAA protease (Anand et al., 2013; Szklarczyk et al., 2014; Truscott et al., 2011; Venkatesh et al., 2012; Voos et al., 2013). These proteases are ATP-dependent and belong to the AAA+ (ATPases associated with various cellular activities) protein superfamily.

### 1.4.1 Overview of AAA+ proteins

Proteins of the AAA+ superfamily are present in eukaryotes, bacteria and archaea. These proteins catalyse essential physiological processes such as DNA replication, membrane fusion as well as protein disaggregation and degradation (Ogura & Wilkinson, 2001). The defining feature of all AAA+ proteins is the highly conserved nucleotide binding domain, also known as the 'AAA domain' containing the Walker A (GXXXXGK[T/S], where X = any amino acid) and Walker B (hhhhDE, where h = any hydrophobic amino acid) motifs that mediate ATP binding and hydrolysis respectively (Hanson & Whiteheart, 2005; Ogura & Wilkinson, 2001).

The fold of the AAA domain forms two distinct subdomains (Figure 1.5). The N-terminal region ('large' subdomain) incorporates the distinctive αβα Rossmann fold of a nucleotide binding domain (Walker A and B motifs) and typically comprises five parallel β-sheets sandwiched between four-five α-helices (Iyer et al., 2004). The C-terminal region of the AAA domain ('small' subdomain) is less conserved but is generally composed of four α-helices forming two hair-pin loops that are connected by two short, parallel β-sheets (Ammelburg et al., 2006). Functional motifs can also be incorporated into this region (Ammelburg et al., 2006).

AAA+ superfamily members can be classified into distinct groups by their distinguishing structural features (Figure 1.5) such as pore loops, linker regions, arginine fingers, sensor motifs (Ammelburg et al., 2006; Erzberger & Berger, 2006; Iyer et al., 2004; Wendler et al., 2012). These include the 'classic' clade, the proteases, chelatases, transcriptional activators and transport proteins (PACTT) clade, the helicases and clamp loaders (HEC) clade, helicase superfamily III clade, ExeA clade and the

signal transduction ATPases with numerous domains (STAND) clade (Ammelburg et al., 2006; Wendler et al., 2012). AAA+ proteins can also interact with other proteins or co-factors to modulate their activity and increase their functional diversity (Iyer et al., 2004).

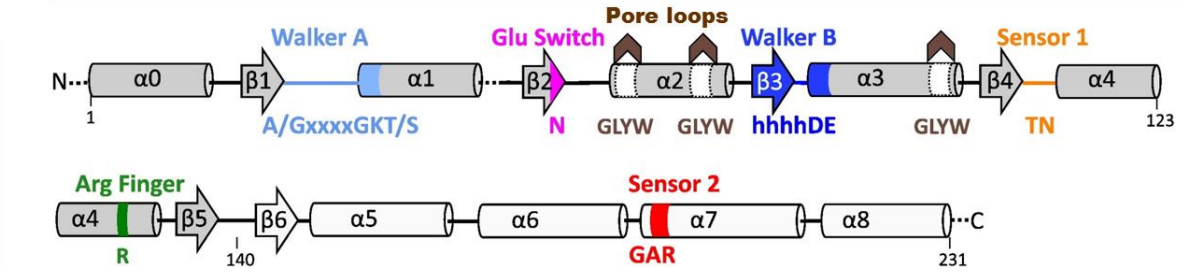


**Figure 1.5:** Typical secondary structural arrangement of the AAA domain of AAA+ proteins. The conserved motifs and sequences that are used to distinguish between the different families of AAA+ proteins are indicated. Highly conserved Walker A and B motifs bind and hydrolyse ATP respectively. The functionality and role of the sensor regions and arginine fingers vary between the AAA+ families. Pore loops are typically arranged around the entrance of the central axial pore of AAA+ proteases. Figure taken from Wendler et al. (2012).

For the majority of AAA+ proteins, oligomerisation is a pre-requisite for ATPase activity (Wendler et al., 2012), and based on numerous structural studies, self-compartmentalised, ring-shaped homohexamers are the most common conformation observed thus far (Zardecki et al., 2016). The binding and hydrolysis of ATP by individual subunits stimulates conformational changes within the AAA domain that drives mechanical force within the AAA+ protein to mediate its function (Ogura & Wilkinson, 2001). Subunits can bind and hydrolyse ATP in a concerted manner (Gai et al., 2004), or sequentially wherein ATP is bound in succession (Adelman et al., 2006; Crampton et al., 2006; Matyskiela et al., 2013) or stochastically (Briggs et al., 2008; Glynn et al., 2009; Yakamavich et al., 2008). In addition, subunits can adopt different conformations depending on the type of nucleotide (e.g. ATP or ADP) that is bound (Cha et al., 2010; Glynn et al., 2009; Sysoeva et al., 2013; Yakamavich et al., 2008).

The mitochondrial AAA+ proteases identified in mammals belong to either the classic (e.g. *i*-AAA and *m*-AAA proteases) or PACTT (e.g. LONM, CLPXP) clades (Truscott et al., 2010).

### 1.4.2 Regulated proteolysis by AAA+ proteases

To ensure the degradation of cellular proteins occurs in a regulated manner, AAA+ proteases must selectively recognise a specific motif or tag on the target protein. For example, the central AAA+ protease in the eukaryotic cytosol, the 26S proteasome, mediates the recognition and degradation of polyubiquitinated proteins (Ravid & Hochstrasser, 2008). In this case proteins destined for degradation by the ubiquitin proteasome system (UPS) display specific motifs that are directly recognised by an E3 ligase, which mediates ubiquitin tagging. For other AAA+ proteases, such as those found in mitochondria, regulated degradation of a target protein occurs after the direct and specific recognition of a particular motif or tag.

In general, these degradation signals, or 'degrons', are only exposed under specific conditions, which provides a level of control to the irreversible turnover of proteins (Baker & Sauer, 2006). For instance, proteins damaged by exposure to heat-shock or ROS can become unfolded that then reveals hydrophobic residues that would normally be buried within the protein structure (Gosslau et al., 2001). These hydrophobic residues act as a degron that is recognised by several AAA+ proteases and as such, structurally compromised proteins are rapidly degraded (Parsell & Lindquist, 1993). Structurally stable 'native' proteins are also degraded by AAA+ proteases and similarly, they require recognition of specific degrons prior to degradation. Intrinsic degrons are often concealed within the tertiary or quaternary structure of the protein and may be exposed only after peptidase cleavage (Flynn et al., 2003), disassembly (Neher et al., 2003a), or partial unfolding by chaperones (Hoskins et al., 2002). Some substrates contain intrinsic degrons that are constantly exposed (e.g. λ CII) and these proteins are generally

transient (Shotland et al., 1997). Furthermore, the post-translational modification of proteins can also target them for degradation, such as the addition of a C-terminal SsrA- (small stable RNA gene A-) tag to stalled translation products in bacteria (Gottesman et al., 1998) or acetylation of the N-terminus of specific proteins in yeast (Hwang et al., 2010). In some cases degradation of a substrate by an AAA+ protease is dependent on recognition and delivery of the substrate by an adaptor protein (Kirstein et al., 2009b). For example, the *Escherichia coli* adaptor protein ClpS is essential for the delivery of N-end rule substrates to its cognate AAA+ protease ClpAP (Erbse et al., 2006). In other cases, adaptor proteins modulate the function of their cognate proteases or regulate substrate specificity (Gur et al., 2013). For example, SsrA-tagged proteins in *E. coli* are recognised directly by ClpXP but this recognition can be enhanced by the adaptor protein SspB and results in the accelerated degradation of the substrate (Dougan et al., 2003; Levchenko et al., 2000; Wah et al., 2003). In general, adaptor proteins dock onto accessory domains (e.g. N-terminal domain) and facilitate the delivery of a substrate to the axial entry pore of the protease where it is then bound by pore loops lining the entrance to central cavity (Gur et al., 2013).

Independent of adaptor proteins, substrates can be bound directly by the AAA+ protease (Hinnerwisch et al., 2005; Martin et al., 2008; Matyskiela & Martin, 2013; Wohlever et al., 2014). This binding is facilitated by two regions of the AAA+ protease; the pore loop (pore-1), that plays an important role in substrate specificity and translocation (Martin et al., 2008; Matyskiela et al., 2013; Park et al., 2005) and the N-terminal accessory domain, which in the case of ClpA, can stimulate the binding of the substrate to the pore loops (Wohlever et al., 2014).

Due to size constraints imposed by the central entrance pore, proteins must be unfolded to permit access to the catalytic chamber of the protease (Nyquist & Martin, 2014), however two strands can be translocated simultaneously (Glynn et al., 2012; Gur et al., 2012). Stochastic ATP binding and hydrolysis via the AAA domain drives

conformational changes in the subunits that creates an unfolding force to facilitate the unravelling of the substrate from the point of recognition/binding (Aubin-Tam et al., 2011; Glynn et al., 2009; Wendler et al., 2012; Yakamavich et al., 2008). Depending on the complexity or stability of the substrate protein, complete unfolding may require numerous cycles of ATP hydrolysis (Kenniston et al., 2003) (depicted in Figure 1.6), after which the polypeptide chain is threaded (step-wise) through the pore and into the catalytic chamber where it is processively cleaved into small peptides typically 5-20 residues in length (Aubin-Tam et al., 2011; Choi & Licht, 2005; Kisselev et al., 1999; Lee et al., 2001; Sauer & Baker, 2011).

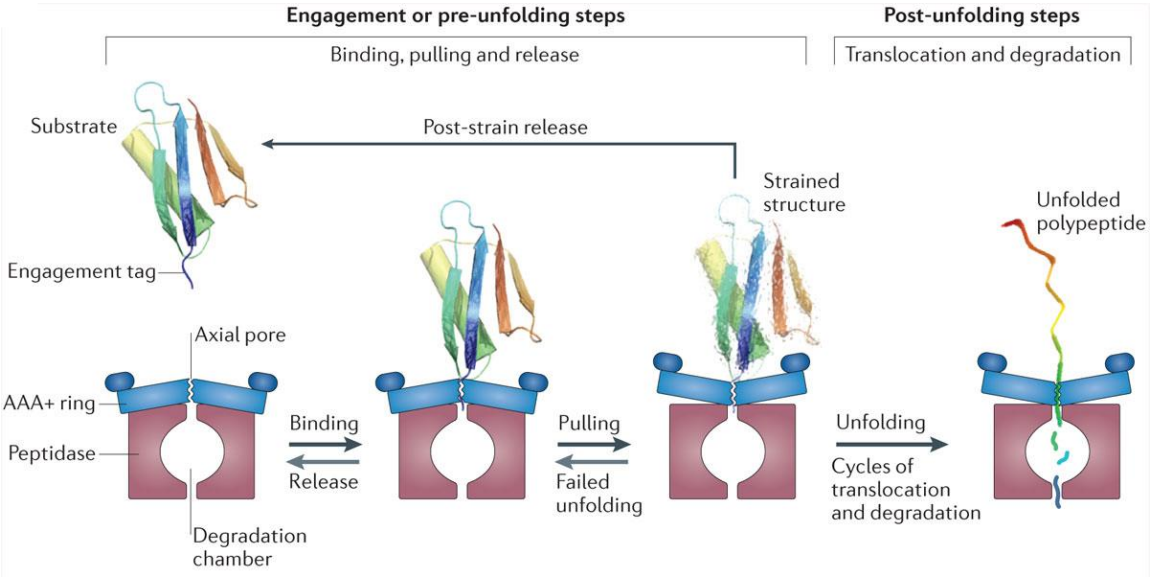


**Figure 1.6:** Recognition, unfolding and degradation of a substrate protein by AAA+ proteases. Substrates are recognised via an engagement tag or regulatory sequence known as a degron. Multiple rounds of ATP hydrolysis via the AAA+ ring drives conformation changes within the subunits to mediate unfolding of the substrate. Depending on their structural stability, substrates may require numerous unfolding attempts. Following unfolding, the substrate is translocated into the catalytic chamber (peptidase domain) where degradation takes place. Figure taken from Olivares et al. (2016)

### 1.4.3 The *m*-AAA protease: an FtsH metalloprotease family member of the mitochondrial inner membrane

The mitochondrial *m*-AAA protease is a member of the conserved FtsH metalloprotease family M41 (Rawlings et al., 2014). It belongs to the classic clade AAA proteins (Iyer et al., 2004; Tomoyasu et al., 1993a) and like FtsH, is composed of N-terminal transmembrane domains, an AAA domain and a C-terminal peptidase domain that contains the conserved motif HExxH (where x represents any residue) (Figure 1.7A) (Tomoyasu et al., 1995; Tomoyasu et al., 1993a; Tomoyasu et al., 1993b). These proteins, like most AAA+ proteases, assemble into homohexamers (Bieniossek et al., 2006). FtsH family members also contain a second region of homology (SRH) which is essential for ATP hydrolysis (Karata et al., 1999) and a C-terminal coiled-coil region that has been proposed to play a role in substrate binding (Figure 1.7A) (Shotland et al., 2000). In *E. coli*, FtsH can function both as a chaperone (Shirai et al., 1996) and as a protease (Jayasekera et al., 2000; Tomoyasu et al., 1995) and is required for optimal growth and viability. Substrates of FtsH include unfolded proteins, SsrA-tagged substrates and regulatory proteins that modulate essential metabolic pathways (e.g. heat shock response) (Herman et al., 2003; Jayasekera et al., 2000; Ogura et al., 1999; Shotland et al., 1997; Tomoyasu et al., 1995).

In yeast, two homologs of *E. coli* FtsH have been identified (*i*-AAA protease and *m*-AAA protease) which are located within mitochondria and anchored to the inner membrane. The *i*-AAA protease contributes to proteostasis of the inner membrane and intermembrane space whilst *m*-AAA protease degrades proteins in the inner membrane and the matrix (Leonhard et al., 1996). As this thesis focuses on protein degradation in the mitochondrial matrix, the *i*-AAA protease is not described further.

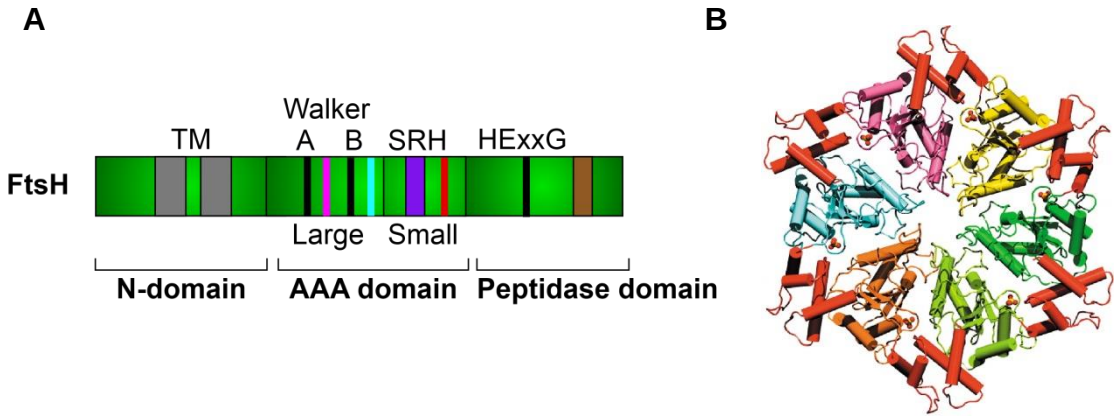


**Figure 1.7:** Conserved domains of FtsH family proteases. **A**, Each subunit of FtsH family members contain an N-domain, the AAA domain (separated into large and small regions) for ATP binding and hydrolysis via Walker A and B motifs respectively and a metallopeptidase domain with a conserved $Zn^{2+}$-binding motif HExxG (where x represents any amino acid). FtsH family members also comprise two transmembrane (TM) domains which span the inner cell membrane in prokaryotes and the inner mitochondrial membrane in eukaryotes (*m*-AAA protease). The position of the conserved pore loop (pink), sensor 1 residue (cyan), sensor 2 motif (red), second region of homology (SRH) (purple) and coiled-coiled region (brown) are also indicated. **B**, Modelled hexamer of *E. coli* FtsH based on the crystal structure of the AAA domain. Figure taken from Krzywda et al. (2002).

The *m*-AAA protease is a heterohexamer composed of two subunits (Yta10p and Yta12p) (Arlt et al., 1996) and both are essential for mitochondrial respiration (Arlt et al., 1998). In mammals, *m*-AAA exists in two forms, as a homohexamer of AFG3L2 (ATPase family gene 3-like 2) subunits and as a heterohexamer composed of alternating subunits of AFG3L2 and paraplegin (Atorino et al., 2003). Mutations in the *SPG7* gene (encoding paraplegin) cause an autosomal recessive form of hereditary spastic paraplegia which is characterised by progressive weakness and spasticity in the lower limbs (Casari et al., 1998). Notably, muscle biopsies of patients revealed impaired mitochondrial respiration and altered morphology (Casari et al., 1998). Consistent with this, paraplegin was found to mediate the efficient processing and maturation of mitochondrial ribosomal protein L32 (MrpL32) prior to its assembly into the mitochondrial ribosome and *paraplegin* null mice further

displayed a significant decrease in the translation of mitochondrial-encoded respiratory chain subunits (Nolden et al., 2005). In addition, the processing of antioxidant cytochrome c peroxidase (Ccp1) and mitochondrial fusion associated protein optic atrophy protein 1 (Opa1) was found to be impaired in yeast lacking the Yta10/Yta12 complex (Esser et al., 2002; Ishihara et al., 2006), highlighting the importance of protein processing and biogenesis to mitochondrial function. Consistently, knockdown of *paraplegin* in HeLa cells resulted in mitochondrial filamentation (Ishihara et al., 2006).

Additionally, mutations in *AFG3L2* cause spinocerebellar ataxia type 28 and spastic ataxia-neuropathy syndrome (Cagnoli et al., 2010; Di Bella et al., 2010; Pierson et al., 2011). Both AFG3L2 and paraplegin are necessary for axonal development and the absence of either protein affects anterograde axonal transport of mitochondria (Ferreirinha et al., 2004; Kondadi et al., 2014). Despite the well-established role of *m*-AAA protease in the maturation of mitochondrial proteins and disease progression, the contribution of *m*-AAA protease in mammalian PQC is poorly characterised.

### 1.4.4 LON protease

The Lon family of proteases (LonA and LonB) are highly conserved serine proteases that play fundamental roles in proteostasis in bacteria, archaea and several organelles of eukaryotes (mitochondria, peroxisomes and chloroplasts) (Bartoszewska et al., 2012; Fukui et al., 2002; Goldberg et al., 1994; Kikuchi et al., 2004; Kutejová et al., 1993; Ostersetzer et al., 2007; Wang et al., 1993; Wang et al., 1994).

The active form of Lon is a self-compartmentalised homohexamer (Figure 1.8) (Botos et al., 2004a; Botos et al., 2005; García-Nafría et al., 2010; Seong-Cheol et al., 2006). LonA family members are largely restricted to bacteria and eukaryotes while LonB is generally limited to archaea (Rotanova et al., 2006). Lon A is composed of three domains, a large N-

domain (predicted site of substrate binding or specificity), a AAA domain and a peptidase domain composed of a serine-lysine catalytic dyad (Figure 1.8A) (Botos et al., 2004b; Ebel et al., 1999; Lee et al., 2004b; Wohlever et al., 2014). In contrast, LonB lacks the large N-domain but contains a single transmembrane domain that separates the large and small subdomain of the AAA domain followed by the conserved peptidase domain (Figure 1.8A) (Botos et al., 2005; Rotanova et al., 2006).

The axial entry pore of the Lon hexamer is ~18 Å in diameter and is predicted to accommodate at least two polypeptide strands during substrate translocation (Gur et al., 2012; Rotanova et al., 2006). The subunits within the homohexamer bind ATP with different affinities and as such display nucleotide-dependent asymmetry (Cha et al., 2010). ATP binding and hydrolysis via the AAA module drives conformational changes in the pore loops that creates an unfolding force to facilitates the threading of substrate into the catalytic chamber of the peptidase domain (Figure 1.8B) (Cha et al., 2010; Gur et al., 2012; Wendler et al., 2012). Due to the positioning of the catalytic dyad observed in most crystal structures of Lon, the binding and hydrolysis of ATP is predicted to alter the orientation of the catalytic residues to facilitate an active conformation (Cha et al., 2010; García-Nafría et al., 2010; Rotanova et al., 2006). Following cleavage, peptides are released from the 13 Å exit pore at the base of the protease (Cha et al., 2010).

*E. coli* Lon (ecLon, also known as La) has been shown to degrade short fluorogenic peptides as well as larger proteins in their native or unfolded state (Waxman & Goldberg, 1985). The capacity to degrade an assortment of substrates demonstrates the ability of ecLon to recognise a broad range of degrons (Gur & Sauer, 2008; Patterson-Ward et al., 2009). Moreover, ecLon degrons can modulate the binding affinity of the pore loops as well as govern the rate of substrate unfolding and degradation (Gur & Sauer, 2009; Koodathingal et al., 2009). Similarly, the location of the degron can determine the direction in which the substrate is sequentially unfolded and degraded (Lee et al., 2001). For instance, dihydrofolate reductase (DHFR) containing a C-terminal degron

was more favourably degraded than internally or N-terminally tagged DHFR (Gur et al., 2012).

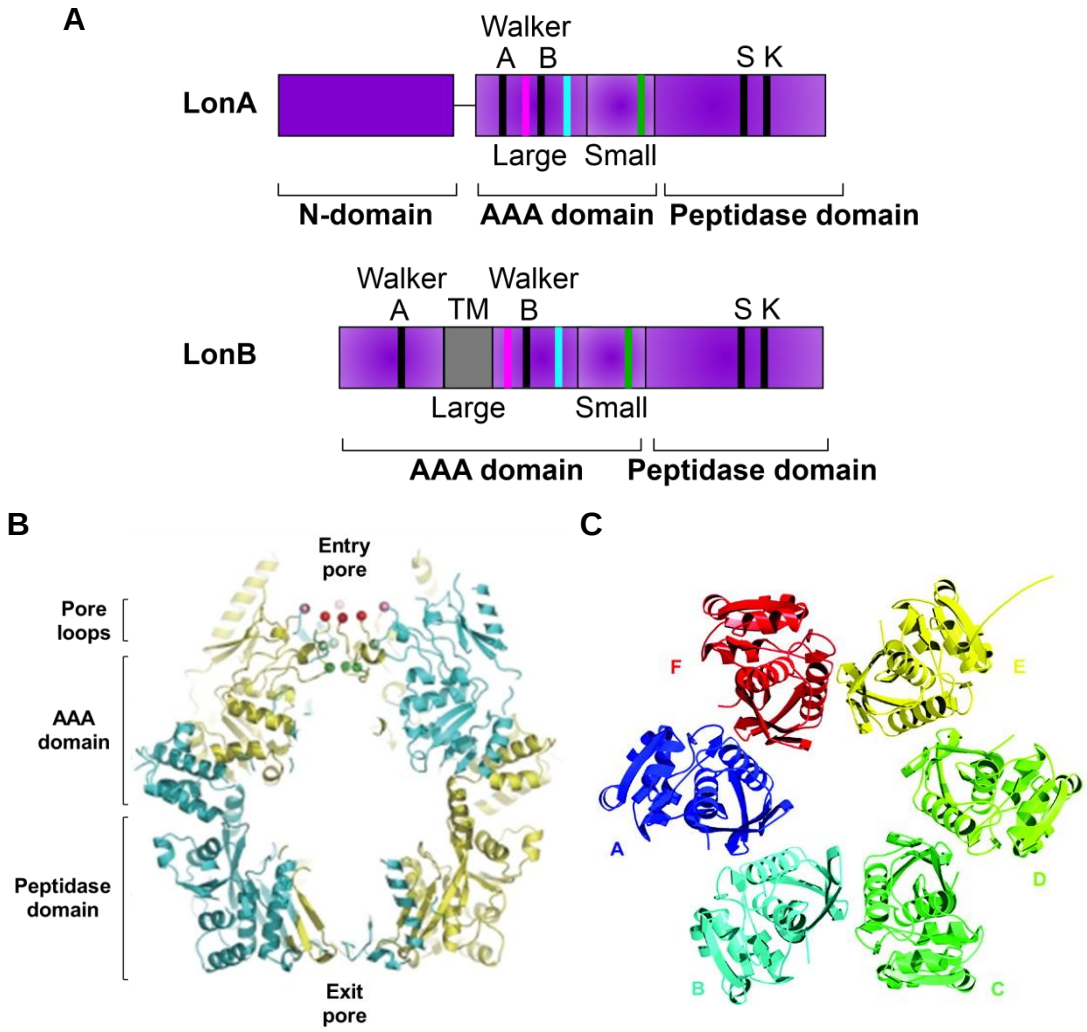


**Figure 1.8:** Structure of Lon family proteases. **A**, Domains of LonA and LonB proteases. LonA proteases comprise a large N-domain (predicted site for substrate recognition), a AAA domain (composed of a large and small subdomain) for ATP binding and hydrolysis via Walker A and B motifs respectively and a peptidase domain containing the serine-lysine catalytic dyad. In the absence of an N-domain, LonB proteases comprise a transmembrane (TM) domain within the AAA domain. The positions of the conserved pore-1 loop (pink), sensor 1 motif (cyan) and sensor 2 motif (green) are indicated. **B**, Ribbon diagram of the crystal structure of *Thermococcus onnurineus* NA1 Lon (LonB family) hexamer that was determined in the absence of the N-terminal transmembrane domain. Side view of the catalytic chamber formed after the assembly of Lon subunits (coloured in alternating blue and yellow). Unfolded substrates enter via the axial entry pore and smaller fragments exit from the base of the protease. Figure adapted from Cha et al. (2010), PDB ID: 3KIJ. **C**, Ribbon diagram of *E. coli* Lon (LonA family) peptidase domain. Axial view of the hexameric configuration of Lon subunits (labelled A-F) that form the base of the protease (exit pore). Figure taken from Botos et al. (2004b), PDB ID: 1RR9.

**Table 1.1: Experimentally determined substrates of LONM**

| LONM substrate | Protein function | Reference |
|---|---|---|
| **Stable, folded proteins** | | |
| Steroidogenic Acute Regulatory Protein (StAR)* ^ # | Rate-limiting step in steroidogenesis. Imported into matrix to terminate function and be cleared from the cell | Ondrovičová et al. (2005)<br>Granot et al. (2007a) |
| Aminoleuvinic Acid Synthase 1 (ALAS-1)^<br>(only in presence of heme) | Rate-limiting step in heme synthesis. Heme production creates a feedback loop to regulate ALAS-1 levels. | Tian et al. (2011) |
| Mitochondrial cystathionine-β-synthase (CBS)^<br>(only in the presence of an oxygenated heme group) | Catalyzes the production of hydrogen sulphide/potential oxygen sensor in mitochondria | Teng et al. (2013) |
| Mitochondrial Transcription Factor A (TFAM)^ # | Promotes transcription of mtDNA. Regulates mtDNA copy number | Matsushima et al. (2010)<br>Lu et al. (2013) |
| Cytochrome c oxidase subunit 4 isoform 1 (COX4-1)^<br>(under hypoxic conditions) | Regulates catalytic activity of cytochrome c oxidase (COX) in non-hypoxic cells | Hori et al. (2002)<br>Fukuda et al. (2007) |
| Cytochrome c oxidase subunit 2 (COX2)^ | Non-catalytic subunit of respiratory chain complex IV | Strauss et al. (2015) |
| **Unassembled proteins** | | |
| Succinate Dehydrogenase Assembly Factor 2 (SDHAF2/SDH5)^ #<br>(when not in complex with SDHA) | Essential for the activity of the catalytic subunit (SDHA) of complex II | Bezawork-Geleta et al. (2014) |
| Mitochondrial processing peptidase subunit alpha (MPPα)** #<br>(when not in complex with MPPβ) | Processes newly imported proteins in the matrix | Ondrovičová et al. (2005) |
| **Structurally compromised proteins** | | |
| Aconitate hydratase (aconitase)^<br>(when oxidatively damaged) | Enzyme in TCA cycle | Bota and Davies (2002) |
| Thioredoxin 2 (Trx2)^<br>(when oxidatively damaged) | Controls mitochondrial redox state. Essential for the reduction of peroxiredoxins after oxidative damage | Zhang et al. (2011) |
| Glutaminase C (GAC)^<br>(after modification by diphenylarsinic acid (DPAA)) | Glutamine metabolism | Kita et al. (2012) |
| Alpha-casein (α-casein)# | model unfolded protein | Wang et al. (1993) |
| Unfolded (but not aggregated) ornithine transcarbamylase (OTC)^# and malate dehydrogenese (MDH)# | Native forms of OTC and MDH are not *in vitro* substrates | Bezawork-Geleta et al. (2015) |
| * recombinant murine substrate, ** recombinant yeast substrate, ^ *in-organello* based investigation (i.e. enrichment of substrate with LONM inhibition or siRNA-mediated knockdown of *LONM*), # demonstrated with recombinant proteins | | |

The unfolding and degradation of larger multi-domain proteins has been shown to cause premature disassociation from the protease and lead to the accumulation of partially cleaved polypeptides (Gur et al., 2012; Koodathingal et al., 2009). Importantly, Lon can only re-engage with these fragments if the degron is still present. Therefore, it is likely that multiple degrons exist within a single protein to permit re-engagement with Lon and other AAA+ proteases (Flynn et al., 2001; Gur & Sauer, 2008; Koodathingal et al., 2009).

In *E. coli*, Lon not only contributes to proteostasis under normal conditions but is also essential for survival under stress conditions such as heat shock, UV irradiation and DNA damage (Phillips et al., 1984; Schoemaker et al., 1984). Substrates of ecLon include damaged or misfolded proteins, as well as folded regulatory proteins that control specific cellular pathways such as the cell cycle, capsule synthesis and the SOS response (Gur, 2013; Nishii et al., 2002; Nishii et al., 2005; Phillips et al., 1984; Schoemaker et al., 1984; Van Melderen et al., 1996). ecLon also binds DNA in a site-specific manner although its specific function in this has not been determined (Fu et al., 1997; Gur, 2013).

Consistent with the recognition of misfolded or unassembled proteins, ecLon binds to hydrophobic patches (abundant in aromatic residues) contained within proteins (Gur & Sauer, 2008). A preference for cleaving between hydrophobic residues has also been established for ecLon across several studies but a consensus cleavage site has yet to be determined (Maurizi, 1987; Nishii et al., 2002; Nishii et al., 2005; Ondrovičová et al., 2005; Van Melderen et al., 1996).

In *Saccharomyces cerevisiae*, the Lon homologue Pim1 (proteolysis in mitochondria) is localised to mitochondria where it plays a vital role in regulating mitochondrial respiration, biogenesis, proteostasis and mtDNA integrity and as such, its depletion leads to mitochondrial dysfunction and accumulation of protein aggregates (Bayot et al., 2010; Bender et al., 2011; Erjavec et al., 2013; Van Dyck et al., 1994; von Janowsky et al., 2005). In addition to misfolded proteins, substrates of

Pim1 typically include oxidatively damaged proteins and native proteins with destabilised tertiary structures that are prone to aggregation at higher temperatures (Bayot et al., 2010; Major et al., 2006). Uniquely, the structure of Pim1 when visualised via cryo-transmission electron microscopy, appeared to be a heptamer (Stahlberg et al., 1999).

In mammals, LonA family member LONM (mitochondrial Lon), also referred to as LONP1, is encoded on nuclear DNA and directed to mitochondria via an N-terminal presequence (Wang et al., 1994). Following import and processing in the matrix, LONM assembles in the presence of ATP to form an active hexamer (García-Nafría et al., 2010; Wang et al., 1994). LONM expression is increased in response to heat-shock, oxidative damage to proteins, ROS, hypoxia, UV irradiation and rapid accumulation of proteins in the matrix (Bahat et al., 2014; Cheng et al., 2013; Hori et al., 2002; Ngo & Davies, 2009; Pinti et al., 2011). LONM binds DNA *in vitro* and *in vivo* and has been found to interact with nucleoids in mitochondria and regulate mtDNA copy number (Bogenhagen et al., 2008; Liu et al., 2004; Matsushima et al., 2010).

Peroxisomal Lon (LONP2/PLN) has ~30% sequence similarity to LONM but its role is not well established is mammals. It has been demonstrated to function both as a chaperone and a protease in peroxisomes to protect proteins from oxidative damage and prevent the accumulation of protein aggregates (Bartoszewska et al., 2012; Okumoto et al., 2011). PLN has also been found to regulate peroxisomal autophagy in plants and yeast (Aksam et al., 2007; Goto-Yamada et al., 2014).

LONM interacts with numerous proteins including subunits of the respiratory chain, antioxidant proteins and stabilises the HSP60/HSP70 complex under environmental stresses which prevents apoptosis (Kao et al., 2015). Elevated LONM expression promotes cell survival and consistent with this, LONM overexpression has been observed in various cancers and is associated with tumorigenesis (Bernstein et al., 2012; Cheng et al., 2013; Gibellini et al., 2014; Nie et al., 2013; Quirós et al., 2014). *LONM* knock-out is embryonically lethal in mice, however

heterozygous expression of LONM (*LONM*$^{+/-}$) exhibits a protective phenotype against colorectal cancer (Quirós et al., 2014). *LONM* knockdown leads to an accumulation of oxidatively damaged proteins, elevated ROS levels, mitochondrial dysfunction and cell death (Bota et al., 2005; Quirós et al., 2014). Clinical homozygous or compound heterozygous mutations in *LONM* that affect the assembly, ATPase activity or proteolytic function of LONM are associated with cerebral, ocular, dental, auricular, and skeletal anomalies (CODAS syndrome) (Strauss et al., 2015).

Listed in Table 1 are the experimentally determined substrates of human LONM. In addition to degrading damaged or unfolded proteins, LONM has been found to degrade proteins in their native conformation that are associated with the respiratory chain and various metabolic pathways (e.g. heme synthesis). However, the degrons that facilitate LONM-mediated recognition and degradation of these substrates have not yet been determined.

### 1.4.5 ClpXP protease

In contrast to Lon and FtsH (where both the AAA+ unfoldase and peptidase components are located on a single polypeptide), ClpXP is a two-component protease in which the unfoldase and peptidase components are located on separate polypeptides. In this case, the AAA+ unfoldase component – Casein-lytic protease X (ClpX) is responsible for substrate recognition and unfolding while substrate degradation is controlled by the peptidase component – Casein-lytic protease P (ClpP) (Figure 1.9). The ClpXP protease is highly conserved, with homologues identified in bacteria and most eukaryotes (where it is located within the mitochondrion). Despite its widespread occurrence, little is known about human CLPXP, and much of our understanding of this machine is based on the *E. coli* protease (ecClpXP), as such the next section(s) will focus primarily on the *E. coli* components of this enzyme.

### 1.4.6 The unfoldase - ClpX

*E. coli* ClpX is composed of an N-terminal C4-type zinc-binding domain (ZBD) and a C-terminal AAA domain (Grimaud et al., 1998) (Figure 1.9A). While the AAA domain is required for the binding and hydrolysis of ATP to facilitate substrate unfolding, the ZBD is essential for the binding of specific substrates and adaptor proteins (Dougan et al., 2003; Wojtyra et al., 2003). Consistent with other AAA+ proteins, the AAA domain of ClpX contains a large and small subdomain, separated by a flexible hinge (Figure 1.10A and B) (Glynn et al., 2009). ATP binds at the cleft between the large and small subdomain within a single subunit and as a result drives oligomerisation of the protein. This architecture ensures that the small AAA subdomain of one subunit interacts with the large subunit of the adjacent (counter-clockwise) subunit to form a 'rigid body' (Figure 1.10B) (Glynn et al., 2009), thereby creating a narrow entry pore (~15 Å diameter) which is lined with various loops (Figure 1.10C). These loops mediate direct recognition of specific substrates and facilitate translocation of the unfolded proteins (Martin et al., 2008).

Similar to Lon, the subunits of ClpX also display nucleotide-dependent asymmetry within the hexamer whereby certain subunits display a greater affinity for ATP than others, however only four subunits of ClpX are able to bind ATP at any given time (Hersch et al., 2005). During cycles of ATP binding and hydrolysis, the hinge separating the AAA subdomains within each subunit adopts a different configuration that creates distinct loadable (can bind ATP) and non-loadable (cannot bind ATP) subunits (Stinson et al., 2013). As the subunits alternate between loadable and non-loadable configurations, step-wise conformational changes are transferred to the adjacent subunits through the rigid-body unit that creates a mechanical unfolding force (Stinson et al., 2013). The unfolding force drives translocation of the linear substrate into the catalytic chamber of the associated peptidase, ClpP (Aubin-Tam et al., 2011; Glynn et al., 2009; Sen et al., 2013)

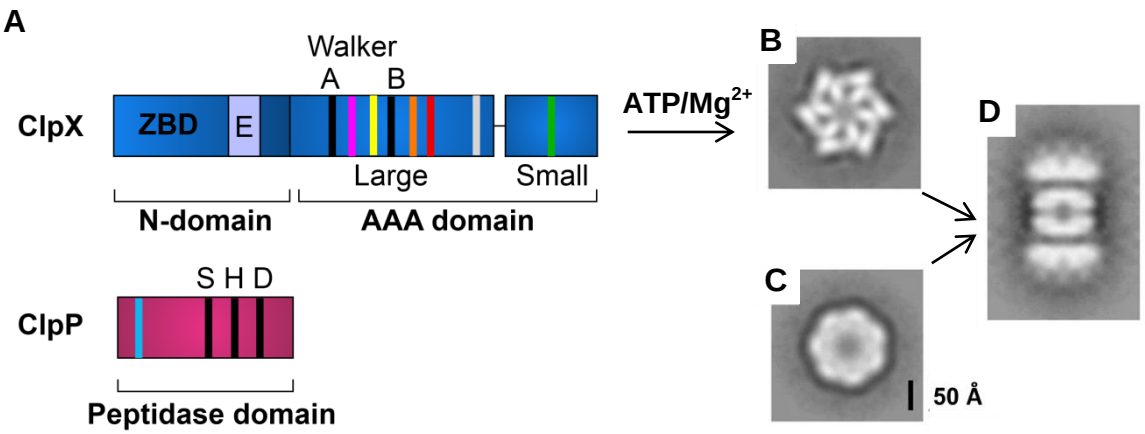


**Figure 1.9:** Conserved domains and assembly of ClpXP proteases. **A**, Domains of ClpX and ClpP. ClpX comprises an N-domain with a C4-type zinc-binding domain (ZBD) for substrate recognition and an AAA domain (divided into large and small regions) where ATP binding and hydrolysis is mediated by the Walker A and B motifs respectively. The E-domain (E) is present only in eukaryotic ClpX. The positions of the conserved pore 1 loop (pink), GYVG loop (yellow), pore 2 loop (orange), RKH loop (red), LGF loop (grey) and sensor 2 motif (green) are indicated. ClpP contains the peptidase domain with a serine, histidine and aspartate catalytic triad. N-terminal loops (cyan) are indicated. **B, C** and **D,** Electron micrographs of human CLPX, hCLPP and hCLPXP respectively, formed *in vitro*. The CLPXP protease is composed of two CLPX hexamers sitting on both ends of a CLPP tetradecamer (composed of two ClpP heptamers). Images taken from Kang et al. (2002).

### 1.4.7 The peptidase - ClpP

Similar to ClpX, ClpP is widely distributed throughout nature from bacteria to the mitochondrial matrix of fungi, plants and mammals (Bross et al., 1995; Maurizi et al., 1990a). Only a distant relative of ClpP has been identified in Archaea (De Castro et al., 2006) but no homologs are present in yeast (Adam et al., 2001; Maurizi et al., 1990b).

*E. coli* ClpP (ecClpP) is a ~25 kDa protein, that contains a short (14 residues) propeptide. The propeptide is autocatalytically removed when the protease assembles into its active conformation (Maurizi et al., 1990b). EcClpP forms a barrel-shaped oligomer (~51 Å in diameter), composed of two heptameric rings stacked back-to-back with the catalytic residues are sequestered inside the barrel (Flanagan et al., 1995; Maurizi et al., 1990a; Wang et al., 1997). Access to the catalytic

chamber is restricted to a 10-12 Å diameter axial pore at either end of the barrel. As such, although ClpP is able to degrade short peptides without an unfoldase component, the turnover of larger proteins requires interaction from a cognate unfoldase (Grimaud et al., 1998; Maurizi et al., 1990a).

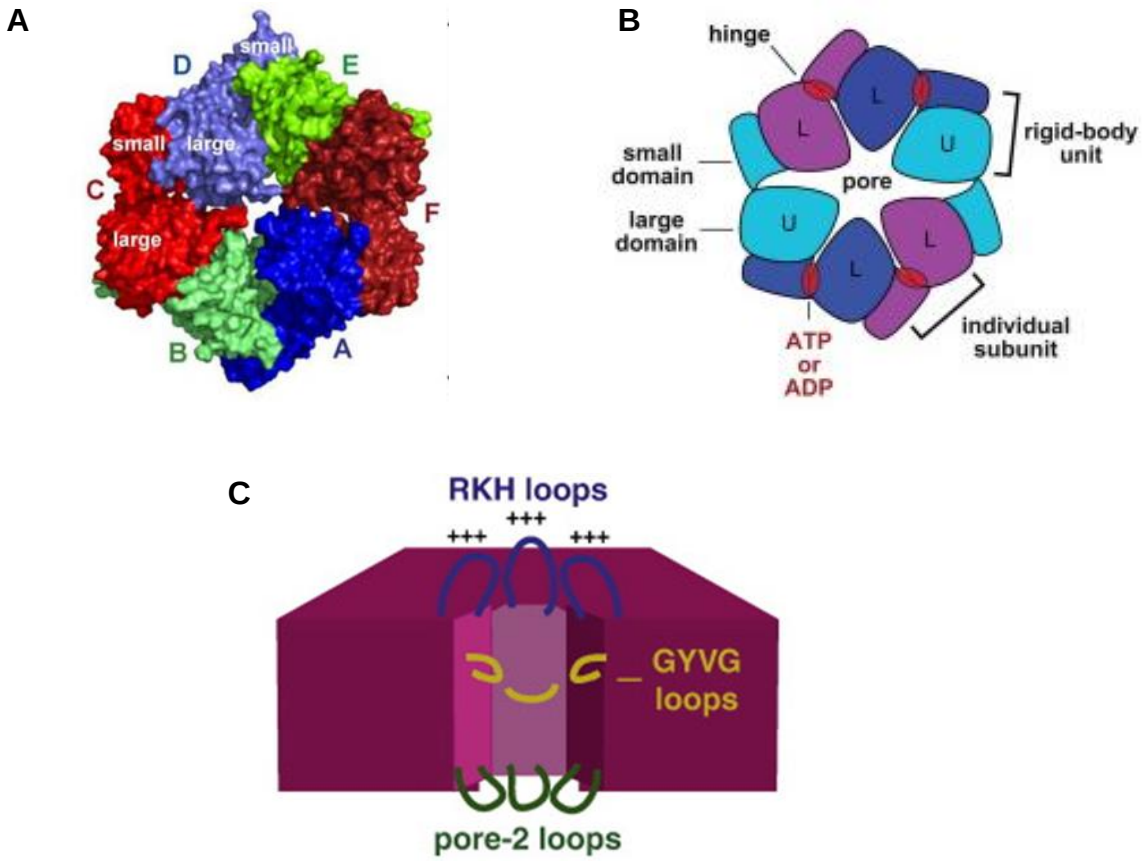


**Figure 1.10:** Structural and functional elements of ClpX. **A**, Surface representation model of *E. coli* ClpX hexamer (top view) with the large and small AAA region indicated on each subunit (A-F). PDB ID: 3HWS. Image taken from Glynn et al. (2009). **B**, Cartoon representation of the packing of ATP-loadable and non-loadable subunits within the ClpX hexamer. ATP is bound within the cleft between the large and small AAA regions while small and large regions from adjacent subunits form rigid-body units. Image taken from Stinson et al. (2013). **C**, Cartoon representation of the pore loops of *E. coli* ClpX (cut-away view) that mediates substrate specificity. RKH loops (RKL in hCLPX), GYVG loops (also GYVG in hCLPX) and pore-2 loops (ecClpX: SRKSDNPSITR, hCLPX: GSVPGIHQLR) are essential for substrate binding, translocation and interaction with ClpP. Image taken from Baker and Sauer (2012).

Complex formation between ClpX and ClpP is stabilised by two distinct sets of molecular interactions. One set of "static" interactions occurs between a conserved tripeptide loop motif ([L/I/V]-G-[F/L]) on the unfoldase (e.g. ClpX) and the hydrophobic pockets on ClpP (Gribun et al., 2005; Joshi et al., 2004; Martin et al., 2007). The second "dynamic" set of interactions occurs between the flexible N-terminal loops of ClpP with the pore-2 loops of ClpX (Figure 1.11C) (Joshi et al., 2004; Kim et al., 2001; Lee et al., 2010; Martin et al., 2007). The interaction of the IGF loops of ecClpX with the hydrophobic pockets of ecClpP stimulates a conformational change in the ClpP subunits that opens the axial pore of ClpP (Joshi et al., 2004; Lee et al., 2010). This mechanism not only facilitates protein translocation of substrate but also enhances access to the catalytic chamber (Baker & Sauer, 2012; Joshi et al., 2004; Lee et al., 2010). ClpP can also be activated by a group of novel antibiotics known as acyldepsipeptides (ADEPs) (Brotz-Oesterhelt et al., 2005; Kirstein et al., 2009a; Lowth et al., 2012; Sass et al., 2011). These compounds bind to the hydrophobic pocket of ClpP and dysregulate the peptidase. Specifically, they do so by (a) preventing ATPase-docking and (b) by triggering opening of the axial pore which activates ClpP, promoting the unregulated degradation of larger proteins both *in vitro* and *in vivo* (Kirstein et al., 2009a; Li et al., 2010).

The ClpXP complex plays several important roles in *E. coli* that range from general proteostasis (e.g. degrading SsrA-tagged substrates) to the control of regulatory pathways such as cell division, the general stress response and the extra-cytoplasmic stress response (Camberg et al., 2009; Farrell et al., 2005; Flynn et al., 2003; Gonzalez et al., 1998; Neher et al., 2003b; Schweder et al., 1996; Truscott et al., 2011; Wojtkowiak et al., 1993). Based on the identification of ~50 ClpXP-substrates in *E. coli*, 5 different degrons have been described (Flynn et al., 2003). Consistent with other AAA+ proteases, these degrons were located at either the C- or N-terminus of the substrate (Flynn et al., 2003; Hoskins et al., 2002). Although many ClpX substrates are recognised directly by the ATPase, several substrates either require, or are modulated by, adaptor proteins.

In *E. coli*, three ClpX-adaptor proteins have been characterised, RssB, SspB and UmuD (Dougan et al., 2003; Gonzalez et al., 2000; Levchenko et al., 2000; Wah et al., 2003; Wawrzynow et al., 1995; Zhou et al., 2001). For an extensive review of adaptor proteins see Kirstein et al. (2009b).

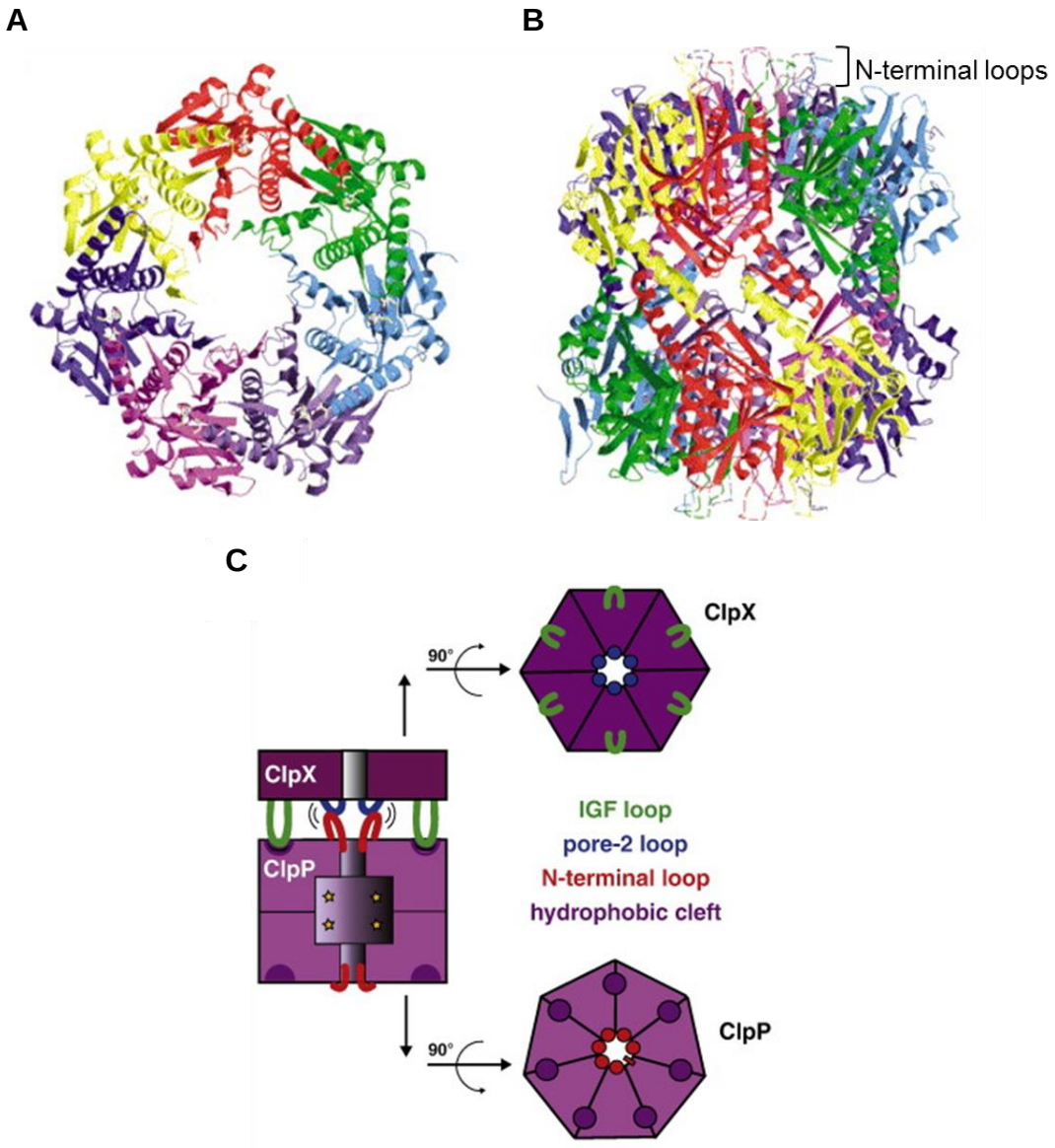


**Figure 1.11:** Structure of ClpP and the interactions stabilising the complex with ClpX. **A**, Ribbon diagram of hCLPP heptamer (top view) with each subunit coloured differently. **B**, Ribbon diagram of hCLPP tetradecamer (based on *E. coli* ClpP structure). N-terminal loops were not clearly resolved in the structure but their predicted locations are marked by dashed lines. PDB ID: 1TG6. Adapted from Kang et al. (2004). **C**, Molecular interactions between ClpX and ClpP that stabilise the ClpXP protease complex. IGF loops of ecClpX (LGF in hCLPX) interact with the hydrophobic clefts of ClpP while loops from the AAA+ pore of ClpX interact with N-terminal loops of ClpP. Taken from Baker and Sauer (2012).

In contrast to bacteria, ClpXP-mediated protein degradation in eukaryotes is poorly understood. Interestingly, the peptidase component (ClpP) is absent from yeast, and hence ClpX (Mcx1p) was predicted to play a chaperone role in the mitochondrial matrix (van Dyck et al., 1998). Although no phenotypic changes were observed in the *Mcx1p* deletion strain (van Dyck et al., 1998) it was recently discovered that Mcx1p stimulates the production of heme by interacting with the rate-limiting enzyme Hem1 and promoting the incorporation of its cofactor (Kardon et al., 2015).

In contrast to yeast, mammals contain both CLPX and CLPP. These proteins are nuclear encoded and directed to the mitochondrial matrix by an N-terminal presequence (Bross et al., 1995; Corydon et al., 2000). Although human CLPX (hCLPX) shares 41% sequence identity with ecClpX, it contains a unique region (73 amino acids), which is located between the N-terminus and AAA+ domain. This domain has been termed the eukaryotic domain (E-domain) (Truscott et al., 2010) but its functionality has yet to be determined (Corydon et al., 2000; Lowth et al., 2012). Despite this difference, hCLPX shares a similar architecture to other ClpX homologues (Kang et al., 2002). Nevertheless, sequence variation on important loops, such as the IGL loop for ClpP docking, can limit the formation of heterologous complexes. For instance, hCLPX is unable to interact with ecClpP, however, ecClpX can interact with hCLPP (Kang et al., 2002). Similarly, sequence variation in the pore loops of ClpX means that hCLPX exhibits different substrate specificity to ecClpX (Kang et al., 2002; Lowth et al., 2012; Martin et al., 2008). Currently, it remains unclear if substrate specificity of hCLPX can be modulated by adaptor proteins, although it has been speculated that p32 (also known as gC1q receptor (gC1qR) or hyaluronic acid binding protein 1 (HABP1)) and polymerase δ interacting protein 2 (POLDIP2/PDIP38) are adaptor proteins for hCLPX (Lowth et al., 2012).

Human CLPP (hCLPP) shares 56% sequence identity with ecClpP and both proteins form a barrel-shaped tetradecamer with similar overall architecture (Kang et al., 2004). Interestingly, hCLPP contains a unique

28 amino acid C-terminal extension that is required for its stability but is not essential for its peptidase activity or complex formation with CLPX (Kang et al., 2004). A major difference between the bacterial and human ClpXP protease system is in the assembly of the final complex. In the case of *E. coli*, each component (ClpX and ClpP) can self-assemble, however assembly of hCLPP into the final tetradecamer first requires interaction of CLPX with the CLPP heptameric intermediate (Figure 1.9D) (Kang et al., 2005).

Several recent studies have identified numerous CLPXP-interacting proteins (including mitochondrial chaperones, ETC subunits and proteins associated with ribosomal biogenesis, the urea cycle, mitophagy and mitochondrial morphology) but no physiological substrates have been validated (Al-Furoukh et al., 2014; Cole et al., 2015; Fischer et al., 2015; Greene et al., 2012; Lowth et al., 2012). Human CLPX has also been found to associate with mitochondrial nucleoids and indirectly regulate mtDNA copy number through its interaction with TFAM (Kasashima et al., 2012).

Despite the lack of identified substrates, CLPXP is thought to play a crucial role in humans as it has been implicated in numerous diseases. In mammals, CLPP expression is transcriptionally upregulated in the mitochondrial unfolded protein response ($UPR^{mt}$) (Zhao et al., 2002) and was shown to be essential for the activation of this signalling pathway in nematode worm *Caenorhabditis elegans* (Haynes et al., 2007). Elevated levels of CLPP have been observed in particular cancers and consequently, CLPP was predicted to contribute to cellular viability as shown by diminished CLPP levels abrogating cancer progression and sensitising cells to other treatments (Cole et al., 2015; Zhang & Maurizi, 2016). Most recently, mutations in *CLPP* were identified in Perrault syndrome 3 patients, characterised by female infertility and sensorineural hearing loss (Ahmed et al., 2015; Jenkinson et al., 2013). These patients also displayed muscle ataxias and neurological symptoms (Ahmed et al., 2015; Jenkinson et al., 2013). Consistent with this, *CLPP* null mice also display infertility, deafness and reduced growth (Gispert et

al., 2013). Knock down of *CLPP* in muscle cells decreased mitochondrial respiration, cell proliferation and impaired mitochondrial dynamics (Deepa et al., 2015).

## 1.5 Aims of this study

Maintaining mitochondrial functionality is critical for the viability of the cell and organism. Constant surveillance of the protein folding environment is required to ensure misfolded proteins do not accumulate to detrimental levels and impede normal protein function. As such, a vast array of chaperones and proteases exist within mitochondria to prevent proteotoxic stress. Within the mitochondrial matrix, AAA+ proteases such as LONM and CLPXP contribute to protein homeostasis by degrading damaged or unwanted protein. Substrate recognition by these proteases is hypothesised to occur via specific degrons exposed on the substrate, however the precise sequence and location of these recognition motifs is not well characterised.

The first part of this study aimed to determine the mechanism of recognition of two 'native' substrates by LONM. Specifically, the identity of the degron and specific requirements for LONM-mediated recognition was examined for SDH5 (Chapter 3) and StAR (Chapter 4) using purified recombinant proteins. These data should provide insights into the molecular determinants regulating LONM recognition and is anticipated that this information could lead to novel approaches to control the metabolic stability of pathogenic forms of mitochondrial proteins.

The second part of the study aimed to establish the role of mitochondrial CLPXP in the pathogenesis of Perrault syndrome 3 (Chapter 5). This was investigated through the biochemical characterisation of three known single point mutations in CLPP associated with Perrault syndrome (T145P, C147S and Y229D). From these data it is anticipated that the different mutations (which lead to varying severity of the disease) may be linked to different biochemical defects.

# Chapter 2: Materials and Methods

## 2.1 General Molecular Biology Techniques

### 2.1.1 Polymerase chain reaction (PCR)

PCR was used to amplify specific regions of DNA for the purpose of cloning or to introduce mutations via site-directed mutagenesis (see the next section). Specific forward and reverse synthetic oligonucleotide primers were designed (listed in Appendix 1, Table 1) and used at a final concentration of 0.5 µM in reactions containing 1-5 ng/µl template plasmid DNA, 0.2 mM of each dNTP, 2 U/µl of Vent or Taq DNA polymerase (New England Biolabs (NEB)) or 0.02 U/µl High Fidelity Phusion® DNA Polymerase (NEB) in 1× reaction buffer (NEB) as appropriate. DNA was amplified using a Mastercycler EP PCR machine (Eppendorf).

### 2.1.2 Site-directed mutagenesis

Non-overlapping partially complementary synthetic oligonucleotide primers (Appendix 1, Table 1) were designed to introduce specific point mutations into newly synthesised DNA (Zheng et al., 2004). Typically, reactions consisting of 0.5 pmol/µl of each primer, 1-100 pg/µl template plasmid DNA, 0.2 mM of each dNTP and 0.02 U/µl High Fidelity Phusion® DNA Polymerase (Thermo Scientifics) were combined in 1× reaction buffer as appropriate. Generally, mutant DNA was synthesised with the following conditions: initial denaturation at 98 °C (15 s) followed by 30 cycles of DNA denaturation (98 °C, 15 s), primer annealing (60-72 °C, 30 s) and elongation (72 °C, 15-30 s/kb DNA). Finally, an additional elongation step (72 °C, 10 min) concluded the reaction. The newly synthesised linear DNA was then phosphorylated at the 5′ end in reactions containing 2 U/µl T4 Polynucleotide Kinase (PNK, NEB) with appropriate 1× reaction buffer (NEB) supplemented with 1 mM ATP and incubated at 37 °C for 45 min. The PNK was then heat-denatured at 65 °C for 20 min and 2 U/µl of T4 DNA Ligase (NEB) was added to facilitate ligation of the plasmid DNA. The reaction was incubated at RT for 2 h or

16 °C overnight prior to transformation into $CaCl_2$-competent XL-1 Blue *E. coli* cells (Section 2.1.8).

### 2.1.3 DNA gel electrophoresis

DNA samples (e.g. PCR products) were separated via Tris-acetate EDTA (TAE)-agarose gel electrophoresis. Agarose gels containing 0.8-1.5% (w/v) agarose in 1× TAE buffer (40 mM Tris-acetate, 0.571% (v/v) glacial acetic acid, 2 mM EDTA, pH 8.0) and 1× SYBR® Safe (Life Technologies) were run in 1× TAE-buffer. DNA samples combined with 1× loading dye (0.2% (w/v) OrangeG, 3% (v/v) glycerol) were loaded into individual wells in the gel. Samples were run alongside 1 kb Plus DNA Ladder (Invitrogen) at 100 V for approximately 40 min. DNA was visualised under a blue light transilluminator (Syngene).

### 2.1.4 Restriction endonuclease digestion of DNA

Sequence-specific digestion of DNA was performed using restriction endonucleases. DNA (0.5-1 µg) was incubated in appropriate 1× reaction buffer (NEB) with 0.5 U/µl restriction enzyme(s) at 37 °C for 15-60 min. Digested DNA fragments were analysed by DNA gel electrophoresis (see above).

### 2.1.5 Extraction of DNA from TAE-agarose gels

Individual DNA fragments were excised from agarose gels and purified using QIAQuick Gel Extraction Kit (QIAGEN) according to the manufacturer's instructions.

### 2.1.6 Ligation of DNA

DNA fragments digested with restriction enzymes were ligated to similarly digested plasmid DNA using DNA ligase. T4 DNA Ligase (4 U/µl, NEB) in 1× Ligase Reaction Buffer (NEB) was combined with digested insert and vector DNA (typically 1:1, 3:1 or 5:1 molar ratio) and incubated for 2 h at RT or 16 °C overnight. The reaction sample was then subjected to a transformation reaction using competent XL-1 Blue *E. coli* cells (Section 2.1.8).

### 2.1.7 Preparing competent E. coli cells

Competent XL-1 Blue *E. coli* cells were prepared using the Inoue method essentially as described by Sambrook and Russell (2006).

### 2.1.8 Transformation of DNA into competent E. coli cells

The heat shock method of transformation was used (Hanahan, 1983). Briefly, 20-100 ng plasmid DNA or 10 µl ligation mixture (Section 2.1.6) was added to the appropriate $CaCl_2$-competent *E. coli* strain (XL-1 Blue, BL21(DE3)-CodonPlus-RIL, BL21(DE3) EN2 (*DnaK* null) and SHuffle® cells, (NEB), see Appendix 1, Table 2) and incubated on ice for 10-30 min. Cells were then 'heat-shocked' at 42 °C for 90 s and then incubated on ice for 3 min. Following incubation (30-60 min with shaking) in 2×YT media (1.6% (w/v) tryptone, 1% (w/v) yeast extract, 0.5% (w/v) NaCl) recovered cells were spread onto LB agar plates (1% (w/v) tryptone, 0.5% (w/v) yeast extract, 1% (w/v) NaCl, 1.5% (w/v) bacteriological agarose) containing appropriate selective antibiotics and incubated overnight at 37 °C.

### 2.1.9 Isolation of plasmid DNA from E. coli (mini & midi prep)

Small (5-15 µg) and moderate (100 µg) amounts of plasmid DNA (outlined in Appendix 1, Table 2) was isolated from XL-1 Blue *E. coli* cells via alkaline lysis (Bimboim & Doly, 1979) using QIAprep Spin Miniprep and QIAGEN Plasmid Midi Kits (QIAGEN) respectively. 2×YT media (5 ml or 50 ml) containing appropriate antibiotics was inoculated with a single colony of freshly transformed bacteria and incubated overnight at 37 °C with shaking (140 rpm). Cells were pelleted via centrifugation (3578 *g*) and plasmid DNA was isolated according to the manufacturer's instructions.

### 2.1.10 DNA sequencing

Sanger sequencing of cloned DNA was performed by the Australian Genome Research Facility (AGRF) on 3730 and 3730xl capillary sequencers (Applied Biosystems) using Big Dye Terminator (BDT) chemistry version 3.1 (Applied Biosystems) under standardised cycling PCR conditions. 600 ng DNA was supplied ready-mixed with 10 pmol of appropriate primer in a 12 µl reaction volume. Chromatograms were viewed using Chromas Lite v2.1.

### 2.1.11 Preparation of glycerol stocks

5 ml 2×YT media containing the appropriate antibiotics was inoculated with a single colony of freshly transformed *E. coli* strain and incubated overnight at 37 °C with shaking (140 rpm). The liquid culture was supplemented with glycerol (final concentration of 15% (v/v)) then snap-frozen using liquid nitrogen and stored at -80 °C.

## 2.2 Protein Chemistry

### 2.2.1 SDS-PAGE

Sodium dodecyl sulphate polyacrylamide gel electrophoresis (SDS-PAGE) was used to separate proteins based on their molecular weight. Protein samples (1-50 µg) mixed 5:1 with 6× Laemmli loading buffer (Laemmli, 1970) (480 mM Tris-HCl pH 6.8, 12% (w/v) SDS, 30% (v/v) glycerol, 1 mM dithiothreitol (DTT), 0.12% (w/v) Bromophenol Blue) and heat-treated (95 °C, 5 min) were loaded onto 12.5% or 15% (w/v) glycine-buffered (Laemmli, 1970) or 16.5% (w/v) Tricine-buffered (Schägger & von Jagow, 1987) polyacrylamide gels. All gels were made in-house and then mounted in a Mini Protean 3 cell apparatus (Bio-Rad) containing 1× SDS running buffer (25 mM Tris-HCl pH 8.3, 190 mM glycine, 0.1% (w/v) SDS) for glycine gels or separate 1× Cathode buffer (100 mM Tris, 100 mM Tricine buffer, 0.1% (w/v) SDS, pH 8.2) and 1× Anode buffer (200 mM Tris-HCl pH 8.9) for Tricine gels. Samples were run alongside Mark12 Unstained Standard molecular weight markers (Invitrogen) or SeeBlue Plus2 Pre-stained Standard molecular weight markers (Invitrogen) at 100-200 V until completion of electrophoresis. For the detection of proteins, immunoblotting (Section 2.2.4), digital autoradiography (Section 2.2.3) or Coomassie Brilliant Blue staining was performed. Gels were placed in Coomassie Brilliant Blue stain (0.1% (w/v) Coomassie Brilliant Blue R-250, 50% (v/v) methanol, 15% (v/v) glacial acetic acid) for at least an hour before destaining in destain solution (10% (v/v) glacial acetic acid, 20% (v/v) ethanol).

### 2.2.2 Blue native-PAGE (BN-PAGE)

For the separation of mitochondrial proteins under native conditions, mitochondria were first resuspended in solubilisation buffer (20 mM Tris-HCl, pH 8, 0.1 mM EDTA, 50 mM NaCl, 10% (v/v) glycerol, 1 mM PMSF, 1% (w/v) n-Dodecyl-β-D-maltoside (DDM)). Following centrifugation (17,000 *g* for 15 min) the supernatant was mixed with BN-

PAGE loading dye to 1× (10 mM Bis-Tris pH 8.0, 50 mM caproic acid, 0.5% (w/v) Coomassie Brilliant Blue G250) and proteins separated using a 5-16.5% gradient gel (made in-house as described by Schagger and von Jagow (1991)). Gels were maintained at 4 °C and run at 120 V for 2 h followed by 600 V for 2 h. Proteins were then fixed in the gel and the gel was dried (see below).

To visualise recombinant proteins under native conditions, samples of purified proteins were mixed with BN-PAGE sample buffer to a 1× concentration (1×: 10 mM Tris-HCl, 10 mM NaCl, 5 mM $MgCl_2$, 10 mM KCl, 5% (v/v) glycerol, pH 7.0) and BN-PAGE loading dye to 1× concentration and separated via pre-cast 4-16% NativePAGE™ Bis-Tris gel (Life Technologies) according to the manufacturer's instructions.

HMW Native molecular markers (GE Healthcare) solubilised in 120 mM Tris-HCl pH 7.0, 50 mM NaCl, 10 mM $MgCl_2$, 10% (v/v) glycerol were mixed with BN-PAGE loading dye to a 1× concentration and run alongside samples.

### 2.2.3 Gel drying & autoradiography

Following protein separation by electrophoresis, polyacrylamide gels were incubated in fixation solution (30% (v/v) methanol and 15% (v/v) acetic acid) for at least 1 h at RT then washed with 30% (v/v) methanol, 4% (v/v) glycerol solution for 15-30 min. The gel was then dried at 80 °C for 1-2 h using a Model 583 gel dryer (Bio-Rad) under vacuum. The molecular weight standards were marked using radioactive dye ([$^{35}$S]Met/Cys in 1× Laemmli loading dye) and covered using adhesive tape. The gels were then exposed to a storage phosphor screen (Molecular Dynamics) for 16-36 h. Digital autoradiography images were acquired by scanning the phosphor screen using a Typhoon™ Trio variable mode imager (GE Healthcare) with Typhoon Scanner Control (v 5.0) software.

### 2.2.4 Western transfer and immuno-decoration

Proteins separated via SDS-PAGE (Section 2.2.1) or BN-PAGE (Section 2.2.2) were transferred to methanol-activated polyvinylidene fluorine (PVDF) membrane (Millipore) by semi-dry method (Harlow & Lane, 1999) using an OWL Separation System electroblotting apparatus (Thermo Fisher Scientific) with 1× transfer buffer (4.8 mM Tris-HCl pH 8.3, 39 mM glycine, 0.037% (w/v) SDS and 20% (v/v) methanol). A 300-350 mA current was applied for 90-120 min. Before immuno-decoration (Harlow & Lane, 1999), the membrane was blocked in 5% (w/v) skim milk powder (Diploma) in 1× Tris-buffered saline supplemented with Tween-20 (TBS-T; 20 mM Tris-HCl pH 7.5, 150 mM NaCl, 0.1% (v/v) Tween-20) for at least 2 h. The membrane was incubated with the primary antibody (see Appendix 2, Table 1) for 1 h. Following wash steps the membrane was incubated (1 h at RT) with Horse Radish Peroxidase- (HRP-) conjugated secondary antibody in TBS-T. Following wash steps and incubation (1 min) with ECL reagent (100 mM Tris-HCl, pH 8.5, 1.25 mM luminol, 0.198 mM coumaric acid, 0.012% (v/v) $H_2O_2$) the membrane was exposed for 1-10 min using a G-Box Chemi-XL1 molecular imager (SynGene) with GeneSys software v1.2.8.0. Membranes were also exposed using x-ray film (Super RX, Fuji Film) for 5-300 s. Film was developed using a medical film processor (SRX-101A, Konica-Minolta).

## 2.3 Recombinant protein expression & purification

### 2.3.1 Small and large scale expression of recombinant proteins

Pre-cultures were prepared by inoculating 5 ml or 200 ml 2×YT media (in preparation for small and large scale expression respectively) containing selective antibiotics with a single colony of transformed *E. coli* strain (see Appendix 1, Table 2) and were grown overnight at 37 °C with shaking (140 rpm). For small-scale expression, the overnight culture was used to inoculate a fresh 5 ml of antibiotic-containing 2×YT to an initial optical density at 600 nm ($OD_{600}$) of 0.1. Cells were then grown at 37 °C with

shaking (140 rpm) until an $OD_{600}$ of between 0.8-1.0 and then protein expression was induced by the addition of IPTG (0.5 mM). The expression culture was grown between 16-37 °C with shaking (140 rpm) for a further 16 h with samples collected at various time intervals.

For large scale protein expression, the overnight culture was used to inoculate 1-1.5 L of antibiotic supplemented 2×YT media contained within a 2 or 5 L baffled flask to an initial $OD_{600}$ of 0.1. Cultures were then grown at 37 °C with shaking (140 rpm) until an $OD_{600}$ of 0.8-1.0 was reached. Protein expression was induced by the addition of IPTG (0.5 mM) and cultures were grown at 20 °C for 4-16 h with shaking (140 rpm) until harvesting (Section 2.3.3).

### 2.3.2 Solubility test for recombinant proteins

Expression cultures (5 ml) were cultivated as described (see above). Harvested cells were resuspended in bacterial extraction buffer (50 mM Tris-HCl pH 8.0, 300 mM NaCl, 1 mM EDTA, 0.05% (v/v) Triton X-100 and 10% (v/v) glycerol) at a ratio of 4 ml/g wet weight of cells then snap-frozen and thawed (repeated 3 times), prior to the addition of chicken egg white lysozyme (0.2 mg/ml). Cells were gently mixed for 45 min at 4 °C prior to sonication at 50 W for 3 × 60 s with 30 s resting intervals using a chilled sonicating water bath. Finally, DNase 1 (10 µg/ml) and $MgCl_2$ (5 mM) were added and the lysate was mixed for 30 min at 4 °C. A sample of lysate (total) was set aside then the remaining sample was separated into soluble and insoluble fractions by centrifugation at 9477 *g* for 15 min at 4 °C. The insoluble pellet was resuspended in extraction buffer (to the initial volume) and equal volumes of total, soluble and insoluble material subjected to SDS-PAGE (see 2.2.1).

### 2.3.3 Extraction of bacterial cells

After completion of large-scale expression (Section 2.3.1), cells were pelleted via centrifugation (3849 *g*) and resuspended in chilled bacterial extraction buffer at a ratio of 4 ml/g wet weight of cells. Cells were subjected to three cycles of snap-freezing in liquid nitrogen and thawing in a water bath prior to the addition of chicken egg white lysozyme (0.2 mg/ml) and mixing for 60 min at 4 °C. The cell suspension was sonicated on ice for total 30 min (60 amplitude, 2 s processing time with 20 s resting intervals) (QSonica) before the addition of DNase I (10 µg/ml), $MgCl_2$ (5 mM) and imidazole (10 mM) and mixing for 30 min at 4 °C. The cell lysate was then centrifuged (24 000 *g*, 50 min, 4 °C) and soluble cell-free fraction retained.

### 2.3.4 Purification of His-tagged recombinant proteins

Recombinant proteins tagged with 6×His ($His_6$) or 10×His ($His_{10}$) were isolated using immobilized metal affinity chromatography (IMAC) using Ni-NTA agarose beads (QIAGEN) at 4 °C. Generally, soluble lysate (see above) was applied to 1 ml settled Ni-NTA agarose pre-equilibrated with 5 bed volumes (BV) of Wash 10 buffer (W10; 20 mM Tris-HCl pH 8.0, 300 mM NaCl and 10 mM imidazole) and allowed to pass over the beads under gravity flow. For $His_6$-tagged proteins the beads were then washed with 5 BV W10 and W20 buffer (20 mM Tris-HCl pH 8.0, 300 mM NaCl and 20 mM imidazole) prior to elution of tagged protein using 6× 1 BV of E250 buffer (20 mM Tris-HCl pH 8.0, 300 mM NaCl, 250 mM imidazole). For purification of $His_{10}$-tagged proteins, the beads were subjected to additional washing steps (typically, 2 BV each of W40, W60, W80 and W100 in succession; the numerical value represents the mM concentration of imidazole made up in 20 mM Tris-HCl pH 8.0 and 300 mM NaCl) prior to elution with 6× 1 BV of E500 buffer (20 mM Tris-HCl pH 8.0, 300 mM NaCl and 500 mM imidazole) supplemented with 10-20% (v/v) glycerol.

### 2.3.5 Cleavage of $His_6$-ubiquitin ($His_6$-Ub)-tagged recombinant proteins

For the generation of authentic recombinant proteins, following initial IMAC purification (see above), $His_6$-Ub fusion proteins (5-12 mg) were incubated in 1× cleavage buffer (20 mM Tris-HCl pH 8.0, 150 mM NaCl and 1 mM DTT) with deubiquitinating (DUB) enzyme Usp2cc (Catanzariti et al., 2004) at a 1:75 ratio at 20 °C for 2 h. Protein samples were then dialysed (50 mM Tris-HCl pH 8.0, 200 mM KCl, 10% (v/v) glycerol and 1 mM DTT) at 4 °C for 2-4 h to remove imidazole. The protein sample was incubated with Ni-NTA agarose beads (100 µl settled beads to 1 mg protein sample) pre-equilibrated with 5 BV of W10 buffer (see above for buffer components) for 20 min at 4 °C. The untagged protein of interest was collected in the unbound fraction ('reverse IMAC'). The beads were then washed with 1 BV of W10 and W20 buffer and 2× 1 BV of E250 buffer to monitor non-specific binding to the column. Protein purity was analysed via SDS-PAGE (Section 2.2.1).

### 2.3.6 Anion exchange chromatography

Following $His_6$-Ub cleavage (Section 2.3.5), where indicated, purified recombinant protein with persisting contaminants was applied to a 1 ml ResourceQ anion exchange column (GE Healthcare) pre-equilibrated in Buffer A (50 mM Tris-HCl pH 8.0, 5% (v/v) glycerol and 20 mM KCl) using an NGC™ Quest Plus (Bio-Rad) chromatography system operated using Chromlab software. Following a 5 BV wash using Buffer A, the protein of interest was eluted using a salt gradient (20 mM KCl – 1 M KCl in 50 mM Tris pH 8.0 and 5% (v/v) glycerol over 20 BV). Throughout the chromatography procedure proteins was monitored by absorbance at 280 nm and samples were collected on a BioFrac™ fraction collector. Aliquots of collected samples were analysed by SDS-PAGE (Section 2.2.1) then the protein of interest was concentrated by ultrafiltration using an Amicon® ultra centrifugal filter (Merck-Millipore) as per the manufacturer's instructions.

### 2.3.7 Size exclusion chromatography (SEC)

Recombinant protein (0.2-20 mg) was applied to size exclusion chromatography columns Superdex 75 10/30 GL, Superdex 75 HiLoad 16/60 pg or Superdex 200 HiLoad 16/60 pg (GE Healthcare). Columns were connected to either an AKTA™ Pure 1.01.2 Purification system (GE Healthcare) with Unicorn v6.3 software or a NGC™ Quest Plus Chromatography System with Chromlab software v3.1.0.06 and equilibrated with appropriate buffer (see Table 2.1). The elution of the protein was monitored by absorbance at 280 nm. Columns were calibrated with molecular weight standards (LMW/HMW Gel Filtration Calibration Kit, GE Healthcare) according to the manufacturer's instructions.

**Table 2.1: SEC Buffer composition for various recombinant proteins.**

| Protein | Buffer components |
|---|---|
| CLPP (WT & mutants) | 50 mM Tris-HCl, 100 mM NaCl, 200 mM KCl, 5% (v/v) glycerol, 0.025% (v/v) Triton X-100, 200 mM $MgCl_2$ and 0.5 mM tris(2-carboxyethyl)phosphine (TCEP), pH 7.5. |
| SDH5 (WT & mutants) | 50 mM Tris-HCl, 100 mM KCl, 20 mM $MgCl_2$ and 5% (v/v) glycerol, pH 8.0. |
| StAR (WT & mutants) | 50 mM Tris-HCl, 150 mM KCl and 5% (v/v) glycerol, pH 7.5. |

### 2.3.8 Determining protein concentration

Protein concentration was estimated using the dye-binding method (Bradford, 1976) using commercially available assay solution (Bio-Rad) as per the manufacturer's instructions. The absorbance at 595 nm was measured against a protein-free blank using a spectrophotometer (Novaspec III, Amersham Biosciences) or microtiter plate reader (Spectra

Max M5e, Molecular Devices). Protein concentration was then determined by comparison to a BSA standard curve.

### 2.3.9 Solubilising lyophilised casein (FITC- or alpha-casein)

In solubilisation buffer (50 mM Tris, 100 mM NaCl, 0.05% (v/v) Triton X-100, pH 8.0), α-casein or fluorescein isothiocyanate (FITC)-casein derived from bovine milk (Sigma) was resuspended to a final concentration of 5 mg/ml. The protein was then snap-frozen and stored at -80 °C until required.

## 2.4 Biochemical characterisation of recombinant proteins

### 2.4.1 *In vitro* proteolysis assays

The proteolytic activity of purified recombinant proteases and half-life of various substrate proteins was determined via degradation assays in the presence or absence of ATP.

In appropriate 1× assay buffer (1× LONM Buffer: 50 mM Tris-HCl pH 8.0, 100 mM KCl, 20 mM $MgCl_2$, 0.05% (v/v) Triton X-100, 10% (v/v) glycerol and 1 mM DTT, or 1× hCLPXP buffer: 50 mM Tris-HCl pH 7.5, 100 mM KCl, 100 mM NaCl, 20 mM $MgCl_2$, 10% (v/v) glycerol, 0.025% (v/v) Triton X-100 and 1 mM DTT), substrate protein (typically 1 μM) and protease (LONM: typically 1.2 μM protomer concentration, hCLPX: 2.4 μM, hCLPP: 5.6 μM) was combined and pre-incubated at 30 °C. The catalytic reaction was initiated by the addition of neutralised ATP (5 mM). Aliquots were taken at various time points as indicated and reactions terminated by treatment with 6× Laemmli buffer (5:1 ratio). Samples were separated via SDS-PAGE (Section 2.2.1) and visualised by Coomassie Brilliant Blue staining or western blotting (Section 2.2.4).

### 2.4.2 *In vitro* fluorometric assays

The peptidase activity of purified recombinant CLPP was determined using a peptide substrate linked to chromophore 7-amino-4-methylcoumarin (AMC). In 1× hCLPXP assay buffer, hCLPP (5.6 μM protomer concentration) was incubated in a black 96-well microplate (Nunc) at 30 °C for 5 min prior to the addition of 1 mM peptide substrate as indicated. The plate was then read every 10 s over 60 min with excitation: 380 nm and emission: 460 nm.

The proteolytic activity of purified recombinant hCLPXP was determined with FITC-labelled casein. In 1× hCLPXP buffer as above, hCLPX (2.4 μM protomer), hCLPP (5.6 μM protomer) and ATP (5 mM) was pre-incubated at 30 °C for 5 min in a black 96-well microplate. The assay was initiated by the addition of FITC-casein (0.3 μM) and the plate was read every 10 s for 60 min at excitation wavelength: 490 nm and emission: 520 nm.

The activity of purified recombinant hCLPP in the presence of purified recombinant *E. coli* ClpX (ecClpX) was determined using the *E. coli* ClpXP substrate GFP-SsrA (SsrA tag AANDENYALAA fused to the C-terminus of GFP). In 1× hCLPXP buffer as above, ecClpX (1.2 μM protomer), hCLPP (2.8 μM protomer) and ATP (5 mM) was pre-incubated at 30 °C for 5 min in a black 96-well microplate. The assay was initiated by the addition of GFP-SsrA (1 μM) and the plate was read every 10 s for 60 min with excitation wavelength: 410 nm and emission: 500 nm.

### 2.4.3 Limited proteolysis

Limited proteolysis experiments were performed to determine the accessibility of $StAR_{\Delta C}$ to proteolytic cleavage in the presence or absence of the $StAR_{pep}$. In 1× thermolysin buffer (50 mM Tris-HCl pH 7.0, 175 mM NaCl and 5 mM $CaCl_2$), 42 μg $StAR_{\Delta C}$ in the absence or presence of $StAR_{pep}$ (1:4 molar ratio) was combined and incubated at (20 °C) prior of the addition of thermolysin (0.5 U) (Sigma) to initiate the reaction.

Aliquots were taken at the indicated time points and the reaction was terminated by treating with 6× Laemmli loading dye and immediately boiling the samples (95 °C, 5 min). Proteins were separated via SDS-PAGE (Section 2.2.1), transferred to PVDF membrane and analysed via immunoblotting (Section 2.2.4)

### 2.4.4 Glutaraldehyde crosslinking

Prior to crosslinking, samples of recombinant protein were dialysed against Tris-free dialysis buffer (50 mM MOPS-KOH pH 7.5, 300 mM NaCl, 0.025% (v/v) Triton X-100, 10% (v/v) glycerol and 1 mM DTT) for 2 h at 4 °C. In 1× crosslinking buffer (50 mM Hepes, 300 mM NaCl, 20 mM $MgCl_2$, 200 mM KCl, 0.025% (v/v) Triton X-100, 10% (v/v) glycerol and 1 mM DTT, pH 7.5) recombinant protein (0.16 µg/µl) was pre-incubated at 25 °C prior to addition of 0.1% (v/v) glutaraldehyde. Aliquots were taken at the time points indicated and added to 4× Laemmli loading dye (6× loading dye diluted to 4× with 1.24 M Tris pH 6.8) and immediately heat-treated (95 °C, 5 min). Samples were separated via SDS-PAGE (2.2.1) and analysed via Coomassie Brilliant Blue staining.

### 2.4.5 Analytical ultra-centrifugation (AUC)

Sedimentation velocity experiments and data analysis were performed in collaboration with Dr. Tatiana Soares da Costa and Associate Professor Matthew Perugini (La Trobe Institute for Molecular Science, La Trobe University). Specifically, sedimentation experiments of CLPP, $CLPP^{C147S}$ and $CLPP^{Y229D}$ (1.2 and 0.90 mg/ml) dissolved in 50 mM Tris-HCl pH 7.5, 100 mM NaCl, 200 mM KCl, 5% (v/v) glycerol, 0.025% (v/v) Triton X-100, 200 mM $MgCl_2$, and 0.5 mM TCEP were performed using a Beckman model XL-A analytical ultracentrifuge equipped with a photoelectric optical absorbance system. Sample (380 µl) and reference (400 µl) solutions were loaded into a conventional double sector quartz

cell and mounted in a Beckman An-60 Ti rotor. The samples were then centrifuged at 40,000 rpm at 20 °C and data were collected at a single wavelength (280 nm) in continuous mode without averaging using a step-size of 0.003 cm. Solvent density (1.02600 g/ml at 20 °C) and viscosity (1.1603 cp at 20 °C), as well as estimates of the partial specific volume, $\bar{v}$ (0.743114 ml/g, 0.743188 ml/g and 0.742661 for wild-type CLPP, $CLPP^{C147S}$ and $CLPP^{Y229D}$ respectively, at 20 °C) were computed using the program SEDNTERP (Laue et al., 1992). Sedimentation velocity data at multiple time points were fitted to a continuous size-distribution model (Perugini et al., 2000; Schuck, 2000; Schuck et al., 2002) using the program SEDFIT.

### 2.4.6 Co-immunoprecipitation (IP) of hCLPP with hCLPX

Human CLPP (hCLPP) binding to human CLPX (hCLPX) was assessed by immunoprecipitation assays using anti-CLPX antibodies. hCLPX antisera raised in rabbit was incubated (15 min, RT) with Protein A Sepharose (PAS) pre-equilibrated in 10 mM Tris-HCl, pH 8. The PAS was washed 3 times with 10 mM Tris-HCl, pH 8 then used directly in IP assays. In 1× IP buffer (50 mM Tris-HCl pH 7.5, 100 mM NaCl, 100 mM KCl, 40 mM Mg-Acetate, 10% (v/v) glycerol, 0.1% (v/v) Triton X-100) protein mixes containing 0.5 μM hCLPP in the presence or absence of 1 μM hCLPX (supplemented with 2 mM ATPγS as required) were combined in a total volume of 400 μl. The samples were incubated at RT for 5 min then added to the CLPX antibody-bound PAS. The PAS and protein mixes were then slowly mixed for 60 min at 4 °C. The PAS was washed three times with 1× IP buffer supplemented with 10 mM ATP prior to eluting bound protein with 50 mM glycine, pH 2.5. Samples were neutralised with excess Tris base then separated via SDS-PAGE (Section 2.2.1) and analysed by immunoblotting (Section 2.2.4).

### 2.4.7 $StAR_{\Delta C}$ pull-down assay

To investigate the interaction between $StAR_{\Delta C}$ and $StAR_{pep}$, a series of pull downs assays were performed. Briefly, 27.5 µg His-tagged protein ($His_6$-Ub-$StAR_{pep}$) was immobilized to Ni-NTA agarose beads pre-equilibrated with 10 BV of 1× Buffer A (50 mM Tris-HCl pH 8.0, 300 mM NaCl, 0.1% (v/v) Triton X-100 and 10 mM imidazole) followed by 5 BV of 1× Buffer C (20 mM Hepes-KOH pH 7.5, 100 mM KOAc, 10 mM MgOAc, 10% (v/v) glycerol, 0.5% (v/v) Triton X-100 and 20 mM imidazole). Interacting protein of interest ($StAR_{\Delta C}$) was added at a molar ratio of 1:4 in 1× Buffer C and the mixture was slowly mixed at 4 °C for 30 min. The bead mixture was then centrifuged (2000 *g*, 10 min, 4 °C) and the supernatant (unbound) was removed. The beads were then resuspended in 5 BV of 1× Buffer C and transferred to Mobicol spin columns (MoBiTec) for subsequent washing steps. The beads were washed with 10 BV 1× Buffer D (20 mM Hepes-KOH pH 7.5, 100 mM KOAc, 10 mM MgOAc, 10% (v/v) glycerol, 0.25% (v/v) Triton X-100 and 20 mM imidazole) by centrifuging for 2 min, 2000 *g*, 4 °C followed by an additional centrifugation step to remove all remaining buffer. The beads were then incubated with 1 BV of 1× Buffer E (50 mM Tris-HCl pH 8.0, 300 mM NaCl and 250 mM imidazole) for 1 min at RT and centrifuged (2000 *g*, 5 min, 4 °C) to elute all bound proteins. Samples were separated via SDS-PAGE (Section 2.2.1) and results visualised via immunoblotting (Section 2.2.4).

### 2.4.8 ATPase activity assay

The ability of LONM to hydrolyse ATP was monitored via a malachite green ATPase assay (Lanzetta et al., 1979). 1× LONM assay buffer, samples containing LONM (0.6 µM, protomer concentration) in the absence or presence of α-casein (3 µM) were pre-incubated at 30 °C or 37 °C for 5 min prior to the addition of ATP (2 mM). The reactions were stopped at the same time by the addition of malachite green solution

(0.034% (w/v) malachite green, 0.1% (v/v) Triton X-100, 1.05% (w/v) ammonium molybdate, 1M HCl) and incubated at RT for 10 min. Colour development was quenched by the addition of 34% (w/v) citrate. Aliquots from each sample were then added to a 96-well microplate and the absorbance was measured at 650 nm.

### 2.4.9 Isolation of crude mitochondria from mammalian cultured cells

Mitochondria were isolated essentially as described by Johnston et al. (2002) but with the following specific details. Fully confluent plates of HeLa or HepG2 cells grown as described (Section 2.5.1) were harvested using a cell scraper. After centrifugation at 800 *g* for 5 min, the cell pellet was washed 3 times in 10 ml 1× Phosphate Buffered Saline (PBS; 137 mM NaCl, 10 mM Phosphate, 2.7 mM KCl, pH 7.4-7.6). The cells were then resuspended in chilled Solution A (20 mM Hepes pH 7.6, 220 mM mannitol, 70 mM sucrose, 1 mM EDTA and 2 mg/ml BSA Fraction V) to a final concentration of 25-30 mg/ml and allowed to swell on ice for 15 min. The cell solution was homogenized (~25 strokes) with a drill–fitted tissue grinder pestle and mortar assembly (Wheaton) at 4 °C. Cell debris was pelleted at 1000 *g* for 15 min at 4 °C while the supernatant containing the mitochondrial fraction was collected and centrifuged again at 10,000 *g* for 15 min at 4 °C. The pellet was then washed in 10 ml Solution B (Solution A without BSA) prior to another 10,000 *g* centrifugation step for 15 min at 4 °C. The mitochondrial pellet was then resuspended in sucrose buffer (0.5 M sucrose, 10 mM Hepes pH 7.6) to a protein concentration of approximately 5 mg/ml. Suspensions of mitochondria were placed at -80 °C for storage.

### 2.4.10 Isolation of crude mitochondria from *Saccharomyces cerevisiae*.

Mitochondria were isolated from *S. cerevisiae*, strain YPH499 as described by Meisinger et al. (2006). To do this, a single colony of yeast grown on YPG agar (1% (w/v) yeast extract, 2% (w/v) peptone, 3% (v/v) glycerol and 2.5% (w/v) agar) was used to inoculate 200 ml of YPG media (1% (w/v) yeast extract, 2% (w/v) peptone and 3% (v/v) glycerol, pH 5.0) and grown overnight at 30 °C with shaking (160 rpm). The starter culture was then used to inoculate fresh YPG media and the cells were grown at 30 °C (160 rpm) until an $OD_{600}$ of ~1.5 was obtained. Following extraction and isolation, mitochondria were resuspended in chilled SEM buffer (250 mM sucrose, 1 mM EDTA, 10 mM MOPS-KOH, pH 7.2) to a final protein concentration of 5 mg/ml. Mitochondria were aliquoted, snap-frozen in liquid $N_2$ and stored at -80°C.

### 2.4.11 Generation of radiolabelled precursor proteins *in vitro*

cDNA coding for the gene of interest was purchased from the I.M.A.G.E consortium (in pOTB7 background, refer to Appendix 1, Table 2). A reaction mix containing no less than 80% SP6 coupled transcription and translation (TNT) rabbit reticulocyte lysate system (Promega), 20 ng/µl of plasmid DNA and typically 0.5 µCi/µl [$^{35}$S]Met/Cys (comprising 73% [$^{35}$S]-L-methionine (specific activity: 1175.0 Ci/mmol) and 22% [$^{35}$S]-L-cysteine (specific activity 1075.0 Ci/mmol) (Perkin Elmer)) was incubated at 30 °C for 70-90 min to generate radiolabelled precursor protein. Successful translation of radiolabelled protein was determined via SDS-PAGE (Section 2.2.1) and autoradiography (Section 2.2.3).

### 2.4.12 Import of radiolabelled precursor proteins into isolated mitochondria

Isolated mitochondria (~600 µg) resuspended in import buffer (mammalian mitochondria: 20 mM Hepes-KOH pH 7.4, 250 mM sucrose, 5 mM Mg-acetate, 80 mM K-acetate, 10 mM Na succinate, 1 mM DTT, 30 mg/ml BSA Fraction V, 5 mM methionine and 2 mM ATP. Yeast mitochondria: 10 mM MOPS-KOH pH 7.2, 250 mM sucrose, 5 mM $MgCl_2$, 2 mM $KH_2PO_4$, 80 mM KCl, 0.03 mg/ml BSA Fraction V, 2 mM NADH, 5 mM methionine and 2 mM ATP) were aliquoted into separate tubes and incubated at either 37 °C for mammalian mitochondria or 25 °C for yeast mitochondria. Valinomycin (f.c. 1 µM in ethanol) was added to specific samples to dissipate the membrane potential ($\Delta\psi$). Reticulocyte lysate (see above) containing radiolabelled precursor protein was added and samples were incubated until import was stopped by the addition of valinomycin (1 µM) and placed on ice.

Samples treated with Proteinase K (50 µg/ml) were incubated on ice for 15 min prior to adding PMSF (6 mM) for 10 min. Alternatively, samples were treated with trypsin (50 µg/ml) and incubated on ice for 30 min (with occasional tapping) prior to the addition of soy bean trypsin inhibitor (SBTI) (1 mg/ml) for 5 min.

Samples were then centrifuged (9000 *g*, 10 min, 4 °C) and the pellet was resuspended in 150 µl of chilled SEM buffer. The samples were centrifuged again and the pellet was resuspended in either 1× solubilisation buffer (20 mM Tris-HCl, pH 8, 0.1 mM EDTA, 50 mM NaCl, 10% (v/v) glycerol, 1 mM PMSF and 1% (w/v) DDM) for analysis via BN-PAGE (Section 2.2.2) or 3× Laemmli buffer for analysis via SDS-PAGE (Section 2.2.1), and the proteins were visualised via autoradiography (Section 2.2.3).

### 2.4.13 *In organello* proteolysis assay (import-chase)

Following import of radiolabelled precursor proteins (see above) and addition of valinomycin (1 µM), an ATP re-generation system was added (1 mM ATP, 10 mM phosphocreatine and 0.1 mg/ml creatine kinase) and the mitochondrial suspension was incubated at 37 °C. At the indicated time points aliquots, equivalent to 50 µg protein, were collected and the mitochondrial pellet formed by centrifugation (9000 *g*, 10 min, 4 °C) was resuspended in 150 µl of chilled SEM buffer. Samples were centrifuged again and the pellet was resuspended in either 1× solubilisation buffer (for analysis via BN-PAGE (Section 2.2.2)) or 3× Laemmli buffer (for analysis via SDS-PAGE (Section 2.2.1)) and the proteins were visualised via autoradiography (Section 2.2.3).

### 2.4.14 Quantitation of protein turnover

After separation of protein samples via SDS-PAGE (Section 2.2.1) and visualisation by Coomassie Brilliant Blue, radiolabelling or immuno-decoration, protein bands of interest were quantitated via densitometry using ImageQuant TL v.8.1 (GE Healthcare). The half-life was then determined by plotting density (relative to initial) over time using GraphPad Prism v6.07.

## 2.5 General cell-culture techniques

### 2.5.1 Culturing and passaging cells

Tissue culture cells were grown and maintained at 70-90% confluency at 37 °C with 5% (v/v) $CO_2$ in Dulbecco's Modified Eagle Medium (DMEM; Invitrogen) supplemented with 10% (v/v) Fetal Bovine Serum (FBS) for a maximum of one month. To passage adherent cells, the media was aspirated and cells were washed with 1× Phosphate Buffered Saline (PBS; 137 mM NaCl, 10 mM Phosphate, 2.7 mM KCl, pH 7.4-7.6) before

adding trypsin solution (0.25% (w/v) Trypsin and 1 mM ETDA; Sigma) for 30-60 s. Cells were then resuspended in DMEM supplemented with 10% (v/v) FBS and seeded to ~50% confluency.

### 2.5.2 Cryopreservation of mammalian cell lines

Adherent cells grown to ~90-100% confluency were harvested from a 14 cm tissue culture plate and centrifuged at 800 *g* for 5 min. The pellet was washed in 1× PBS, centrifuged again and then resuspended in complete growth media supplemented with 5-10% (v/v) DMSO (Sigma). The freezing-media suspension was then separated into 1 ml aliquots in cell-culture cryogenic tubes (Thermo-Scientific) and stored in a Mr Frosty™ Freezing Container (Thermo-Scientific) at -80 °C overnight before being transferred to a liquid nitrogen cryogenic freezer until required.

# Chapter 3: Dissecting the molecular determinants of substrate recognition by LONM

## 3.1 Introduction

The contribution of LONM to mitochondrial matrix proteostasis through the selective degradation of unfolded or oxidatively damaged proteins has been well established *in vitro* and *in vivo* (Bezawork-Geleta et al., 2015; Bota & Davies, 2002; Bota et al., 2002; Venkatesh et al., 2012). However, the specific recognition determinants for LONM-mediated degradation of native proteins are poorly understood. Substrates of ecLon and other AAA+ proteases are recognised via specific sequences or structural motifs known as degrons (degradation signals). In regard to ecLon, these degrons regulate the recognition of the substrate which in turn influences the unfolding and translocation efficiency of the protein (Gur & Sauer, 2009). Co-evolution of degrons and proteases has allowed for the selection of specific proteins to be rapidly removed from the cell without causing proteotoxic stress or affecting cellular viability (Gur et al., 2012). Moreover, multiple degrons are likely to exist within a single protein substrate to facilitate the complete turnover of a protein by the concerted action of resident proteases (Gur & Sauer, 2009).

In the mitochondrial matrix, LONM has been established as the primary protease responsible for the degradation of unfolded (but not aggregated) proteins that are typically recognised via the exposure of hydrophobic residues that would normally be buried within the structure of the folded protein (Bezawork-Geleta et al., 2015; Bota & Davies, 2002). Consistently, Pim1 in yeast mitochondria has been demonstrated to recognise and degrade oxidatively damaged or unstable proteins that are prone to aggregation (Bayot et al., 2010; Bender et al., 2011). Similar to ecLon, LONM has been shown to regulate the turnover of several native substrates (outlined in Table 1.1), indicating a conserved regulatory role for this protease. The current understanding is that LONM degrades native, stable proteins to control protein levels within the cell (e.g. StAR), to regulate metabolic pathways (e.g. heme biosynthesis) and to maintain proteostasis by removing unassembled complex subunits (e.g. MPPα) (Granot et al., 2007a; Ondrovičová et al., 2005; Tian et al., 2011). LONM

is also proposed to play a role in the progression of paraganglioma type 2 (PGL2) as it is responsible for the turnover of the pathogenic form of SDH5 (also known as SDHAF2, succinate dehydrogenase assembly factor 2) (Bezawork-Geleta et al., 2014). However, the elements that promote LONM-mediated degradation of these substrates have yet to be identified. In contrast, several recognition motifs have been identified for ecLon, such as β-20 (a 20 residue internal fragment of β-galactosidase), Sul20C (the last C-terminal residues of SulA) and the UmuD tag (N-terminal residues of UmuD), that promote recognition and binding with different affinities (Gonzalez et al., 1998; Gur & Sauer, 2008; Ishii et al., 2000). Additionally, hydrophobic and aromatic residues were determined to be critical elements in ecLon-mediated recognition (Gur & Sauer, 2008).

The ability of LONM to recognise folded proteins as substrates can be strongly influenced by genetic or acquired mutation and ultimately can have detrimental consequences for the cell if not properly controlled. For instance, many diseases have been linked to the aberrant tagging or degradation of proteins by the Ubiquitin Proteasome System (UPS), and it is now evident that a change in protein levels can have global effects on the viability of the cell and/or organism (Lecker et al., 2006; Reinstein & Ciechanover, 2006). Similarly, changes in the levels of mitochondrial proteins can result in a variety of disease states from impaired metabolism to cancer, myopathies and neurodegenerative disorders (Angelini et al., 2009; Tuppen et al., 2010). The direct function of mitochondrial proteases and chaperones under these circumstances however, has not been thoroughly examined. Approximately half of the known disease-causing mutations in humans are due to amino acid substitutions within proteins that lead to impaired signalling pathways or structural instability (Ng & Henikoff, 2006). Other mutations are seemingly innocuous with the protein demonstrating functionality and biochemical stability *in vitro* but exhibiting reduced expression levels *in vivo* (Bezawork-Geleta et al., 2014; Correia et al., 2006). To date, the

contribution of LONM and other mitochondrial proteases to the pathology of particular diseases has not been extensively explored.

To determine if the recognition and subsequent degradation of substrates by LONM can be predicted or manipulated, the location and features of the degron(s) used by LONM first needs to be identified. MPPα (Ondrovičová et al., 2005), TFAM (Matsushima et al., 2010), ALAS-1, (Tian et al., 2011), StAR (Granot et al., 2007a) and SDH5 (Bezawork-Geleta et al., 2014) have all been characterised as substrates of LONM but the specific degrons influencing their turnover have not been determined.

### 3.1.1 LONM-mediated turnover of SDH5 is regulated by its interaction with SDHA.

Succinate dehydrogenase (SDH) assembly factor 2 (SDHAF2/SDH5) was first described by Hao et al. (2009) as an assembly factor for SDH (complex II) as it is responsible for the flavinylation of the catalytic subunit SDHA which is vital for complex II activity. Patients with a missense mutation (G78R) in SDH5 displayed ~95% reduction in levels of flavinylated SDHA compared to control samples and develop paraganglioma type 2 (PGL2) which is characterised by benign neuroendocrine tumours in the head and neck (Hao et al., 2009).

Characterisation of wild-type SDH5 and the clinical mutant ($SDH5^{G78R}$) *in vitro* revealed that both proteins share similar biochemical properties and were degraded by LONM at comparable rates (Bezawork-Geleta et al., 2014). However *in organello*, SDH5 was protected from LONM-mediated degradation by SDHA, while $SDH5^{G78R}$ was not. It was found that the SDHA-$SDH5^{G78R}$ complex formation was less stable than the SDHA-SDH5 complex and as such $SDH5^{G78R}$ was more susceptible to degradation by LONM *in vivo* (Bezawork-Geleta et al., 2014). The reduced half-life of $SDH5^{G78R}$ may partially or fully account for the reduced levels of flavinylated SDHA seen in patients with PGL2 (Hao et al., 2009). As

the interaction with SDHA influences the stability of SDH5 *in organello* and *in vitro*, it was proposed that a degron of SDH5 is protected within the SDHA-SDH5 complex.

Therefore, by increasing the levels of $SDH5^{G78R}$ (as a result of reducing the degradation), the interaction with SDHA may be restored and the levels of flavinylated SDHA may increase. Indeed the 90 kDa complex of SDHA-$SDH5^{G78R}$ was seemingly stabilised in LONM depleted mitochondria (Bezawork-Geleta et al., 2014). The aim of this study was to establish the primary regulatory elements for LONM-mediated recognition of folded substrates. Using SDH5 as a model substrate for understanding the degradation of native proteins, the essential requirements for LONM-mediated degradation *in vitro* and *in organello* was established.

Previously the N-terminal sequence of mature FLAG-tagged SDH5, isolated from HeLa mitochondria was experimentally determined (Bezawork-Geleta et al., 2014). This revealed two possible cleavage sites (1: between F34 and Y35 or 2: between R36 and G37) for the removal of the presequence (outlined in Appendix 3, Supplementary Figure 1A). The stability of both forms of recombinant SDH5, ($SDH5_{35\text{-}166}$, herein referred to as YR-SDH5 or $SDH5_{37\text{-}166}$, herein referred to as G-SDH5), were analysed *in vitro* in the presence of LONM. Both YR-SDH5 and G-SDH5 were rapidly degraded by LONM but at different rates, with YR-SDH5 having a slightly shorter half-life (Bezawork-Geleta et al., 2014). A molecular explanation for this difference was not experimentally determined. It did however suggest that the N-termini of SDH5 influenced its recognition by LONM and therefore all the information required for LONM mediated degradation may reside within the N-terminal region of the protein.

## 3.2 Results

### 3.2.1 Determining the region(s) of SDH5 that are essential for LONM-mediated recognition

To investigate the specific degron mediating LONM-recognition and degradation of SDH5 in this study, the conditions facilitating the turnover of YR- and G-SDH5 by LONM were replicated. Initially, YR- and G-SDH5 were expressed individually in *E. coli* with an N-terminal $His_6$-Ubiquitin ($His_6$-Ub) tag for initial purification via IMAC (see Section 2.3.4) which was then cleaved using deubiquitinating enzyme Usp2cc to generate untagged, mature YR- or G-SDH5 (Section 2.3.5 and Appendix 3, Supplementary Figure 1B-C). The turnover of YR- or G-SDH5 was monitored in the presence of recombinant LONM in an *in vitro* degradation assay (Section 2.4.1 and Appendix 3, Supplementary Figure 1D). Similar to the results previously observed by Bezawork-Geleta et al. (2014), YR-SDH5 (t½ ~7 min) was degraded faster than G-SDH5 (t½ ~11 min) (Appendix 3, Supplementary Figure 1E).

As the N-terminus of SDH5 appears to influence LONM-mediated degradation, the requirement for an accessible (free) N-terminus on SDH5 for recognition by LONM was examined next. To test this, the turnover of the $His_6$-Ub-YR-SDH5 fusion protein (Figure 3.1B, upper construct) was monitored in an *in vitro* degradation assay in the presence of LONM (Figure 3.1C). Consistent with the involvement of the N-terminus in LONM-mediated recognition of SDH5, and the requirement of a free N-terminus in this recognition, $His_6$-Ub-YR-SDH5 was protected from turnover by LONM (Figure 3.1D, grey line).

Upon closer examination of the predicted secondary structure of SDH5 generated using Jpred 4 (Drozdetskiy et al., 2015), two random coil regions were identified at the N-terminus (Figure 3.1A, highlighted in blue). To examine if these regions contributed to LONM-mediated recognition of SDH5, N-terminal truncations of each random coil region were generated. The first deletion mutant started at D46 and lacked the first 11 residues of SDH5 (herein referred to as Δ11 SDH5) while the

second mutant started at T59 and lacked both random coil regions (herein referred to as Δ24 SDH5) (represented in Figure 3.1B, lower constructs). Similar to full-length SDH5, these proteins and all proteins mentioned hereafter were expressed with an N-terminal $His_6$-Ub tag, purified and cleaved as described in Section 2.3.4 and 2.3.5. Next, the stability of each protein was monitored in the presence of LONM (Figure 3.1C).

Consistent with previous findings, YR-SDH5 was rapidly degraded by LONM (t½ ~7 min) (Figure 3.1D, purple line). Consistent with a crucial role for the N-terminal random coil regions in mediating recognition by LONM, deletion of one or both regions resulted in a dramatic increase in the half-life of the protein (Figure 3.1D, blue and green lines). Surprisingly, the longer N-terminal truncation (Δ24-SDH5) was degraded more rapidly (t½ ~ 20 min) than the shorter truncation Δ11-SDH5 (t½ >30 min). One possibility is that there was a new recognition motif exposed or alternatively, the overall structure of Δ24 SDH5 was somewhat compromised. As a method to directly investigate the contribution of the N-terminal region of SDH5 to LONM mediated-degradation, the first 21 N-terminal residues of SDH5 ($SDH5_{21}$) were fused to *Mus musculus* dihydrofolate reductase (DHFR) (herein referred to as $SDH5_{21}$-DHFR, see Figure 3.2A)

DHFR is a stable, well-folded protein that lacks any intrinsic recognition motifs. It is commonly used to investigate the capacity of a protein sequence motif or structural element to act as a degron for recognition by AAA+ proteases (Gur et al., 2012; Koodathingal et al., 2009; Lee et al., 2001). Additionally, in the presence of methotrexate (MTX), the unfolding and turnover of DHFR can be inhibited, or substantially decreased, irrespective of the attached degron because its quaternary structure is highly stabilised in the presence of this folic acid analogue (Eilers & Schatz, 1986; Lee et al., 2001). Therefore, the turnover of $SDH5_{21}$-DHFR by LONM was monitored in the absence or presence of MTX to determine if this region of SDH5 was sufficient to mediate recognition and degradation of the fusion protein (Figure 3.2B).

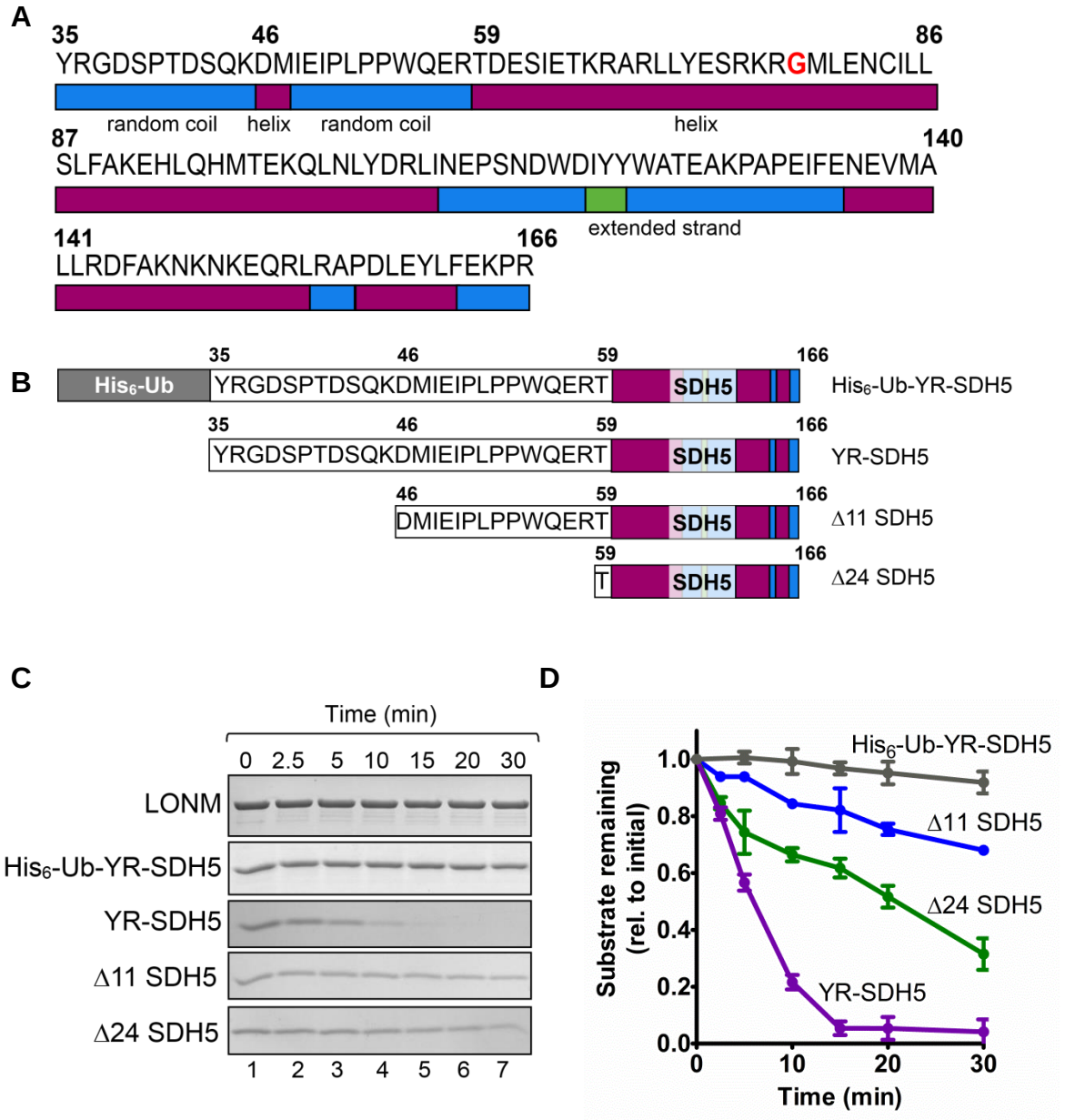


**Figure 3.1:** The N-terminus of SDH5 regulates LONM-mediated degradation *in vitro*. **A**, Results of the secondary structure prediction of mature YR-SDH5 generated using Jpred 4. The various secondary structure features are indicated in different colours. The location of clinical mutation of SDH5 (SDH5$^{G78R}$) is highlighted in red. **B**, Cartoon representation of the proteins used to investigate SDH5 stability with the N-terminus blocked or truncated. **C**, Representative Coomassie Brilliant Blue stained SDS-polyacrylamide gel strips of *in vitro* degradation assays using recombinant LONM (0.2 μM hexamer) and the various forms of SDH5 (1 μM) as indicated. **D**, The amount of wild-type SDH5 (purple line), His$_6$-Ub-YR-SDH5 (grey line), Δ11 SDH5 (blue line) and Δ24 SDH5 (green line) was quantitated via densitometry (n=3, error bars represent SEM).

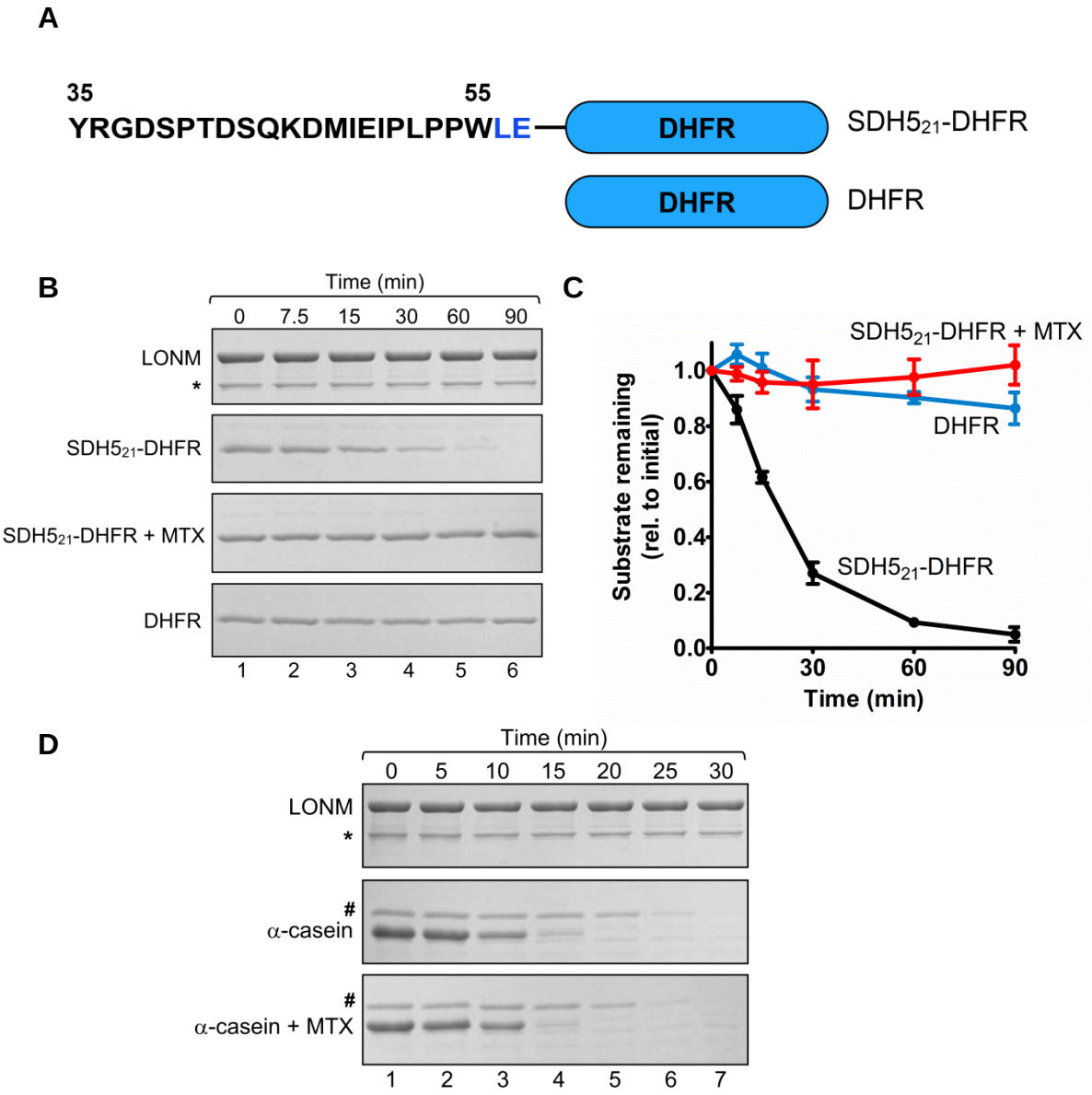


**Figure 3.2:** The N-terminus of SDH5 is sufficient to promote LONM-mediated recognition. **A**, Cartoon representation of the first 21 residues (35-55) of YR-SDH5 fused to mouse DHFR to generate SDH5$_{21}$-DHFR. Residues highlighted in blue are linker residues. **B**, Coomassie Brilliant Blue stained SDS-polyacrylamide gel strips of an *in vitro* degradation assay with LONM (0.2 μM hexamer), DHFR and SDH5$_{21}$-DHFR (1 μM each) in the absence or presence of 10 μM methotrexate (MTX) as indicated. **C**, The amount of DHFR (blue line) or SDH5$_{21}$-DHFR in the absence (black line) or presence (red line) of MTX (10 μM) was quantitated via densitometry (n=3, error bars represent SEM). **D**, Coomassie Brilliant Blue stained SDS-polyacrylamide gel strips showing the turnover of α-casein (α-S1) (3 μM) by LONM (0.2 μM hexamer) in the absence or presence of MTX as indicated. * indicates degradation product of LONM, # indicates second isoform of α-casein (α-S2).

As expected, native DHFR was completely resistant to LONM-mediated degradation validating its use as a reporter of degron-driven turnover (Figure 3.2B, lower panel and 3.2C, blue line). In comparison, $SDH5_{21}$-DHFR was completely degraded by LONM with a half-life of ~20 min (Figure 3.2C, black line). These data indicate that the N-terminus of SDH5 is sufficient for LONM recognition and degradation. To exclude the possibility that the N-terminal fusion irreversibly destabilised the overall structure of DHFR, the degradation was also monitored in the presence of MTX (Figure 3.2B). As expected, the turnover of $SDH5_{21}$-DHFR was completely inhibited by the addition of MTX (Figure 3.2C, red line). As an additional control, the turnover of α-casein was monitored in the presence of MTX to ensure that MTX had no adverse effects on LONM. Consistently, the activity of LONM was not affected by the presence of MTX (Figure 3.2D, compare middle and lower panel).

### 3.2.2 Determining key residues for LONM recognition

Next, to identify the motif (within this region) responsible for LONM recognition, a series of mutations were generated within the 21 amino acid sequence (attached to DHFR) in which four consecutive residues were replaced with alanine (see Figure 3.3A, also refer to Appendix 1, Table 2). As it has been demonstrated that the length of the degron or initiating region from the N-terminus is an important factor influencing recognition by AAA+ proteases (Gur & Sauer, 2008; Inobe et al., 2011; von Janowsky et al., 2005), the length of the SDH5 sequence was kept constant as opposed to generating truncations. Next, the turnover of each $SDH5_{21}$-DHFR alanine replacement mutant ($SDH5_{21}^{PTDS}$-DHFR, $SDH5_{21}^{QKDM}$-DHFR, $SDH5_{21}^{IEIP}$-DHFR and $SDH5_{21}^{LPPW}$-DHFR,) was monitored over time in the presence of LONM (Figure 3.3B). Interestingly, with the exception of $SDH5_{21}^{LPPW}$-DHFR (Figure 3.3C, green line), all fusion proteins were degraded with a similar half-life (t½ ~20 min) (Figure 3.3C, compare orange, grey and pink lines). These data suggest

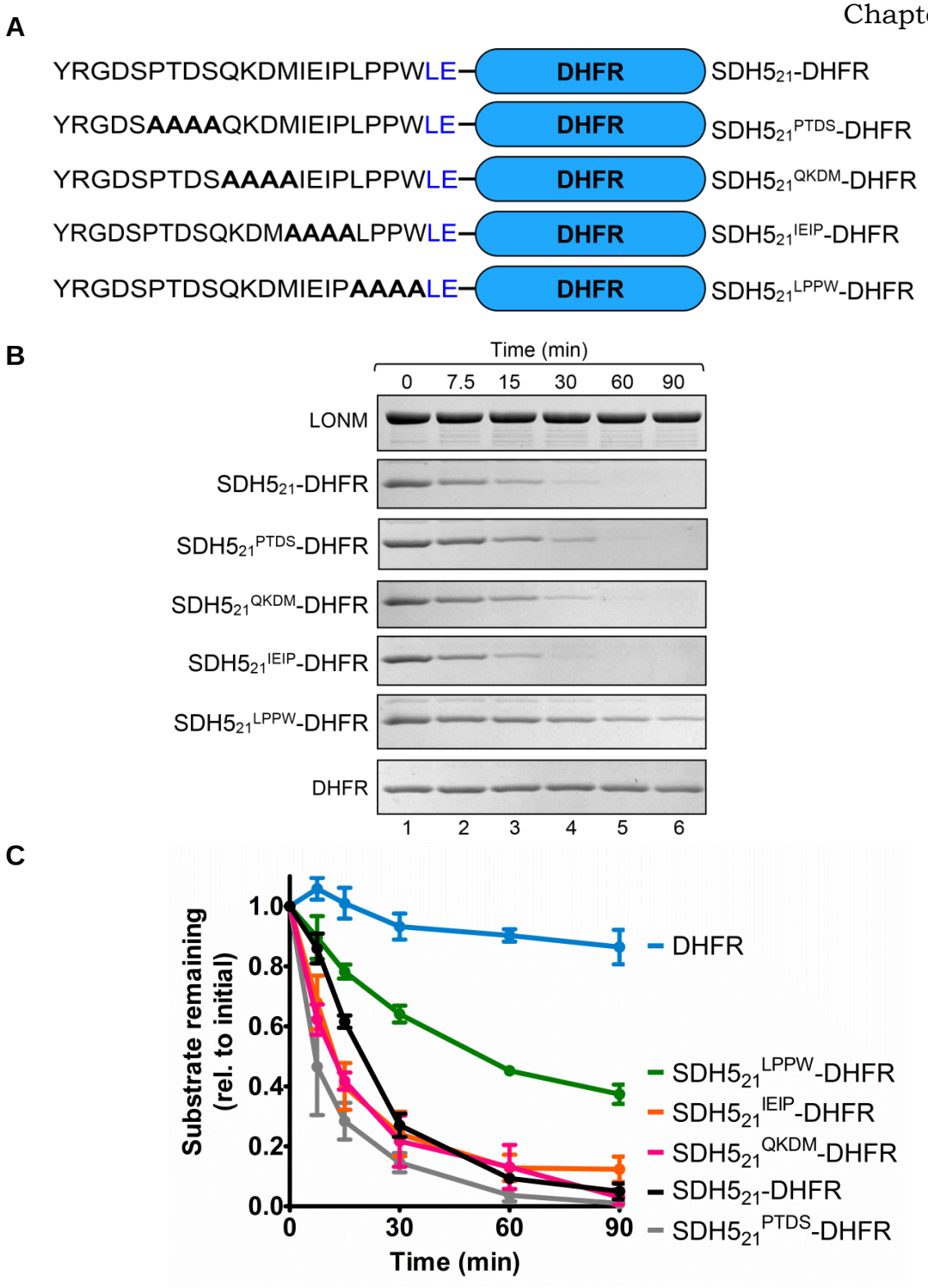


**Figure 3.3:** Identifying the residues within the N-terminus of SDH5 responsible for LONM-mediated recognition. **A**, Cartoon representation of SDH5$_{21}$-DHFR fusion mutants generated to investigate the critical residues influencing LONM-mediated recognition. The location of the alanine replacement mutations in each variant are indicated in bold. **B**, Coomassie Brilliant Blue stained SDS-polyacrylamide gel strips representing a typical *in vitro* degradation assay using LONM (0.2 μM hexamer) and each SDH5$_{21}$-DHFR fusion protein (1 μM) as indicated. **C**, The amount of DHFR (blue line), wild-type SDH5$_{21}$-DHFR (black line), SDH5$_{21}^{PTDS}$-DHFR (grey line), SDH5$_{21}^{QKDM}$-DHFR (pink line), SDH5$_{21}^{IEIP}$-DHFR (orange line) and SDH5$_{21}^{LPPW}$-DHFR (green line) was quantitated via densitometry (n=3, error bars represent SEM).

that the 'LPPW' motif plays an important role in LONM-mediated recognition.

Next, to validate these findings, and to account for any effects relating to the DHFR linker region (highlighted in blue, Figure 3.3A), the same alanine replacement mutations were generated in full-length SDH5 (both YR- and G- forms) (depicted in Figure 3.4A and D). The relative purity of these proteins was assessed after separation by SDS-PAGE and staining with Coomassie Brilliant Blue (See Appendix 3, Supplementary Figure 2A). Surprisingly, the mobility of some alanine replacement mutants (for both YR- and G-SDH5) following SDS-PAGE was altered in comparison to their wild-type (WT) counterparts (e.g. Appendix 3, Supplementary Figure 2A, compare lanes 1 and 5).

The stability of each YR-SDH5-derived (YR-SDH5$^{PTDS}$, YR-SDH5$^{QKDM}$, YR-SDH5$^{IEIP}$ and YR-SDH5$^{LPPW}$) and G-SDH5-derived (G-SDH5$^{QKDM}$, G-SDH5$^{IEIP}$ and G-SDH5$^{LPPW}$) alanine replacement mutant was monitored in the presence of LONM in a series of *in vitro* degradation assays (Figure 3.4B, and E, respectively). Due to technical difficulties, G-SDH5$^{PTDS}$ was not included in this analysis. Similar to previous (Figure 3.1D), the half-life of YR-SDH5 was ~7 min (Figure 3.4C, purple line). YR-SDH5$^{IEIP}$ and YR-SDH5$^{LPPW}$ only generated a modest increase in SDH5 stability (Figure 3.4C, orange and green lines, respectively), while YR-SDH5$^{PTDS}$, decreased the half-life of SDH5 to ~5 min (Figure 3.4C, grey line). In contrast, a stabilising effect was observed for all G-SDH5 mutants (Figure 3.4F). Interestingly, consistent with the data obtained for the SDH5$_{21}$-DHFR fusion proteins (Figure 3.3C), mutation of the LPPW motif resulted in the greatest stability of both YR-SDH5 (YR-SDH5$^{LPPW}$, t½ ~12 min) and G-SDH5 (G-SDH5$^{LPPW}$, t½ >30 min), (Figure 3.4C and F, green line).

Collectively, these data indicate that both the N-terminus and the LPPW motif influence LONM-mediated recognition of SDH5. Recognition of more than one site is similar to substrate recognition by the 26S proteasome wherein the ubiquitin tag and an unstructured region on a

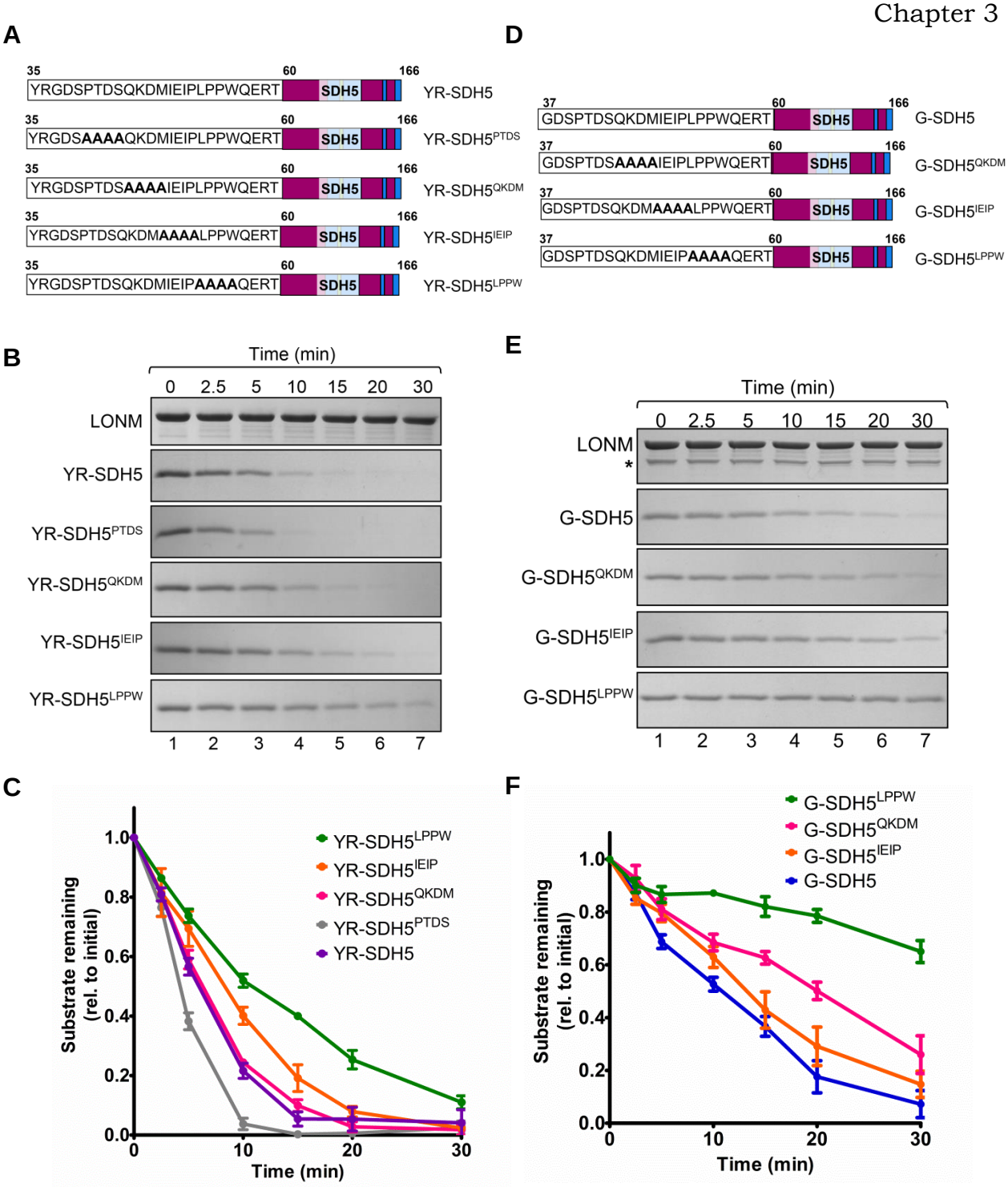


**Figure 3.4:** LONM-mediated recognition of SDH5 is regulated by two sites within the N-terminus. **A** and **D**, Cartoon representation of the alanine replacement mutations introduced into full-length YR- and G-SDH5, respectively, to determine the regions that are essential for LONM-mediated recognition. The location of the alanine replacement mutations in each variant are indicated in bold. **B** and **E**, Coomassie Brilliant Blue stained SDS-polyacrylamide gel strips representing *in vitro* degradation assays using LONM (0.2 μM hexamer) and YR-SDH5 or G-SDH5 mutant variants respectively, (1 μM each), as indicated. **C** and **F**, The amount of each YR-SDH5 and G-SDH5 mutant variant, respectively, was quantitated via densitometry (n=3, error bars represent SEM), the colour scheme for each mutation are similar to Figure 3.3C with the addition of wild-type YR-SDH5 (purple line) and wild-type G-SDH5 (royal blue line). * indicates degradation product of LONM

substrate is necessary for binding and enhancing degradation (Prakash et al., 2004). In this regard, the residues LPPW and others within that region may represent a potential binding site for LONM.

### 3.2.3 Examining turnover of clinically-relevant SDH5 mutant (SDH5$^{G78R}$)

The stability of SDH5$^{G78R}$ was next examined to establish whether inhibiting the turnover of this mutant protein could potentially improve complex formation with SDHA. As the replacement of the LPPW motif conferred the greatest stability to SDH5, only this particular mutation was introduced into SDH5$^{G78R}$ but as the precise N-terminus of SDH5 is still undetermined, the stability of both YR- and G-SDH5$^{G78R}$ forms were examined. The LPPW>AAAA mutation was generated in both forms of the pathogenic mutant, herein referred to as YR-SDH5$^{G78R\text{-}LPPW}$ and G-SDH5$^{G78R\text{-}LPPW}$ (outlined in Figure 3.5A), and turnover was monitored in the presence of LONM (Figure 3.5B and D). Consistent with previous findings, SDH5$^{G78R}$ was less stable than SDH5 (Bezawork-Geleta et al., 2014) with both forms of YR- and G-SDH5$^{G78R}$ being degraded faster than their wild-type equivalents (Figure 3.5C and E, compare dashed lines to solid lines).

Specifically, YR-SDH5$^{G78R}$ was less stable than YR-SDH5 with half-life of ~4 min compared to ~7 min (Figure 3.5C, compare dashed line to solid line). Replacement of LPPW with AAAA in YR-SDH5$^{G78R}$ negated this minor destabilising effect returning the half-life to ~7 min (Figure 3.5C, dotted line). A similar pattern was observed for G-SDH5$^{G78R}$ when introducing the LPPW>AAAA mutation in this background except that the stabilising effect was much more profound shifting the half-life from ~8 min to greater than 30 min (Figure 3.5E, compare dashed line to dotted line).

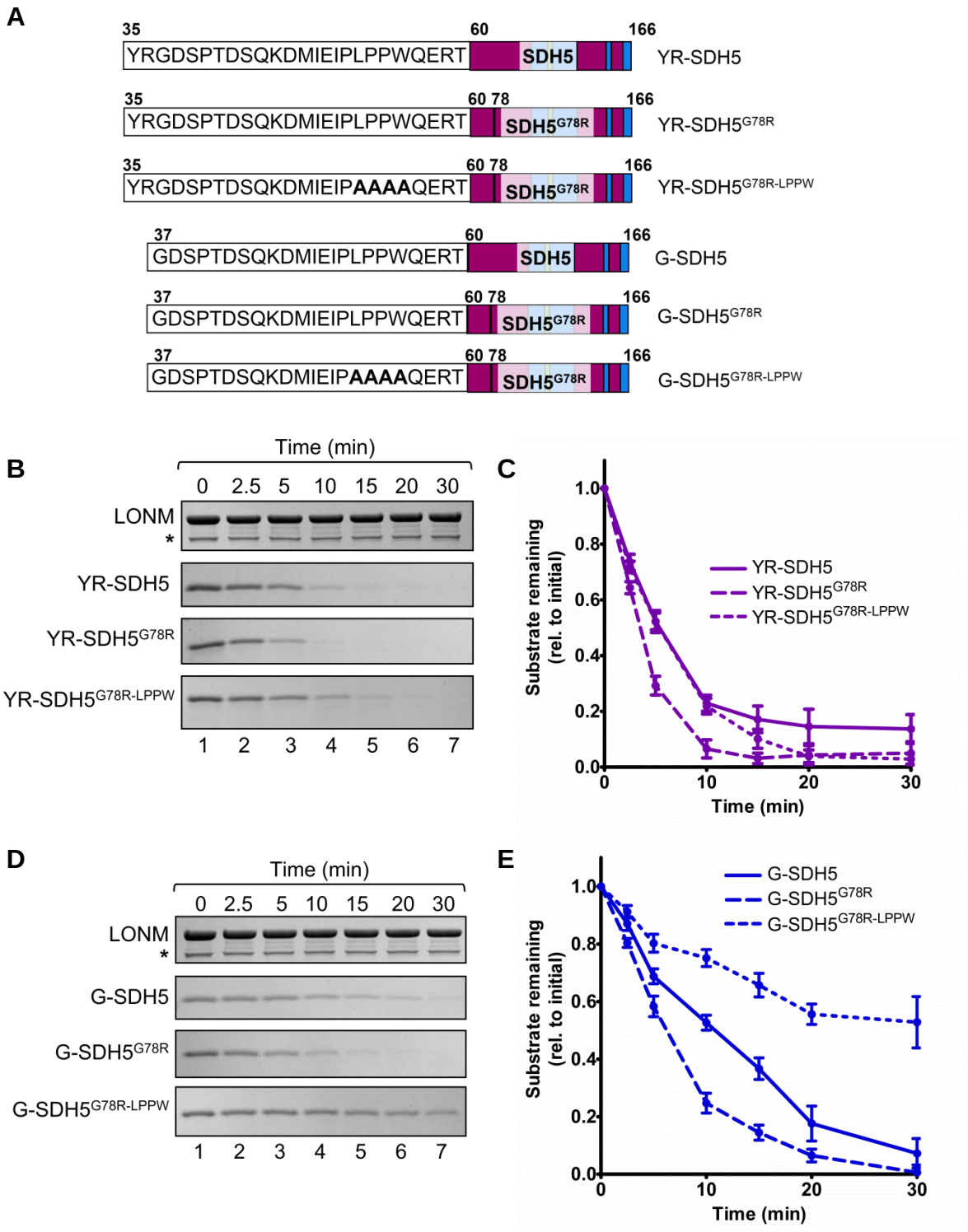


**Figure 3.5:** Removal of LPPW motif stabilises SDH5$^{G78R}$ *in vitro*. **A**, Cartoon representation of the proteins used in this study to monitor stability of SDH5$^{G78R}$ and SDH5$^{G78R\text{-}LPPW}$. **B** and **D**, Coomassie Brilliant Blue stained SDS-polyacrylamide gel strips representing *in vitro* degradation assays using LONM (0.2 μM hexamer) and YR- or G-SDH5 variants, respectively, (1 μM), as indicated. **C** and **E**, The amount of wild-type SDH5 (solid line), SDH5$^{G78R}$ (dashed line) and SDH5$^{G78R\text{-}LPPW}$ (dotted line) derived from YR-SDH5 (purple) or G-SDH5 (blue), respectively, was quantitated via densitometry (n=3, error bars represent SEM). * indicates degradation product of LONM

These data reinforces the model that the pathological mutation G78R does not create a new degron in SDH5, rather the degradation signal, intrinsic to the protein, drives LONM-mediated recognition and turnover. Removal of these intrinsic signals appears to be the key to stabilising SDH5 *in vitro*. However, how such changes affect the stability of the protein *in vivo* and how it partitions between its functional partner SDHA and the terminal pathway of LONM-mediated degradation remain unknown. To address this, the stability of degron-manipulated SDH5$^{G78R}$ was investigated *in organello*.

To do so, radiolabelled preSDH5, preSDH5$^{G78R}$ and preSDH5$^{G78R\text{-}LPPW}$ was first generated using a coupled transcription and translation (TNT) reticulate lysate system supplemented with $^{35}$S-Met/Cys (Section 2.4.11) and template cDNA coding for each SDH5 precursor protein variant (Appendix 1, Table 2). Initially, the conditions for mitochondrial import were established in mitochondria isolated from HepG2 cells (Section 2.4.12). Following the addition of radiolabelled preSDH5, preSDH5$^{G78R}$ or preSDH5$^{G78R\text{-}LPPW}$ to HepG2 mitochondria, the import of each was stopped by the addition of valinomycin. Mitochondrial lysate was then separated by SDS-PAGE and visualised by autoradiography (Figure 3.6A).

Consistent with successful import and cleavage of the presequence, a smaller (~16 kDa) radiolabelled species of SDH5 appeared after 20 min that represents the mature form of SDH5 (m-SDH5) (Figure 3.6A, lane 1). This import and processing was dependent on membrane potential ($\Delta\psi$) as the ~16 kDa radiolabelled band was not observed in depolarised mitochondria (Figure 3.6A, lane 2). Similar to wild-type, preSDH5$^{G78R}$ and preSDH5$^{G78R\text{-}LPPW}$ were also successfully imported and processed to their mature forms in a membrane-dependent manner (Figure 3.6A, lanes 3 and 5 respectively). Consistent with previous reports, the migration of m-SDH5$^{G78R}$ was retarded slightly compared to wild-type m-SDH5, most likely due to an increase in the overall charge of the protein (Bezawork-Geleta et al., 2014). Similarly, the LPPW mutation resulted in further retardation of the protein (Figure 3.6, compare lane 5 to lane 3),

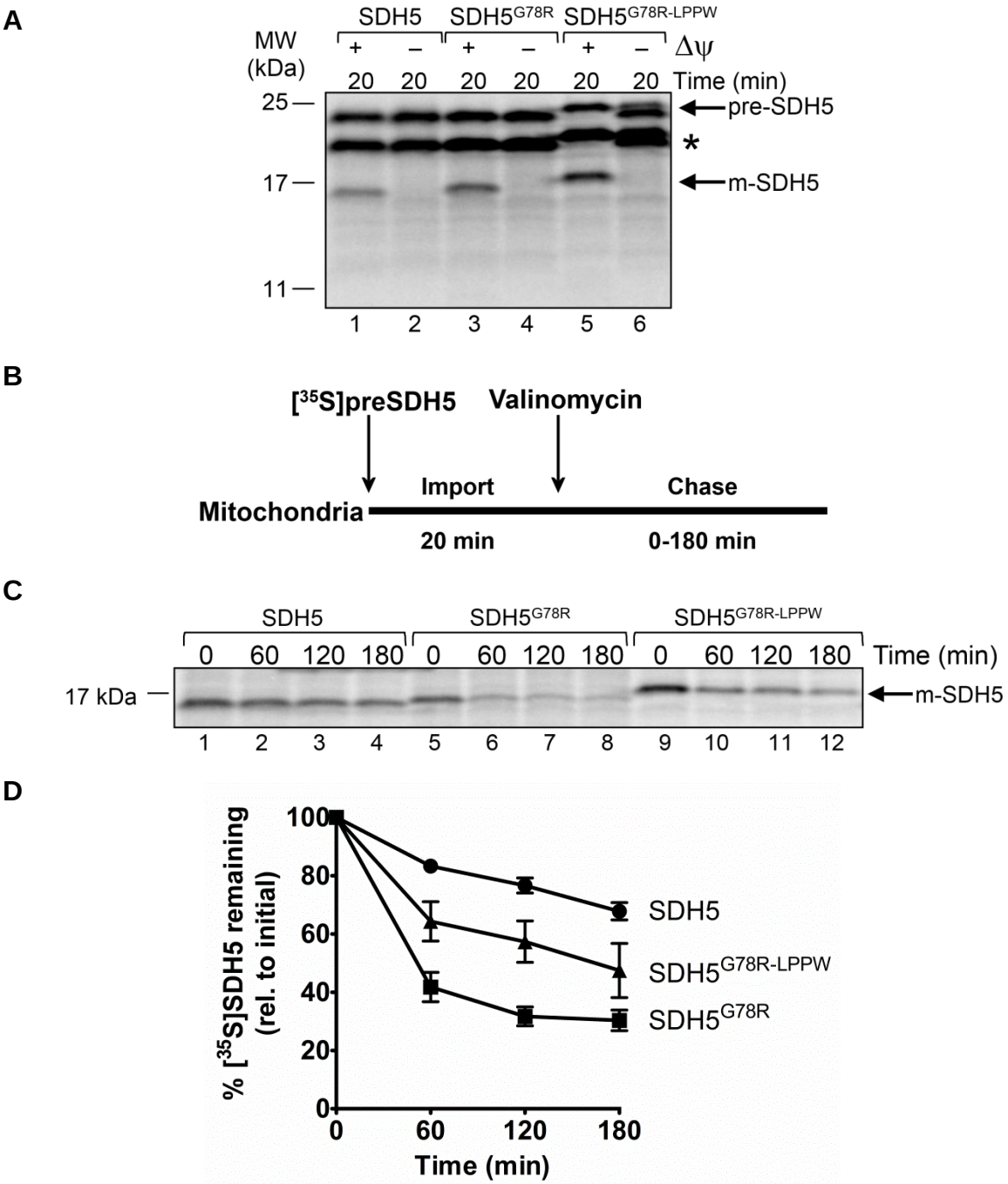


**Figure 3.6:** LPPW>AAAA mutation increases the stability of SDH5$^{G78R}$ *in organello*. **A**, Autoradiography image of the import of wild-type preSDH5 (lanes 1-2), preSDH5$^{G78R}$ (lanes 3-4) and preSDH5$^{G78R\text{-}LPPW}$ (lanes 5-6) into isolated HepG2 mitochondria, monitored in the absence or presence of membrane potential (Δψ) after separation by SDS-PAGE. Mature SDH5 (m-SDH5) migrates at ~16 kDa. *possible internal translation site. **B**, Outline of the experimental procedure employed to monitor stability of m-SDH5 *in organello*. **C**, The stability of radiolabelled wild-type m-SDH5 (lanes 1-4), m-SDH5$^{G78R}$ (lanes 5-8) and m-SDH5$^{G78R\text{-}LPPW}$ (lanes 9-12) in isolated HepG2 mitochondria was monitored over 3 h in an import-chase assay. Protein samples containing mitochondrial lysate were separated by SDS-PAGE and visualised by autoradiography. **D**, The radioactive signal from wild-type m-SDH5 (black circles), m-SDH5$^{G78R}$ (black squares) or SDH5$^{G78R\text{-}LPPW}$ (black triangles) was quantitated via densitometry (n=3, error bars represent SEM).

which is consistent with the same mutation in recombinant SDH5$^{G78R}$ (Appendix 3, Supplementary Figure 2B, compare lane 3 with 4 and lane 5 with 6).

To examine the metabolic stability of m-SDH5 *in organello*, an import-chase assay was performed (outlined in Figure 3.6B). After import (20 min), the level of each radiolabelled m-SDH5 (wild-type and mutants) was monitored over 3 h (Figure 3.6C). Under the conditions examined, m-SDH5 was relatively stable with ~ 70% of the protein still remaining after 3 h (Figure 3.6D, black circles) whereas in comparison, m-SDH5$^{G78R}$ was unstable with a half-life of ~50 min (Figure 3.6D, black squares). Interestingly, mutation of LPPW to AAAA within the pathogenic mutant resulted in a significant change to the *in vitro* half-life of the protein SDH5$^{G78R}$ (t½ ~180 min) (Figure 3.6D, black triangles). These data further support a role for this region (LPPW) in mediating LONM recognition of SDH5 under physiologically relevant conditions.

Finally, to determine if preventing turnover of SDH5$^{G78R}$ through mutation of the LONM degron could stabilise the SDHA-SDH5 complex, another import-chase assay was performed (as above) and complex formation was monitored following separation of the DDM-solubilised mitochondrial lysate by BN-PAGE (outlined in Figure 3.7A). In this case, different amounts of radiolabelled lysate were applied in an attempt to start the import-chase reaction with the same levels of radiolabelled SDH5 (Figure 3.7B). Consistent with published results, a 90 kDa complex of SDHA-SDH5 was observed on BN-PAGE for wild-type and mutant SDH5 (Bezawork-Geleta et al., 2014; Hao et al., 2009) (Figure 3.7B). Also consistent with previous data, m-SDH5$^{G78R}$ disassociated rapidly from the SDHA-SDH5 complex (Figure 3.7B, lanes 5-8 and C, black squares). However, despite observing increased stability of m-SDH5$^{G78R\text{-}LPPW}$ compared to m-SDH5$^{G78R}$ (Figure 3.6D), the complex that formed with SDHA was unstable and appeared to dissociate much more rapidly than m-SDH5$^{G78R}$ (Figure 3.7B, lanes 9-12 and C, black triangles). This indicated that residues LPPW in SDH5 may be pivotal for its interaction with SDHA.

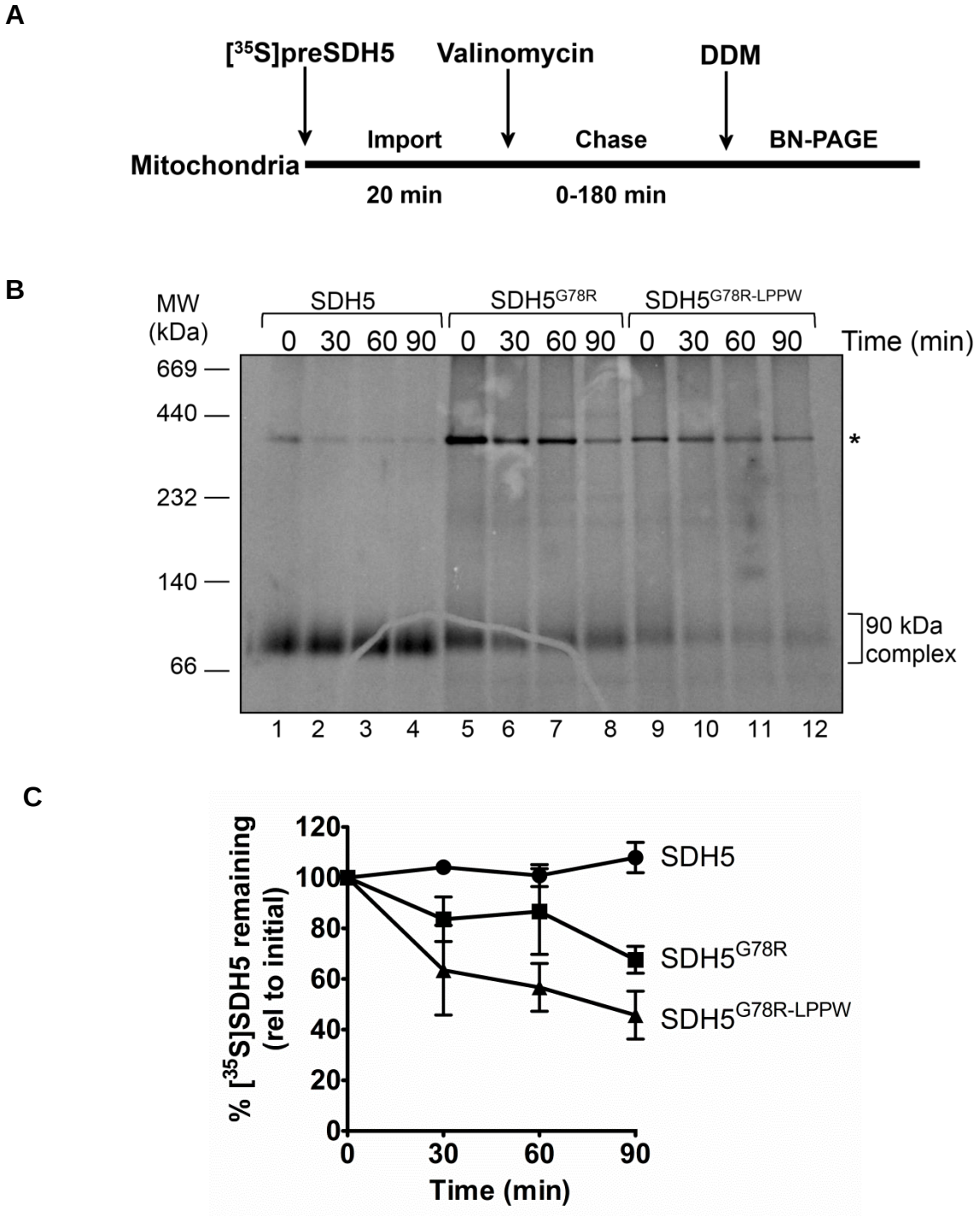


**Figure 3.7:** LPPW>AAAA mutation destabilises the SDHA-SDH5$^{G78R}$ complex *in organello*. **A**, Outline of experimental procedure to analyse SDHA-SDH5 complex formation under native conditions. **B**, Autoradiography image of a BN-polyacrylamide gel demonstrating complex formation between SDHA and radiolabelled wild-type SDH5 (lanes 1-4), SDH5$^{G78R}$ (lanes 5-8) and SDH5$^{G78R-LPPW}$ (lanes 9-12) after import. **C**, The radioactive signal of wild-type SDH5 (black circles), SDH5$^{G78R}$ (black squares) or SDH5$^{G78R-LPPW}$ (black triangles) in complex with SDHA (~90 kDa) was quantitated via densitometry (n=3, error bars represent SEM).

## 3.3 Discussion

To prevent the detrimental and pervasive degradation of proteins, AAA+ proteases must recognise substrates via particular sequential or structural motifs that are only exposed under specific conditions, (e.g. heat-shock) (Gur et al., 2013). These elements are known as degradation signals or 'degrons' and together with the conformation of the protein, determine the protein's metabolic stability. Similarly, the substrate specificity of a protease is determined by the repertoire of degrons that it recognises as well as its unfolding strength (Koodathingal et al., 2009). In regards to LONM, the substrates identified thus far include unfolded and oxidatively damaged proteins as well as functional, folded substrates, indicating that LONM is able of recognising a broad range of degrons (Bezawork-Geleta et al., 2014; Bota & Davies, 2002; Granot et al., 2007a; Ondrovičová et al., 2005; Tian et al., 2011). While unfolded or damaged proteins are recognised via the exposure of hydrophobic residues that would normally be buried within the protein structure (Gur & Sauer, 2008), folded proteins must contain specific degrons that facilitate selective recognition by LONM. So far, only a handful of native, folded substrates of LONM have been identified and the recognition motifs that regulate their degradation have not been determined. This chapter has established the primary regulatory elements for LONM-mediated recognition of SDH5 and revealed crucial residues that promote degradation of this native substrate.

In this study, in order to dissect the sequence elements required for LONM-mediated recognition, the degradation of several protein constructs of SDH5 (fusions and mutants) was examined. Initial experiments revealed that fusion of $His_6$-Ub to the N-terminus of SDH5 inhibited its degradation suggesting that exposure of the N-terminus, or access to the N-terminal region of SDH5 was a crucial element in LONM-mediated recognition (Figure 3.1D). It could be argued however, the $His_6$-Ub moiety was unable to be unfolded and degraded by LONM due to its stable conformation, but the unrestricted LONM-mediated turnover of a separate $His_6$-Ub-tagged substrate has been observed (see Chapter 4),

which indicates the stability of $His_6$-Ub-YR-SDH5 specifically relates to a lack of recognition. Consistent, with an important role for a free N-terminus, it was previously shown that YR-SDH5 was degraded more rapidly by LONM than G-SDH5 (Bezawork-Geleta et al., 2014). Interestingly, the accelerated degradation of YR-SDH5 is reminiscent of an N-terminal degradation pathway, known as the N-end rule (Varshavsky, 2011) in which N-terminal residues such as Tyr are responsible for the metabolic instability of a protein. Despite this intriguing similarity to the N-end rule pathway, a classic form of this pathway does not exist in mitochondria. Nevertheless, these data did suggest that the N-terminus of SDH5 played an important role in regulating LONM-mediated recognition.

To investigate this possibility further, the LONM-mediated degradation of two N-terminal truncations of SDH5 was examined. While both truncations stabilised SDH5 substantially, the longer truncation (Δ24 SDH5) also exhibited a small destabilising effect on the protein (relative to the shorter construct, Δ11 SDH5). This artificial construct (Δ24 SDH5) is likely to have exposed a downstream “non-physiological” degron or destabilised the structure of the protein, making interpretation of these results difficult. Therefore, as an alternative approach to identify the region or motif within the N-terminal region of SDH5 responsible for mediating degradation by LONM, the first 21 residues of YR-SDH5 were fused to the stable reporter protein DHFR. Consistent with a critical role for the first 21 residues of SDH5 in promoting recognition by LONM, the fusion protein was rapidly degraded by LONM (Figure 3.2C), while untagged DHFR was not. This indicated that all the information required for LONM recognition and degradation was contained within this part of the protein. This construct ($SDH5_{21}$-DHFR) was used as a reporter to further probe the elements within SDH5 required for LONM degradation. Alanine replacements (in blocks of 4 contiguous residues) across the length of the SDH5 N-terminal region revealed the last 4 residues of the N-terminal tag (LPPW) played a key role in recognition by LONM. However, replacement of this motif with alanine residues did not abolish

degradation suggesting that alanine residues (in this position) may support weak recognition by LONM. Further interrogation of this region, i.e. substituting LPPW residues with polar or charged residues, would verify if the hydrophobic nature of the LPPW motif is critical for LONM-mediated recognition. Alternatively, this patch may simply be involved in modulating the interaction with LONM while the N-terminal residues (YR) drive primary recognition by LONM. Consistent with this idea, mutation of the LPPW motif in G-SDH5 almost completely abolished degradation by LONM (t½ >30 min). This bipartite recognition of the substrate is comparable to the recognition of cytosolic substrates by the proteasome, wherein substrates are recognised by the ubiquitin tag and an unstructured initiation site (Prakash et al., 2004). It is possible that the proline-rich nature of this sequence (LPPW) contributes to recognition LONM, likewise the hydrophobicity of this region is also a likely to be the contributing factor for recognition by human LONM as it has been demonstrated for ecLon (Gur & Sauer, 2008; Gur & Sauer, 2009). In summary, the *in vitro* half-life of SDH5 is influenced by the exposed N-terminus, the identity of the N-terminal residue and by the hydrophobic patch approximately 10-15 residues downstream of the N-terminus. In this regard it would be highly interestingly to establish the physiologically relevant N-terminus of SDH5 (Y- or G-) but it has yet to be identified in N-terminome studies of mitochondrial proteins (Vaca Jacome et al., 2015).

The metabolic stability of SDH5 *in vivo* is largely determined by its interaction with SDHA (Bezawork-Geleta et al., 2014; Hao et al., 2009). In terms of the disease-causing mutant of SDH5 ($SDH5^{G78R}$), this protein was more susceptible to LONM-mediated degradation as a result of decreased complex formation with SDHA (Bezawork-Geleta et al., 2014). We sought to determine if a reduction in LONM-mediated recognition of $SDH5^{G78R}$ would confer an increase in metabolic stability. Similar to wild-type SDH5, the N-terminal residue significantly influenced the half-life of $SDH5^{G78R}$ (Figure 3.5). Introducing the LPPW>AAAA mutation into YR-$SDH5^{G78R}$ only conferred a modest increase in the half-life (Figure

3.5C) but for G-SDH5$^{G78R}$, t½ increased from 6 min to >30 min (Figure 3.5E). Additionally, under native conditions, the turnover of radiolabelled SDH5$^{G78R}$ (t½ = 50 min) was significantly reduced (t½ = 180 min) by mutation of the LPPW motif (Figure 3.6D), illustrating that modification of this motif could increase the metabolic stability of the substrate *in organello*. Unfortunately, an increase in stability of the complex with SDHA was not observed (Figure 3.7C), instead the SDHA-SDH5 complex was destabilised by mutation of the LPPW motif which suggests these residues form part of binding interface between SDHA and SDH5 or the mutation has altered the structure of SDH5 and no longer permits the interaction with SDHA. Further investigation of the SDHA-SDH5 complex, in particular determining the X-ray crystal structure, would provide valuable insight into the residues at the binding interface. Also defining the mechanism involved in SDHA flavinylation would be essential to ensure modulation of the LONM degron does not directly impact SDH5 activity or association with other proteins.

Collectively these data clearly demonstrate the N-terminus of SDH5 contains a bipartite degron that promotes turnover by LONM. However, despite removal of these elements from SDH5 (e.g. G-SDH5$^{LPPW}$), LONM-mediated degradation was not abolished. In future experiments, it will be important to establish if the N-terminal residues (GDS) also contribute to recognition by LONM as part of a longer motif (YRGDS). Alternatively the globular domain of SDH5 may expose further degrons if it samples a partially unfolded state due to structural plasticity ("breathing") under normal conditions or following stress. Proteins comprising multiple degrons would ensure their complete and efficient degradation is achieved by single or multiple proteases (Gur et al., 2012; Patterson-Ward et al., 2009). In the case of SDH5, the presence of other recognition motifs would enable LONM to recognise and re-engage with fragments of SDH5 if either the unfolding or translocation steps were inefficient. This would ensure that SDH5 function was completely abolished and prevent proteotoxic stress generated by the accumulation of protein fragments.

This study has demonstrated that modulation of the LONM degron can increase the half-life and metabolic stability of folded substrates, including a disease-causing pathological mutant of SDH5. Targeting the degron for LONM or other proteases may have practical uses for other diseases caused by impaired proteostasis or deleterious mutations in particular proteins. For instance, Friedreich's Ataxia (FRDA) is caused by homozygous GAA triplet expansions or compound heterozygous GAA triplet expansions and point mutations within the gene encoding frataxin (*FXN*), resulting in a loss of protein expression or function (Campuzano et al., 1997; Campuzano et al., 1996). Frataxin is a mitochondrial protein associated with the assembly of iron-sulphur clusters, iron homeostasis and heme biosynthesis (Stehling et al., 2004) and a loss of function leads to progressive ataxia, cardiomyopathy and diabetes mellitus (Galea et al., 2016). Analysis of frataxin mutants (caused by point mutations) identified a decrease in steady state levels of mutant frataxin in patient samples and also after import into isolated mitochondria (Campuzano et al., 1997; Cavadini et al., 2000). Interestingly, biochemical characterisation of frataxin mutants (caused by point mutations) *in vitro* revealed only a partial decrease of protein stability and capacity to bind iron under physiological conditions in comparison to wild-type frataxin (Correia et al., 2006; Correia et al., 2008). It was speculated that the associated loss of protein function in FRDA patients carrying these frataxin mutants may be due to protein aggregation or increased turnover of frataxin *in vivo* (Correia et al., 2006; Cossée et al., 1999; Galea et al., 2016). Interestingly, in a FRDA cardiac mouse model, the expression levels of LONM and CLPP were specifically increased in the affected tissues, however the contribution of these proteins to mitochondrial function or disease progression has yet to be examined (Guillon et al., 2009).

The manipulation of residues within a protein (i.e. protein engineering) requires the delicate balance between improving one function while simultaneously not causing adverse changes to another part of the protein (Page et al., 2003). Nonetheless, enhanced substrate specificity

and functionality have been observed in the directed evolution of molecular chaperones (e.g. GroEL/S and DnaK), indicating that significant practical advancements can be made without detrimental consequences (Aponte et al., 2010; Wang et al., 2002). Manipulation of the protein folding environment through the use of 'chemical chaperones' has also been used to increase the metabolic stability of particular proteins associated with diabetes, colitis and other diseases (Cao et al., 2013; Fan et al., 1999; Özcan et al., 2006; Porto et al., 2009). Thus, decreasing the susceptibility of certain mitochondrial proteins to degradation could also provide therapeutic options for diseases associated with acquired protein instability and increased turnover. Alternatively, preventing the recognition of proteins by proteases such as LONM, through the direct manipulation of a degron may prevent the premature degradation of a protein recognised via this molecular mechanism.

To improve our understanding of substrate recognition by LONM is vital to establish not only the location of the degron but also the key residues required for this interaction. Therefore, characterisation of the other known substrates of LONM would be useful to determine the regions involved in promoting LONM-mediated recognition and potentially reveal new degrons or binding sites.

# Chapter 4: Investigating molecular determinants for the degradation of steroidogenic acute regulatory protein (StAR).

## 4.1 Introduction

LONM is the key AAA+ protease involved in the quality control of mitochondrial matrix proteins. In addition to its role in the turnover of misfolded matrix proteins, LONM has also been found to degrade folded proteins which are involved in numerous metabolic pathways (Venkatesh et al., 2012). One such example is the regulated turnover of steroidogenic acute regulatory (StAR or STARD1) protein. Following steroidogenesis, StAR is imported into the mitochondrion and the native protein is degraded in the matrix by LONM (Granot et al., 2007a). In order to ensure that StAR is rapidly degraded by LONM, it is believed that StAR contains a strong recognition motif (Granot et al., 2002) however the identity and location of this motif has yet to be determined.

StAR is upregulated in response to trophic hormone stimulus and promotes the rapid production of steroids (Clark et al., 1994). StAR is expressed in 'classical' steroidogenic cells such as adrenal glands and reproductive organs but is also present in 'non-classical' tissues such as the brain, kidney and liver (a complete list can be found in a recent review by Anuka et al. (2013)). Although the exact mechanism of action of StAR remains elusive, extensive research has determined that StAR (via its mitochondrial targeting sequence) is directed to the mitochondrial outer membrane (OM) where it interacts with various proteins i.e. Peripheral benzodiazepine receptor/mitochondrial transporter protein (PBR/TSPO) and voltage-dependent anion channel (VDAC), which together promote the transport of cholesterol from the cytosol to the inner mitochondrial membrane (IM) (Besman et al., 1989; Bose et al., 2002; Liu et al., 2006; Papadopoulos et al., 2006; Prasad et al., 2015). Cholesterol is then converted to pregnenolone by cytochrome P450scc (CYP11A1), which is located at the IM. Pregnenolone is used to synthesise hormone steroids in mitochondria or smooth endoplasmic reticulum (Motohashi et al., 2016; Privalle et al., 1983). The rate-limiting step in this reaction is the StAR-mediated transport of cholesterol from the OM to the IM (Petrescu et al., 2001).

Similar to other STAR-related lipid transfer (START) domain proteins, human StAR contains a typical 'helix-grip' fold (Thorsell et al., 2011). This fold is composed of anti-parallel β-sheets flanked by an N- and C-terminal α-helix (Figure 4.1) (Tsujishita & Hurley, 2000). A U-shaped cavity is formed by the β-sheets to facilitate the binding of a ligand, which in the case of StAR, is a single molecule of cholesterol (Tsujishita & Hurley, 2000). This sterol binding pocket (SBP) of StAR is predominantly hydrophobic in nature and inherited mutations within this protein are also often associated with congenital lipoid adrenal hyperplasia (CAH) or other diseases related to impaired cholesterol transport (Bose et al., 1998; Strauss III et al., 2003; Tsujishita & Hurley, 2000).

A single molecule of newly synthesised StAR is predicted to bind 400 molecules of cholesterol per minute which indicates that StAR must be able to bind cholesterol rapidly and reversibly (Artemenko et al., 2001). Currently the mode of cholesterol binding and release by StAR is controversial as a conformational change within the structure of StAR is required to facilitate access of a cholesterol molecule (Tsujishita & Hurley, 2000). Some groups have proposed that StAR exists as a molten globule with minimal tertiary structure prior to cholesterol binding (Baker et al., 2005; Bose et al., 1999; Christensen et al., 2001; Song et al., 2001) while other groups suggest that only the C-terminal α-helix or the Ω1 loop (Figure 4.1) moves or unfolds to 'gate' entry of cholesterol to the SBP (Mathieu et al., 2002; Murcia et al., 2006; Roostaee et al., 2008).

In the absence of hormone stimulus, StAR expression is arrested and all remaining StAR is either degraded at the mitochondrial OM by the 26S proteasome or imported into the mitochondrial matrix where it is degraded by resident proteases (Clark et al., 1994; Granot et al., 2007b; Granot et al., 2002; Stocco & Sodeman, 1991). Once imported, the presequence is removed by processing enzymes to generate a mature ~30 kDa protein (Clark et al., 1994; Stocco & Sodeman, 1991). Interestingly, the accumulation of StAR in the mitochondrion results in the upregulation of several protein quality control proteases (i.e. LONM,

AFG3L2 and SPG7) in a signalling pathway that has been termed the StAR overload response (SOR) (Bahat et al., 2014). Therefore it appears that the levels of StAR within the mitochondrion need to be effectively managed to prevent mitochondrial dysfunction.

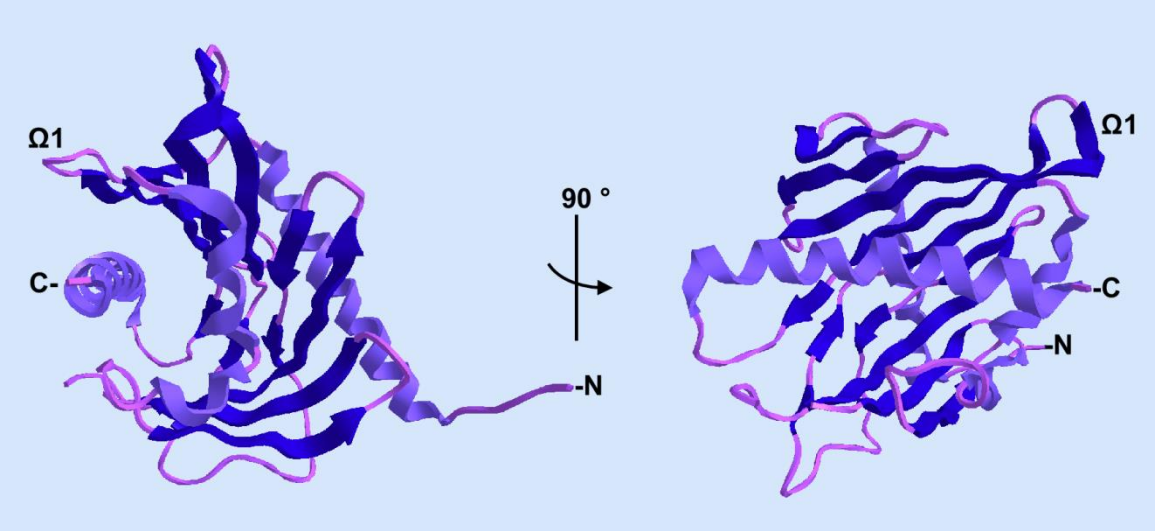


**Figure 4.1:** Ribbon diagram of the structure of human StAR. Characteristic of other lipid binding proteins, StAR is composed of the helix-grip fold where semi-parallel β-sheets (blue) are 'gripped' by α-helices (purple) at the N- and C- termini. The U-shaped cavity (sterol binding pocket) formed by the β-sheets, facilitates binding of a single molecule of cholesterol. The Ω1 loop and C-terminus is predicted to stabilise the StAR:cholesterol complex after binding. PDB ID: 3P0L. Image generated with Chem3D 15.0 software (PerkinElmer).

Through the use of protease inhibitors and siRNA-mediated knock-down, LONM was shown to be the primary protease responsible for the turnover of StAR within the mitochondrion (Bahat et al., 2014; Granot et al., 2007a). However, consistent with the upregulation of SPG7 and AFG3L2 in SOR it has been proposed that multiple mitochondrial proteases are involved in StAR turnover (Bahat et al., 2014; Ronen-Fuhrmann et al., 1998). Interestingly, depletion of *AFG3L2* and *SPG7* in the presence of MG132 (which inhibits both the 26S proteasome and LONM) did not stabilise StAR completely (Bahat et al., 2014; Granot et al., 2007a; Lee & Goldberg, 1998) suggesting that another mitochondrial protease may also contribute to the turnover of StAR (Bahat et al., 2014).

Surprisingly, CLPXP (the only other known matrix AAA+ protease) is not believed to be involved in the turnover of human StAR, as recombinant CLPXP was unable to degrade murine StAR *in vitro* (Granot et al., 2007a).

Nevertheless, regardless of whether additional mitochondrial proteases are involved in the turnover of human StAR, the molecular determinants for StAR recognition and degradation by LONM are poorly defined (Ondrovičová et al., 2005). Therefore the aim of this chapter is to provide a detailed understanding of LONM-mediated recognition and degradation of StAR.

## 4.2 Results

### 4.2.1 Purification of recombinant, authentic human StAR

To determine the structural elements that control the LONM-mediated degradation of StAR, an *in vitro* approach was pursued using purified recombinant proteins. Given that the N- or C-termini of a substrate can play an important role in facilitating recognition by AAA+ proteases, this study used an untagged (authentic) form of StAR. With respect to targeting information, StAR is synthesised with an N-terminal presequence but the cleavage site for the generation of mature StAR has yet to be experimentally determined. Despite this, Arakane et al. (1996) demonstrated that N-terminal truncations of StAR (Δ48 and Δ62) failed to import into mitochondria and these proteins were found to migrate with a similar molecular weight to processed StAR (in untreated cells). Therefore, despite not fitting to the typical rules of presequence cleavage by mitochondrial processing peptidases (Gakh et al., 2002), those data suggest that the StAR is processed between residues 48 and 62 (Arakane et al., 1996). Consistent with these findings, mature human StAR starting at position Leu63 (or Met48 for rodent StAR) has been used for most *in vitro* studies (Bose et al., 1999; Granot et al., 2002; Ondrovičová et al., 2005; Roostaee et al., 2008). Nevertheless, for this study, Ser56

was assigned as the N-terminal residue of mature StAR (Figure 4.2A), (based on prediction of the mitochondrial presequence cleavage site using MitoProt II (Claros & Vincens, 1996)). Importantly, this site is consistent with the R-2 rule for cleavage by MPP (Gakh et al., 2002).

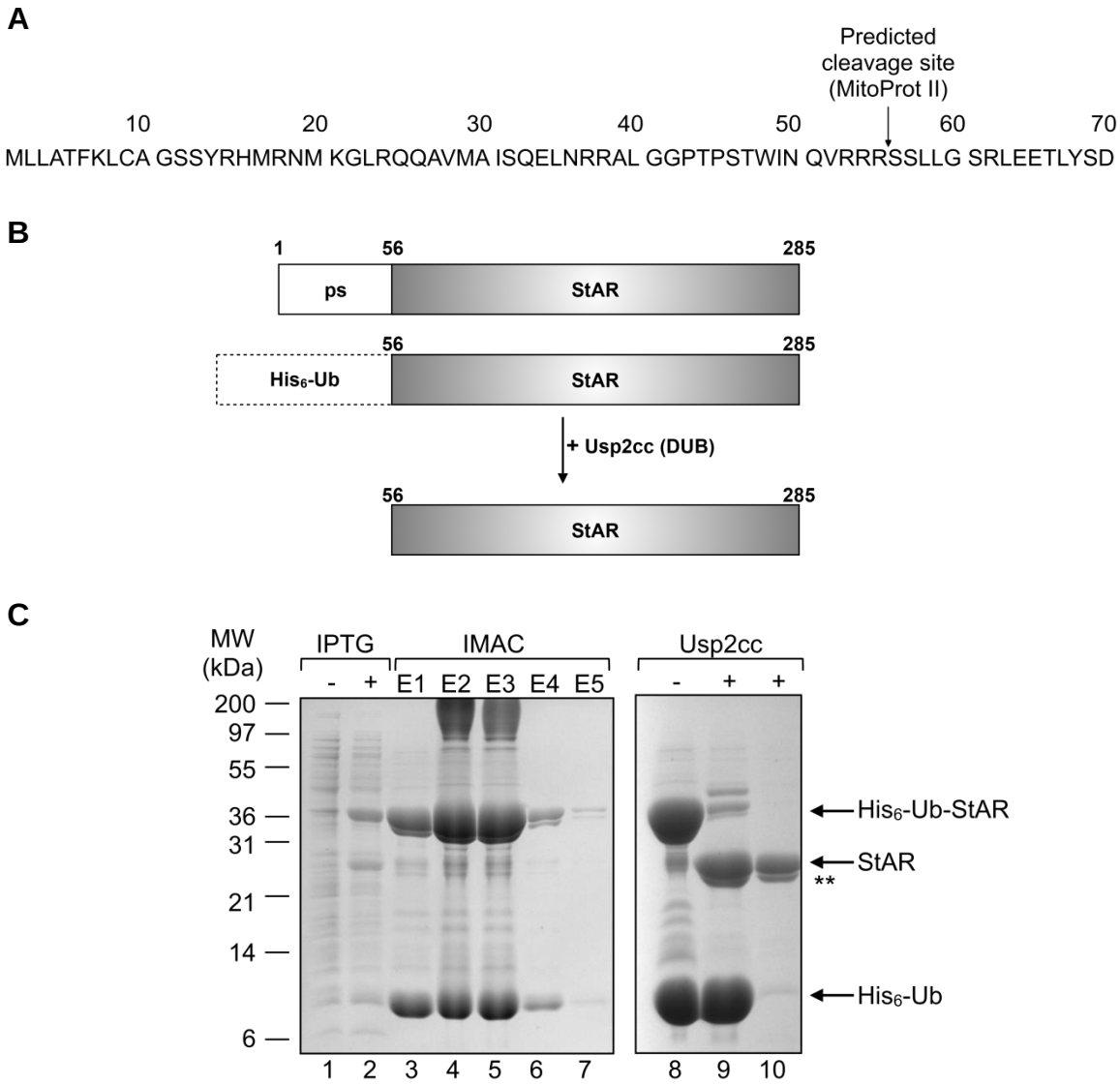


**Figure 4.2:** Generating mature, untagged human StAR. **A**, First 70 amino acids of StAR precursor protein depicting the predicted cleavage site of the mitochondrial presequence (ps). **B**, Schematic showing full-length StAR including the 55 amino acid ps that is removed following import into mitochondria. This mature form of StAR (starting at Ser56) was expressed in *E. coli* with an N-terminal $His_6$-Ub tag which was removed with the deubiquitinating (DUB) enzyme Usp2cc to generate untagged, mature StAR. **C**, Coomassie Brilliant Blue stained 16.5% Tricine-buffered SDS-polyacrylamide gels showing pre- and post-induction samples of StAR expression in *E. coli* (lanes 1-2), eluted fractions (E1-E5) from IMAC purification of $His_6$-Ub-StAR (lanes 3-7), cleavage of $His_6$-Ub from StAR by Usp2cc (lanes 8-9) to generate untagged, mature StAR (lane 10). ** indicates degradation product of StAR.

To generate untagged recombinant StAR the ubiquitin-fusion system was used (Catanzariti et al., 2004). Specifically cDNA encoding the mature form of human StAR was amplified via PCR using specific primers (see Appendix 1, Table 1) and cloned into pHUE, downstream and in frame with the DNA sequence coding for $His_6$-Ub (depicted in Figure 4.2B). Following expression and initial purification via IMAC, $His_6$-Ub-StAR was cleaved using DUB enzyme Usp2cc and the untagged StAR was isolated from the free $His_6$-Ub tag or the uncleaved fusion protein via reverse IMAC (Figure 4.2C). With the exception of the presence of a minor degradation product, StAR was >90% pure (Figure 4.2C, lane 10).

### 4.2.2 Recombinant StAR is degraded by LONM *in vitro*

In order to confirm that StAR was recognised by LONM, a series of *in vitro* degradation assays were performed with purified recombinant components. Consistent with published data (Ondrovičová et al., 2005), StAR was degraded by LONM (Figure 4.3A) and the degradation was ATP-dependent. Interestingly, at 30 °C, the half-life (t½) of human StAR was ~30 min (Figure 4.3B) while the half-life decreased significantly (t½ ~15 min) at the biologically-relevant temperature (37 °C) (Figure 4.3B, compare blue and black lines). Next, to determine if a temperature-induced change in the ATPase activity of LONM was responsible for a change in substrate turnover, the ATPase activity of LONM was monitored in the absence or presence of a substrate (Figure 4.3C). Importantly, the ATPase activity of LONM was similar at 30 °C and 37 °C (Figure 4.3C, compare white and hatched bars) even in the presence of α-casein, indicating that substrate engagement and not ATPase activity played an important role in StAR turnover at 37 °C. Therefore, the enhanced proteolytic activity towards StAR at 37 °C compared to 30 °C was likely due to improved exposure of the LONM degron(s) at the higher temperature.

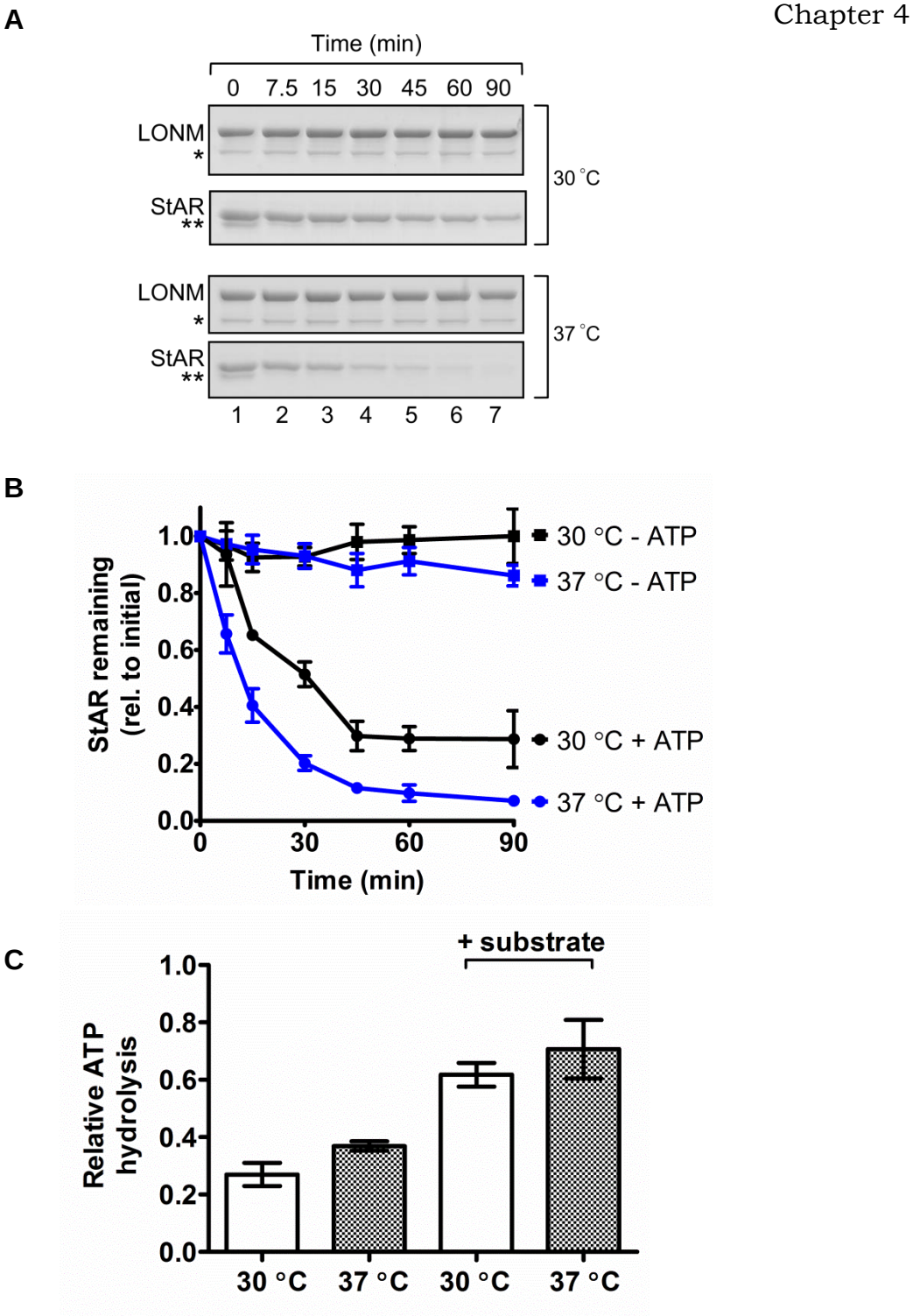


**Figure 4.3:** The LONM-mediated degradation of StAR is accelerated at a higher temperature. **A**, Coomassie Brilliant Blue stained SDS-polyacrylamide gel strips showing *in vitro* degradation of StAR (3 μM) by LONM (0.2 μM hexamer) in the presence or absence of ATP (5 mM) at 30 °C (upper panels) or 37 °C (lower panels). **B**, The amount of StAR following incubation with LONM at 30 °C (black lines) or 37 °C (blue lines) in the presence (circles) or absence (squares) of ATP (5 mM) was quantitated via densitometry (n=3, error bars represent SEM). **C**, Relative rates (0-15 min) of LONM (0.1 μM hexamer) ATPase activity at 30 °C (white bars) or 37 °C (hatched bars) in the absence or presence of excess substrate (3 μM α-casein), (n=2, error bars represent SD). * indicates degradation product of LONM, ** indicates degradation product of StAR.

### 4.2.3 A free N-terminus is not required for recognition by LONM

Next, to determine the location of the degron in StAR, the requirements for an exposed N- and C-terminus of StAR for LONM-mediated recognition were examined. To investigate the role of the N-terminus in StAR recognition, the *in vitro* turnover of $His_6$-Ub-StAR was monitored at 30 °C and 37 °C (Figure 4.4A). Interestingly, the presence of the $His_6$-Ub moiety at the N-terminus of StAR did not alter the turnover of StAR at either 30 °C or 37 °C (Figure 4.4B) indicating that LONM-mediated recognition of StAR did not require a free N-terminus.

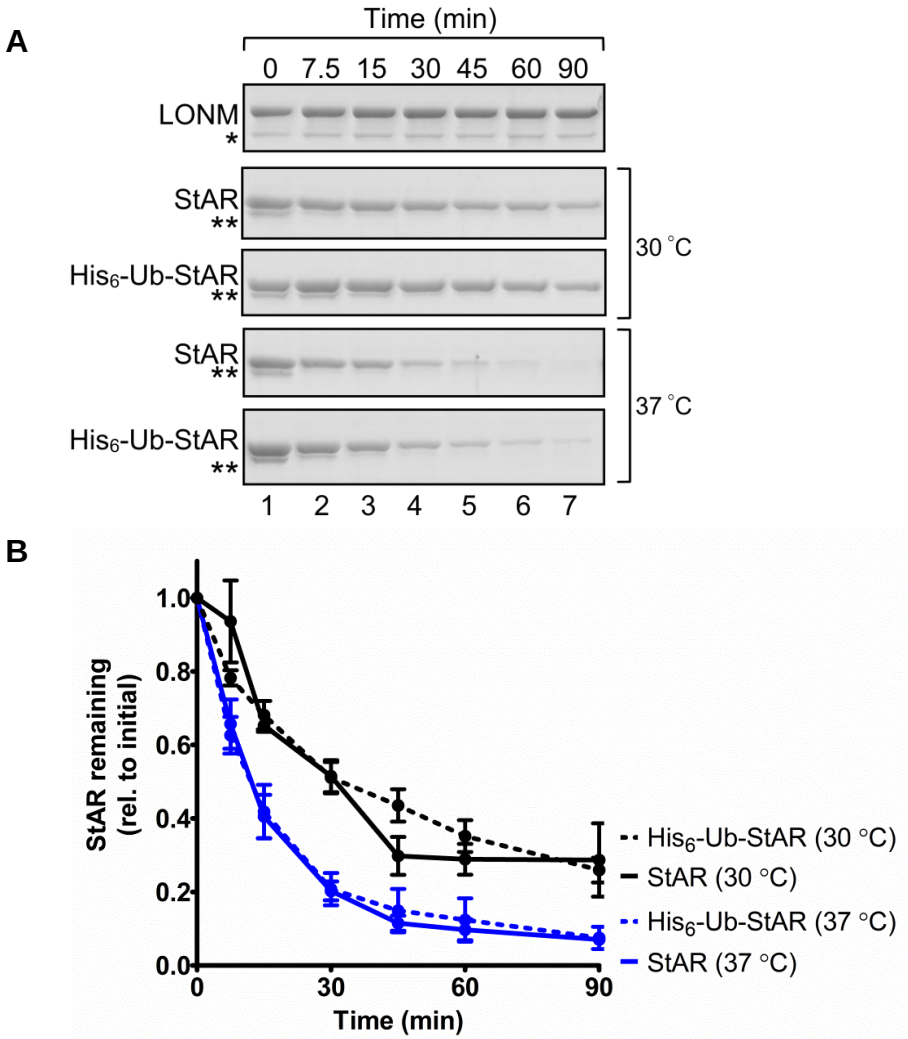


**Figure 4.4:** A free N-terminus is not required for LONM-mediated degradation of StAR. **A**, The turnover of StAR or $His_6$-Ub-StAR (3 µM each) was monitored in the presence of LONM (0.2 µM hexamer) and ATP (5 mM) at 30 °C or 37 °C. Proteins were separated by SDS-PAGE and visualised by staining with Coomassie Brilliant Blue. **B**, The amount of StAR (solid lines) or $His_6$-Ub-StAR (dashed lines) at 30 °C (black circles) or 37 °C (blue circles) was quantitated via densitometry (n=3, error bars represent SEM). * indicates degradation product of LONM, ** indicates degradation product of StAR.

Next, as the C-terminal α-helix is reported to be highly flexible and partially unstructured at neutral pH (Roostaee et al., 2008; Yaworsky et al., 2005), this region was speculated to contain the degron for LONM recognition. Initially, to determine if the degron was located within the C-terminal α-helix, a mutant of StAR was generated that lacked this helix ($StAR_{56-249}$, herein referred to as $StAR_{\Delta C}$, Figure 4.5A). Consistent with the loss of the 36 residue α-helix, $StAR_{\Delta C}$ migrated at ~ 25 kDa following separation by SDS-PAGE (Figure 4.5B). Next, the effect of removing the C-terminal α-helix was examined in an *in vitro* degradation assay (Figure 4.5C). Surprisingly, the turnover of $StAR_{\Delta C}$ was more rapid than the turnover of StAR (Figure 4.5D, compare solid and open circles) suggesting that the C-terminus of StAR does not contain the degron, rather its removal resulted in exposure of the degron. Given the C-terminal α-helix is thought to gate entry to hydrophobic SBP of StAR (Alpy & Tomasetto, 2005), it is possible that exposure of this region promotes enhanced recognition by LONM. Alternatively, the C-terminal α-helix is simply required for the structural integrity of StAR and its deletion adversely affected the conformation of StAR.

To monitor the overall fold of $StAR_{\Delta C}$, size exclusion chromatography was performed on StAR and $StAR_{\Delta C}$ (Figure 4.6). Importantly, little to no $StAR_{\Delta C}$ eluted at the void volume ($V_0$) indicating that this protein was not prone to aggregation. Interestingly, $StAR_{\Delta C}$ eluted earlier than StAR (Figure 4.6A, compare red and black lines), suggesting it had a larger hydrodynamic radius. Collectively these data suggest that $StAR_{\Delta C}$ exhibits a more 'open' conformation. To determine if $StAR_{\Delta C}$ was in a stable conformation or simply misfolded, the interaction with the C-terminal α-helix of StAR ($His_6$-Ub-$StAR_{250-285}$, herein referred to as $StAR_{pep}$) (Figure 4.7A) was monitored using a number of different assays.

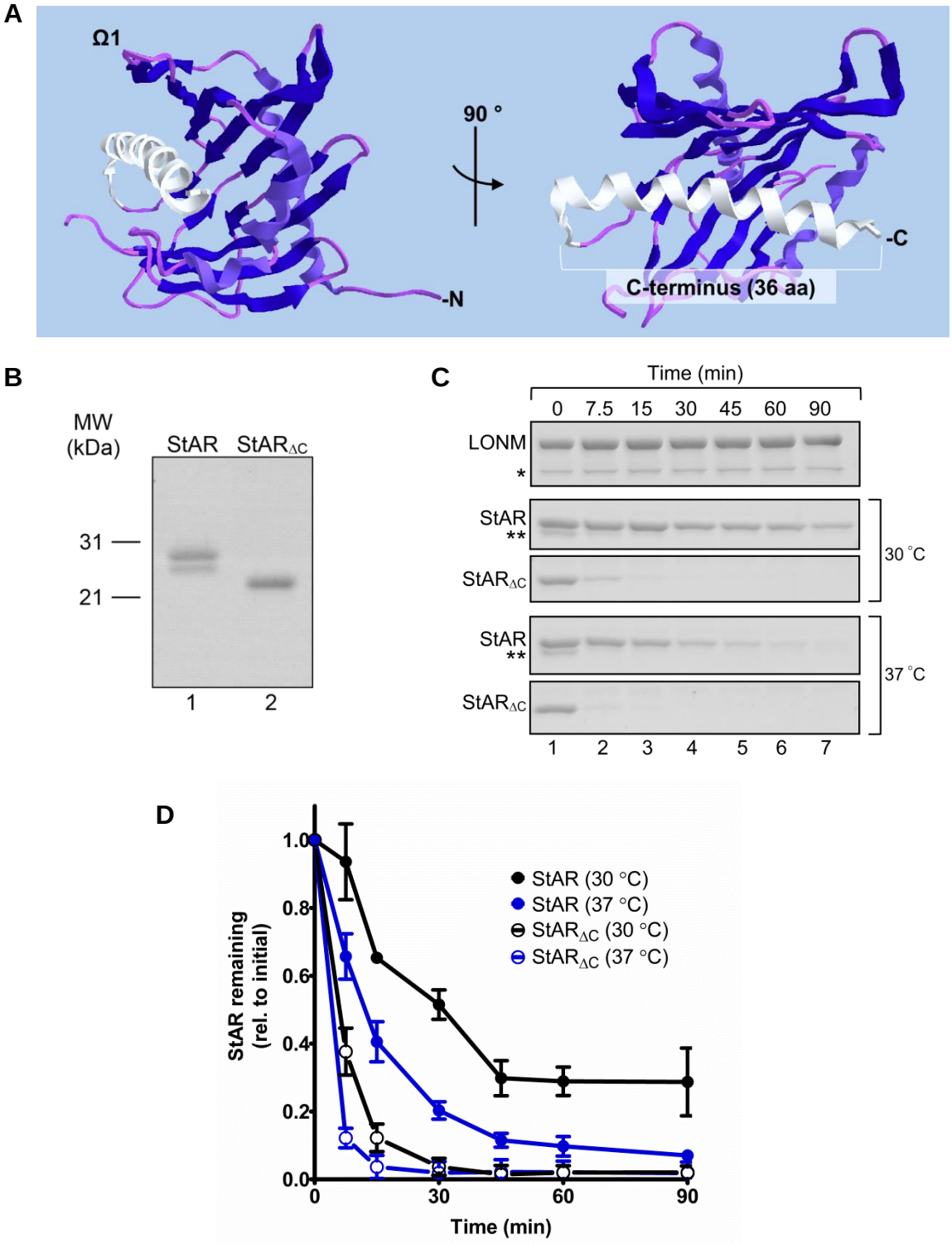


**Figure 4.5:** Deletion the C-terminus enhances LONM-mediated degradation of StAR. **A**, Ribbon diagram of human StAR with the residues truncated from the C-terminal α-helix indicated in white. Image generated with Chem3D 15.0 software. PDB ID: 3P0L. **B**, Coomassie Brilliant Blue stained SDS-polyacrylamide gel strip showing the relative molecular weight of recombinant StAR (lane 1) and StAR$_{\Delta C}$ (lane 2) (2 µg each). **C**, Coomassie Brilliant Blue stained SDS-polyacrylamide gel strips showing *in vitro* degradation of StAR and StAR$_{\Delta C}$ (3 µM each) by LONM (0.2 µM hexamer) at 30 °C and 37 °C as indicated. **D**, The amount of StAR (solid circles) or StAR$_{\Delta C}$ (open circles) at 30 °C (black lines) or 37 °C (blue lines) was quantitated via densitometry (n=3, error bars represent SEM). * indicates degradation product of LONM, ** indicates degradation product of StAR.

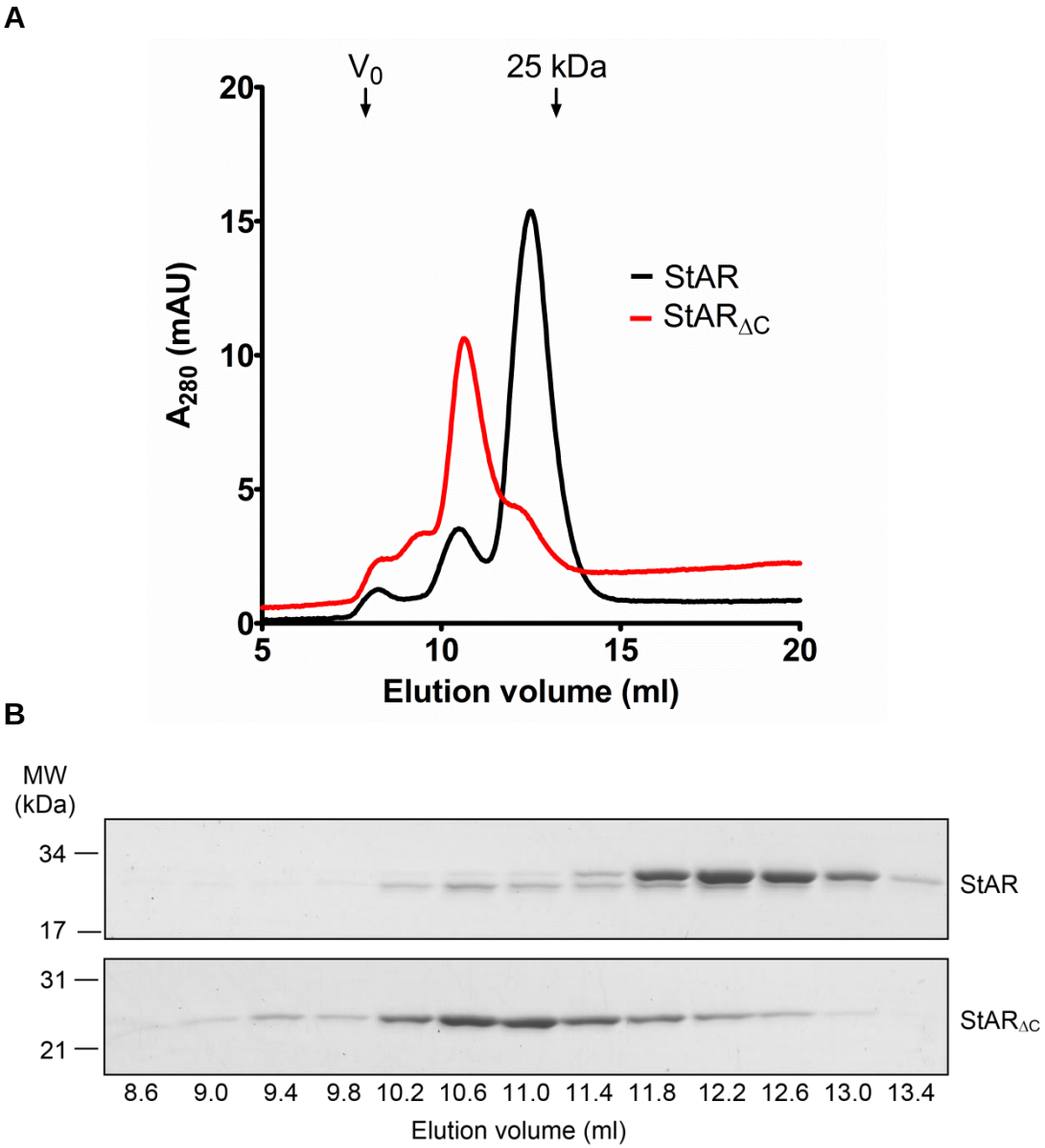


**Figure 4.6:** Size exclusion chromatography of StAR and $StAR_{\Delta C}$. **A**, Elution profiles of wild-type StAR (black line) and ΔC StAR (red line) separated using a Superdex 75 column. The protein absorbance was measured 280 nm ($A_{280}$). Arrows indicate the peak elution volume of blue dextran (void volume ($V_0$)) and chymotrypsin A (25 kDa). **B**, Proteins from the indicated fractions were separated by SDS-PAGE and visualised by staining with Coomassie Brilliant Blue.

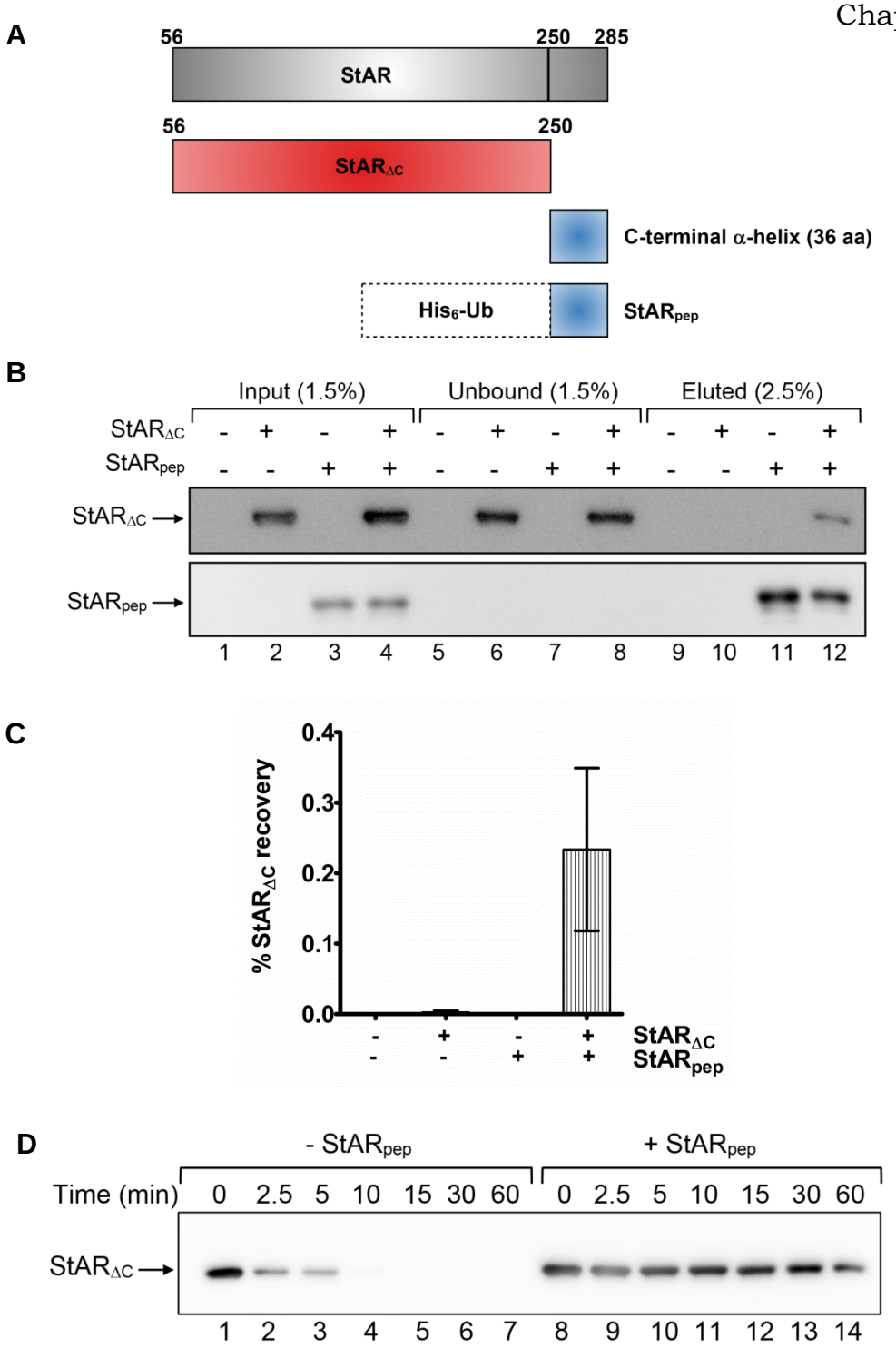


**Figure 4.7:** StAR$_{pep}$ interacts with StAR$_{\Delta C}$ *in trans* and stabilises StAR$_{\Delta C}$. **A**, Cartoon representation of the proteins used to examine the interaction between StAR$_{\Delta C}$ and StAR$_{pep}$. Numbering based on the StAR preprotein. **B**, Representative western blot of input (lanes 1-4), unbound (lanes 5-8) and eluted (lanes 9-12) samples from a series of pull-down assays between StAR$_{\Delta C}$ and StAR$_{pep}$ (1:4 molar ratio). StAR$_{\Delta C}$ (upper panel) and StAR$_{pep}$ (lower panel) levels were visualised by α-StAR and α-His antisera respectively. **C**, The percentage (%) of StAR$_{\Delta C}$ recovery relative to input was determined for each sample (n=3, error bars represent SEM). **D**, Immunoblot of StAR$_{\Delta C}$ levels showing limited proteolysis of StAR$_{\Delta C}$ in the absence (lanes 1-7) or presence (lanes 8-14) of StAR$_{pep}$ (1:4 molar ratio) using thermolysin at 20 °C.

Initially, to determine if $StAR_{pep}$ could form a stable interaction with $StAR_{\Delta C}$, a series of pull-down assays were performed (Figure 4.7B). In this case $StAR_{pep}$ was immobilised to Ni-NTA agarose beads and then incubated with $StAR_{\Delta C}$. While there was a small amount of non-specific binding of $StAR_{\Delta C}$ to the Ni-NTA beads alone (Figure 4.7C), the binding of $StAR_{\Delta C}$ was significantly enriched in the presence of $StAR_{pep}$ (Figure 4.7B, lane 12 and Figure 4.7C, grey bar) indicating that $StAR_{\Delta C}$ was able to interact with $StAR_{pep}$ *in trans*. This association also suggests the structure of StAR was not compromised by deletion of the C-terminus.

Next, to determine if the interaction of $StAR_{pep}$ could stabilise the structure of $StAR_{\Delta C}$, limited proteolysis (Section 2.4.3) was performed using thermolysin. Importantly, in the absence of $StAR_{pep}$ $StAR_{\Delta C}$ was rapidly cleaved (Figure 4.7D, lanes 1-7). Consistent with an increase in structural stability, $StAR_{\Delta C}$ was less susceptible to cleavage by thermolysin in the presence of $StAR_{pep}$ (Figure 4.7D, compare lanes 7 and 14). Given that the SBP is largely hydrophobic in nature and that thermolysin exhibits specificity for hydrophobic residues, the stability of $StAR_{\Delta C}$ was consistent with the docking of $StAR_{pep}$ to the hydrophobic cavity of StAR.

### 4.2.4 StAR C-terminal α-helix regulates exposure of LONM degron

To determine if $StAR_{pep}$ could also prevent the LONM-mediated turnover of $StAR_{\Delta C}$, an *in vitro* degradation assay was performed using LONM. In this case, $StAR_{\Delta C}$ was pre-incubated in the absence or presence of $StAR_{pep}$ prior to the addition of LONM (Figure 4.8A). Similar to previous results, $StAR_{\Delta C}$ was rapidly degraded by LONM (Figure 4.8, solid line). Remarkably, the addition of $StAR_{pep}$ inhibited LONM-mediated turnover of $StAR_{\Delta C}$ in a concentration-dependent manner (Figure 4.8B, compare solid line with dotted and dashed lines). No evidence of $StAR_{pep}$ degradation was observed (data not shown). As a control, the turnover of α-casein was also monitored in the presence of $StAR_{pep}$ and importantly no significant change in α-casein turnover was observed (Appendix 4,

Supplementary Figure 1). These data indicate that $StAR_{pep}$ does not negatively inhibit LONM activity, rather the specific protection conferred to $StAR_{\Delta C}$ is due to the degron being obstructed by $StAR_{pep}$ which is expected to be bound within the SBP.

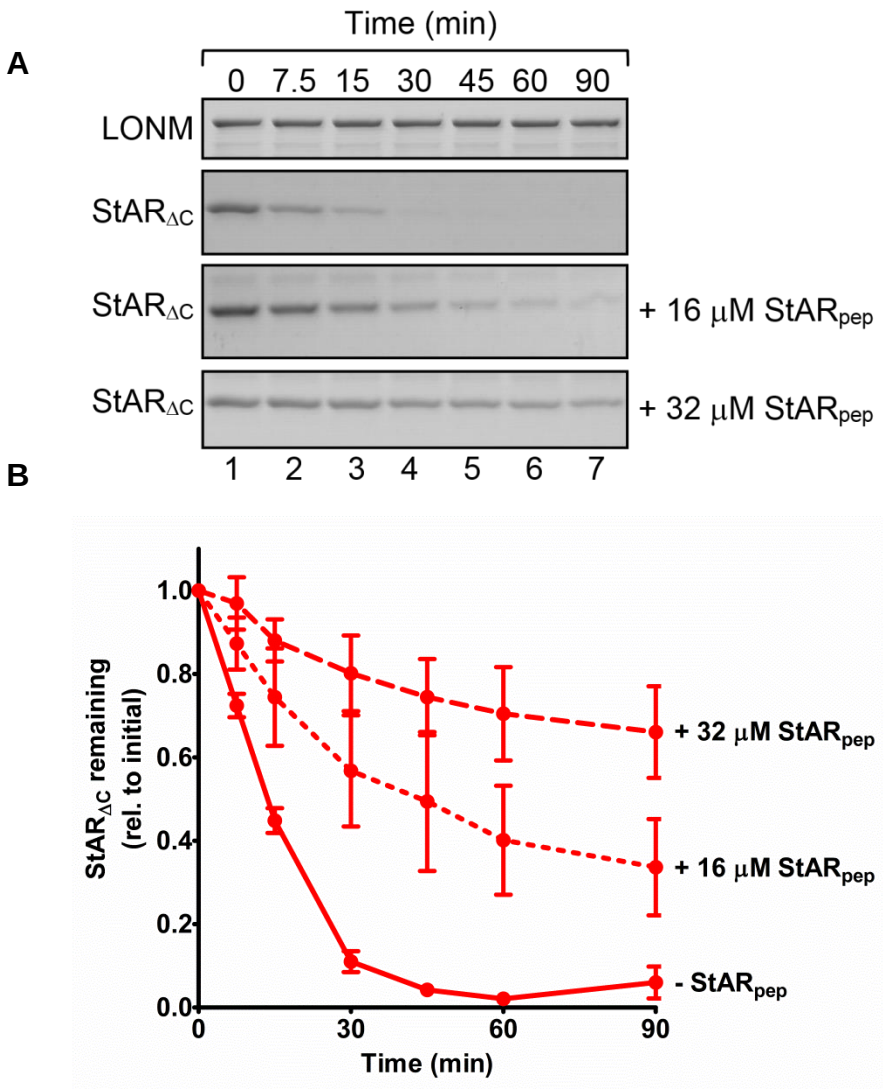


**Figure 4.8:** LONM-mediated degradation of $StAR_{\Delta C}$ is inhibited in the presence of $StAR_{pep}$. **A**, The turnover of $StAR_{\Delta C}$ (2 µM) by LONM (0.1 µM hexamer) was monitored in the absence or presence of increasing concentration of $StAR_{pep}$ (16 µM and 32 µM) at 30 °C. Protein samples were separated by SDS-PAGE and visualised by staining with Commassie Brilliant Blue. **B**, The amount of $StAR_{\Delta C}$ in the absence (solid line) or presence of 16 µM (dotted line) or 32 µM (dashed line) $StAR_{pep}$ was quantitated via densitometry (n=3, error bars represent SEM). * indicates degradation product of LONM

To confirm that access to the hydrophobic cavity is modulated by movement of the C-terminal α-helix, which in turn regulates the LONM-mediated turnover of StAR, a mutant form of StAR was generated where the C-terminus could be reversibly tethered to the wall of the SBP through a disulphide bond. For this, a double mutant of StAR was used in which Asp127 and Ala189 were each replaced with a cysteine residue (Baker et al., 2005). This mutant protein ($StAR_{56\text{-}285}^{A268C/D106C}$, herein referred to as $StAR^{DA}$), depicted in Figure 4.9A, under reducing conditions was previously shown to bind cholesterol and promote steroidogenesis in isolated mitochondria similar to wild-type StAR (Baker et al., 2005). However, when oxidised, the C-terminal α-helix was tethered and all cholesterol binding activity was lost (Baker et al., 2005). To ensure disulphide bonds were formed and remained oxidised, StAR and $StAR^{DA}$ were expressed in SHuffle® T7 *E. coli* (NEB) cells and the proteins were purified in the absence of any reducing reagents.

Initially, the turnover of the oxidised form of wild-type StAR ($StAR_{OX}$) was monitored in the presence or absence of DTT (Figure 4.9B). Importantly, although there was a small change in the half-life of wild-type StAR purified under oxidising conditions (compare Figure 4.3B to Figure 4.9C), the half-life of $StAR_{OX}$ did not change greatly with the addition of DTT (Figure 4.9C, compare blue solid and dashed lines). Consistently, the turnover of reduced $StAR^{DA}$ was similar to wild-type StAR (Figure 4.9C, compare solid blue and green lines). In contrast, the turnover of $StAR^{DA}$ under oxidising conditions was significantly decreased (Figure 4.9C, green dashed line) confirming that tethering of the C-terminal α-helix was able to block recognition by LONM.

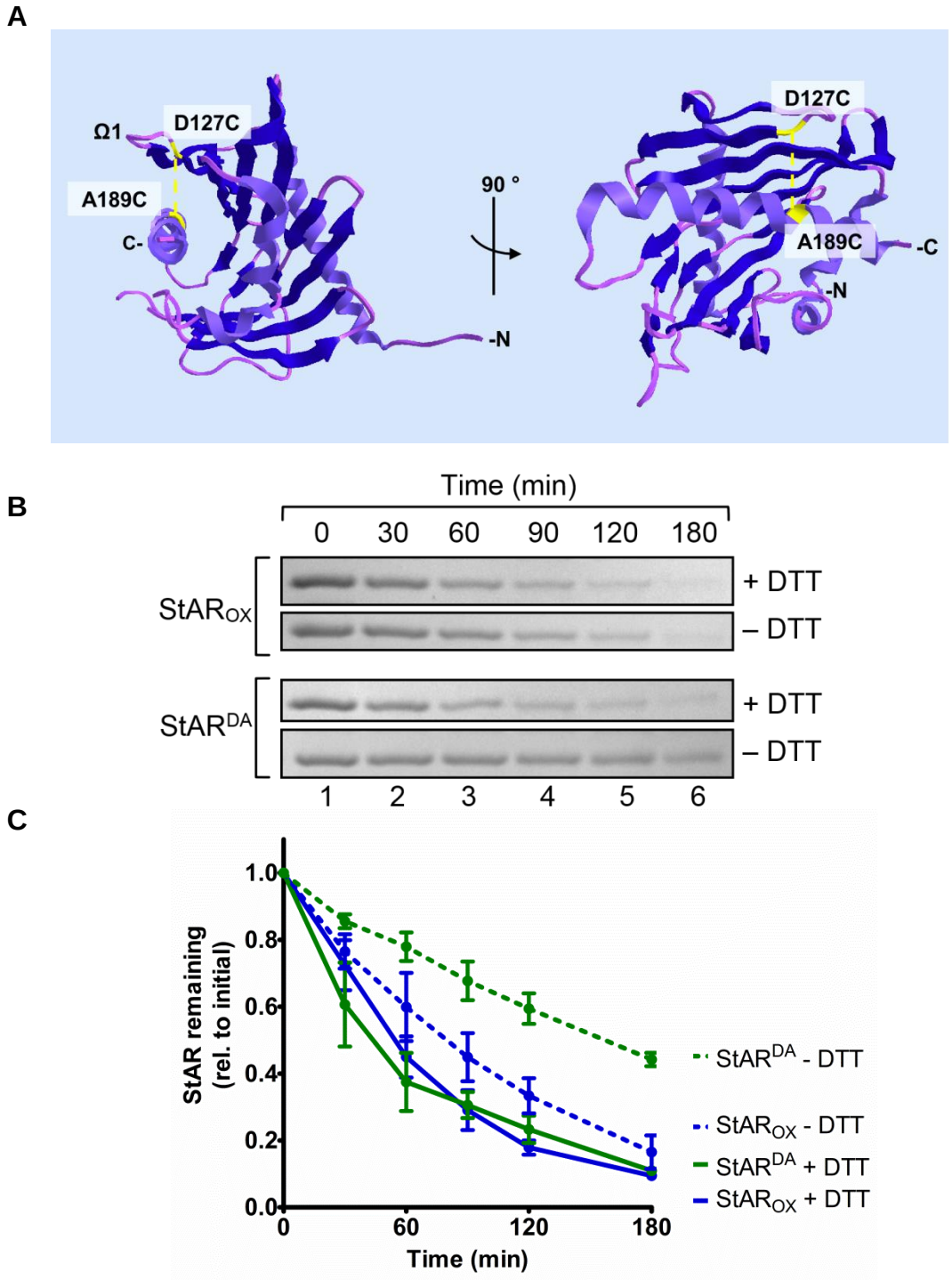


**Figure 4.9:** LONM-mediated recognition of StAR is regulated by movement of the C-terminal α-helix. **A**, Ribbon diagram of human StAR (PDB ID: 3P0L) indicating the position of the residues (Asp127 and Ala189) that were replaced with Cys to generate StAR$^{DA}$ highlighted in yellow. Theoretical disulphide bond formation indicated by a yellow dotted line. Image generated with Chem3D 15.0 software. **B**, *In vitro* degradation of oxidised wild-type StAR (StAR$_{OX}$) and mutant StAR (StAR$^{DA}$) (1 μM each) by LONM (0.2 μM hexamer) at 37 °C in the presence or absence of DTT (1 mM) as indicated. Protein samples were separated by SDS-PAGE and visualised by staining with Coomassie Brilliant Blue. **C**, The amount of wild-type StAR (blue circles) or StAR$^{DA}$ (green circles) in the presence (solid lines) or absence (dotted lines) of DTT (1 mM) was quantitated via densitometry (n=3, error bars represent SEM).

### 4.2.5 StAR is degraded by hCLPXP *in vitro*

Recently it was proposed that the turnover of StAR within the mitochondrion could involve an additional protease (Bahat et al., 2014). In order to examine a possible role for hCLPXP in StAR turnover, an *in vitro* degradation assay was performed (Figure 4.10A). Because StAR and hCLPP co-migrate during SDS-PAGE (Appendix 4, Supplementary Figure 2), α-StAR antisera was used to monitor the degradation of StAR by hCLPXP (Figure 4.10A, lower panel). Interestingly, the turnover of StAR was observed in an ATP-dependent manner (Figure 4.10A, lanes 1-6) with a half-life of ~180 min (Figure 4.10B, black circles).

Next, to determine if recognition by hCLPXP was mediated via the same degron as LONM, the turnover of $StAR_{\Delta C}$ was monitored in the absence or presence of $StAR_{pep}$ (Figure 4.10C). Similar to the LONM-mediated degradation of $StAR_{\Delta C}$, the turnover of $StAR_{\Delta C}$ by CLPXP was faster than that of StAR (Figure 4.10D, solid line). However in contrast, the CLPXP-mediated degradation of $StAR_{\Delta C}$ was not significantly altered by the addition of $StAR_{pep}$ (Figure 4.10D, compare solid line to dotted and dashed lines), indicating LONM and CLPXP recognise StAR via different degrons.

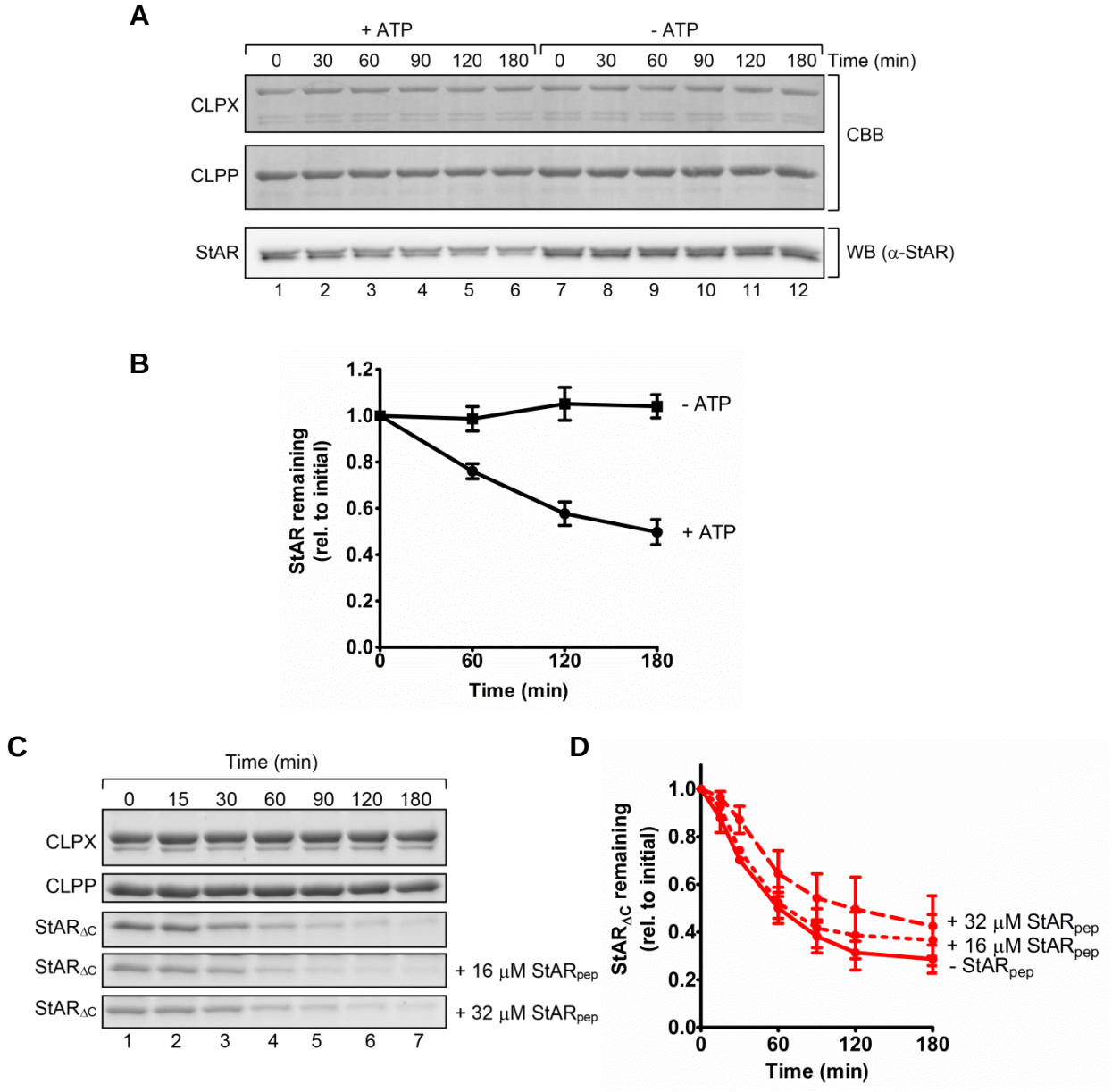


**Figure 4.10:** StAR is an *in vitro* substrate of human CLPXP. **A**, The stability of StAR (0.1 µM) in the presence of hCLPP (5.6 µM protomer) and hCLPX (2.4 µM protomer) was monitored in the presence (lanes 1-6) or absence (lanes 7-12) of ATP (5 mM) at 30 °C. Protein samples were separated by SDS-PAGE and transferred to PVDF membrane. Prior to probing with α-StAR, the membrane was stained with Coomassie Brilliant Blue (CBB) to visualise hCLPX and hCLPP. **B**, The amount of StAR remaining in the presence (black circles) or absence (black squares) of ATP (5 mM) was quantitated via densitometry (n=4, error bars represent SEM). **C**, CBB stained SDS-polyacrylamide gel strips showing the turnover of $StAR_{\Delta C}$ (2 µM) in the absence or presence of increasing concentrations of $StAR_{pep}$ (16 µM and 32 µM) by hCLPXP at 30 °C. **D**, The amount of $StAR_{\Delta C}$ in the absence (solid lines) or presence of 16 µM (dotted lines) or 32 µM (dashed lines) $StAR_{pep}$ was quantitated via densitometry (n=3, error bars represent SEM).

## 4.3 Discussion

The rapid clearance of StAR from mitochondria post-steroidogenesis is essential to prevent proteotoxic stress and mitochondrial dysfunction. The StAR overload response promotes the upregulation of specific proteases responsible for the turnover of StAR (Bahat et al., 2014) so that the clearance of StAR is accomplished rapidly and efficiently after import into the matrix. LONM was determined to be the primary protease contributing to StAR turnover (Bahat et al., 2014; Granot et al., 2007a) and is also largely responsible for maintaining proteostasis within the mitochondrial matrix (Bezawork-Geleta et al., 2015). As substrates of LONM include unfolded, oxidatively damaged, unassembled and native proteins, LONM must be capable of recognising a variety of different degrons but still retain substrate specificity (Bezawork-Geleta et al., 2015; Bezawork-Geleta et al., 2014; Bota & Davies, 2002; Granot et al., 2007a; Matsushima et al., 2010; Ondrovičová et al., 2005; Tian et al., 2011).

This study investigated the molecular determinants governing LONM-mediated recognition of StAR and has established the primary degron for LONM is located within the SBP of StAR and its exposure is regulated by the movement of the C-terminal α-helix. As the SBP is largely hydrophobic in nature, it is speculated that LONM-mediated recognition of StAR is enhanced through the exposure of these hydrophobic residues. Consistent with this, hydrophobic residues have been demonstrated to be crucial for optimal recognition and degradation of folded and unfolded substrates by ecLon (Gur & Sauer, 2008; Gur & Sauer, 2009) and for recognition of unfolded proteins by LONM (Bezawork-Geleta et al., 2015).

### 4.3.1 Exposure of LONM degron is regulated by the C-terminal α-helix

StAR is reported to exist in multiple conformational states that are influenced by pH and the binding of cholesterol (Bose et al., 1999; Mathieu et al., 2002; Roostaee et al., 2008). However, at neutral pH in the absence of cholesterol, StAR was predicted to be predominantly stable (Bose et al., 1998) but may also exhibit a partially open or unfolded state caused by the C-terminal α-helix folding away from the SBP (Mathieu et al., 2002). At neutral pH, the C-terminal α-helix was also predicted to be partially unfolded (Yaworsky et al., 2005) which would likely contribute to its flexibility and facilitate the exposure of the SBP.

During this study, to investigate the regions of StAR that would contribute to LONM-mediated recognition within the mitochondrion, all *in vitro* degradation assays were performed at physiological pH (7.0-8.0) and temperature (37 °C). Interestingly, the LONM-mediated recognition of StAR was enhanced at 37 °C compared to 30 °C (Figure 4.3B). The ATP-dependent unfolding and translocation of substrates has been determined as the rate-limiting step in the regulated degradation by ecLon and other AAA+ proteases (Gur & Sauer, 2009; Peth et al., 2013; Sundar et al., 2010; Vineyard et al., 2005) and substrates, such as α-casein, can enhance the ATPase activity of ecLon (Waxman & Goldberg, 1986). Consistent with this, the presence of model unfolded substrate α-casein also stimulated the ATPase activity of LONM (Figure 4.3C). However, in this study, the ATPase activity of LONM was not increased further at the higher temperature (37 °C) indicating that the increased proteolytic activity towards StAR at 37 °C was likely due to enhanced recognition of StAR by LONM. An increase in the thermodynamics of StAR at the higher temperature (37 °C) may lead to greater flexibility of the C-terminal α-helix and increased exposure of the SBP, accounting for the increased recognition by LONM. In support of the SBP playing a key role in LONM recognition, StAR turnover was not affected by the addition of the N-terminal $His_6$-Ub moiety at either temperature.

Despite the predicted disordered state of the C-terminus, no degradation of $StAR_{pep}$ by LONM was observed *in vitro* (data not shown). In the absence of cholesterol, the C-terminal α-helix can be stabilised by a core group of conserved hydrophobic residues (Lavigne et al., 2010), which may be the binding site between $StAR_{\Delta C}$ and $StAR_{pep}$ *in vitro*, as observed during the pull-down assay (Figure 4.7B). In support of $StAR_{pep}$ binding within the SBP, the interaction between $StAR_{pep}$ and $StAR_{\Delta C}$ provided protection against proteolytic cleavage by thermolysin (Figure 4.7D). As thermolysin exhibits a preference for cleaving substrates with hydrophobic residues (i.e. Ile, Leu, Val, Ala, Met, Phe) in position P1', the reduction in the cleavage of $StAR_{\Delta C}$ suggests $StAR_{pep}$ is binding within, and blocking access to, the hydrophobic SBP. The LONM-mediated degradation of $StAR_{\Delta C}$ was selectively reduced in the presence of $StAR_{pep}$ (Figure 4.8), indicating stabilisation of the $StAR_{\Delta C}$ structure and competitive binding of the degron. Finally, the location of the degron was determined specifically by using a double cysteine mutant of StAR ($StAR^{DA}$) that prevented movement of the C-terminus via a reversible disulphide bond (Baker et al., 2005). Under reducing conditions, $StAR^{DA}$ was degraded at a similar rate as wild-type StAR, but under oxidising conditions the turnover of $StAR^{DA}$ was significantly reduced (Figure 4.9C). This revealed the primary degron for LONM was the hydrophobic SBP underneath the C-terminal α-helix and the susceptibility to LONM-mediated degradation is regulated by the movement of the C-terminus. However, the exact conformation of the C-terminal region in the mitochondrial matrix, either partially unfolded or completely α-helical, is yet to be determined. The data observed here supports either model.

Interestingly, it has been reported that under acidic conditions, the C-terminus is completely α-helical and access to the SBP by cholesterol is optimal (Baker et al., 2005; Yaworsky et al., 2005). Consistent with this, acidification of the mitochondrial matrix (by the addition of the ionophore nigericin) increased the turnover of imported StAR (Akhmedov et al., 2010; Bose et al., 1999; Granot et al., 2003; Lavigne et al., 2010; Mathieu et al., 2002; Roostaee et al., 2008) which further supports the

notion that the metabolic stability of StAR is regulated by the C-terminal α-helix and exposure of the hydrophobic SBP.

However, tethering the C-terminal α-helix did not abolish StAR turnover completely, suggesting the presence of other degrons, possibly via specific surface properties of StAR (Ondrovičová et al., 2005), may contribute to LONM-mediated recognition. Alternatively, the remaining flexibility of the C-terminus or Ω1 loop (Figure 4.9A) may be leading to the partial exposure of residues within the SBP. More investigation would be required to determine if any particular residues, or arrangement of residues within the pocket, are crucial for stimulating LONM recognition of StAR.

The direct recognition of StAR by LONM is conflicting with the proposal made by Ondrovičová et al. (2005) who examined the peptides generated by the LONM-mediated degradation of StAR and MPPα *in vitro* and concluded that LONM preferentially cleaves folded substrates to generate easily accessible polypeptides which are then degraded. However, the external cleavage of a substrate is not consistent with the process of regulated proteolysis determined for ecLon (Edmunds & Goldberg, 1986; Gur & Sauer, 2008; Gur & Sauer, 2009; Gur et al., 2012; Nishii et al., 2005; Waxman & Goldberg, 1986). Substrate engagement by ecLon first requires direct or indirect recognition of a specific degron that then promotes binding, unfolding and translocation of the protein it is attached to (Gur & Sauer, 2008; Gur & Sauer, 2009; Gur et al., 2012). The step-wise translocation of the unfolded substrate into the catalytic chamber allows the substrate to be processively degraded and the resulting peptides (between 5-25 residues) are released from the exit pore (Cha et al., 2010; Gur et al., 2012; Rotanova et al., 2006). Thus, the fragments produced during StAR 'cleavage' by LONM (Ondrovičová et al., 2005) may actually represent the peptides produced post-proteolysis. Consistent with this, the accumulation of irregular fragments has also been observed after the processive degradation of substrates by the *E. coli* ClpAP protease (Thompson et al., 1994) and the mammalian 26S proteasome (Kisselev et al., 1999). Partially cleaved fragments of StAR

may also occur if LONM disassociates prematurely from StAR during translocation and degradation, similar to what has been observed during *in vitro* degradation of larger substrates by ecLon (Gur et al., 2012; Patterson-Ward et al., 2009). These partially cleaved peptides derived from StAR may also occur *in vivo* but they would most likely be re-engaged and degraded by LONM or other proteases.

### 4.3.2 StAR is cleared from mitochondria by multiple proteases

As StAR is degraded by different proteases (e.g. LONM and *m*-AAA protease) in the mitochondrion (Bahat et al., 2014), it would be reasonable to assume that recognition and binding is also mediated by different degrons. Substrate overlap and cooperation between mitochondrial proteases would ensure the efficient degradation of StAR is accomplished to prevent proteotoxic stress. The turnover of imported StAR is reported to occur in at least two phases (Bahat et al., 2014). The first phase relies upon the contribution of LONM, followed by the next phase that involves the *m*-AAA protease (AFG3L2 subunit only) (Bahat et al., 2014). After this phase, remaining StAR was observed to be degraded by another protease that was resistant to MG132 inhibition (Bahat et al., 2014). Preliminary data reported here (Figure 4.10) suggests that CLPXP could be responsible for StAR turnover in the matrix and it recognises StAR via a different degron to LONM. Additionally, CLPXP is resistant to inhibition by MG132 (Bezawork-Geleta et al., 2015) and other protease inhibitors (Kang et al., 2002) which suggests this protease would have been active in the assays reported by Bahat et al. (2014). Previously, Granot et al. (2007a) performed a series of assays investigating the turnover of murine StAR *in vitro*. Surprisingly, they observed no turnover of murine StAR by hCLPXP in an *in vitro* degradation assay after 90 min (Granot et al., 2007a). However, no positive controls were included in this particular assay to demonstrate their recombinant proteins (hCLPX and hCLPP) were active. Another method employed to monitor StAR turnover *in vitro* was the overexpression of hLONM or hCLPP in

combination with hStAR in a *Lon* knock-out strain of *E. coli* (Granot et al., 2007a). In this case, the turnover of StAR was observed with hLONM overexpression but not with hCLPP overexpression (Granot et al., 2007a) indicating a lack of activity towards hStAR by the complex formed between ecClpX and hCLPP. However, while ecClpX can indeed interact with hCLPP and form an active complex, ecClpX and hCLPX display different substrate specificity (Kang et al., 2002; Martin et al., 2008). In this regard, it was likely that StAR was not recognised by ecClpX and as a result it was not degraded by hCLPP. Consistently, StAR was observed to be stable in the presence of ecClpXP during an *in vitro* degradation assay (data not shown).

While StAR was an *in vitro* substrate of hCLPXP (Figure 4.10), it may not be preferentially degraded within the mitochondrion by this protease. Substrate specificity of AAA+ proteases is determined, in part, by how well a substrate is recognised and how readily it can be unfolded (Koodathingal et al., 2009). In this respect, LONM and *m*-AAA protease may out-compete CLPXP for degradation of StAR. In contrast to the other proteases, neither CLPX nor CLPP were found to be transcriptionally upregulated in the StAR overload response. However, CLPXP may still contribute to the gradual turnover of StAR within the matrix or provide a PQC role in cases when the other proteases are over-burdened. More investigation *in organello* is required to determine the contribution of CLPXP to the clearance of StAR from the matrix.

In conclusion, the hydrophobic residues lining the SBP of StAR greatly enhance LONM-mediated recognition and degradation and the exposure of this degron is regulated by the C-terminal α-helix. The rapid turnover of StAR by LONM, in addition to other AAA+ proteases, is likely to be a conserved mechanism between steroidogenic and non-steroidogenic cells to prevent proteotoxic stress within the mitochondrial matrix.

# Chapter 5: Understanding the molecular defect underlying Perrault syndrome due to mutations in CLPP.

## 5.1 Introduction

### 5.1.1 Perrault syndrome

Perrault syndrome (PRLTS) is a rare, autosomal recessive disorder characterised by sensorineural hearing loss (SNHL) in both genders and premature ovarian failure (POF) in females. Clinical symptoms can also include growth retardation, epilepsy, ataxia, spasticity and other neurological defects which differ in their onset and severity between patients (Jenkinson et al., 2012). It is a genetically heterogeneous disease wherein mutations in five different causative genes have been identified thus far (see Table 5.1), however for many other reported cases of Perrault syndrome, a causative gene has yet to be defined (Jenkinson et al., 2013; Marlin et al., 2008; Morino et al., 2014; Pierce et al., 2011; Pierce et al., 2013; Pierce et al., 2010).

### 5.1.2 Point mutations in *CLPP* cause Perrault syndrome 3 (PRLTS3)

Patients from four unrelated families were reported to be homozygous for mutations in the *CLPP* gene (on chromosome 19p13.3) as determined by genome-wide sequencing (Ahmed et al., 2015; Jenkinson et al., 2013). One *CLPP* variant c.270+4A>G abolished normal intron splicing of the CLPP mRNA while the other *CLPP* variants were generated by point mutations (c.433A>C, c.440G>C and c.685T>G) resulting in amino acid substitutions in the translated CLPP protein (Thr145Pro, Cys147Ser and Tyr229Asp respectively, see Figure 5.1) (Ahmed et al., 2015; Jenkinson et al., 2013).

In support of a vital role for CLPP in development and a link to Perrault syndrome, *CLPP* null mice ($CLPP^{-/-}$) also display infertility, deafness and growth retardation (Gispert et al., 2013). The similarity between the phenotype of *CLPP* null mice and the symptoms displayed by the patients of Perrault syndrome suggests this syndrome is caused by a loss of CLPP function, either as a result of reduced levels of CLPP or a loss of

CLPP activity. However to date, neither the structural or functional consequences of these mutations in CLPP have been examined.

**Table 5.1: Summary of Perrault syndrome cases with an identified causative gene.**

| Type | Gene | Protein | Protein function | Other symptoms (in addition to SNHL & ovarian dysgenesis) | Reference |
|---|---|---|---|---|---|
| 1 | *HSD17B4* | Peroxisomal Hydroxysteroid (17-β) Dehydrogenase or D-Bifunctional protein (DBP) | Fatty acid β-oxidation and steroid metabolism in peroxisomes | short stature, mild mental retardation, progressive sensory and motor peripheral neuropathy | McMillan et al. (2012) Pierce et al. (2010) |
| *2* | *HARS2* | Mitochondrial histidyl-tRNA synthetase 2 | Mitochondrial protein translation | minor developmental abnormalities | Pierce et al. (2011) |
| 3 | *CLPP* | Mitochondrial caseinolytic peptidase protease subunit | Protein quality control of the mitochondrial matrix | cerebellar ataxia, learning disability, peripheral neuropathy, short stature, epilepsy | Jenkinson et al. (2013) Ahmed et al. (2015) |
| 4 | *LARS2* | Mitochondrial leucyl-tRNA synthetase 2 | Mitochondrial protein translation | None reported | Pierce et al. (2013) |
| 5 | *C10orf2* | Mitochondrial T7-Like mtDNA Helicase (Twinkle) | mtDNA replication | ataxia, peripheral neuropathy, epilepsy | Morino et al. (2014) |

CLPP is encoded on nuclear DNA and targeted to the mitochondrial matrix by the presence of a positively-charged N-terminal targeting sequence (Bross et al.) which is initially cleaved by mitochondria processing peptidases (at an undefined position) (Corydon et al., 1998). Human CLPP (hCLPP) exhibits ~56% sequence identity with *E. coli* ClpP (ecClpP) and both proteins, not only share a common fold, (root mean square (r.m.s) deviation of 0.63 Å), but they also share a similar overall architecture based on the crystal structures (Kang et al., 2004). Both proteins form a barrel-shaped tetradecamer that encloses an aqueous chamber (58 Å in diameter) with a narrow axial entrance pore (~10 Å) (Kang et al., 2004). However, different to ecClpP, hCLPP contains a 28

amino acid C-terminal extension that is required for its stability but not for its activity or interaction with CLPX (Kang et al., 2004).

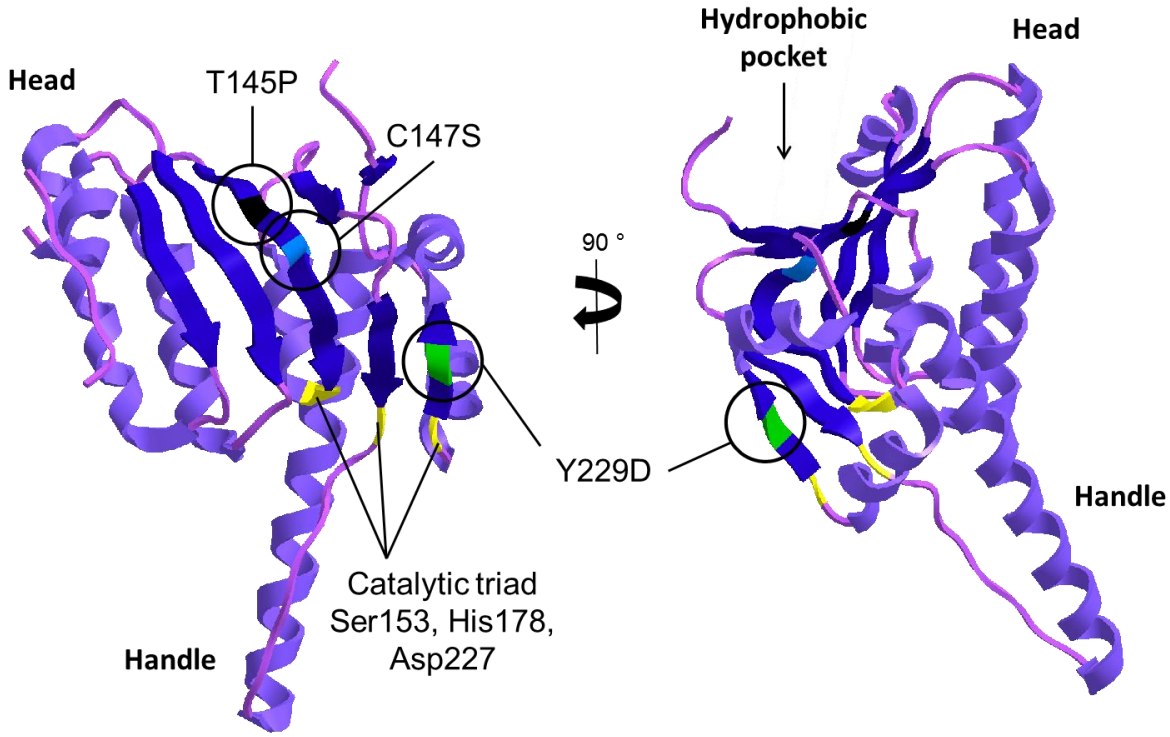


**Figure 5.1:** Ribbon diagram of human CLPP illustrating the location of each point mutation (T145P (black), C147S (blue) and Y229D (green)) that has been determined to cause Perrault syndrome type 3. CLPP monomers interact via the head region to form a heptameric ring. Heptameric rings of CLPP associate via their handle regions to form a tetradecamer with all active sites facing inwards. CLPX hexamers bind on one or both ends of the CLPP tetradecamer to form the active CLPXP protease complex. Molecular interactions between CLPP and CLPX stabilise the complex: LGF loops of CLPX bind to the hydrophobic pockets of CLPP while the pore-2 loops of CLPX interact with CLPP N-terminal loops. Active site residues Ser153, His178 and Asp227 are highlighted in yellow. Numbering of residues based on the precursor protein. Figure of hCLPP (PDB ID: ITG6) was generated using Chem3D (v15.0).

In *E. coli*, the first 14 amino acids of ecClpP are cleaved from the N-terminus in an autocatalytic process to generate the mature protein (Maurizi et al., 1990a; Maurizi et al., 1990b). Similar to ecClpP, autocatalytic processing of recombinant hCLPP has also been observed (Kang et al., 2004), however the precise location of this processing *in vivo* has yet to be determined. A summary of the potential cleavage sites of

preCLPP are outlined in Figure 5.2. Consistent with the autocatalytic processing of hCLPP *in vitro* (Kang et al., 2004), Thr53 was also identified as the mature N-terminus of exogenously expressed $hCLPP_{FLAG}$ isolated from HeLa mitochondria (Saiyed, Dougan & Truscott, manuscript in preparation). However, a recent proteomics study identified Pro57 as the mature N-terminus of hCLPP (Vaca Jacome et al., 2015).

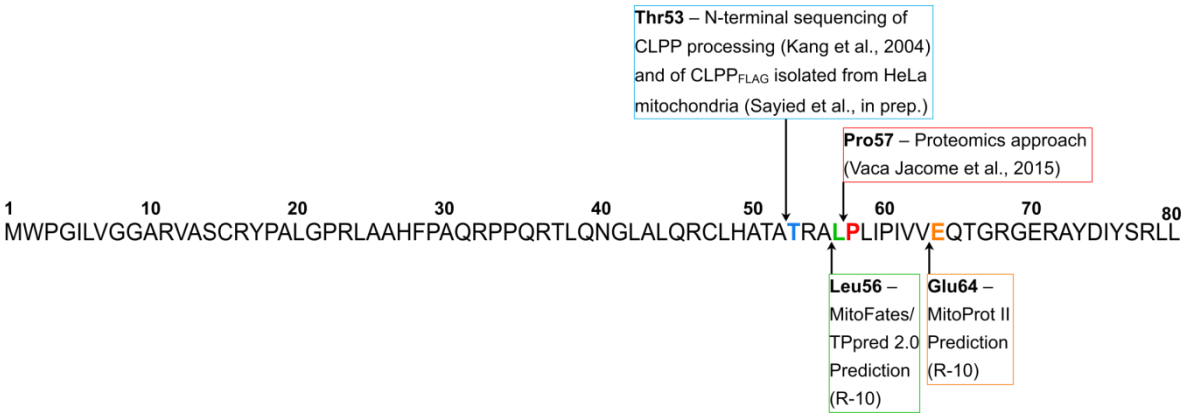


**Figure 5.2:** Summary of the cleavage sites determined or predicted to generate mature CLPP. The experimentally determined and predicted cleavage sites are indicated by arrows above and below, respectively, of the first 80 residues of preCLPP. The resulting N-termini of CLPP are indicated in bold and colour coordinated with a description of how they were derived. Cleavage sites determined by MitoFates, TPred and MitoProt II follow the R-10 rule (R-10) of mitochondrial precursor protein cleavage.

After processing in the mitochondrial matrix, mature hCLPP folds and assembles into a ring-shaped heptamer (Kang et al., 2005). hCLPP then interacts with hCLPX to form a functional protease complex composed of a hCLPX hexamer that docks onto either or both ends of a hCLPP tetradecamer (Kang et al., 2002). Figure 5.1 illustrates the position of each pathological amino acid substitution mapped together onto a single subunit of hCLPP. The Thr145Pro and Cys147Ser substitutions flank Trp146 which is located in the hydrophobic pocket and is thought to be important for interaction with the LGF loop of hCLPX (Jenkinson et al., 2013; Joshi et al., 2004). Based on the position of these mutations it was proposed that these mutants will exhibit compromised CLPXP complex assembly and hence demonstrate impaired protease activity (Jenkinson

et al., 2013). Human CLPP belongs to the S14 family of serine proteases and contains a catalytic triad composed of residues Ser153, His178 and Asp171 (Corydon et al., 1998). Assembly of the heptamer results in the active sites of CLPP facing towards the centre of the ring which creates the catalytic chamber that is ultimately protected from the external environment in the final tetradecamer (Kang et al., 2004). Mutation of residues in the vicinity of the active site alters the proteolytic activity of CLPP (Kang et al., 2005) which suggests that the Tyr229Asp substitution (identified in patients with PRLTS3) may lead to an altered or reduced proteolytic activity.

Alternatively, the amino acid substitution in each CLPP variant could affect the import of the precursor protein or affect its folding or its assembly into the final active complex after import. A defect in any of these processes could alter the metabolic stability of CLPP and cause it to be susceptible to degradation. Thus characterisation of the stability and activity of each CLPP would allow us to determine the role of CLPP in the pathology of Perrault syndrome.

## 5.2 Results

### 5.2.1 *In vitro* import and biogenesis of wild-type and mutant preCLPP

To determine if the amino acid substitution in each the CLPP protein affected their import and/or biogenesis in mitochondria, a series of *in vitro* import reactions were performed. Initially, conditions of import were established using the precursor form of wild-type CLPP (preCLPP). Radiolabelled preCLPP was generated using a coupled transcription and translation (TNT) system supplemented with $^{35}$S-Met/Cys (Section 2.4.11). Aliquots of isolated HeLa mitochondria were resuspended in appropriate buffer and pre-incubated at 37 °C prior to the addition of radiolabelled preCLPP to initiate the import reaction. To stop import at the indicated times, the membrane potential ($\Delta\psi$) was dissipated by the

addition of valinomycin. Washed mitochondria were then resolved by SDS-PAGE and radiolabelled CLPP was visualised by autoradiography (Figure 5.3).

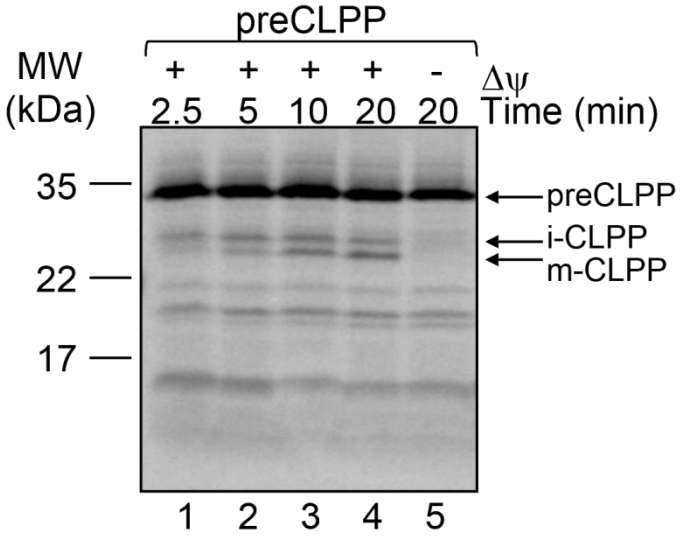


**Figure 5.3:** Import of wild-type preCLPP into isolated HeLa mitochondria in the presence (lanes 1-4) and absence (lane 5) of a membrane potential (Δψ). Protein samples were separated via 12.5% glycine-buffered SDS-PAGE and visualised by autoradiography. Precursor protein (preCLPP) is initially processed into an intermediate species (i-CLPP) before being processed further into the mature form (m-CLPP).

Consistent with successful import and 2-step processing of CLPP, 2 radiolabelled bands appeared in a time-dependent fashion. Initially, a ~27 kDa intermediate form of CLPP (i-CLPP) appeared at 2.5 min (Figure 5.3, lane 1). Following this, a second radiolabelled band appeared (~26 kDa) which represents the mature form of CLPP (m-CLPP) (Figure 5.3, lane 4). Import and processing was dependent on a membrane potential (+Δψ) as no intermediate or mature forms of CLPP were observed in depolarised mitochondria (Figure 5.3, lane 5). Unfortunately, attempts to remove unimported preCLPP from the surface of mitochondria through the addition of Proteinase K or Trypsin were unsuccessful as this resulted in the appearance of non-specific radioactive species which migrated at the same molecular weight as m-CLPP (Appendix 5, Supplementary Figure 1).

To generate the Perrault syndrome-causing mutations in preCLPP, site-directed mutagenesis was performed on cDNA coding for preCLPP using specific primers (see Appendix 1, Table 1). The presence of the mutations was confirmed by DNA sequencing. Radiolabelled preCLPP (wild-type and mutants) was prepared as above and added to isolated HeLa mitochondria to monitor the import and maturation of each CLPP variant in an import reaction (Figure 5.4). Compared to wild-type preCLPP, all mutants displayed similar import and processing capacity (Figure 5.4, lanes 2, 5, 8 and 11), with the intermediate species (i-CLPP) forming after 5 min before a second processing event resulted in the appearance of mature CLPP (m-CLPP) by 20 min. Surprisingly, the migration of preCLPP$^{Y229D}$ and its processed forms was slightly retarded (Figure 5.4, lanes 10-12) in comparison to wild-type CLPP, possibly due to the change in charge of the mutant protein.

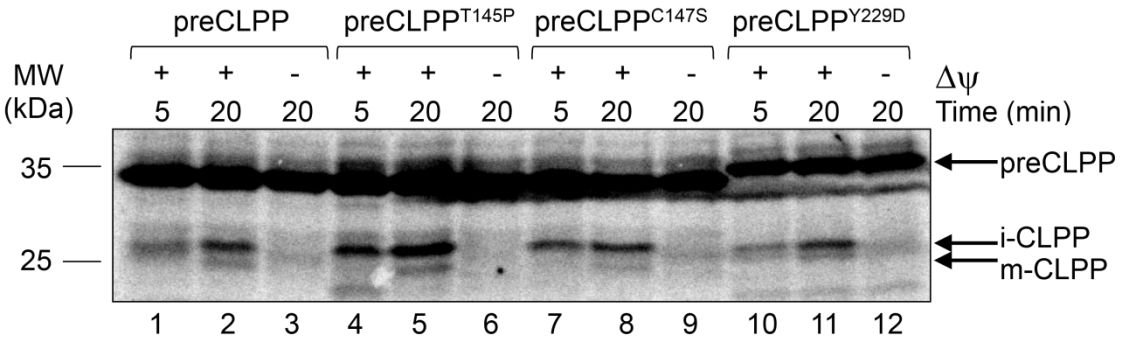


**Figure 5.4:** Import of radiolabelled preCLPP (wild-type and PRLTS3 mutants) into isolated HeLa mitochondria. The import of wild-type preCLPP (lanes 1-3), preCLPP$^{T145P}$ (lanes 4-6), preCLPP$^{C147S}$ (lanes 7-9) and preCLPP$^{Y229D}$ (lanes 10-12) was monitored in the presence and absence of a membrane potential (Δψ). Proteins were separated by 12.5% glycine-buffered SDS-PAGE and visualised by autoradiography.

Next, to monitor assembly of each CLPP variant, following import (20 min), the samples were solubilised in DDM (1% (w/v)) and the radiolabelled proteins were separated by 5-16.5% Blue Native (BN)-PAGE and visualised by autoradiography (Figure 5.5). Recombinant mature Thr53-CLPP (CLPP), purified as described in Section 2.3.4 and 2.3.5, was also examined by BN-PAGE and visualised by staining with Coomassie Brilliant Blue.

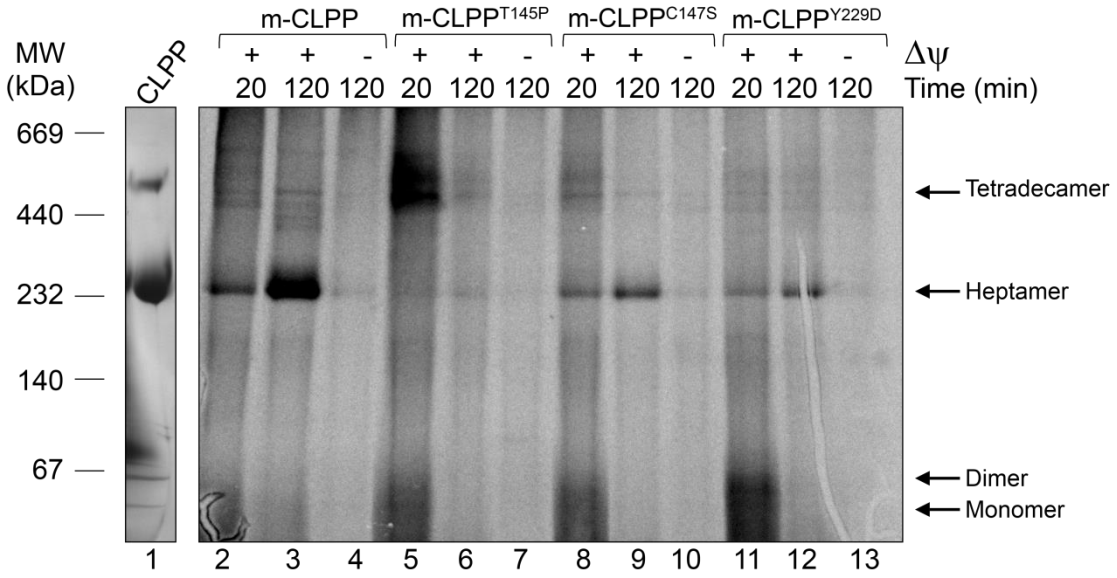


**Figure 5.5:** Import of radiolabelled preCLPP (wild-type and mutants) into isolated HeLa mitochondria. The import and assembly of radiolabelled wild-type CLPP (lanes 2-4), CLPP$^{T145P}$ (lanes 5-7), CLPP$^{C147S}$ (lanes 8-10) and CLPP$^{Y229D}$ (lanes 11-13) was monitored in the presence or absence of a membrane potential (Δψ). Protein complexes were separated by 5-16.5% BN-PAGE. Lane 1 contains 20 µg of recombinant CLPP stained with Coomassie Brilliant Blue. Lanes 2-13 contain ~75 µg solubilised mitochondrial lysate analysed via autoradiography. The different complexes observed, and their predicted configurations, are indicated by arrows.

Interestingly, wild-type recombinant CLPP migrated as two separate bands on BN-PAGE (Figure 5.5, lane 1) which based on the molecular weight markers, suggests the formation of both heptamers and tetradecamers and is consistent with the findings by Fischer et al. (2015). Following import (20 min), wild-type CLPP formed heptamers (~232 kDa, Figure 5.5, lane 2) which increased in intensity over time and

resulted in the formation a small amount of tetradecamer (~500 kDa). Importantly, both species were dependent on a membrane potential (Figure 5.5, compare lanes 3 and 4) demonstrating that they are forming within mitochondria. Interestingly, no heptamers were observed for CLPP$^{T145P}$ although there was evidence of possible tetradecamer formation after 20 minutes which dissipated with time (Figure 5.5, lanes 5-6). In contrast, both CLPP$^{C147S}$ and CLPP$^{Y229D}$ formed heptamers and tetradecamers similar to wild-type CLPP however the levels of these larger complexes were substantially reduced.

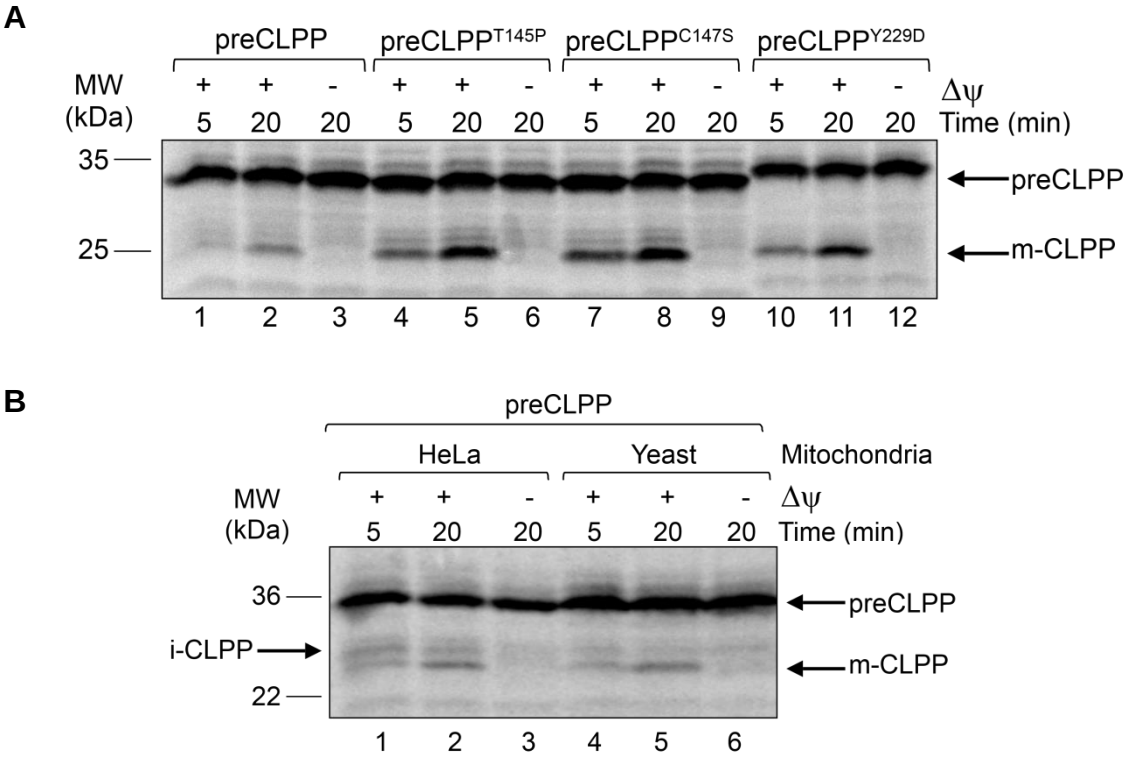


**Figure 5.6:** Import of radiolabelled human preCLPP into mitochondria isolated from *S. cerevisiae*. **A**, The import of wild-type preCLPP (lanes 1-3), preCLPP$^{T145P}$ (lanes 4-6), preCLPP$^{C147S}$ (lanes 7-9) and preCLPP$^{Y229D}$ (lanes 10-12) was monitored in the presence or absence of a membrane potential (Δψ). Proteins were separated by 12.5% glycine-buffered SDS-PAGE and visualised by autoradiography. **B**, import of wild-type preCLPP into isolated HeLa (lane 1-3) and *S. cerevisiae* (yeast) mitochondria (lanes 4-6) at 37 °C and 25 °C respectively in the presence or absence of a membrane potential (Δψ). Proteins were separated via 12.5% glycine-buffered SDS-PAGE and visualised via autoradiography.

Next, to eliminate the possibility that endogenous CLPP in HeLa mitochondria was forming mixed oligomers with the newly imported radiolabelled mutant CLPP and artificially creating stable complexes that would not exist in patients with homozygous *CLPP* mutations, mitochondria were isolated from *S. cerevisiae* (which lacks a CLPP homologue) and used in subsequent import reactions.

Similar to import into HeLa mitochondria, wild-type preCLPP was processed to a ~25 kDa species after 5 min (Figure 5.6A, lane 1), although there was no evidence of an intermediate processing event. The single processed radiolabelled species increased in intensity over time and is denoted as the mature form of CLPP (m-CLPP). Import and processing of CLPP was dependent on a membrane potential (+Δψ) as no processing was observed in depolarised mitochondria (Figure 5.6A, lane 3). Similar to wild-type, all three mutants were processed to m-CLPP (Figure 5.6A, compare lanes 2, 5, 8 and 11). To ensure that CLPP was correctly processed in yeast mitochondria, the processing of wild-type CLPP was directly compared following import into isolated HeLa and yeast mitochondria (Figure 5.6B). Consistent with correct processing in yeast mitochondria, CLPP migrated with the same molecular weight in both HeLa and yeast mitochondria (Figure 5.6B, compare lanes 2 and 5).

Next, the assembly of hCLPP was examined in yeast mitochondria. However, despite successful import and processing of CLPP in yeast mitochondria, assembly of CLPP was not observed (data not shown).

To examine the stability of CLPP after import, the half-life of radiolabelled CLPP was monitored in an import-chase reaction (outlined in Figure 5.7A). Due to the absence of CLPP oligomers forming in yeast mitochondria after import, the stability was not examined in this system and was instead monitored in isolated HeLa mitochondria. Following import (20 min), mitochondria were incubated at 37 °C and the levels of radiolabelled CLPP monitored over a 3 h chase period (Figure 5.7B). Consistent with Figure 5.4, two forms of CLPP (i-CLPP and m-CLPP) were observed after import (Figure 5.7B, lanes 1, 4, 7 and 10). In order to

determine the overall stability of each CLPP variant, both imported species (i- and m-CLPP) were quantitated (Figure 5.7C). Although wild-type CLPP was stable throughout the 3 h chase (Figure 5.7C, red circles), all three mutants exhibited reduced stability (Figure 5.7C).

As the formation of oligomers was previously observed with recombinant wild-type CLPP (Figure 5.5), the stability of each CLPP variant was examined in a cell-free assay using purified recombinant protein. Similar to wild-type CLPP, all CLPP mutants were expressed in BL21(DE3)-CodonPlus-RIL *E. coli* strain as an N-terminal $His_6$-Ub fusion protein. Following preliminary expression and purification trials, significant amounts of DnaK were seen to specifically co-purify with $CLPP^{T145P}$ indicating that this protein may be partially misfolded. To eliminate the co-purification of DnaK, the expression of $CLPP^{T145P}$ was performed in Δ*dnaK E. coli* strain (EN2) (Ratelade et al., 2009). Following expression of wild-type and mutant CLPP fusion proteins (in the appropriate *E. coli* strain, see Appendix 1, Table 2), $His_6$-Ub-CLPP was purified via IMAC and the $His_6$-Ub tag cleaved from CLPP using the deubiquitinating enzyme Usp2cc (Catanzariti et al., 2004). Authentic CLPP (starting at Thr53) was then isolated from the free $His_6$-Ub tag by reverse IMAC. In the case of $CLPP^{T145P}$, this protein was subjected to a further purification step (anion exchange chromatography) (Appendix 5, Supplementary Figure 2). The relative purity of each recombinant protein was determined after separation by SDS-PAGE and staining with Coomassie Brilliant Blue (Figure 5.8). Despite removal of DnaK, $CLPP^{T145P}$ (Figure 5.8, lane 2) still contained two major impurities compared to the other CLPPs. Based on the molecular weight, the major contaminants were speculated to be the *E. coli* molecular chaperonin GroEL (~60 kDa) and uncleaved $His_6$-Ub-CLPP (~38 kDa).

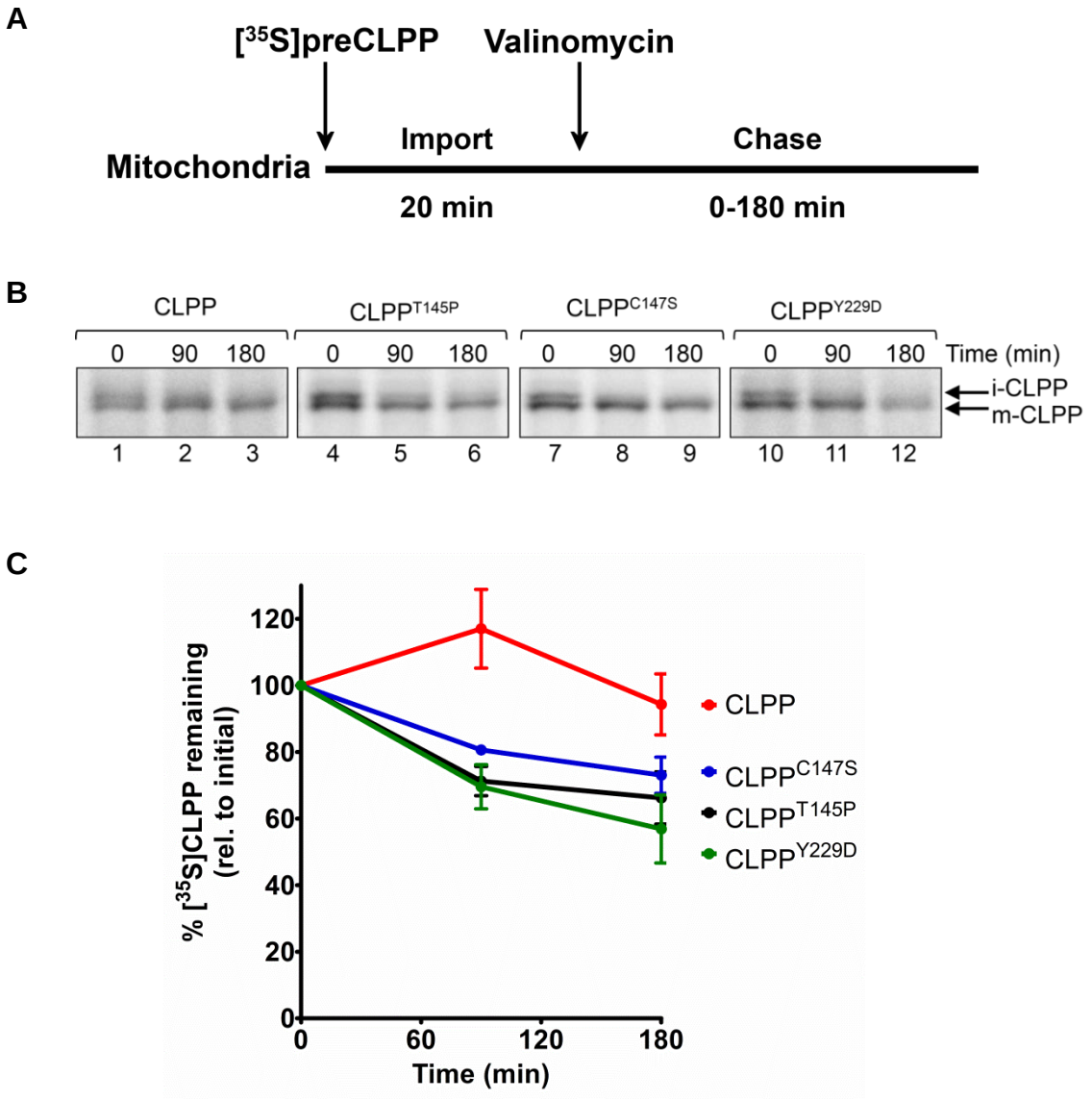


**Figure 5.7:** The level of each CLPP mutant variant decreases after import into isolated HeLa mitochondria. **A**, Outline of the experimental procedure used in an import-chase assay **B**, The stability of radiolabelled wild-type CLPP (lanes 1-3), CLPP$^{T145P}$ (lanes 4-6), CLPP$^{C147S}$ (lanes 7-9) and CLPP$^{Y229D}$ (lanes 10-12) was monitored over 3 h. Proteins were separated by 16.5% Tricine-buffered SDS-PAGE and visualised via autoradiography. **C**, Both imported species (m-CLPP and i-CLPP) were quantitated from wild-type CLPP (red line), CLPP$^{T145P}$ (black line), CLPP$^{C147S}$ (blue line) or CLPP$^{Y229D}$ (green line) by densitometry of the autoradiography image from three separate experiments (error bars represent SEM).

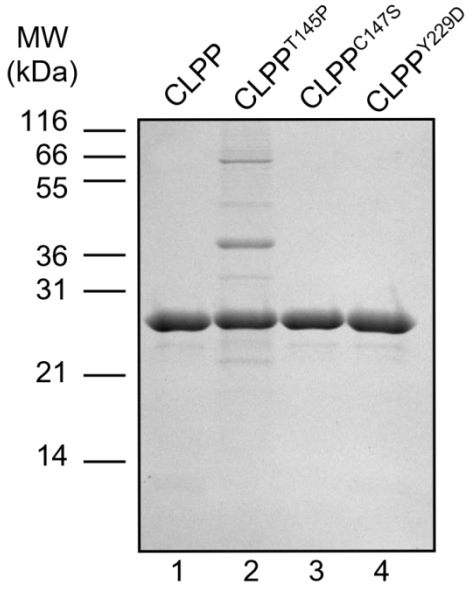


**Figure 5.8:** Relative purity of recombinant wild-type and mutant CLPP variants used in this study. Proteins (2 µg) were separated by 16.5% Tricine-buffered SDS-PAGE and visualised by staining with Coomassie Brilliant Blue.

While it may not replicate physiological conditions entirely, examining the half-life of each CLPP variant *in vitro* would determine the stability of each CLPP without the potential for the formation of mixed oligomers. As LONM has been reported to recognise and degrade a wide range of native substrates *in vitro* (Bezawork-Geleta et al., 2015; Bezawork-Geleta et al., 2014; Bota & Davies, 2002; Granot et al., 2007a; Ondrovičová et al., 2005), it was chosen as a 'model' protease to investigate CLPP stability. The turnover of each recombinant CLPP was monitored in the presence of recombinant LONM in an *in vitro* degradation assay (Appendix 5, Supplementary Figure 3). Wild-type CLPP was stable throughout the time course (t½ >2 h), presumably due to its capacity to form a stable heptamer or tetradecamer. Similar to wild-type, CLPP$^{C147S}$ was resistant to LONM-mediated degradation (t½ ~2 h), indicating stable assembly of this mutant. In contrast, both CLPP$^{T145P}$ and CLPP$^{Y229D}$ were susceptible to LONM-mediated degradation (t½ <15 min), suggesting these CLPP variants were misfolded or lack the capacity to assemble into a stable complex like wild-type CLPP (Appendix 5, Supplementary Figure 3).

### 5.2.2 Analysing oligomerisation of recombinant PRLTS3 CLPP mutants *in vitro*

To directly examine assembly of wild-type and mutant CLPP into higher order oligomeric complexes, glutaraldehyde crosslinking was performed. Protein samples were monitored before and after the addition of glutaraldehyde. Cross-linked proteins were then separated by SDS-PAGE and visualised via staining with Coomassie Brilliant Blue (Figure 5.9).

For wild-type CLPP, seven distinct bands could be observed by 30 min (Figure 5.9, lane 3) which represent the assembly intermediates between a monomer and a heptamer. Similar to wild-type CLPP, CLPP$^{C147S}$ and CLPP$^{Y229D}$ also displayed seven individual species of increasing molecular weight indicating that both these mutants were able to form heptamers. In contrast, CLPP$^{T145P}$ appeared to only form dimers which then rapidly cross-linked to form a very high molecular weight species (Figure 5.9, lanes 5 and 6), indicating possible aggregation. It was likely that the contaminating proteins co-purifying with CLPP$^{T145P}$ (Figure 5.8, lane 2) also interfered with the crosslinking reaction and contributed to this high molecular weight species.

Next, the assembly of recombinant wild-type and mutant CLPP proteins was examined under native conditions using BN-PAGE (Figure 5.10). Consistent with the previous experiment (Figure 5.5, lane 1), wild-type CLPP predominantly migrated as two separate bands (heptamers and tetradecamers) on BN-PAGE (Figure 5.10, lane 2). Similar to wild-type CLPP, CLPP$^{C147S}$ and CLPP$^{Y229D}$ formed both of these species (Figure 5.10, lanes 4 and 5) although only a very small amount of the tetradecamer was observed for CLPP$^{Y229D}$ (Figure 5.10, lane 5). Other smaller species representing possible monomers or dimers of CLPP were also observed for wild-type CLPP, CLPP$^{C147S}$ and CLPP$^{Y229D}$ (Figure 5.10, indicated by arrows). In contrast, and consistent with the glutaraldehyde crosslinking, CLPP$^{T145P}$ formed a lower molecular weight species (~170 kDa) while the majority of the protein remained in the loading well, possibly due to aggregation (Figure 5.10, lane 3). The 170 kDa species

may be an assembly intermediate of CLPP or could be formed by interactions with or between the proteins co-purifying with CLPP$^{T145P}$ (as in Figure 5.8, lane 2).

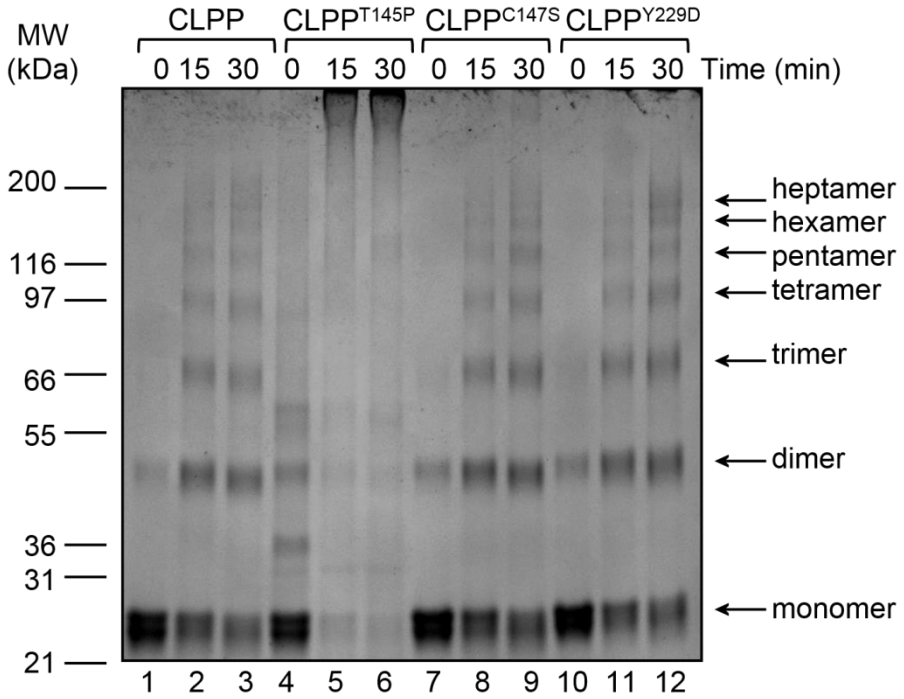


**Figure 5.9:** Assembly of recombinant CLPPs analysed by glutaraldehyde crosslinking. Glutaraldehyde (0.1% (v/v)) was incubated with 50 µg wild-type CLPP (lanes 1-3), CLPP$^{T145P}$ (lanes 4-6), CLPP$^{C147S}$ (lanes 7-9) or CLPP$^{Y229D}$ (lanes 10-12) at 25 °C. Samples were separated by 5-12.5% MES-buffered SDS-PAGE and visualised by staining with Coomassie Brilliant Blue.

To further characterise the oligomeric state of the mutant CLPP variants, size exclusion chromatography (SEC) was performed (Figure 5.11). Consistent with the band observed during BN-PAGE (Figure 5.10), wild-type CLPP eluted at a theoretical molecular weight ~500 kDa (Figure 5.11A, red line), indicative of tetradecamer formation. Interestingly, no heptamer formation was observed. Similar to wild-type, CLPP$^{C147S}$ (Figure 5.11A, blue line) also eluted in a single peak ~500 kDa. In contrast to wild-type, CLPP$^{Y229D}$ eluted later (~61 ml) forming a ~200 kDa species (Figure 5.11A, green line) which was consistent with the heptamer band observed during BN-PAGE for this mutant (Figure 5.10, lane 5). Consistent with both the BN-PAGE (Figure 5.10, lane 3) and

glutaraldehyde crosslinking (Figure 5.9, lanes 4-6), much of CLPP$^{T145P}$ eluted as either a small molecular weight peak (~170 kDa) or as a larger, potentially misfolded, species (Figure 5.11A, black line). Surprisingly, elution of this peak after the void volume ($V_0$), indicated this species may not be aggregated or insoluble.

Next, to better define the molecular weight of the CLPP oligomers observed on BN-PAGE (Figure 5.10) and size exclusion chromatography (Figure 5.11), wild-type CLPP, CLPP$^{C147S}$ and CLPP$^{Y229D}$ were subjected to analytical ultracentrifugation (AUC) (Section 2.4.5). Due to the low yield and contaminating proteins, CLPP$^{T145P}$ was excluded from this particular examination.

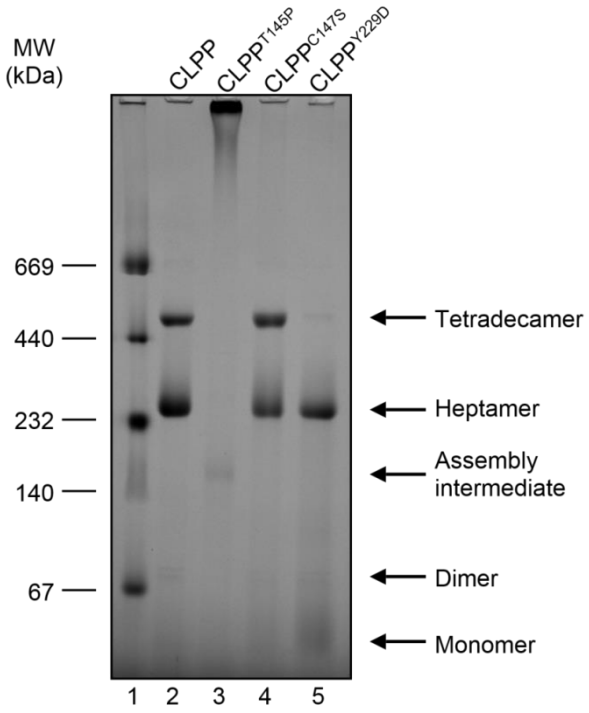


**Figure 5.10:** Assembly of wild-type and mutant CLPPs under native conditions. Recombinant CLPP (4 μg) were separated by BN-PAGE (4-16.5% NativePAGE) and visualised by staining with Coomassie Brilliant Blue. Lane 1: Native molecular weight markers. The different oligomeric species are indicated by arrows.

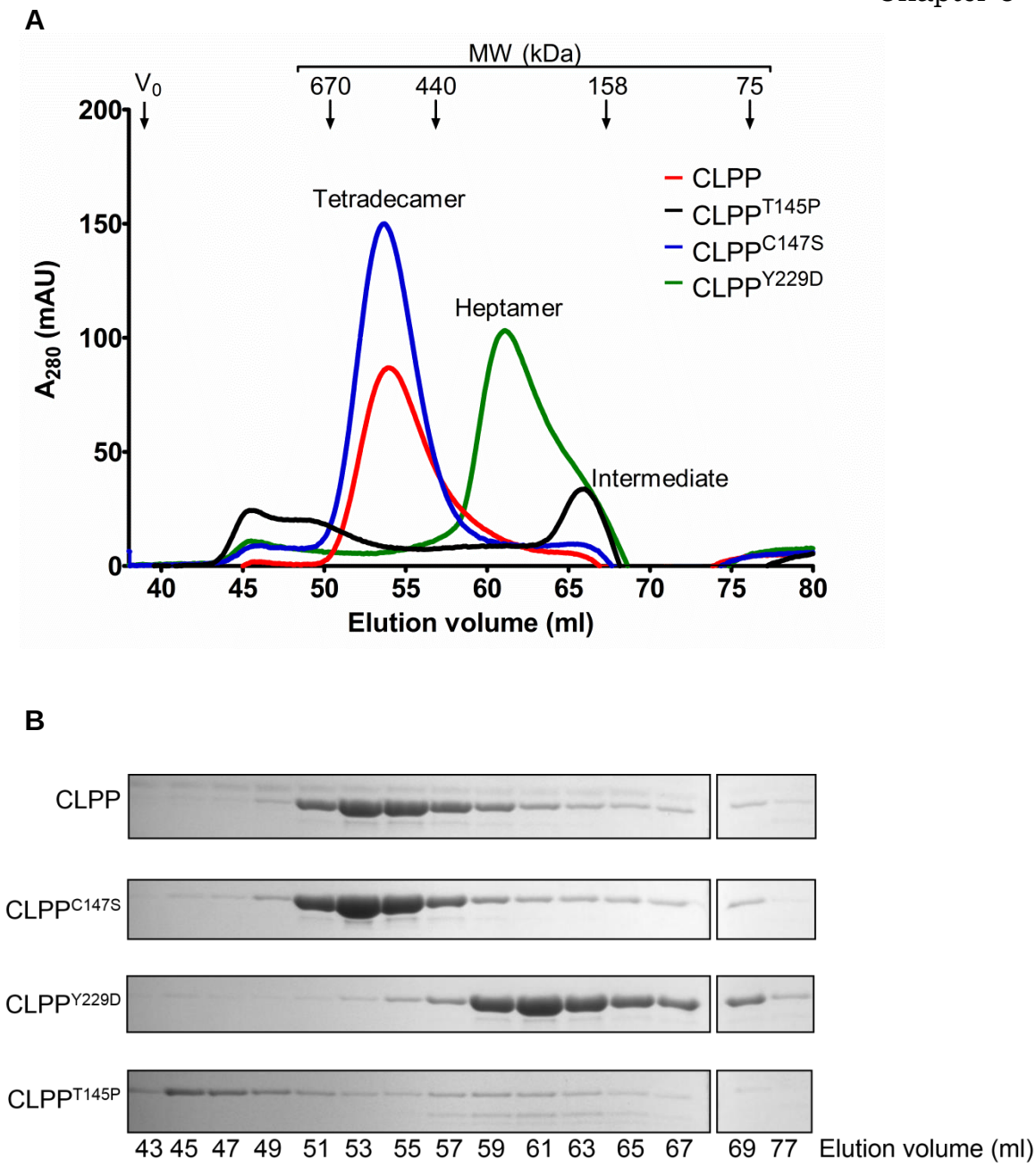


**Figure 5.11:** Size exclusion chromatography (SEC) of wild-type and mutant CLPPs. **A**, Elution profiles of wild-type CLPP (red line), CLPP$^{C147S}$ (blue line), CLPP$^{Y229D}$ (green line) and CLPP$^{T145P}$ (black line) separated using a Superdex 200 SEC column. The protein absorbance was measured at 280 nm ($A_{280}$). Arrows indicate the peak elution volume of Blue Dextran (void volume, $V_0$), thyroglobulin (670 kDa), ferritin (440 kDa), aldolase (158 kDa) and conalbumin (75 kDa). The predicted oligomeric state of each peak is also indicated. 3 mg of each wild-type CLPP, CLPP$^{C147S}$ and CLPP$^{Y229D}$ and 0.3 mg of CLPP$^{T145P}$ was applied to the column. **B**, Proteins from the indicated fractions were separated by SDS-PAGE and visualised by staining with Coomassie Brilliant Blue.

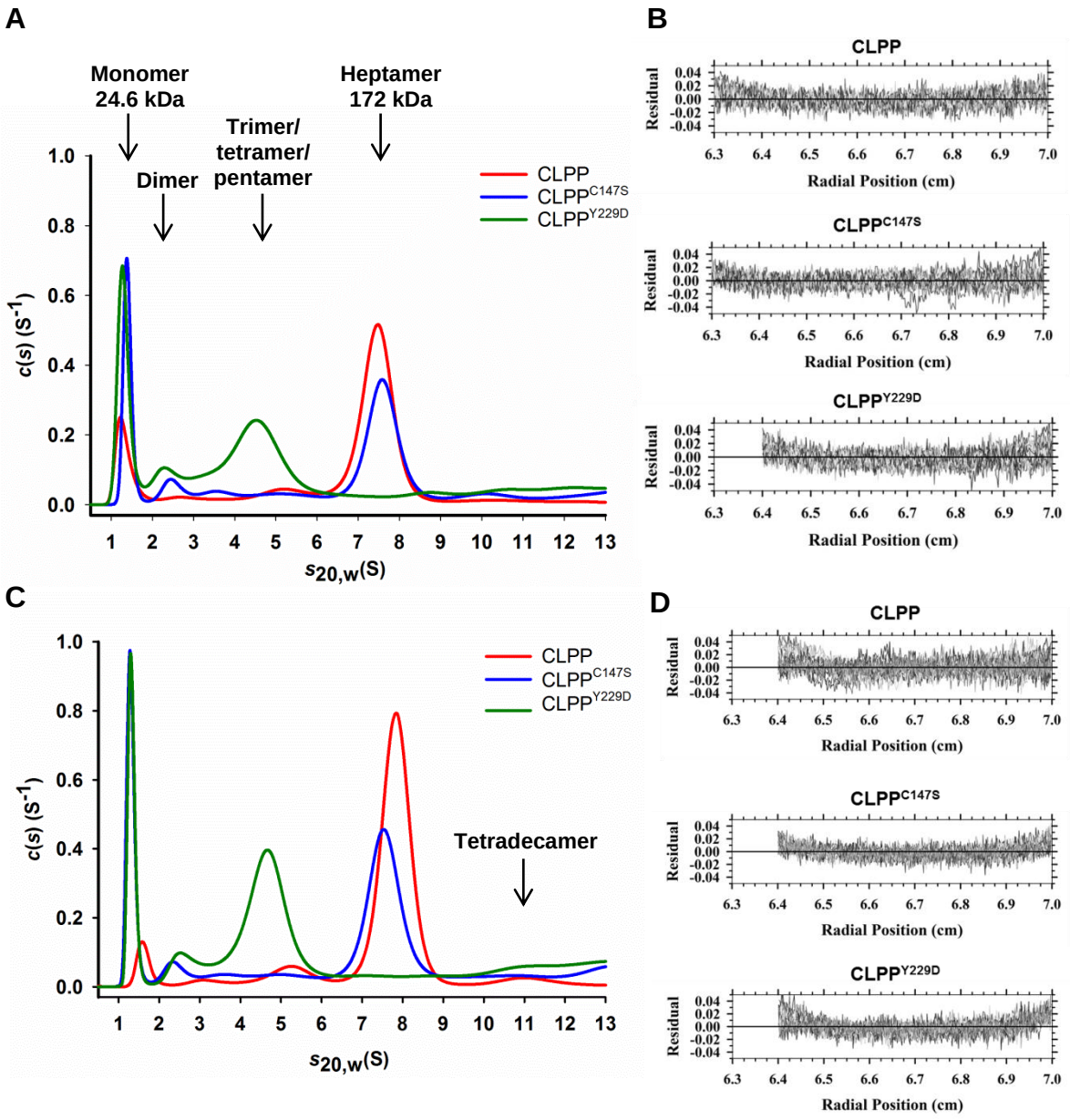


**Figure 5.12:** Sedimentation velocity experiments of wild-type CLPP, CLPP$^{C147S}$ and CLPP$^{Y229D}$ at 0.9 and 1.2 mg/ml (20 °C). **A** and **C**, Distribution c(s) of each species vs sedimentation coefficient $^{S}20$ in Svedberg units (S) at 0.9 mg/ml and 1.2 mg/ml respectively. The oligomeric state and the calculated molecular weight for the major peaks of wild-type CLPP (red line), CLPP$^{C147S}$ (blue line) and CLPP$^{Y229D}$ (green line) are indicated. **B** and **D**, residuals of each CLPP sample at 0.9 mg/ml and 1.2 mg/ml respectively, showing <0.05 absorbance deviation from the global fits. Refer to materials and methods for specific details.

The sedimentation coefficient(s) of each CLPP protein was determined at different concentrations (Figure 5.12). At a concentration of 0.9 mg/ml (Figure 5.12A, red line), wild-type CLPP existed as two species, the predominant species had a sedimentation coefficient of 7.8 S (~170 kDa), while the minor species had a smaller sedimentation coefficient of 1.7 S (~25 kDa). The 7.8 S peak was consistent with heptamer formation while the 1.5 S peak was consistent with a monomer. Additionally, a small, broad peak (~5.4 S) was also observed for wild-type CLPP, indicative of a tetramer/pentamer equilibrium (average MW ~112 kDa). At the higher concentration (1.2 mg/ml), the amount of the 1.7 S species decreased while the size of the larger molecular weight peaks (5.4 S and 7.8 S) increased, indicating that the oligomerisation of CLPP was concentration dependent (Figure 5.12C, red line). Evidence of another broad peak (~11 S) was also observed at 1.2 mg/ml, suggestive of a tetradecamer.

Similar to wild-type CLPP, CLPP$^{C147S}$ formed two species, a 7.6 S species (indicative of a heptamer) and a 1.5 S monomeric species (Figure 5.12A, blue line) although the relative amounts of monomer and heptamer was different to wild-type. In addition to the heptamer and monomer, CLPP$^{C147S}$ also formed a 2.3 S species which was indicative of a dimer. Interestingly, at the higher concentration, the 7.6 S (heptamer) peak of CLPP$^{C147S}$ did not follow the same increase as observed for wild-type CLPP (Figure 5.12C, blue line), rather the 1.5 S (monomer) peak increased, suggesting that CLPP$^{C147S}$ does not favour heptamer formation. Similar to CLPP$^{C147S}$, CLPP$^{Y229D}$ also formed a 1.3 S monomeric species and a 2.5 S dimeric species however no evidence of heptamer formation was observed at either concentration (Figure 5.12A and C, green line). Instead, a broad peak (~4.5 S) was also observed for CLPP$^{Y229D}$, which was indicative of a rapid equilibrium between trimer and pentamer. Similar to CLPP$^{C147S}$, the assembly of CLPP$^{Y229D}$ is likely to be impaired as both the broad peak (~4.5 S) and the monomeric peak (1.3 S) of CLPP$^{Y229D}$ increased at the higher concentration (1.2 mg/ml) (Figure 5.12C, green line) whilst heptamer formation was not observed.

### 5.2.3 Investigating peptidase activity of PRLTS3 CLPP mutants

Similar to ecCLPP, hCLPP retains the ability to degrade small peptide substrates in the absence of its cognate unfoldase, although this activity is considerably reduced compared to ecClpP (Corydon et al., 1998). To determine the effect of each mutation on the peptidase activity of CLPP, the cleavage of model peptide N-Suc-Leu-Tyr linked to chromophore 7-Amino-4-methylcoumarin (AMC) was monitored (Figure 5.13). As expected, wild-type CLPP had low but measurable peptidase activity towards N-Suc-Leu-Tyr-AMC (Figure 5.13, inset image, red circles). Similar to wild-type, CLPP$^{C147S}$ also demonstrated low peptidase activity (Figure 5.13, inset image, blue circles). However, in contrast to both wild-type CLPP and CLPP$^{C147S}$, no peptidase activity for CLPP$^{Y229D}$ was observed (Figure 5.13, inset image, green circles) indicating this mutant was unable to cleave peptides. Surprisingly, CLPP$^{T145P}$ exhibited a >15-fold increase in peptidase activity (Figure 5.13, black circles). Similar profiles of CLPP$^{T145P}$ "hyper-activation" were also observed with other peptide substrates (Appendix 5, Supplementary Figure 4).

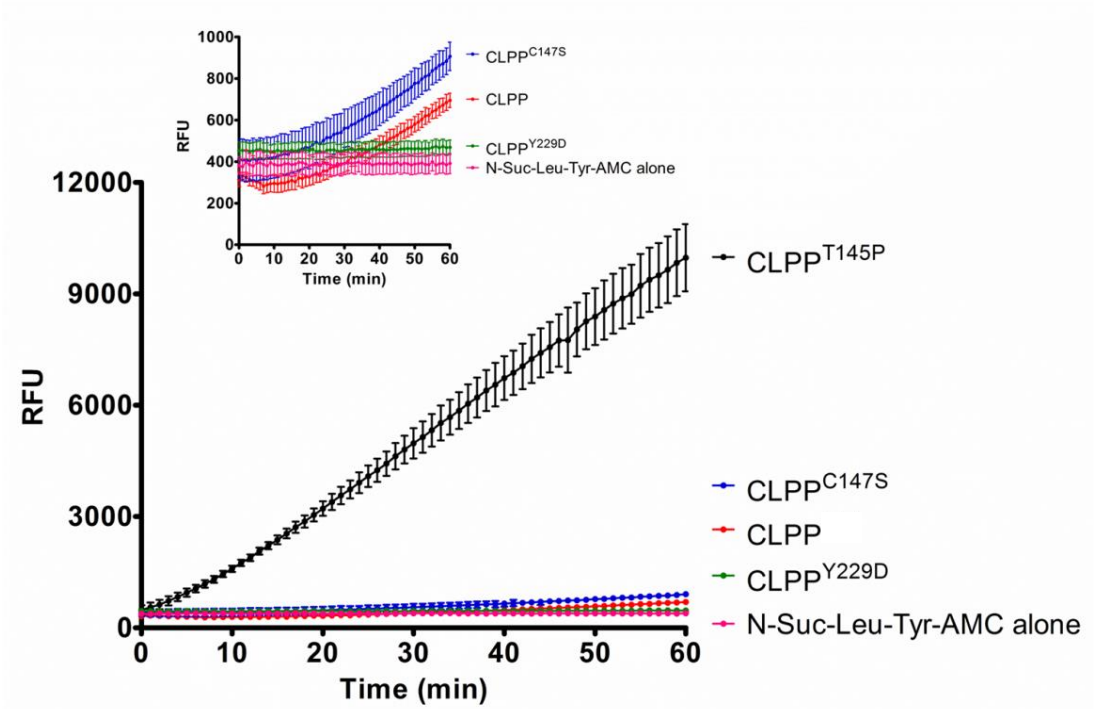


**Figure 5.13:** Peptidase activity of wild-type and mutant CLPP variants. Fluorogenic peptide substrate N-Suc-Leu-Tyr-AMC (1 μM) was combined with CLPP (0.8 μM heptamer) and the peptidase activity of wild-type CLPP (red circles), CLPP$^{T145P}$ (black circles), CLPP$^{C147S}$ (blue circles) or CLPP$^{Y229D}$ (green circles) was monitored over time (n=3, error bars represent SEM). RFU, relative fluorescent units.

### 5.2.4 Determining interaction between CLPX and PRLTS3 CLPP mutants

To determine if the amino acid substitutions in each mutant CLPP affected their ability to interact with CLPX, a series of assays were performed. Initially, the degradation of model unfolded substrate FITC-labelled casein was used to assess hCLPX-hCLPP (hCLPXP) complex formation and activity (Section 2.4.2). As expected, FITC-casein was recognised and degraded in the presence of wild-type CLPP and hCLPX (Figure 5.14, red circles). Similar to wild-type CLPP, CLPP$^{C147S}$ also facilitated the hCLPX-mediated degradation of FITC-casein, albeit at a reduced rate (Figure 5.14, blue circles). In contrast to both wild-type and CLPP$^{C147S}$, neither CLPP$^{T145P}$ (Figure 5.14, black circles) nor CLPP$^{Y229D}$ (Figure 5.14, green circles) were able to mediate the degradation of FITC-casein suggesting that these CLPP variants were not able to interact with hCLPX or were unable to degrade larger protein substrates.

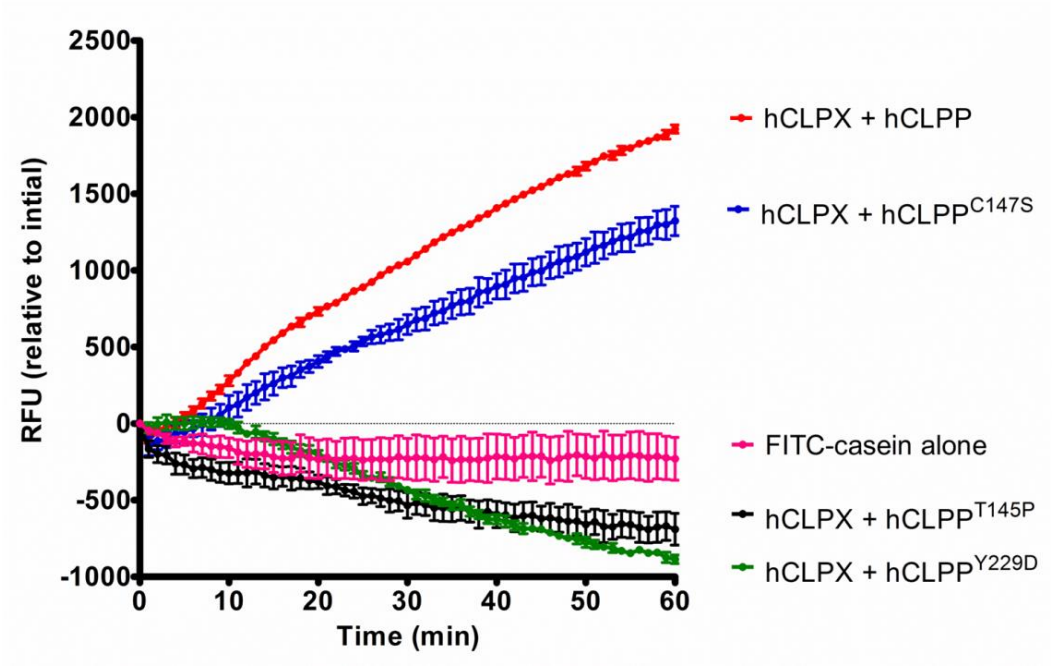


**Figure 5.14:** Protease activity of wild-type and mutant CLPPs toward hCLPX-dependent substrate. FITC-casein (0.3 μM) was added to hCLPX (0.4 μM hexamer) in combination with wild-type CLPP (red circles), CLPP$^{T145P}$ (black circles), CLPP$^{C147S}$ (blue circles) or CLPP$^{Y229D}$ (green circles) (0.8 μM heptamer each) and the degradation was monitored over time, (n=3, error bars represent SEM). RFU, relative fluorescence units.

Next, to examine the interaction of CLPP with hCLPX more directly, a series of immunoprecipitation (IP) experiments were performed (Section 2.4.6). Specifically, hCLPX antisera was immobilised to Protein A Sepharose (PAS) and then incubated with wild-type CLPP, CLPP$^{T145P}$, CLPP$^{C147S}$ or CLPP$^{Y229D}$ in the absence or presence of hCLPX. Following incubation of the protein with the beads and washing off non-specifically bound proteins from the PAS, the eluted protein samples were separated by SDS-PAGE and transferred to PVDF membrane for analysis via immunoblotting (Figure 5.15). Despite some weak non-specific binding of wild-type CLPP with the PAS-immobilised α-CLPX antisera (Figure 5.15A, lane 3), there was a significant increase in the recovery of CLPP in the presence of hCLPX (Figure 5.15A, lane 7 and Figure 5.15C), indicating successful co-IP of hCLPP with hCLPX. Similar to wild-type CLPP, there was little non-specific binding of CLPP$^{C147S}$ to α-CLPX antisera but significant enrichment of CLPP$^{C147S}$ binding was observed in the presence of hCLPX (Figure 5.15A, compare lane 9 with lane 5). In contrast to wild-type CLPP and CLPP$^{C147S}$, neither CLPP$^{T145P}$ nor CLPP$^{Y229D}$ displayed any significant interaction with hCLPX (Figure 5.15C) indicating the lack of CLPX-mediated degradation of FITC-casein by CLPP$^{T145P}$ and CLPP$^{Y229D}$ (Figure 5.14), was due to their lack of interaction with hCLPX.

Finally in an alternate, albeit indirect, approach to examine the interaction between CLPP and an unfoldase, the interaction of hCLPP with ecClpX was monitored via degradation of GFP-SsrA (Figure 5.16). Previously it has been shown that hCLPP can interact with ecClpX to facilitate the degradation of *E. coli* ClpXP substrate GFP-SsrA (Kang et al., 2002). This tag is not recognised by hCLPX and GFP cannot be degraded by CLPP alone (data not shown). As expected, ecClpX-ecClpP recognised and degraded GFP-SsrA, indicated by a loss of fluorescence (Figure 5.16, orange circles). Consistent with published results, wild-type hCLPP facilitated the degradation of GFP-SsrA in the presence of ecClpX (Figure 5.16, red circles). Similar to the results of the FITC-casein

degradation assay (Figure 5.14), hCLPP$^{C147S}$ mediated the degradation of GFP-SsrA similar to wild-type hCLPP (Figure 5.16, blue circles).

Surprisingly, hCLPP$^{T145P}$ also facilitated the degradation of GFP-SsrA (Figure 5.16, black circles), indicating that an active complex formed between hCLPP$^{T145P}$ and ecClpX. This interaction appears to be specific to ecClpX as no previous activity (Figure 5.14, black circles) or interaction (Figure 5.15C, black bar) was detected in the presence of hCLPX. Consistent with the FITC-casein degradation assay (Figure 5.14, green circle) and co-IP (Figure 5.15C, green bar), CLPP$^{Y229D}$ showed no activity towards GFP-SsrA (Figure 5.16, green circles) indicating that impaired oligomerisation of CLPP$^{Y229D}$ also leads to a loss of ClpX-mediated binding and activity.

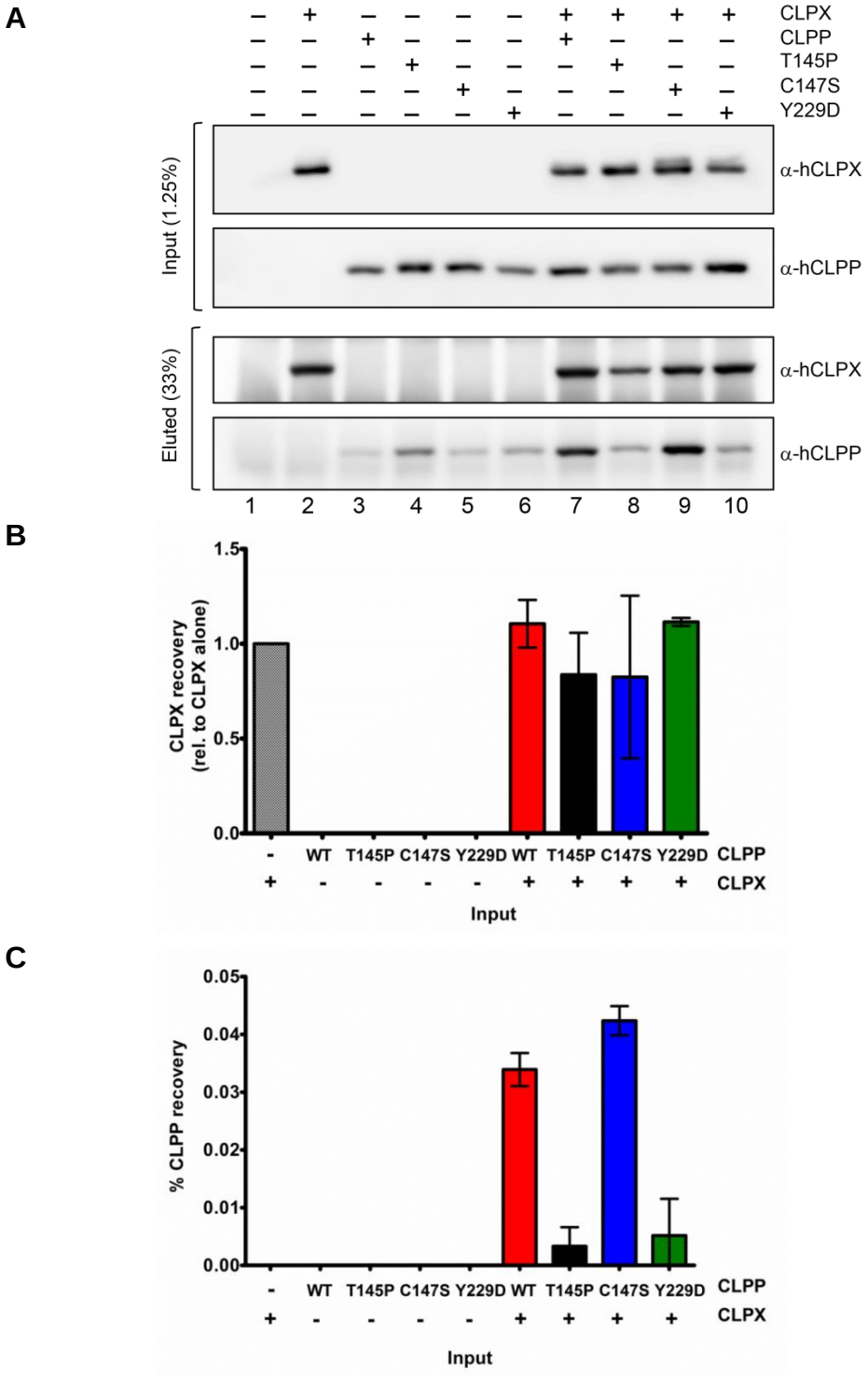


**Figure 5.15:** Co-immunoprecipitation of hCLPP (wild-type and mutants) with hCLPX. **A**, Representative western blot showing input (upper panels) and eluted (lower panels) samples probed with either α-hCLPX or α-hCLPP antisera. Protein mixes comprise CLPX alone (lane 2) and wild-type CLPP (lanes 3 and 7), $CLPP^{T145P}$ (lanes 4 and 8), $CLPP^{C147S}$ (lanes 5 and 9) and $CLPP^{Y229D}$ (lanes 6 and 10) in the absence (lanes 3-6) or presence (lanes 7-10) of hCLPX. **B**, The recovery of hCLPX in each protein mix was determined relative to hCLPX (lane 2) alone. **C**, The recovery of CLPP relative to input (lanes 3-6) of the eluted samples was determined after subtracting respective non-specific binding (CLPP alone) signal. (n=3, error bars represent SEM).

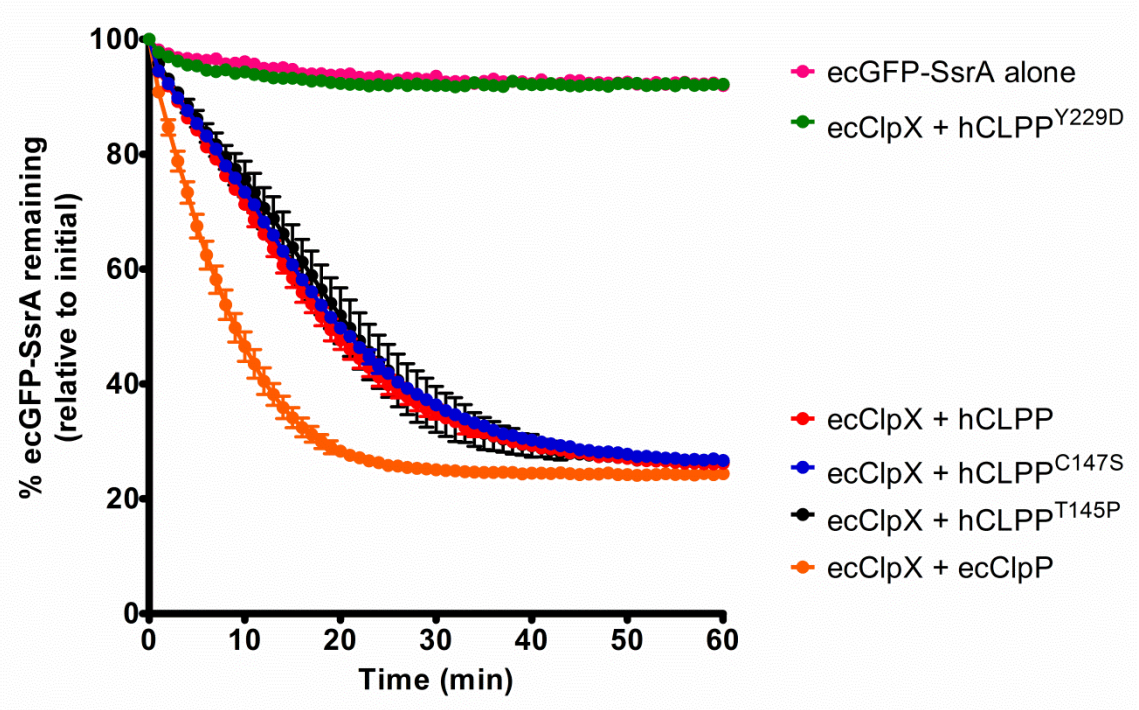


**Figure 5.16:** Protease activity of wild-type and mutant CLPP variants towards ecClpX-dependent substrate. Positive control ecClpP (0.2 µM heptamer) (orange circles) or wild-type hCLPP (red circles), hCLPP$^{T145P}$ (black circles), hCLPP$^{C147S}$ (blue circles) or hCLPP$^{Y229D}$ (green circles) (0.4 µM heptamer each) was combined with ecClpX (0.2 µM hexamer) and GFP-SsrA (1 µM) and the activity was monitored over time, (n=3, error bars represent SEM).

## 5.3 Discussion

The role of CLPP (and CLPX) in mammalian mitochondria is not well understood. *CLPP* null mice (CLPP$^{(-/-)}$) display both female and male infertility and deafness which demonstrates a direct link between mutations of *CLPP* and Perrault syndrome 3. The tissue-specific effects of *CLPP* reduction suggest a vital role of CLPP in these cells that is able to be reasonably tolerated in other tissues. However, it has been demonstrated that CLPP is necessary to prevent mitochondrial dysfunction as reduced growth and cellular respiratory defects are shared between CLPP$^{(-/-)}$ mice and *CLPP*-depleted cultured mammalian cells (Cole et al., 2015; Deepa et al., 2015; Gispert et al., 2013; Greene et al., 2012). While reduced motor activity was a common feature in PRLTS3 patients and *CLPP*$^{(-/-)}$ mice, major neurological impairments

such as epilepsy, microcephaly or learning difficulties were unique to certain PRLTS3 patients indicating a potential gain of toxic function due to the specific mutations in *CLPP*.

In this chapter, the import, maturation, assembly and activity of three PRLTS3 associated CLPP mutants has been determined *in vitro* and the interaction with cognate unfoldase hCLPX has been assessed. Together these data provide a greater understanding of the role of CLPP in the pathogenesis of PRLTS3.

### 5.3.1 Import and processing of each PRLTS3 CLPP mutant is not affected

To determine if reduced CLPP activity in patients with Perrault syndrome was due to impaired import or biogenesis of CLPP in mitochondria, the import and processing for each mutant CLPP variant was compared to wild-type CLPP (Figure 5.4). These data indicate the amino acid substitutions did not abolish the import or maturation of CLPP. In HeLa mitochondria two forms of CLPP (i-CLPP and m-CLPP) were observed which suggest CLPP is processed in two steps.

The processing of wild-type human preCLPP is controversial; Figure 5.2 describes the theoretical and experimentally derived cleavage sites of m-CLPP. Generally, mitochondrial proteins follow the R-2, R-3 or R-10 motif rule in which an arginine residue is located 2, 3 or 10 residues upstream of the scissile bond (Gakh et al., 2002). Surprisingly, the experimentally determined cleavage sites do not follow these rules which suggest that another mechanism may be responsible for generating mature CLPP. Importantly, ecClpP and ClpPs from other organisms are autocatalytically processed (Benaroudj et al., 2011; Maurizi et al., 1990b), so it is reasonable to expect that hCLPP can also undergo autocatalytic processing after import into the mitochondrial matrix. Similar to maturation of the subunits of inner membrane-bound *m*-AAA protease (Koppen et al., 2009), autocatalytic cleavage of CLPP monomers

may occur prior to, or following, assembly into the tertiary structure. hCLPP has been determined to preferentially cleave substrates after hydrophobic residues (Gersch et al., 2015) which is consistent with the experimentally determined cleavage sites (Figure 5.2).

The absence of a two-step processing of hCLPP in yeast mitochondria further suggests that CLPP undergoes an autocatalytic processing step mediated by endogenous CLPP in human cells. However, the molecular weight of m-CLPP generated in HeLa mitochondria was very similar to the single processed form of CLPP generated in yeast mitochondria (Figure 5.6B). It is possible that imported CLPP is immediately auto-processed by itself but this is unlikely as the $CLPP^{Y229D}$ mutant, which demonstrated no catalytic activity *in vitro*, was also processed to the same extent as wild-type CLPP (Figure 5.6A). Alternatively, the difference in processing may result from an altered cleavage specificity of yeast MPP that ultimately results in the formation of the same final m-CLPP species (Figure 5.6B), such as the direct cleavage between Ala55 and Leu56 which is a potential R-2 cleavage site. It would be interesting to examine the maturation of imported preCLPP in mitochondria isolated from a *CLPP* knock-out cell line to determine the requirement of endogenous CLPP in autocatalytic processing.

Of note, in contrast to  results, Corydon et al. (1998) examined the import of precursor hCLPP in isolated rat liver mitochondria and observed only a single form of processed CLPP. However the longer time course of the import (45 min) and the dissimilarity between the species of imported protein and mitochondria may contribute to the lack of i-CLPP observed.

### 5.3.2 Human CLPP exists in multiple oligomeric states

In this study, the assembly of wild-type and mutant CLPP variants was monitored by a variety of different techniques such as cross-linking, SEC, BN-PAGE and AUC. Interestingly, wild-type CLPP was observed to

form two predominant oligomeric states (heptamer and tetradecamer) throughout this study which is conflicting with a previous report that demonstrates hCLPP can only form a stable heptamer in the absence of CLPX (Kang et al., 2005). However, the formation of heptamers and tetradecamers on BN-PAGE (Figure 5.10) is consistent with the previous findings reported by Corydon et al. (1998) and Fischer et al. (2015) who observed hCLPP migrating as two different species on native electrophoresis. The formation of multiple species during AUC (Figure 5.12A and C) is also consistent with data reported by Kimber et al. (2010) who indicated that other peaks (10% of the total) were observed in addition to the major 6.3 S (heptamer) species of hCLPP which suggests the presence of smaller peaks, possibly assembly intermediates.

In this study, in addition to heptamer and tetradecamer formation, other oligomers of CLPP were observed to form during sedimentation velocity experiments (Figure 5.12) and also during BN-PAGE (Figure 5.10) that indicate CLPP regularly forms assembly intermediates between a monomer and heptamer. No other species were observed between the heptamer and tetradecamer which indicates heptamer formation in a prerequisite for tetradecamer formation. In this regard, the lack of multiple peaks formed by wild-type CLPP during SEC is surprising and intriguing (Figure 5.11A). Potentially, the column matrix and system pressure stabilises the assembly of CLPP and supports the formation of tetradecamers (~500 kDa) that was maintained throughout the run. The migration of hCLPP oligomers on SEC was also monitored by Kang et al. (2005) who observed hCLPP eluting at a higher-than-expected molecular weight due to its C-terminal extension which is anticipated to protrude from the globular structure. However, the molecular weight of the complex they reported (~200 kDa) is more consistent with the formation of a heptamer and is considerably smaller than the major peak observed for wild-type CLPP (~500 kDa) in this study (Figure 5.11). The concentration of protein applied to the column in each case may account for these differences and consistently, the sedimentation velocity experiments indicated the formation of tetradecamers is concentration-

dependent (Figure 5.12A and C). Likewise, this may explain the absence of larger molecular weight species (e.g. >200 kDa) observed during glutaraldehyde crosslinking (Figure 5.9) wherein only heptamer formation (~180 kDa) was observed.

Interestingly, after import, radiolabelled wild-type CLPP was observed to assemble into multiple oligomeric species on BN-PAGE (Figure 5.5). The migration of hCLPX on BN-PAGE is significantly impaired (data not shown) which implies that the assembly of CLPP after import, as visualised after separation by BN-PAGE, is likely to be independent of hCLPX. Despite the predominant formation of a heptamer (~232 kDa), wild-type CLPP was also observed to form a small amount of tetradecamer (Figure 5.5), which indicates tetradecamer formation *in vivo* is possible and further supports the hypothesis that CLPX is not essential for the assembly of CLPP tetradecamers.

The absence of hCLPP complexes forming in yeast mitochondria after import (data not shown) would suggest the mature form of CLPP (m-CLPP) (Figure 5.6B) is unable to fold properly or interact with other subunits due to the differences in processing compared to that in HeLa mitochondria (Figure 5.3). However, Kang et al. (2004) examined the effect of N-terminal truncations on CLPP assembly and activity and determined that the assembly was similar to wild-type CLPP in each case which suggests that oligomerisation of m-CLPP is not being prohibited by the different processing in yeast mitochondria. One rationale is that CLPP requires a minimum level of pre-existing CLPP to aid in the assembly and the amount of hCLPP imported and processed into yeast mitochondria was not sufficient enough to act as a platform for CLPP oligomerisation. However, further experimental investigation would be required to verify this.

### 5.3.3 PRLTS3 CLPP mutants display impaired assembly and stability

The assembly of the PRLTS3 mutant variants ($CLPP^{T145P}$, $CLPP^{C147S}$ and $CLPP^{Y229D}$) were monitored alongside wild-type CLPP *in organello* and also *in vitro* (summarised in Table 5.2). After import, similar to wild-type CLPP, all mutants demonstrated the ability to form both heptamers and tetradecamers over the course of the import reaction (Figure 5.5). However, endogenous CLPP may be interacting with radiolabelled CLPP and subsequently influencing the assembly and stability of the CLPP oligomers. The formation of mixed oligomers would explain the differences observed between complex formation of radiolabelled $CLPP^{T145P}$ and $CLPP^{Y229D}$ *in organello* and the assembly of these homogenous CLPP samples *in vitro* (compare Figure 5.5 and 5.10). During assembly *in organello*, a brief yet intense band of $CLPP^{T145P}$ appeared after 20 min that was indicative of a tetradecamer or larger complex (Figure 5.5) but it was absent in the next time point (Figure 5.5). The rapid accumulation of radiolabelled $CLPP^{T145P}$ and the high molecular weight (>500 kDa) would also be consistent with oligomers of $CLPP^{T145P}$ associating with molecular chaperones (e.g. HSP60 or HSP70). As a similar recruitment of chaperones was observed for $CLPP^{T145P}$ *in vitro* (Figure 5.8, lane 2), the association with molecular chaperones *in organello* and *in vivo* would be probable. Additionally, the assembly of mixed oligomers may be protecting the mutant CLPP variants against turnover in the matrix (Figure 5.7C) that would not be true for the homozygous *CLPP* mutations found in the patients with PRLTS3. The inability to fold or form a stable complex *in vivo* may result in a greater susceptibility to proteolytic degradation and result in a loss of CLPP. In support of this, the LONM-mediated turnover of each mutant CLPP variant was increased compared to wild-type CLPP (Appendix 5, Supplementary Figure 3). Examining the assembly and turnover of each CLPP mutant in a *CLPP* knock-out cell line would be useful to determine the likely scenario in mitochondria of patients with PRLTS3.

Under native conditions *in vitro*, the defects in the assembly of each CLPP mutant was more evident. On BN-PAGE (Figure 5.10) and SEC

(Figure 5.11) the assembly of CLPP$^{C147S}$ (heptamer and tetradecamer) was very similar to wild-type CLPP. However, during sedimentation velocity experiments, heptamer and tetradecamer formation did not increase in a concentration-dependent manner for CLPP$^{C147S}$ as it did for wild-type CLPP (Figure 5.12A and C) indicating impaired complex formation. Similarly, on BN-PAGE (Figure 5.10) and SEC (Figure 5.11), CLPP$^{Y229D}$ demonstrated the formation of stable heptamer (~ 232 kDa) but the reduced capacity to form a tetradecamer (Figure 5.10). The sedimentation velocity experiments further revealed impaired oligomerisation for CLPP$^{Y229D}$ as there was no evidence to suggest heptamer formation (Figure 5.12A and C) which indicates CLPP$^{Y229D}$ can only form heptamers if it is artificially stabilised (e.g. via gel matrix during SEC, BN-PAGE or chemical cross-linking). Due to it being aggregation-prone and its inherent instability, the analysis of CLPP$^{T145P}$ assembly is limited. Evidence of a ~170 kDa species was observed on BN-PAGE (Figure 5.10) and SEC (Figure 5.11) which may represent an assembly intermediate (formed with CLPP$^{T145P}$ and/or residual $His_6$-Ub-CLPP$^{T145P}$) or artefactual complex formed via the interaction between CLPP$^{T145P}$ and the contaminating molecular chaperones that it was co-purifying with (e.g. Figure 5.8, lane 2).

### 5.3.4 Correlation between assembly and activity of PRLTS3 CLPP mutants

Stable heptamer formation of CLPP is not only essential for the assembly of a tetradecamer but also for its interaction with hCLPX, and hence the proteolytic activity of the hCLPXP complex. This study has determined that the amino acid substitutions in each CLPP mutant have affected their ability to assemble into a stable heptamer which impacted on their peptidase and protease activity in different ways (summarised in Table 5.2).

**Table 5.2: Summary of the assembly and activity of each PRLTS3 mutant CLPP variant determined in this study and their associated clinical symptoms.**

| CLPP variant | Oligomeric state: | | Peptidase activity (compared to WT) | Interacts with hCLPX | Displays protease activity | | Metabolic stability | | Associated symptoms (in addition to SNHL) |
|---|---|---|---|---|---|---|---|---|---|
| | *in vitro* | *in vivo* | | | h CLPX | ec ClpX | HeLa mito | *in vitro* | |
| Wild-type (WT) | 7mer/ 14mer | 7mer/ 14mer | - | Yes | Yes | Yes | - | >2 h | - |
| T145P | 2mer-5mer | 2mer-5mer | Hyper-activated | No | No | Yes | ↓ | <15 min | Premature ovarian failure (POF), epilepsy, short stature, microce-phaly & moderate learning difficulties. (In some cases, successful pregnancy and uncomplicated birth was achieved prior to developing POF) |
| C147S | 7mer/ 14mer | Less stable 7mer/ 14mer | Similar | Yes | Yes | Yes | ↓ | ~2h | Hypergonadotropic hypogonadism |
| Y229D | ~3-4-5mer (7mer only if stabilised) | ~3-4-5mer | Inactive | No | No | No | ↓ | <15 min | Sudden inability to walk or maintain acquired skills. Inability to speak, spasticity of lower limbs. (hormone testing not conducted in these cases) |

As the position of the amino acid substitution was located next to the hydrophobic pocket, the CLPP$^{C147S}$ mutant was predicted to exhibit impaired interaction with hCLPX (Jenkinson et al., 2013). Surprisingly, compared to wild-type CLPP, a greater recovery of CLPP$^{C147S}$ was demonstrated during the co-IP assays, indicating the interaction with hCLPX was not decreased. Accordingly, CLPP$^{C147S}$ also facilitated the degradation of larger substrates (e.g. FITC-casein and GFP-SsrA) that were delivered via ClpX-mediated recognition and translocation. However, compared to wild-type CLPP, the degradation of FITC-casein was decreased (Figure 5.14) which is consistent with the reduced

capacity of CLPP$^{C147S}$ to form stable heptamers and tetradecamers in solution and indicates hCLPX cannot effectively stabilise CLPP$^{C147S}$ despite their interaction being seemingly unaffected. However, interestingly, CLPP$^{C147S}$ facilitated the ecClpX-mediated degradation of GFP-SsrA in a similar manner to wild-type CLPP indicating ecClpX is able to establish a more stable interaction with CLPP$^{C147S}$ compared to hCLPX.

Compared to wild-type CLPP, the CLPP$^{Y229D}$ mutant exhibited impaired heptamer assembly, no significant interaction with CLPX and no activity towards peptides or larger substrates. While the assembly of native CLPP$^{Y229D}$ heptamers is unlikely to occur *in vivo*, all the experiments monitoring assembly of this mutant *in vitro* indicated heptamer formation was possible for this mutant but only with artificial stabilisation. As the formation of mixed oligomers created *in organello* contributed to the assembly of radiolabelled CLPP$^{Y229D}$ after import (Figure 5.5), mixed oligomer experiments were performed with wild-type CLPP and CLPP$^{Y229D}$ *in vitro* and the resulting peptidase activity of this mixed species was examined (data not shown). Unfortunately, no stimulation of peptidase activity was observed which was consistent with CLPP$^{Y229D}$ being catalytically inactive, or still unable to form heptamers even with the stabilisation by wild-type CLPP. As the location of the amino acid substitution, Tyr229, is close to active site residue Asp227, this mutant was predicted to have impaired catalytic activity (Ahmed et al., 2015). While Tyr229 is not a conserved residue contributing to the conformational stability of the active site (Kang et al., 2005), the data from this study indicate that this residue is not only vital for CLPP activity but contributes to the overall structural conformation of CLPP. Unlike CLPP$^{T145P}$ which also displays structural instability, CLPP$^{Y229D}$ could not form a heptamer even in the presence of human or *E. coli* ClpX. As demonstrated by Kang et al. (2002), catalytic activity of CLPP is not a pre-requisite for maintaining heptamer formation. Active site mutants of CLPP can still form a complex with ClpX and can also be used to 'trap' substrates translocated by ClpX such as GFP-SsrA, which

is indicated by a fluctuation of GFP fluorescence (Kang et al., 2002). In the case of CLPP$^{Y229D}$, no variation of fluorescence was observed in the GFP-SsrA degradation assay to indicate translocation and release of GFP-SsrA (Figure 5.16), nor was there detectable activity towards any of the peptide substrates tested (Figure 5.13 and Appendix 5, Supplementary Figure 4) or FITC-casein (Figure 5.14) which together signifies CLPP$^{Y229D}$ was not active due to impaired heptamer formation. Further investigation is required to determine whether the catalytic activity of CLPP$^{Y229D}$ could be restored if the assembly was stabilised (e.g. with a reducible cross-linker or mutational analysis).

In contrast to CLPP$^{Y229D}$, CLPP$^{T145P}$ displayed impaired assembly but retained peptidase and protease activity. Despite no indication of proper heptamer assembly during glutaraldehyde cross-linking, BN-PAGE or SEC, the CLPP$^{T145P}$-mediated degradation of GFP-SsrA indicated heptamer (and tetradecamer) formation was possible for this mutant. Mutational studies on the IGF loops of ecClpX demonstrate that all the subunits must interact with ecClpP for maximal protein degradation (Martin et al., 2007). Compared to wild-type CLPP, the degradation of GFP-SsrA by CLPP$^{T145P}$ was similar (Figure 5.16, compare red and black dots), suggesting that the assembly and oligomeric state of CLPP$^{T145P}$ must also be equivalent to wild-type under the conditions tested. The difference in activity towards GFP-SsrA compared to FITC-casein is presumably due to the variation in the unfoldase. ecClpX shares 41% identity with hCLPX with one of the major difference being the interacting IGF loop (LGF in hCLPX) which binds to the hydrophobic pockets on CLPP (Lowth et al., 2012; Martin et al., 2008). Like CLPP$^{C147S}$, the location of amino acid substitution in CLPP$^{T145P}$ is located around the hydrophobic pocket and consequently this mutant was predicted to have impaired interaction with CLPX (Jenkinson et al., 2013). While the interaction with hCLPX was indeed diminished, the interaction with ecClpX was remarkably unaffected. A similar result was recently reported by Gersch et al. (2015) who investigated the activity of CLPP$^{C147S}$ and CLPP$^{T145P}$ in the presence of ecClpX (but not hCLPX). In

contrast, the peptidase activity of CLPP$^{T145P}$ was reported to be only 60% of wild-type CLPP activity with an optimised substrate (Ac-Phe(3,4-$Cl_2$)-hArg-Leu-ACC) which is conflicting with the 'hyper' CLPP$^{T145P}$ peptidase activity observed in this study (Figure 5.13 and Supplementary Figure 4, black circles). Yet consistently, CLPP$^{C147S}$ displayed similar peptidase activity to wild-type CLPP (Gersch et al., 2015). Perhaps the increased specificity of wild-type CLPP towards the optimised substrate, compared to N-Suc-Leu-Tyr-AMC, would cause the negative effects of the amino acid substitutions in the mutant CLPPs to be made more apparent. Alternatively, the different methods used to generate recombinant CLPP$^{T145P}$ *in vitro*, (e.g. authentic CLPP compared to CLPP fused with a C-terminal StrepII tag), may influence the assembly or activity of CLPP$^{T145P}$ while the interaction with ecClpX is maintained.

The oligomeric state of CLPP$^{T145P}$ which was contributing to the observed 'hyper' peptidase activity compared to wild-type CLPP (Figure 5.13 and Supplementary Figure 4) is yet to be defined. Hyper-activation of ClpP peptidase and proteolytic function has been observed in the presence of acyldepsipeptides (ADEPs), which mimic the interaction of an ATPase to open the axial pore of ClpP and promote uncontrolled degradation of large polypeptides (Brotz-Oesterhelt et al., 2005; Kirstein et al., 2009a; Li et al., 2010; Lowth et al., 2012; Sass et al., 2011). In prokaryotes, this results in cell death due to the dysregulated degradation of essential proteins (Brotz-Oesterhelt et al., 2005). However, results from SEC and glutaraldehyde crosslinking experiments indicate that CLPP$^{T145P}$, while being aggregation prone, is likely to exist in an oligomeric state between a dimer and a pentamer. Presumably a dimer would be the minimal conformation required for catalytic activity of CLPP and without the active sites being sequestered in the ring conformation there would be unlimited access to the cleavage of substrates. Surprisingly, CLPP$^{T145P}$ hyper-activity does not extend towards the cleavage of larger substrates such as FITC-casein (data not shown), rather a gradual decrease of fluorescence was observed (similar to the trend in Figure 5.14, black circles) which suggested aggregation of FITC-casein and CLPP$^{T145P}$ was

occurring instead. Consequently, an ADEP-like activation of CLPP$^{T145P}$ is doubtful and the selective hyper-stimulation towards peptides may be due to active dimer formation or open/unstable heptamer formation that is not sustained with hCLPX. *In vivo,* the impaired assembly of CLPP$^{T145P}$ would negatively impact the metabolic stability of CLPP or potentially result in the formation of aggregates.

### 5.3.5 PRLTS3 is caused by a loss of CLPP (and CLPXP) function

The phenotypic similarities (SNHL and premature ovarian failure) between the CLPP$^{(-/-)}$ mice and patients with PRLTS3 implies CLPP has an essential role in the development and viability of specific cells. CLPP is upregulated during rat ovarian follicular development (Bahat et al., 2014) and was observed in relative high abundance in certain cells within adult mouse ovaries and organ of Corti (inner ear) (Jenkinson et al., 2013). All patients with PRLTS3 presented with SNHL but the age of onset, severity and progression of premature ovarian failure was variable among the tested individuals (and in some cases hormone testing could not be performed) (Ahmed et al., 2015; Jenkinson et al., 2013).

Due to the direct association with function and stability, the proper assembly of CLPP heptamers (and tetradecamers) is required for a healthy phenotype in mammals. Consistent with this, CLPP$^{C147S}$ exhibited similar activity to wild-type CLPP in all aspects except the formation of stable complexes and as such, patients with this particular mutation all displayed hearing loss and ovarian dysfunction (Jenkinson et al., 2013), suggesting loss of CLPP function due to decreased levels of CLPP heptamers. Consistently, a splice mutation of *CLPP* that was established to reduce but not abolish CLPP expression was also reported to cause PRLTS3 (Jenkinson et al., 2013). These patients did not report any notable symptoms apart from SNHL but hormone testing was not performed to determine the extent of gonadal dysgenesis (Jenkinson et al., 2013). In contrast, the patients carrying CLPP$^{T145P}$ and CLPP$^{Y229D}$ mutations reported additional symptoms (e.g. microcephaly, learning

difficulties and muscle spasticity) indicating a severe loss of CLPP or a potential gain of toxic function due to the mutation in CLPP (Ahmed et al., 2015; Jenkinson et al., 2013). The observed *in vitro* instability of $CLPP^{T145P}$ (prone to aggregation) and $CLPP^{Y229D}$ (formed smaller assembly intermediates) would suggest that the accumulation of partially folded protein intermediates may be a possible scenario *in vivo*. The cytotoxicity of protein aggregation, even with non-disease-related proteins, has been observed *in vitro* (Bucciantini et al., 2002) and is the underlying cause of the pathogenesis of various neurodegenerative diseases (Jucker & Walker, 2013). Alternatively, as $CLPP^{T145P}$ has been shown to associate with molecular chaperones *in vitro* (Figure 5.5 and Figure 5.8), this mutant may also recruit mitochondrial chaperones *in vivo* and reduce the total amount of chaperones available to other mitochondrial proteins. The accumulation misfolded proteins may ultimately contribute to mitochondrial dysfunction and consistent with this, reduced chaperone activity of HSP60 has been associated with an autosomal dominant form of spastic paraplegia (SPG13) characterised by progressive muscle paralysis within the lower limbs (Hansen et al., 2008).

Without CLPX, the activity of CLPP is limited to cleaving small peptides (Kang et al., 2002) which implies that the greater part of CLPP function(s) would involve its cognate unfoldase CLPX. Despite the roles of CLPP or CLPXP not being well-established in mammalian mitochondria, several studies have revealed CLPXP-interacting proteins to include PQC chaperones, subunits of respiratory chain complexes and others associated with mitochondrial dynamics and ribosome biogenesis (Al-Furoukh et al., 2014; Cole et al., 2015; Fischer et al., 2015; Lowth et al., 2012). Consistent with this, *CLPP*-depleted tissues exhibited a decrease of subunits from Complex I and IV, impaired cellular respiration, elevated levels of reactive oxygen species (ROS) and altered mitochondrial morphology (Cole et al., 2015; Deepa et al., 2015; Gispert et al., 2013). These data and the variable phenotype of PRLTS3 patients would indicate CLPP or CLPXP contributes to the regulation or assembly of

respiratory chain complexes and potentially a broad role in the regulation of other metabolic pathways in a direct or indirect capacity.

Similar characteristics are observed in patients with mutations within *SPG7*, the gene encoding paraplegin, which is linked to an autosomal recessive form of spastic paraplegia (Casari et al., 1998). Subunits of paraplegin and AFG3L2 form the inner membrane-bound *m*-AAA protease complex that regulates mitochondrial morphology and also plays a crucial processing role to mediate the biogenesis of specific proteins such as mitoribosome subunit MrpL32 and ROS scavenger Ccp1 (Esser et al., 2002; Ishihara et al., 2006; Nolden et al., 2005). Consequently, mutations in *SPG7* cause a range of symptoms including progressive weakness and spasticity of lower limbs, learning difficulties, ataxias and cerebellar atrophy (Casari et al., 1998).

Accordingly, the associated phenotype of PRLTS3 (e.g. learning difficulties, ataxias, reduced growth, diminished motor control etc) are typical symptoms of impaired mitochondrial function and are commonly associated with diseases caused by mutations in mitochondrial genes (Angelini et al., 2009; Calvo & Mootha, 2010; Chinnery, 2014). Likewise, three out of the four remaining assigned causative genes of Perrault syndrome are associated with mitochondrial DNA replication or protein translation (Morino et al., 2014; Pierce et al., 2011; Pierce et al., 2013) (Table 5.1), indicating that regulating the levels of mtDNA-encoded proteins i.e. respiratory chain subunits, is vital for mitochondrial functional integrity and cell viability. Consistently, mutations within mtDNA are commonly associated with hearing loss and respiratory chain defects (Chinnery, 2014; Yano et al., 2014).

It is still unclear whether PRLTS3 is directly caused by a loss of CLPP (or CLPXP) activity or is indirectly caused by the subsequent mitochondrial dysfunction arising from a reduction in CLPP(X) activity (e.g. due to elevated ROS production). The accumulation of misfolded subunits of $CLPP^{T145P}$ and $CLPP^{Y229D}$, in addition to the loss of CLPP(X) function, may also be contributing to the more severe neurological defects observed in

patients with these particular mutations. In this regard, it would be valuable to examine the levels of CLPP in patient tissues to determine if a general depletion of CLPP is observed or if the selective vulnerability of specific cells is due to variable CLPP expression or toxic accumulation.

Future experiments would involve introducing the Perrault CLPP mutants in a *CLPP* knock out cell line to verify their metabolic stability and determine the effect on mitochondrial viability and cellular respiration. Additionally, analysing changes to the mitochondrial proteome would allow us to determine novel substrates or interacting proteins of CLPP that would provide greater functional insights into role of CLPP or CLPX and establish their contribution to the symptoms associated with PRLTS3.

# Chapter 6: Discussion

## 6.1 Regulated proteolysis by LONM

LONM contributes to proteostasis of the mitochondrial matrix by degrading misfolded proteins to prevent their toxic accumulation or the formation of aggregates (Bezawork-Geleta et al., 2015; Bota & Davies, 2002). The controlled degradation of folded substrates also contributes to mitochondrial proteostasis by clearing unwanted proteins (e.g. StAR) or those that have the potential to misfold (e.g. unassembled protein subunits) (Granot et al., 2007a; Ondrovičová et al., 2005).

The first part of this study analysed LONM-mediated degradation of folded substrates SDH5 and StAR and determined the location of each degron influencing recognition by LONM. Constant exposure of the degron, (e.g. from the N terminus or internal site), increased the proteolytic activity of LONM and facilitated the rapid turnover of the substrate *in vitro*. StAR and SDH5 differed in their requirements for LONM-mediated recognition which suggests distinct mechanisms of substrate binding and unfolding may exist between substrates. In regards to StAR, the turnover of this protein was significantly increased upon exposure of the hydrophobic sterol binding pocket. Further investigation is required to determine which, if any, specific residues are crucial for this recognition. The general recognition of hydrophobic sequences is likely to be a conserved mechanism between proteins and AAA+ proteases that enables the non-selective degradation of damaged or denatured proteins (Gur & Sauer, 2008). As StAR has no discernible function in the mitochondrial matrix the exposure of this degron, regulated by the C-terminal α-helix, is favourable for its expedited turnover which ultimately benefits the cell. In the case of SDH5 however, the exposure of the degron is regulated by its interaction with SDHA and constant exposure of this degron is detrimental to its function and also mitochondrial and cellular homeostasis, as demonstrated by the development of paraganglioma type 2 in patients with a destabilising mutation in SDH5 ($SDH5^{G78R}$) (Hao et al., 2009). Interestingly, the exposed N-terminus of SDH5 was essential for LONM-mediated

recognition. The degradation of SDH5 was further enhanced by the exposure of a specific cluster of hydrophobic/aromatic residues (LPPW), indicating this region may be a potential initiation or binding site for LONM. This bipartite recognition and/or binding of substrates may represent a novel mechanism for LONM-mediated degradation. Similarly, degradation of native proteins by the 26S proteasome is enhanced by the presence of an unstructured region, contingent on it being in close proximity to the ubiquitination site (Prakash et al., 2004). Additionally, degradation of a folded substrate can be influenced by the unstructured region *in trans* (Prakash et al., 2009). Certainly more investigation is required to determine if bipartite engagement is a common recognition strategy by LONM or is selective to SDH5. The N-terminal residue may be the crucial element for initial engagement by LONM and during substrate unfolding the exposure of this LPPW motif enhances LONM activity. Removal of this motif does not completely abolish degradation which indicates other residues within the random coil regions are likely to be contributing to LONM-mediated recognition. However, as this motif does appear to stimulate turnover of SDH5, it would be interesting to examine if the length between the N-terminus and LPPW motif is an important feature influencing LONM recognition. Additionally, another aspect would be to determine if this motif can enhance the recognition of other substrates *in cis* or *in trans*.

### 6.1.1 Targeting LONM as a therapy for proteostasis imbalance in mitochondria

As a reduction in the exposure of the primary LONM degron on each substrate significantly increased its half-life in the presence of LONM, it may represent a viable approach to prevent or reduce the turnover of LONM substrates *in vivo*. Deleterious structural changes in proteins is commonly associated with genetic mutation (Kowarsch et al., 2010) and can be the cause of disease if this mutation has a direct impact on protein activity (MacArthur et al., 2012). Similarly, the depletion (or

aggregation) of a functional protein within a cell has also been implicated to cause human disease (Hipp et al., 2014). The pathogenic mutation within SDH5$^{G78R}$ has a negative impact on its stability within mitochondria due to the interaction with SDHA being impaired (Bezawork-Geleta et al., 2014; Hao et al., 2009). As such, reducing the degradation of SDH5$^{G78R}$ was predicted to restore complex formation with SDHA and potentially its function (Bezawork-Geleta et al., 2014). Direct, but non-invasive, targeting of the LONM degron within SDH5$^{G78R}$ may be a viable method to increase stability of this protein *in vivo*. Similar to the use of chemical chaperones to stabilise structurally impaired proteins (Powers et al., 2009), the addition of small peptides or compounds specifically targeted to bind and mask LONM degrons could protect SDH5$^{G78R}$ or other proteins from degradation.

However, without knowing the critical residues involved in maintaining the stability or function of a protein, the manipulation or blockage of LONM degron(s) could have deleterious effects. For instance, in the case of SDH5$^{G78R}$, removal of the LPPW motif significantly reduced the capacity to interact with SDHA despite leading to an increase in the half-life of the protein. This indicates that the residues mediating LONM recognition are the same residues that form part of the binding interface between SDHA and SDH5. The co-evolution of proteases and substrates has allowed for the selection of mutations that increase the stability, and less so function, of a particular protein (Bershtein et al., 2013). Thus, the residues that simultaneously facilitate an increase in both stability and functionality are more likely to be conserved. Additionally, the disassembly of protein complexes, (either spontaneously or mediated by molecular chaperones or motor proteins), may be an essential process to abolish protein function or regulate metabolic pathways within a cell (Sauer et al., 2004) and as such, the accumulation of unassembled subunits would need to be effectively regulated. For instance, LONM has been demonstrated to degrade unassembled MPPα subunit but not when in complex with MPPβ (Ondrovičová et al., 2005), indicating the residues forming the protein binding interface of MPPα promote LONM-mediated

recognition. Similarly, the LONM degron for SDH5 may be the residues that would normally be buried within the SDHA-SDH5 complex and recognition and degradation of SDH5 is a natural process to maintain correct stoichiometry or inhibit its function *in vivo*.

However, there may be other proteins that carry LONM degron(s) in non-essential sites on their structure and the targeted blockage of these degrons may lead to increased stability *in vivo*. As an alternative, the direct manipulation of substrate binding site(s) on LONM and other AAA+ proteases (e.g. N-domain, pore-1 loops) may substantially decrease the turnover of particular protein substrates. Investigation into substrate recognition via ecClpXP revealed that the recognition and binding of substrates can occur via different mechanisms (Farrell et al., 2007; Wojtyra et al., 2003). Certain substrates (e.g. SsrA-tagged proteins) were bound directly to the pore loops while other substrates, both dependent and independent of adaptor proteins, were bound via the N-terminal ZBD (Wojtyra et al., 2003). Accordingly, manipulation of the ZBD stabilised the turnover of certain substrates while SsrA-tagged proteins were still degraded (Wojtyra et al., 2003). It is possible that substrate recognition by LONM may also occur via different mechanisms. Further investigation is required to determine the locations(s) for substrate binding on LONM and establish whether manipulation of these regions (e.g. via site-directed mutagenesis) would discriminate between certain substrates or if the global degradation of substrates would be effected. However, as patches of hydrophobic residues appear to be common degrons amongst LONM substrates, they may also bind to LONM via a common mechanism. Nonetheless, improving our understanding about the roles of the various domains of LONM in facilitating recognition and binding of substrates would provide valuable functional insights into regulated proteolysis in the mitochondrion.

Targeting LONM as a therapy to treat mitochondrial diseases associated with a proteostasis imbalance would need to be managed effectively as a decline in LONM expression and function has been associated with mammalian aging (Bakala et al., 2003; Bota et al., 2002), cellular

senescence (Ngo et al., 2011), reduced mtDNA copy number (Matsushima et al., 2010), impaired mitochondrial dynamics (Gibellini et al., 2014) and apoptosis (Bota et al., 2005; Gibellini et al., 2015). Although on the opposite spectrum, an increase in LONM levels has been associated with different malignancies such as lymphoma (Bernstein et al., 2012), colon cancer (Gibellini et al., 2014), cervical cancer (Nie et al., 2013), bladder cancer (Liu et al., 2014) and has been implicated to play a central role in tumorigenesis (Cheng et al., 2013) and maintaining mitochondrial function under oxidative stress (Kao et al., 2015; Luciakova et al., 1999). Consequently, LONM has become an appealing target for the treatment of cancers and a reduction or inhibition of LONM in these cells decreased proliferation and enhanced their sensitivity to other cancer therapies (Bernstein et al., 2012; Liu et al., 2014; Wang et al., 2010). However, difficulties encountered with targeting LONM with specific compounds include penetrating the impermeable IM and potential off-target effects that may impact peroxisomal LON or other AAA+ proteases (Pinti et al., 2015).

## 6.2 Implications for the role of CLPP in mammalian cells

The second part of this study characterised three mutant CLPP variants associated with Perrault syndrome in an effort to determine their respective activities and thus establish a functional link between the clinical phenotype and the role of CLPP in mitochondria. The *in vitro* activity and stability of each PRLTS3 mutant CLPP, in association with the phenotype of *CLPP* null mice, indicates the associated SNHL and premature ovarian failure of Perrault syndrome is caused by a loss of CLPP, and possibly CLPXP, function. In the case of $CLPP^{C147S}$, wherein patients displayed a milder phenotype (Jenkinson et al., 2013), the loss of CLPP function appears to be associated with impaired assembly and stability as opposed to a negative impact on the catalytic site. In contrast, $CLPP^{T145P}$ and $CLPP^{Y229D}$ both exhibit impaired assembly and stability in combination with aberrant peptidase and proteolytic activity.

Patients carrying these mutations display a more severe phenotype with accompanying neurological symptoms (e.g. microcephaly, learning difficulties, muscle weakness) (Ahmed et al., 2015; Jenkinson et al., 2013), indicative of a gain of toxic function, potentially through the formation of protein aggregates. Of note, one of the patients carrying the $CLPP^{Y229D}$ mutation was also heterozygous for mutations in *HSD17B4*, another causative gene of Perrault syndrome (Ahmed et al., 2015; Pierce et al., 2010).

The role of CLPP (and CLPXP) in mammalian mitochondrial is poorly defined which limits the capacity to determine the specific cause of the observed phenotypes associated with a loss of *CLPP* or CLPP function (Ahmed et al., 2015; Gispert et al., 2013; Jenkinson et al., 2013). The diverse symptoms associated with a loss of CLPP function indicate a broad role in regulating numerous metabolic pathways within mitochondria (e.g. cellular respiration, mitochondrial dynamics, mtDNA replication etc) (Ahmed et al., 2015; Gispert et al., 2013; Jenkinson et al., 2013). However, similar tissue-specific effects and variable phenotypes of PRLTS3 are also observed in patients with mutations in BCS1 (BC1 (Ubiquinol-Cytochrome C Reductase) Synthesis). BCS1 is an inner-membrane bound chaperone associated with the insertion of Rieske Fe/S proteins to facilitate the assembly of cytochrome $bc_1$ complex (complex III) in yeast (Cruciat et al., 1999). Consistently, mutations within the BCS1-like (BCS1L) gene cause complex III deficiencies in humans including GRACILE (growth retardation, aminoaciduria, cholestasis, iron overload, lactacidosis and early death) syndrome (de Lonlay et al., 2001; Visapää et al., 2002). Interestingly, point mutations in *BCS1L* that result in impaired protein-protein interaction cause Björnstad syndrome, which is characterised by SNHL and pili torti (brittle hair) (Hinson et al., 2007). Patients with Björnstad syndrome also displayed increased ROS production and mild complex III deficiencies (Hinson et al., 2007). While the symptoms of PRLTS3 are not indicative of complex III deficiencies, similarly the elevated levels of ROS

may be affecting global mitochondrial function that is more apparent in selective cells (e.g. from the inner ear) (Hinson et al., 2007).

The association with respiratory chain complex subunits and metabolic proteins indicate a crucial role of CLPP(X) in regulating molecular quality control within mitochondria in a direct or indirect capacity (Cole et al., 2015; Deepa et al., 2015; Fischer et al., 2015; Gispert et al., 2013). Interestingly, inhibition of CLPP (not CLPX) in human acute myeloid leukaemia cells reduced oxidative phosphorylation and growth of these cells *in vitro* and *in vivo* (Cole et al., 2015), indicating a vital requirement for CLPP peptidase or protease activity. Similarly, siRNA-mediated knock down of *CLPP* in HeLa cells increased the sensitivity to the chemotherapy drug cisplatin (Zhang & Maurizi, 2016). Interestingly, *CLPX* knockdown also increased the chemosensitivity of HeLa cells, but to only half the extent of the *CLPP* knock down (Zhang & Maurizi, 2016) indicating a greater reliance on CLPP activity for cisplatin resistance.

Introducing each PRLTS3 CLPP mutant into a *CLPP* knock-out cell line would be useful to monitor assembly and stability of each CLPP variant and also test for the formation of aggregates. This would provide a greater understanding of PRLTS3 pathogenesis at the molecular level and complement the *in vitro* functional assays reported here. Additionally, the accumulation of specific proteins may reveal novel substrates of CLPP(X). It would also be useful to determine the separate roles of CLPX and CLPP in the mitochondrion and identify whether they perform unique functions in regulating metabolic pathways. In this regard, examining the phenotype and characteristics of *CLPX* null mice would be interesting to determine if there are similarities to *CLPP* null mice and establish whether CLPP or CLPXP function is essential in mitochondria.

# Appendix 1

**Table 1: Oligonucleotide primers used in this thesis**

| Primer | Oligonucleotide sequence (5`-3`) | Gene/ mutation | Features |
|---|---|---|---|
| **Proteases/peptidases** | | | |
| T145P_1 | GGCAGATCGGG TTGAGGATGTAC TGCATCG | *CLPP*$^{T145P}$ | Introduces ACC>CCC point mutation into human *CLPP* by Phusion site-directed mutagenesis, includes an *Nco* I restriction enzyme site for screening |
| T145P_2 | CATGGTGCGTG GGCCAGGCCGC CAGCATG | | |
| C147S_1 | GTGCATATGGG GTTGAGGATGTA CTGCATC | *CLPP*$^{C147S}$ | Introduces TGC>AGT point mutation into human *CLPP* by Phusion site-directed mutagenesis, includes a *Nde* I restriction enzyme site for screening |
| C147S_2 | CTGGAGTGTGG GCCAGGCCGCC AGCATGGGC | | |
| Y229D_Fwd | CGCGACATGAG CCCCATGGAGG CCCAGGAG | *CLPP*$^{Y229D}$ | Introduces TAC>GAC point mutation into human *CLPP* by Phusion site-directed mutagenesis, include a *Pvu* I restriction enzyme site for screening |
| Y229D_Rev | ATCGCGCTCCAT GGCGGACTCGA TCACCTG | | |
| **Substrates – model** | | | |
| XhoI_DHFR | CTCGAGGTTCG ACCATTGAACTG CATCGTC | *DHFR* | Forward primer for amplification of *Mus musculus DHFR*. Introduces *Xho* I restriction enzyme site for cloning into pDT-SDH5-*Xho* I (pDT3179) |
| DHFR_Hind III | ACTTGCAAGCTT AGTCTTTCTTCT CGTAGACTTC | *DHFR* | Reverse primer for amplification of *Mus musculus DHFR*. Introduces *Hind* III restriction enzyme site for cloning into pDT-SDH5-*Xho* I (pDT3179). |

| Primer | Oligonucleotide sequence (5`-3`) | Gene/ mutation | Features |
|---|---|---|---|
| **Substrates – SDH5** | | | |
| DM-SDH5 | GCGCCTCCGCGGTGGAGACATGATTGAAATCCCTTTG | *SDH5*$_{46\text{-}166}$ *(Δ11 SDH5)* | Forward primer for amplification of *SDH5* (encoding residues 46(D)-166). Includes *Sac* II restriction enzyme site for cloning into pHUE. |
| SDH5_Hind | TCTGCAAAGCTTCAACGTGGCTTTTCAAAGAGGTACTC | *SDH5*$_{46\text{-}166}$ *(Δ11 SDH5)* | Reverse primer for amplification of *SDH5*. Includes *Hind* III restriction enzyme site for cloning into pHUE. |
| TDE-SDH5 | GCGCCTCCGCGGTGGAACTGATGAATCCATAGAAACC | *SDH5*$_{59\text{-}166}$ *(Δ24 SDH5)* | Forward primer for amplification of *SDH5* (encoding residues 59(T)-166). Includes *Sac* II restriction enzyme site for cloning into pHUE. |
| sdh10_A | GAGAGAACTGATGAATCCATAGAAACCAAAAG | *SDH5*$_{XhoI}$ | Amplifies *SDH5* gene using pDT2658 as template |
| sdh10_B | GAGCCATGGAGGCAAAGGGATTTCAATCATG | *SDH5*$_{XhoI}$ | Introduces *Xho* I restriction enzyme site into SDH5 (at the equivalent of residue 56) |
| PTDS_Fwd | GCTGCCCAAAAGGACATGATTGAAATCCCTTTG | *SDH5*$^{PTDS>AAAA}$ *(SDH5*$^{PTDS}$*)* | Introduces mutation in *SDH5* (encoding residues 40-43, replacing PTDS with AAAA) using Phusion site-directed mutagenesis. Incorporates *Pst* I restriction enzyme site for screening. |
| PTDS_Rev | TGCAGCGCTGTCACCTCGATATCCACCGC | | |
| QKDM_Fwd | GGCCGCGATTGAAATCCCTTTGCCTCCATGG | *SDH5*$^{QKDM>AAAA}$ *(SDH5*$^{QKDM}$*)* | Introduces mutation in *SDH5* (encoding residues 44-47, replacing QKDM with AAAA) via Phusion site-directed mutagenesis. Incorporates *Not* I restriction enzyme site for screening. |
| QKDM_Rev | GCTGCGGAATCTGTTGGGCTGTCACCTC | | |

| **Primer** | **Oligonucleotide sequence (5`-3`)** | **Gene/ mutation** | **Features** |
|---|---|---|---|
| IEIP_Fwd | GCCGCTTTGCC TCCATGGCTCG AGGTTCG | *SDH5*$_{35\text{-}55}^{IEIP>AAAA}$ *(SDH5*$_{21}^{IEIP}$*)* | Introduces mutation in *SDH5* (encoding residues 48-51, replacing IEIP with AAAA), via Phusion site-directed mutagenesis. Incorporates *Pst* I restriction enzyme site for screening |
| IEIP_Rev | TGCAGCCATGT CCTTTTGGGAAT CTGTTGGGC | | |
| LPPW_Fwd | GCCGCGCTCGA GGTTCGACCATT GAACTGC | *SDH5*$_{35\text{-}55}^{LPPW>AAAA}$ *(SDH5*$_{21}^{LPPW}$*)* | Introduces mutation in *SDH5* (encoding residues 52-55, replacing LPPW with AAAA), via Phusion site-directed mutagenesis. Incorporates *Not* I restriction enzyme site for screening |
| LPPW_Rev | CGCCGCAGGGA TTTCAATCATGT CCTTTTGGGAAT C | | |
| FL_IEIP_F | GCCGCTTTGCC TCCATGGCAGG AGAGAAC | *SDH5*$^{IEIP>AAAA}$ *(SDH5*$^{IEIP}$*)* | Introduces mutation in *SDH5* (encoding residues 48-51, replacing IEIP with AAAA), via Phusion site-directed mutagenesis. Incorporates *Pst* I restriction enzyme site for screening. |
| FL_LPPW_F | GCCGCGCAGGA GAGAACTGATG AATCCATAG | *SDH5*$^{LPPW>AAAA}$ *(SDH5*$^{LPPW}$*)* | Introduces mutation in *SDH5* (encoding residues 52-55, replacing LPPW with AAAA), via Phusion site-directed mutagenesis. Incorporates *Not* I restriction enzyme site for screening. |

| Primer | Oligonucleotide sequence (5`-3`) | Gene/ mutation | Features |
|---|---|---|---|
| **Substrates – StAR** | | | |
| SacII_StAR | CGCCTCCGCGG TGGAAGCTCTCT ACTCGGTTC | *StAR*$_{56-285}$ *(StAR)* | Forward primer for amplification of *StAR* (encoding residues 56-285). Introduces *Sac* II restriction enzyme site for sub-cloning into pHUE. Using IMAGE clone 4153601 (pDT2389) as template |
| StAR_HindIII | ATGCTGAAGCTT AACACCTGGCTT CAGAGGC | *StAR*$_{56-285}$ *(StAR)* | Reverse primer for amplification of *StAR* (encoding residues 56-285). Introduces *Hind* III restriction enzyme site for cloning into pHUE. Using IMAGE clone 4153601 (pDT2389) as template |
| StAR-193_F | AGCTGCCCAAG AGCATCATCAAC CAGG | *StAR*$_{56-249}$ *(StAR*$_{\Delta C}$*)* | Introduces a stop codon (TGG>TGA) in *StAR* (at the equivalent of residue 250) via Phusion site-directed mutagenesis. Incorporates *Nhe* I restriction enzyme site introduced for screening. |
| StAR-193_R | AGCCCTTGAGG TCGATGCTGAGT AGCC | | |
| StARCpep_F | CCGCGGGGGGT GGCTGCCCAAG AGCATCATC | *StAR*$_{250-285}$ *(StAR*$_{pep}$*)* | Amplifies *StAR* C-terminus and introduces *Sac* II restriction enzyme site for cloning into pHUE. |
| StARCpep_R | AGGCGCAACAC CAGGTGCAGGG TGGACTC | | |
| A268C_1 | TGCAACCACCT GCGCAAGCGCC TGGAG | *StAR*$_{56-285}^{A268C}$ *(StAR*$^{A268C}$*)* | Introduces GCC>TGC mutation (encoding A268C) in *StAR* via Phusion site-directed mutagenesis. Incorporates *Sal* I restriction enzyme site for screening. |
| A268C_2 | AAAGTCGACCT GGGTCTGGGAC AGGACC | | |

| **Primer** | **Oligonucleotide sequence (5`-3`)** | **Gene/ mutation** | **Features** |
|---|---|---|---|
| D106C_1 | GCAAAGTGATG AGTAAAGTGGTC CCAGATG | *StAR*$^{A268C/D106C}$ (StAR$^{DA}$) | Introduces GAC>TGC mutation (encoding D106C) in *StAR* via Phusion site-directed mutagenesis. Using *StAR*$_{56\text{-}285}^{A268C}$ as template |
| D106C_2 | ACCCATTGTCCT GCTGACTCTCCT TCTTCC | | |

# Appendix 1

**Table 2: List of plasmids generated or used in this thesis**

| Name | Gene | Plasmid | Source | Method/ *E. coli* strain used to express recombinant protein |
|---|---|---|---|---|
| **Proteases/peptidases** | | | | |
| pDD117 | *Ec ClpP* | pUHIS | Dougan et al. (2002) | BL21(DE3)-CodonPlus-RIL |
| pDD250 | *Ec ClpX* | pNHIS | Dougan et al. (2003) | BL21(DE3)-CodonPlus-RIL |
| pDT1279 | $CLPX_{66\text{-}633}$ | pET10C | Lowth et al. (2012) | BL21(DE3)-CodonPlus-RIL |
| pDT1407 | $Usp2_{cc}$ | pET15b | Catanzariti et al. (2004) | BL21(DE3)-CodonPlus-RIL |
| pDT2015 | *pre-hCLPP* | pOTB7 | IMAGE clone 3542292 | SP6 coupled reticulocyte lysate system |
| pDT2590 | $LONM_{108\text{-}959}$ | pET10C | Bezawork-Geleta et al. (2014) | BL21(DE3)-CodonPlus-RIL |
| pDT2772 | $CLPP_{53\text{-}277}$ ($T_{53}$-*CLPP*) | pHUE | Bezawork-Geleta et al. (2014) | BL21(DE3)-CodonPlus-RIL |
| pDT3001 | $T_{53}$-$CLPP^{C147S}$ | pHUE | DD/KT Laboratory | BL21(DE3)-CodonPlus-RIL |
| pDT3002 | $T_{53}$-$hCLPP^{T145P}$ | pHUE | DD/KT Laboratory | BL21(DE3) EN2 (*DnaK* null) |
| pDT3268 | *pre-hCLPP*$^{C147S}$ | pOTB7 | Phusion site-directed mutagenesis using pDT2015 and primers C147S_1 and C147S_2 | SP6 coupled reticulocyte lysate system |

| **Name** | **Gene** | **Plasmid** | **Source** | **Method/ *E. coli* strain used to express recombinant protein** |
|---|---|---|---|---|
| pDT3269 | *pre-hCLPP$^{T145P}$* | pOTB7 | Phusion site-directed mutagenesis using pDT2015 and primers T145P_1 and T145P_2 | SP6 coupled reticulocyte lysate system |
| pDT3384 | *$T_{53}$-hCLPP$^{Y229D}$* | pHUE | Phusion site-directed mutagenesis using pDT2772 and primers Y229D_1 and Y229D_2 | BL21(DE3)-CodonPlus-RIL |
| pDT3391 | *pre-hCLPP$^{Y229D}$* | pOTB7 | Phusion site-directed mutagenesis using pDT2015 and primers Y229D_1 and Y229D_2 | SP6 coupled reticulocyte lysate system |
| **Substrates – model** | | | | |
| pDD173 | *GFP-SsrA* | pNHIS | Dougan et al. (2002) | BL21(DE3)-CodonPlus-RIL |
| pDT2900 | *Mus musculus DHFR (mature)* | pHUE | DD/KT Laboratory | BL21(DE3)-CodonPlus-RIL |
| **Substrates – SDH5** | | | | |
| pDT2407 | *pre-SDH5* | pOTB7 | Bezawork-Geleta et al. (2014) | SP6 coupled reticulocyte lysate system |
| pDT2420 | *pre-SDH5$^{G78R}$* | pOTB7 | Bezawork-Geleta et al. (2014) | SP6 coupled reticulocyte lysate system |
| pDT2658 | *SDH5$_{35-166}$ (YR-SDH5)* | pHUE | Bezawork-Geleta et al. (2014) | BL21(DE3)-CodonPlus-RIL |
| pDT2659 | *YR-SDH5$^{G78R}$* | pHUE | Bezawork-Geleta et al. (2014) | BL21(DE3)-CodonPlus-RIL |
| pDT2665 | *SDH5$_{37-166}$ (G-SDH5)* | pHUE | Bezawork-Geleta et al. (2014) | BL21(DE3)-CodonPlus-RIL |

| **Name** | **Gene** | **Plasmid** | **Source** | **Method/ *E. coli* strain used to express recombinant protein** |
|---|---|---|---|---|
| pDT2755 | *G-SDH5$^{G78R}$* | pHUE | Bezawork-Geleta et al. (2014) | BL21(DE3)-CodonPlus-RIL |
| pDT3137 | *SDH5$_{46-166}$ (Δ11 SDH5)* | pHUE | Amplified *SDH5* from pDT2658 using primers DM-SDH5 and SDH5_HindIII, digested with *Sac* II and *Hind* III and cloned into pHUE | BL21(DE3)-CodonPlus-RIL |
| pDT3138 | *SDH5$_{59-166}$ (Δ24 SDH5)* | pHUE | Amplified *SDH5* from pDT2658 using primers TDE-SDH5 and SDH5_HindIII, digested with *Sac* II and *Hind* III and cloned into pHUE | BL21(DE3)-CodonPlus-RIL |
| pDT3178 | *SDH5$_{XhoI}$* | pHUE | Amplified *SDH5* from pDT2658 using primers sdh10_A and sdh10_B to introduce *Xho* I restriction enzyme site (at the equivalent of residue 56) | N/A |
| pDT3230 | *SDH5$_{35-55}$-DHFR (SDH5$_{21}$-DHFR)* | pHUE | Amplified *DHFR* from pDT2900 using primers XhoI_DHFR and HindIII_DHFR, digested with *Xho* I and *Hind* III and cloned into pDT3178 | BL21(DE3)-CodonPlus-RIL |

| **Name** | **Gene** | **Plasmid** | **Source** | **Method/ *E. coli* strain used to express recombinant protein** |
|---|---|---|---|---|
| pDT3271 | *$SDH5_{21}^{PTDS}$-DHFR* | pHUE | Phusion site-directed mutagenesis using pDT3230 and primers PTDS_Fwd and PTDS_Rev | BL21(DE3)-CodonPlus-RIL |
| pDT3272 | *$SDH5_{21}^{QKDM}$-DHFR* | pHUE | Phusion site-directed mutagenesis using pDT3230 and primers QKDM_Fwd and QKDM_Rev | BL21(DE3)-CodonPlus-RIL |
| pDT3273 | *$SDH5_{21}^{IEIP}$-DHFR* | pHUE | Phusion site-directed mutagenesis using pDT3230 and primers IEIP_Fwd and IEIP_Rev | BL21(DE3)-CodonPlus-RIL |
| pDT3274 | *$SDH5_{21}^{LPPW}$DHFR* | pHUE | Phusion site-directed mutagenesis using pDT3230 and primers LPPW_Fwd and LPPW_Rev | BL21(DE3)-CodonPlus-RIL |
| pDT3275 | *YR-$SDH5^{PTDS}$* | pHUE | Phusion site-directed mutagenesis using pDT2658 and primers PTDS_Fwd and PTDS_Rev | BL21(DE3)-CodonPlus-RIL |
| pDT3276 | *YR-$SDH5^{QKDM}$* | pHUE | Phusion site-directed mutagenesis using pDT2658 and primers QKDM_Fwd and QKDM_Rev | BL21(DE3)-CodonPlus-RIL |

| **Name** | **Gene** | **Plasmid** | **Source** | **Method/ *E. coli* strain used to express recombinant protein** |
|---|---|---|---|---|
| pDT3290 | *YR-SDH5$^{IEIP}$* | pHUE | Phusion site-directed mutagenesis using pDT2658 and primers FL_IEIP_F and IEIP_Rev | BL21(DE3)-CodonPlus-RIL |
| pDT3291 | *YR-SDH5$^{LPPW}$* | pHUE | Phusion site-directed mutagenesis using pDT2658 and primers FL_LPPW_F and LPPW_Rev | BL21(DE3)-CodonPlus-RIL |
| pDT3298 | *G-SDH5$^{QKDM}$* | pHUE | Phusion site-directed mutagenesis using pDT2665 and primers QKDM_Fwd and QKDM_Rev | BL21(DE3)-CodonPlus-RIL |
| pDT3299 | *G-SDH5$^{IEIP}$* | pHUE | Phusion site-directed mutagenesis using pDT2665 and primers FL_IEIP_Fwd and IEIP_Rev | BL21(DE3)-CodonPlus-RIL |
| pDT3300 | *G-SDH5$^{LPPW}$* | pHUE | Phusion site-directed mutagenesis using pDT2665 and primers FL_LPPW_F and LPPW_Rev | BL21(DE3)-CodonPlus-RIL |
| pDT3301 | *YR-SDH5$^{G78R-LPPW}$* | pHUE | Phusion site-directed mutagenesis using pDT2659 and primers FL_LPPW_F and LPPW_Rev | BL21(DE3)-CodonPlus-RIL |

| **Name** | **Gene** | **Plasmid** | **Source** | **Method/ *E. coli* strain used to express recombinant protein** |
|---|---|---|---|---|
| pDT3302 | *G-SDH5*$^{G78R-LPPW}$ | pHUE | Phusion site-directed mutagenesis using pDT2755 and primers FL_LPPW_F and LPPW_Rev | BL21(DE3)-CodonPlus-RIL |
| pDT3303 | *pre-SDH5*$^{G78R-LPPW}$ | pOTB7 | Phusion site-directed mutagenesis using pDT2420 and primers FL_LPPW_F and LPPW_Rev | SP6 coupled reticulocyte lysate system |
| **Substrates – StAR** | | | | |
| pDT2857 | *StAR*$_{56-285}$ *(StAR)* | pHUE | Amplified *StAR* from pDT2389 using primers SacII_StAR and HindIII_StAR, digested with *Sac* II and *Hind* III and cloned into pHUE | BL21(DE3)-CodonPlus-RIL/ SHuffle® T7 lysY |
| pDT2883 | *StAR*$_{56-249}$ *(StAR*$_{\Delta C}$*)* | pHUE | Phusion site-directed mutagenesis using pDT2857 and primers StAR193_F and StAR193_R to introduce stop codon (at the equivalent of residue 250) | BL21(DE3)-CodonPlus-RIL |
| pDT2963 | *StAR*$_{250-285}$ *(StAR*$_{pep}$*)* | pHUE | Amplified *StAR* from pDT2857 using primers StARCpep_F and StARCpep_R, digested with *Sac* II and *Hind* III and cloned into pHUE | BL21(DE3)-CodonPlus-RIL |

| **Name** | **Gene** | **Plasmid** | **Source** | **Method/ *E. coli* strain used to express recombinant protein** |
|---|---|---|---|---|
| pDT3076 | *$StAR_{56\text{-}285\ A268C/D106C}$ ($StAR^{DA}$)* | pHUE | Phusion site-directed mutagenesis using pDT2857 and primers A268C_1 and A268C_2. Phusion site-directed mutagenesis was conducted again using the PCR product ($StAR^{A268C}$) and primers D106C_1 and D106C_2 | SHuffle® T7 lysY |

# Appendix 2

**Table 1: List of antibodies used in this thesis**

| Antigen | Name | Raised in | Dilution/diluent | Source |
|---|---|---|---|---|
| hStAR | anti-StAR | Mouse | 1:10,000, 3% blotto in TBS-T | Abcam, Ab58013 |
| hCLPP | Purified CLPP monoclonal antibody | Mouse | 1:1000, 3% BSA in TBS-T | Origene, TA502075, clone OTI1D3 |
| hCLPX | 125/71 | Rabbit | 1:1000, 3% blotto in TBS-T | DD/KT Laboratory, bleed 6, affinity purified fraction C |
| Penta His | Penta His Antibody | Mouse | 1:2000, 3% BSA in TBS-T | QIAGEN |
| Rabbit IgG | anti-rabbit IgG whole molecule, HRP conjugate | Goat | 1:5000, 3% blotto in TBS-T | Sigma |
| Murine IgG | anti-mouse IgG whole molecule, HRP conjugate | Rabbit | 1:5000, 3% BSA in TBS-T | QIAGEN |

# Appendix 3

## Supplementary Figures for Chapter 3

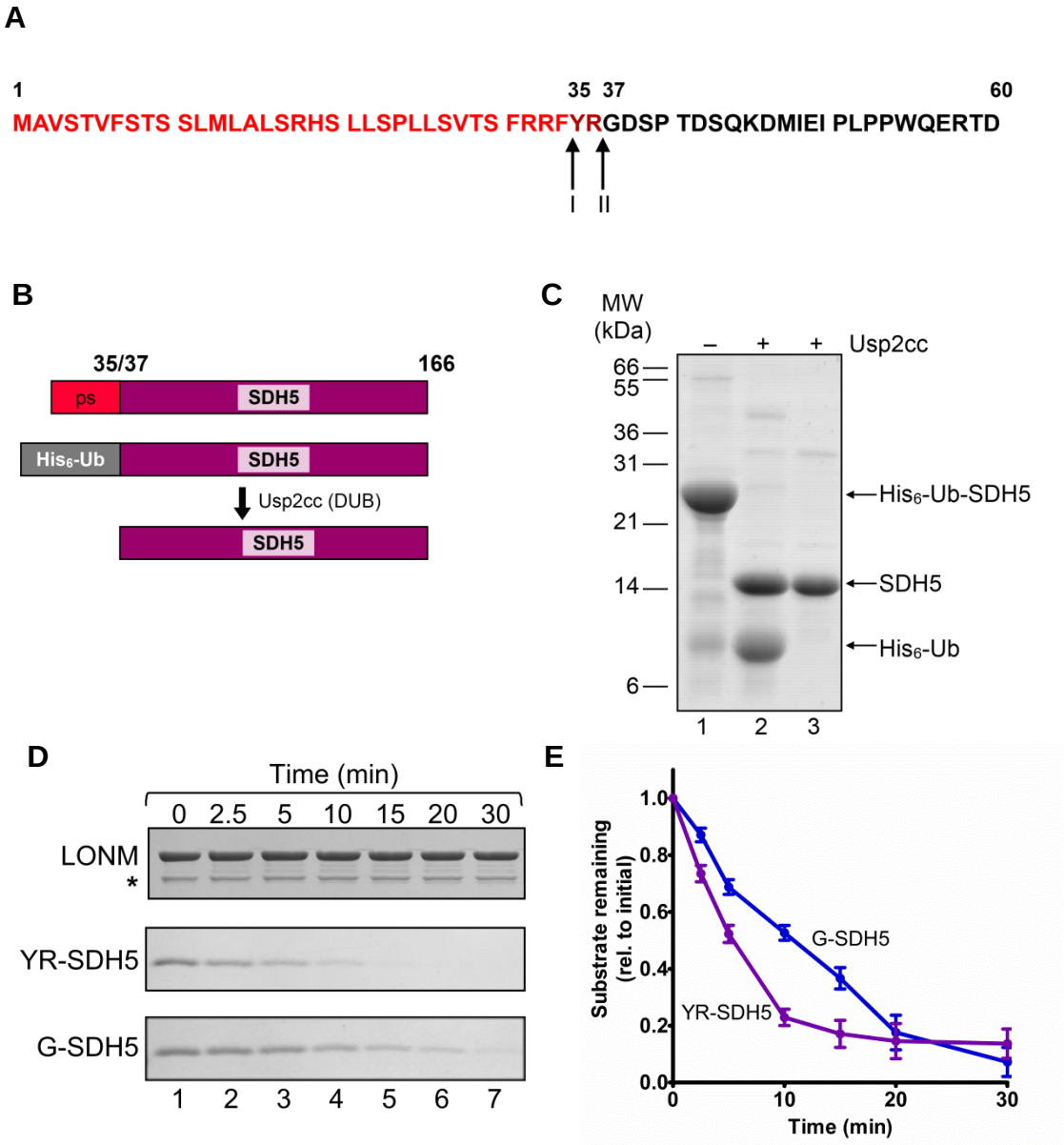


**Supplementary Figure 1:** Experimental plan for generating authentic SDH5 and replicating *in vitro* degradation of YR- and G-SDH5 by recombinant LONM. **A**, The first 60 residues of the SDH5 precursor protein are highlighted in red and black to represent the presequence and the mature protein, respectively. N-terminal sequencing of $SDH5_{FLAG}$ isolated from HeLa mitochondria revealed two possible cleavage sites (indicated by arrows) for the maturation of SDH5. **B**, Schematic showing the generation of authentic, untagged SDH5. SDH5 lacking its presequence (ps) was expressed in *E. coli* with an N-terminal $His_6$-Ubiquitin ($His_6$-Ub) tag which was then cleaved off by deubiquitinating (DUB) enzyme Usp2cc to yield mature SDH5. **C**, Coomassie Brilliant Blue stained SDS-polyacrylamide gel strip containing samples derived from the cleavage (lanes 1 and 2) and purification (lane 3) of untagged

(authentic) SDH5. **D**, Representative Coomassie Brilliant Blue stained SDS-polyacrylamide gel strips of an *in vitro* degradation assay using recombinant LONM (0.2 µM hexamer concentration) (top panel) and recombinant YR-SDH5 (middle panel) or G-SDH5 (bottom panel) (1 µM each) with ATP (5 mM) at 30 °C. **E**, The amount of YR-SDH5 (purple line) and G-SDH5 (blue line) in the presence of LONM were quantitated individually via densitometry and plotted against time (n=3, error bars represent SEM). * indicates degradation product of LONM

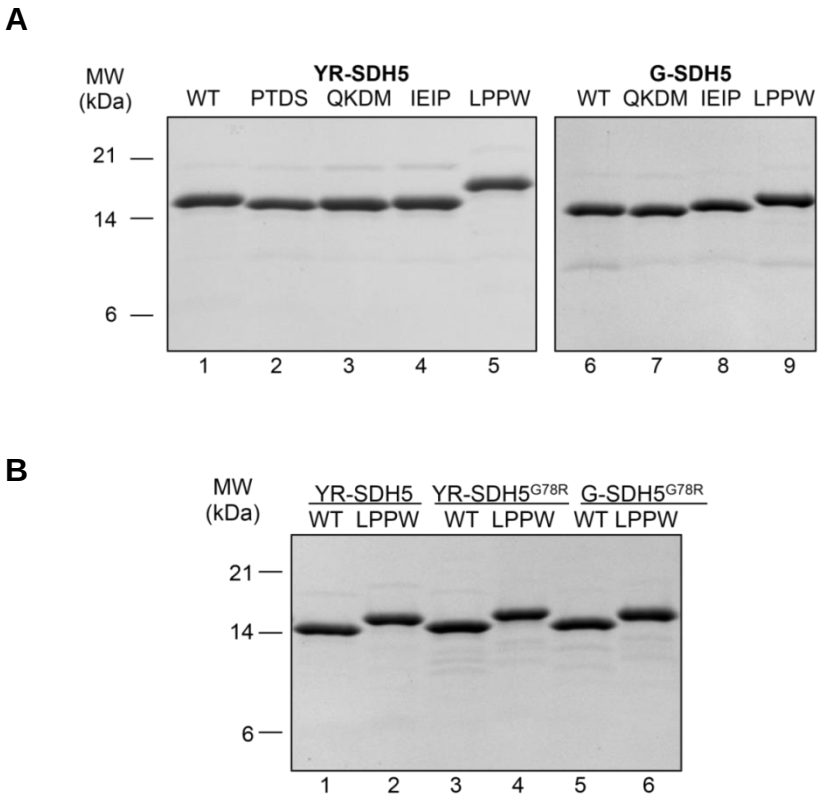


**Supplementary Figure 2:** Comparison of the mobility of full-length YR- and G-SDH5 variants. Coomassie Brilliant Blue stained SDS-polyacrylamide gels of (**A**) wild-type (WT) YR-SDH5 (lanes 1-5) and G-SDH5 (lanes 6-9) derived alanine replacement mutant variants (2 µg each) and (**B**) YR-SDH5 (lanes 1-2), YR-SDH5$^{G78R}$ (lanes 3-4) and G-SDH5$^{G78R}$ (lanes 5-6) derived WT and LPPW>AAAA mutant protein (2 µg each).

# Appendix 4

## Supplementary Figures for Chapter 4

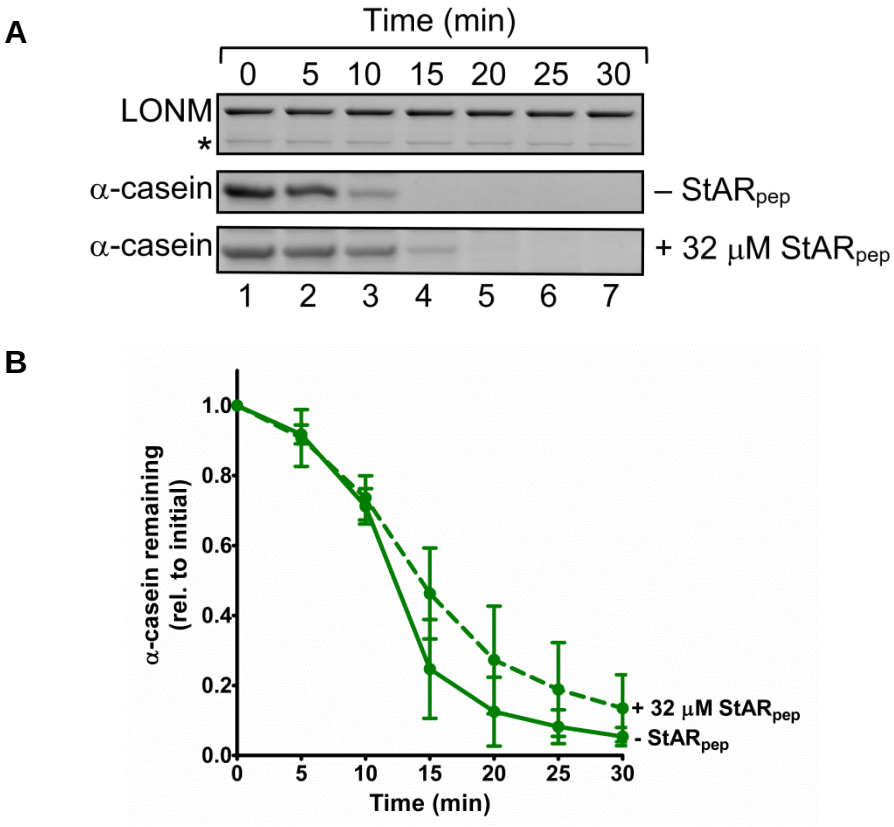


**Supplementary Figure 1:** StAR$_{pep}$ does not inhibit protease activity of LONM. **A**, The turnover of α-casein (3 μM) by LONM (0.1 μM hexamer) was monitored in the absence or presence of StAR$_{pep}$ (32 μM). **B**, The amount of α-casein in the absence (solid line) or presence (dashed line) of StAR$_{pep}$ (32 μM) was quantitated via densitometry (n=3, error bars represent SEM). * indicates degradation product of LONM

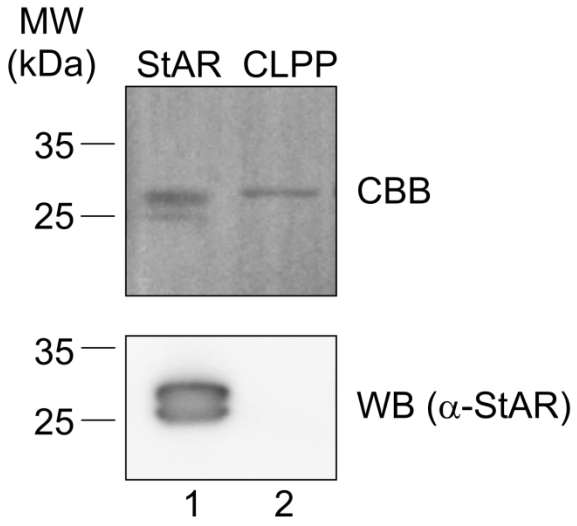


**Supplementary Figure 2:** CLPP migrates at a similar molecular weight as StAR following SDS-PAGE. Recombinant StAR and CLPP (25 ng each) were separated by SDS-PAGE and transferred to PVDF membrane. Prior to immuno-decoration, the membrane was stained with Coomassie Brilliant Blue (CBB) to visualise both StAR and CLPP (upper panel, lane 1 and 2 respectively). The PVDF membrane was then probed with α-StAR antisera to reveal StAR (lower panel, lane 1) but not CLPP (lane 2).

# Appendix 5

## Supplementary Figures for Chapter 5

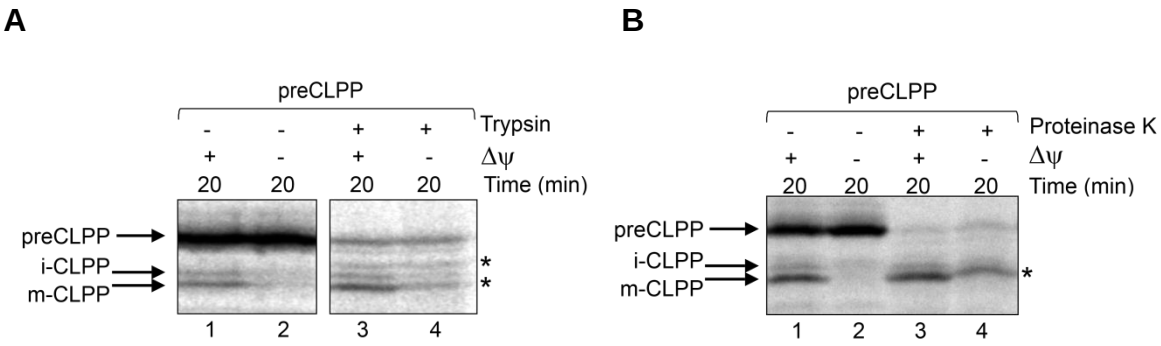


**Supplementary Figure 1:** Comparison of preCLPP import reactions treated with either (**A**) trypsin or (**B**) proteinase K. **A** and **B**, Radiolabelled preCLPP was imported into isolated HeLa mitochondria in the presence or absence of a membrane potential (Δψ). Following import, samples either remained untreated (lanes 1-2) or were treated with protease (lanes 3-4). Proteins were separated via 12.5% glycine-buffered SDS-PAGE and visualised by autoradiography. * indicates non-specific radioactive fragments produced by trypsin or proteinase K treatment.

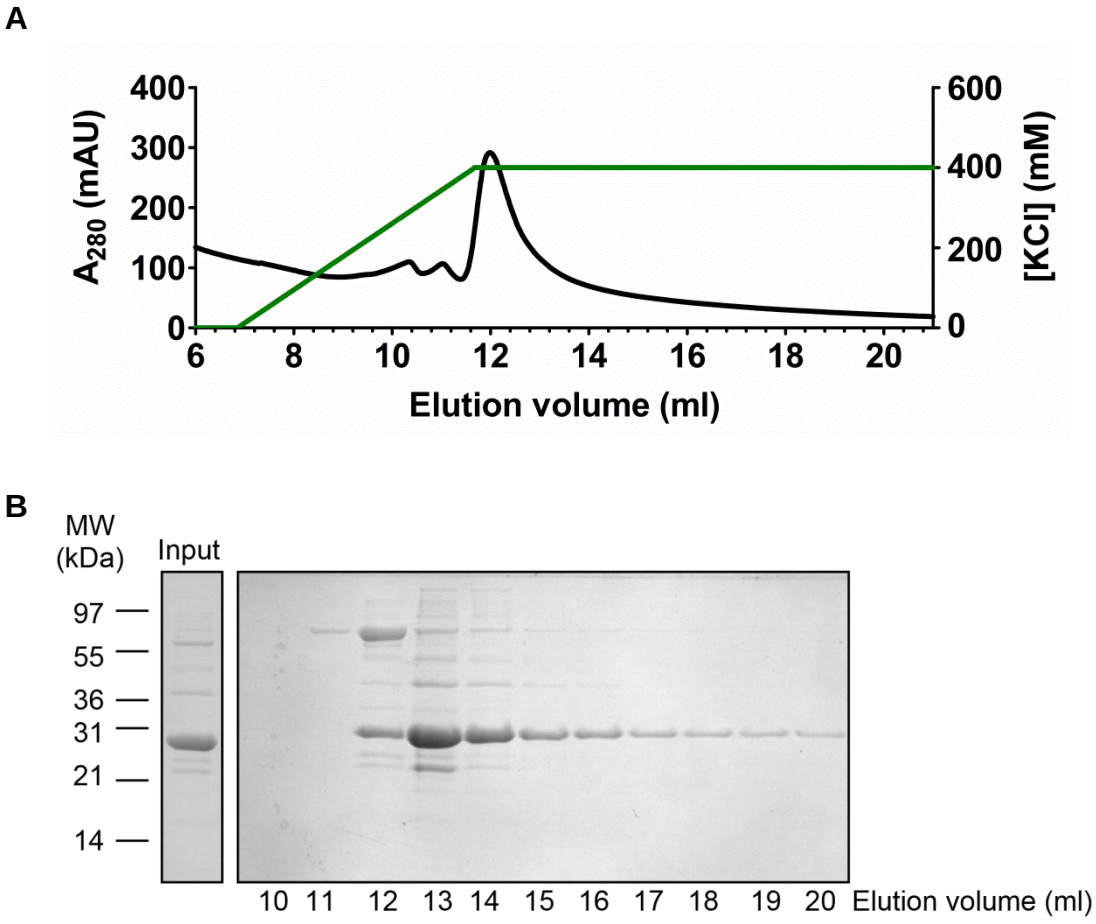


**Supplementary Figure 2:** Anion exchange chromatography of recombinant CLPP$^{T145P}$. **A**, Typical elution profile of CLPP$^{T145P}$ (black line) following application of a salt gradient (green line) to the column. The protein absorbance was measured at 280 nm ($A_{280}$). **B**, Protein samples from the indicated fractions were separated by SDS-PAGE and visualised by staining with Coomassie Brilliant Blue.

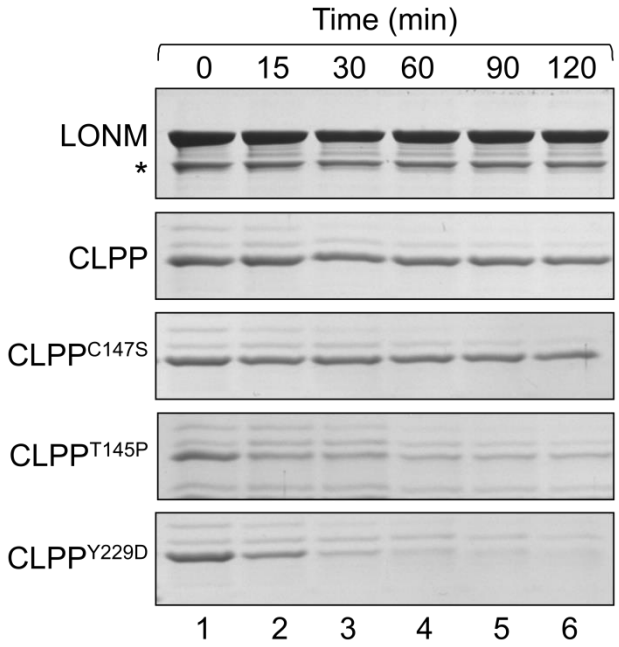


**Supplementary Figure 3:** PRLTS3 mutant CLPPs are susceptible to LONM-mediated degradation. The turnover of wild-type CLPP, CLPP$^{T145P}$, CLPP$^{C147S}$ and CLPP$^{Y229D}$ (1 µM each) was monitored in the presence of LONM (0.4 µM hexamer) and ATP (5 mM) at 30 °C. The protein samples were separated by SDS-PAGE and stained with Coomassie Brilliant Blue. * indicates degradation product of LONM

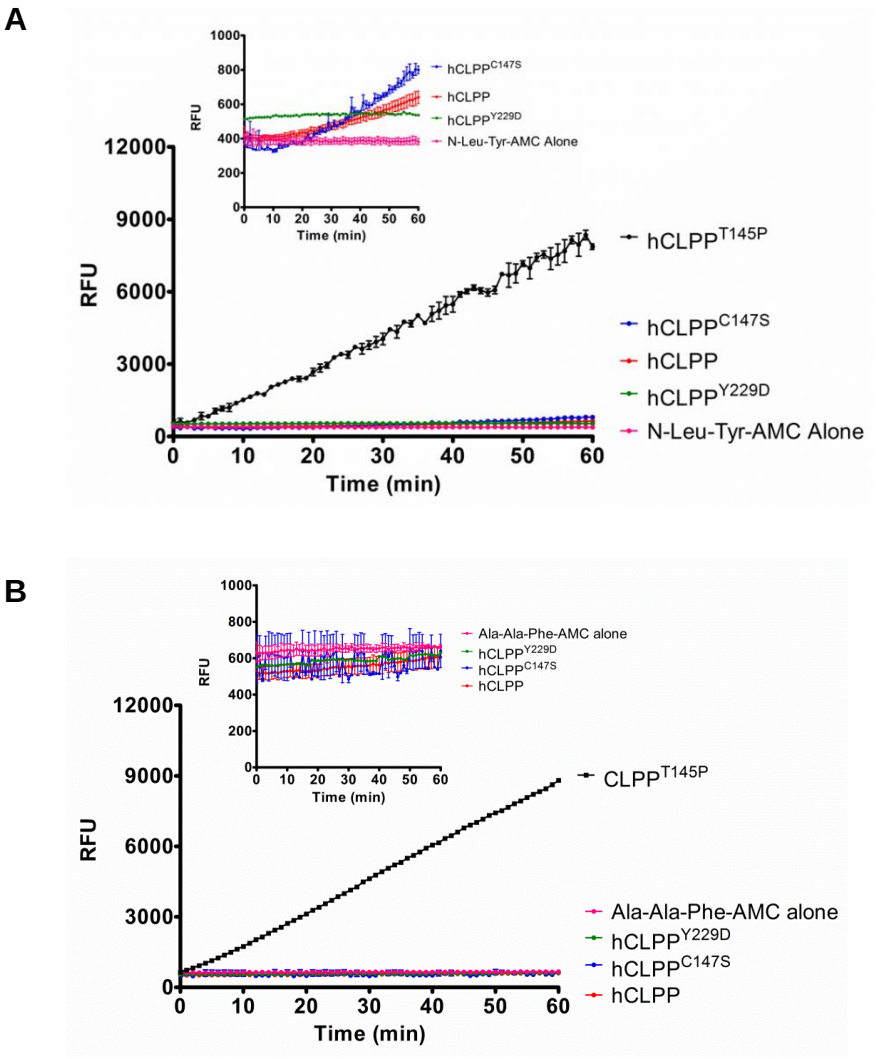


**Supplementary Figure 4:** Peptidase activity of wild-type and mutant CLPP variants towards (**A**) N-Leu-Tyr-AMC and (**B**) Ala-Ala-Phe-AMC. Wild-type CLPP (red circles), $CLPP^{T145P}$ (black circles), $CLPP^{C147S}$ (blue circles) or $CLPP^{Y229D}$ (green circles) (0.8 µM heptamer each) was incubated with peptide substrate (1 µM) as indicated and activity monitored for 60 min. (n=1-3, error bars represent SEM).

# References


Adam, L., Saurabh, A., Matthew, A. C., Anupam, A.& Sadis, M. (2015). Heme Dependent Mitochondrial Stress and Apoptosis are Hallmarks of Bromine Toxicity *C53. PULMONARY TOXICOLOGY AND CASE REPORTS* (pp. A4662-A4662): American Thoracic Society.

Adam, Z., Adamska, I., Nakabayashi, K., Ostersetzer, O., Haussuhl, K., Manuell, A., Zheng, B., Vallon, O., Rodermel, S. R., Shinozaki, K.& Clarke, A. K. (2001). Chloroplast and Mitochondrial Proteases in Arabidopsis. A Proposed Nomenclature. *Plant Physiology, 125*(4), 1912-1918.

Adelman, J. L., Jeong, Y.-J., Liao, J.-C., Patel, G., Kim, D.-E., Oster, G.& Patel, S. S. (2006). Mechanochemistry of Transcription Termination Factor Rho. *Molecular Cell, 22*(5), 611-621.

Ahmed, S., Jelani, M., Alrayes, N., Mohamoud, H. S. A., Almramhi, M. M., Anshasi, W., Ahmed, N. A. B., Wang, J., Nasir, J.& Al-Aama, J. Y. (2015). Exome analysis identified a novel missense mutation in the CLPP gene in a consanguineous Saudi family expanding the clinical spectrum of Perrault Syndrome type-3. *Journal of the Neurological Sciences, 353*(1–2), 149-154.

Akhmedov, D., Braun, M., Mataki, C., Park, K.-S., Pozzan, T., Schoonjans, K., Rorsman, P., Wollheim, C. B.& Wiederkehr, A. (2010). Mitochondrial matrix pH controls oxidative phosphorylation and metabolism-secretion coupling in INS-1E clonal β cells. *The FASEB Journal, 24*(11), 4613-4626.

Aksam, E. B., Koek, A., Kiel, J. A. K. W., Jourdan, S., Veenhuis, M.& van der Klei, I. J. (2007). A peroxisomal lon protease and peroxisome degradation by autophagy play key roles in vitality of Hansenula polymorpha cells. *Autophagy, 3*(2), 96-105.

Al-Furoukh, N., Kardon, J. R., Krüger, M., Szibor, M., Baker, T. A.& Braun, T. (2014). NOA1, a Novel ClpXP Substrate, Takes an Unexpected Nuclear Detour Prior to Mitochondrial Import. *PLoS ONE, 9*(7), e103141.

Alexander, C., Votruba, M., Pesch, U. E. A., Thiselton, D. L., Mayer, S., Moore, A., Rodriguez, M., Kellner, U., Leo-Kottler, B., Auburger, G., Bhattacharya, S. S.& Wissinger, B. (2000). OPA1, encoding a dynamin-related GTPase, is mutated in autosomal dominant optic atrophy linked to chromosome 3q28. *Nature Genetics, 26*(2), 211-215.

Alpy, F.& Tomasetto, C. (2005). Give lipids a START: the StAR-related lipid transfer (START) domain in mammals. *Journal of Cell Science, 118*(13), 2791-2801.

Ammelburg, M., Frickey, T.& Lupas, A. N. (2006). Classification of AAA+ proteins. *Journal of Structural Biology, 156*(1), 2-11.

Anand, R., Langer, T.& Baker, M. J. (2013). Proteolytic control of mitochondrial function and morphogenesis. *Biochimica et Biophysica Acta (BBA) - Molecular Cell Research, 1833*(1), 195-204.

Anderson, S., Bankier, A. T., Barrell, B. G., de Bruijn, M. H. L., Coulson, A. R., Drouin, J., Eperon, I. C., Nierlich, D. P., Roe, B. A., Sanger, F., Schreier, P. H., Smith, A. J. H., Staden, R.& Young, I. G. (1981). Sequence and organization of the human mitochondrial genome. *Nature, 290*(5806), 457-465.

Andersson, S. G. E., Zomorodipour, A., Andersson, J. O., Sicheritz-Ponten, T., Alsmark, U. C. M., Podowski, R. M., Naslund, A. K., Eriksson, A.-S., Winkler, H. H.& Kurland, C. G. (1998). The genome sequence of Rickettsia prowazekii and the origin of mitochondria. *Nature, 396*(6707), 133-140.

Angelini, C., Bello, L., Spinazzi, M.& Ferrati, C. (2009). Mitochondrial disorders of the nuclear genome. *Acta Myologica, 28*(1), 16-23.

Anuka, E., Gal, M., Stocco, D. M.& Orly, J. (2013). Expression and roles of steroidogenic acute regulatory (StAR) protein in 'non-classical', extra-adrenal and extra-gonadal cells and tissues. *Molecular and Cellular Endocrinology, 371*(1–2), 47-61.

Aponte, R. A., Zimmermann, S.& Reinstein, J. (2010). Directed Evolution of the DnaK Chaperone: Mutations in the Lid Domain Result in Enhanced Chaperone Activity. *Journal of Molecular Biology, 399*(1), 154-167.

Arakane, F., Sugawara, T., Nishino, H., Liu, Z., Holt, J. A., Pain, D., Stocco, D. M., Miller, W. L.& Strauss, J. F. (1996). Steroidogenic acute regulatory protein (StAR) retains activity in the absence of its mitochondrial import sequence: Implications for the mechanism of StAR action. *Proceedings of the National Academy of Sciences, 93*(24), 13731-13736.

Arlt, H., Steglich, G., Perryman, R., Guiard, B., Neupert, W.& Langer, T. (1998). The formation of respiratory chain complexes in mitochondria is under the proteolytic control of the m-AAA protease. *The EMBO Journal, 17*(16), 4837-4847.

Arlt, H., Tauer, R., Feldmann, H., Neupert, W.& Langer, T. (1996). The YTA10–12 Complex, an AAA Protease with Chaperone-like Activity in the Inner Membrane of Mitochondria. *Cell, 85*(6), 875-885.

Artemenko, I. P., Zhao, D., Hales, D. B., Hales, K. H.& Jefcoate, C. R. (2001). Mitochondrial Processing of Newly Synthesized Steroidogenic Acute Regulatory Protein (StAR), but Not Total StAR, Mediates Cholesterol Transfer to Cytochrome P450 Side Chain

Cleavage Enzyme in Adrenal Cells. *Journal of Biological Chemistry, 276*(49), 46583-46596.

Atorino, L., Silvestri, L., Koppen, M., Cassina, L., Ballabio, A., Marconi, R., Langer, T.& Casari, G. (2003). Loss of m-AAA protease in mitochondria causes complex I deficiency and increased sensitivity to oxidative stress in hereditary spastic paraplegia. *The Journal of Cell Biology, 163*(4), 777-787.

Aubin-Tam, M.-E., Olivares, Adrian O., Sauer, Robert T., Baker, Tania A.& Lang, Matthew J. (2011). Single-Molecule Protein Unfolding and Translocation by an ATP-Fueled Proteolytic Machine. *Cell, 145*(2), 257-267.

Bahat, A., Perlberg, S., Melamed-Book, N., Lauria, I., Langer, T.& Orly, J. (2014). StAR Enhances Transcription of Genes Encoding the Mitochondrial Proteases Involved in Its Own Degradation. *Molecular Endocrinology, 28*(2), 208-224.

Bakala, H., Delaval, E., Hamelin, M., Bismuth, J., Borot-Laloi, C., Corman, B.& Friguet, B. (2003). Changes in rat liver mitochondria with aging. *European Journal of Biochemistry, 270*(10), 2295-2302.

Baker, B. M.& Haynes, C. M. (2011). Mitochondrial protein quality control during biogenesis and aging. *Trends in Biochemical Sciences, 36*(5), 254-261.

Baker, B. Y., Yaworsky, D. C.& Miller, W. L. (2005). A pH-dependent Molten Globule Transition Is Required for Activity of the Steroidogenic Acute Regulatory Protein, StAR. *Journal of Biological Chemistry, 280*(50), 41753-41760.

Baker, T. A.& Sauer, R. T. (2006). ATP-dependent proteases of bacteria: recognition logic and operating principles. *Trends in Biochemical Sciences, 31*(12), 647-653.

Baker, T. A.& Sauer, R. T. (2012). ClpXP, an ATP-powered unfolding and protein-degradation machine. *Biochimica et Biophysica Acta (BBA) - Molecular Cell Research, 1823*(1), 15-28.

Bartoszewska, M., Williams, C., Kikhney, A., Opaliński, Ł., van Roermund, C. W. T., de Boer, R., Veenhuis, M.& van der Klei, I. J. (2012). Peroxisomal Proteostasis Involves a Lon Family Protein That Functions as Protease and Chaperone. *Journal of Biological Chemistry, 287*(33), 27380-27395.

Bayot, A., Gareil, M., Rogowska-Wrzesinska, A., Roepstorff, P., Friguet, B.& Bulteau, A.-L. (2010). Identification of Novel Oxidized Protein Substrates and Physiological Partners of the Mitochondrial ATP-dependent Lon-like Protease Pim1. *Journal of Biological Chemistry, 285*(15), 11445-11457.

Benaroudj, N., Raynal, B., Miot, M.& Ortiz-Lombardia, M. (2011). Assembly and proteolytic processing of mycobacterial ClpP1 and ClpP2. *BMC Biochemistry, 12*(1), 1-15.

Bender, T., Lewrenz, I., Franken, S., Baitzel, C.& Voos, W. (2011). Mitochondrial enzymes are protected from stress-induced aggregation by mitochondrial chaperones and the Pim1/LON protease. *Molecular Biology of the Cell, 22*(5), 541-554.

Bernstein, S. H., Venkatesh, S., Li, M., Lee, J., Lu, B., Hilchey, S. P., Morse, K. M., Metcalfe, H. M., Skalska, J., Andreeff, M., Brookes, P. S.& Suzuki, C. K. (2012). The mitochondrial ATP-dependent Lon protease: a novel target in lymphoma death mediated by the synthetic triterpenoid CDDO and its derivatives. *Blood, 119*(14), 3321-3329.

Bershtein, S., Mu, W., Serohijos, Adrian W. R., Zhou, J.& Shakhnovich, Eugene I. (2013). Protein Quality Control Acts on Folding Intermediates to Shape the Effects of Mutations on Organismal Fitness. *Molecular Cell, 49*(1), 133-144.

Besman, M. J., Yanagibashi, K., Lee, T. D., Kawamura, M., Hall, P. F.& Shively, J. E. (1989). Identification of des-(Gly-Ile)-endozepine as an effector of corticotropin-dependent adrenal steroidogenesis: stimulation of cholesterol delivery is mediated by the peripheral benzodiazepine receptor. *Proceedings of the National Academy of Sciences, 86*(13), 4897-4901.

Bezawork-Geleta, A., Brodie, E. J., Dougan, D. A.& Truscott, K. N. (2015). LON is the master protease that protects against protein aggregation in human mitochondria through direct degradation of misfolded proteins. *Scientific Reports, 5*, 17397.

Bezawork-Geleta, A., Saiyed, T., Dougan, D. A.& Truscott, K. N. (2014). Mitochondrial matrix proteostasis is linked to hereditary paraganglioma: LON-mediated turnover of the human flavinylation factor SDH5 is regulated by its interaction with SDHA. *The FASEB Journal, 28*(4), 1794-1804.

Bieniossek, C., Schalch, T., Bumann, M., Meister, M., Meier, R.& Baumann, U. (2006). The molecular architecture of the metalloprotease FtsH. *Proceedings of the National Academy of Sciences of the United States of America, 103*(9), 3066-3071.

Bimboim, H. C.& Doly, J. (1979). A rapid alkaline extraction procedure for screening recombinant plasmid DNA. *Nucleic Acids Research, 7*(6), 1513-1523.

Bird, M. J., Thorburn, D. R.& Frazier, A. E. (2014). Modelling biochemical features of mitochondrial neuropathology. *Biochimica et Biophysica Acta (BBA) - General Subjects, 1840*(4), 1380-1392.

Bogenhagen, D. F., Rousseau, D.& Burke, S. (2008). The Layered Structure of Human Mitochondrial DNA Nucleoids. *Journal of Biological Chemistry, 283*(6), 3665-3675.

Boland, M. L., Chourasia, A. H.& Macleod, K. F. (2013). Mitochondrial Dysfunction in Cancer. *Frontiers in Oncology, 3*, 292.

Bose, H. S., Baldwin, M. A.& Miller, W. L. (1998). Incorrect Folding of Steroidogenic Acute Regulatory Protein (StAR) in Congenital Lipoid Adrenal Hyperplasia. *Biochemistry, 37*(27), 9768-9775.

Bose, H. S., Lingappa, V. R.& Miller, W. L. (2002). The steroidogenic acute regulatory protein, StAR, works only at the outer mitochondrial membrane. *Endocrine Research, 28*(4), 295-308.

Bose, H. S., Whittal, R. M., Baldwin, M. A.& Miller, W. L. (1999). The active form of the steroidogenic acute regulatory protein, StAR, appears to be a molten globule. *Proceedings of the National Academy of Sciences, 96*(13), 7250-7255.

Bota, D. A.& Davies, K. J. A. (2002). Lon protease preferentially degrades oxidized mitochondrial aconitase by an ATP-stimulated mechanism. *Nature Cell Biology, 4*(9), 674-680.

Bota, D. A., Ngo, J. K.& Davies, K. J. A. (2005). Downregulation of the human Lon protease impairs mitochondrial structure and function and causes cell death. *Free Radical Biology and Medicine, 38*(5), 665-677.

Bota, D. A., Van Remmen, H.& Davies, K. J. A. (2002). Modulation of Lon protease activity and aconitase turnover during aging and oxidative stress. *FEBS Letters, 532*(1-2), 103-106.

Botos, I., Melnikov, E. E., Cherry, S., Khalatova, A. G., Rasulova, F. S., Tropea, J. E., Maurizi, M. R., Rotanova, T. V., Gustchina, A.& Wlodawer, A. (2004a). Crystal structure of the AAA+ α domain of *E. coli* Lon protease at 1.9 Å resolution. *Journal of Structural Biology, 146*(1–2), 113-122.

Botos, I., Melnikov, E. E., Cherry, S., Kozlov, S., Makhovskaya, O. V., Tropea, J. E., Gustchina, A., Rotanova, T. V.& Wlodawer, A. (2005). Atomic-resolution Crystal Structure of the Proteolytic Domain of Archaeoglobus fulgidus Lon Reveals the Conformational Variability in the Active Sites of Lon Proteases. *Journal of Molecular Biology, 351*(1), 144-157.

Botos, I., Melnikov, E. E., Cherry, S., Tropea, J. E., Khalatova, A. G., Rasulova, F., Dauter, Z., Maurizi, M. R., Rotanova, T. V., Wlodawer, A.& Gustchina, A. (2004b). The Catalytic Domain of *Escherichia coli* Lon Protease Has a Unique Fold and a Ser-Lys Dyad in the Active Site. *Journal of Biological Chemistry, 279*(9), 8140-8148.

Bradford, M. M. (1976). A rapid and sensitive method for the quantitation of microgram quantities of protein utilizing the principle of protein-dye binding. *Analytical Biochemistry, 72*(1), 248-254.

Bragoszewski, P., Wasilewski, M., Sakowska, P., Gornicka, A., Böttinger, L., Qiu, J., Wiedemann, N.& Chacinska, A. (2015). Retro-translocation of mitochondrial intermembrane space proteins. *Proceedings of the National Academy of Sciences, 112*(25), 7713-7718.

Bratic, A.& Larsson, N.-G. (2013). The role of mitochondria in aging. *The Journal of Clinical Investigation, 123*(3), 951-957.

Briggs, L. C., Baldwin, G. S., Miyata, N., Kondo, H., Zhang, X.& Freemont, P. S. (2008). Analysis of Nucleotide Binding to P97 Reveals the Properties of a Tandem AAA Hexameric ATPase. *The Journal of Biological Chemistry, 283*(20), 13745-13752.

Bross, P., Andresen, B. S., Knudsen, I., Kruse, T. A.& Gregersen, N. (1995). Human ClpP protease: cDNA sequence, tissue-specific expression and chromosomal assignment of the gene. *FEBS Letters, 377*(2), 249-252.

Brotz-Oesterhelt, H., Beyer, D., Kroll, H.-P., Endermann, R., Ladel, C., Schroeder, W., Hinzen, B., Raddatz, S., Paulsen, H., Henninger, K., Bandow, J. E., Sahl, H.-G.& Labischinski, H. (2005). Dysregulation of bacterial proteolytic machinery by a new class of antibiotics. *Nature Medicine, 11*(10), 1082-1087.

Bucciantini, M., Giannoni, E., Chiti, F., Baroni, F., Formigli, L., Zurdo, J., Taddei, N., Ramponi, G., Dobson, C. M.& Stefani, M. (2002). Inherent toxicity of aggregates implies a common mechanism for protein misfolding diseases. *Nature, 416*(6880), 507-511.

Bulua, A. C., Simon, A., Maddipati, R., Pelletier, M., Park, H., Kim, K.-Y., Sack, M. N., Kastner, D. L.& Siegel, R. M. (2011). Mitochondrial reactive oxygen species promote production of proinflammatory cytokines and are elevated in TNFR1-associated periodic syndrome (TRAPS). *The Journal of Experimental Medicine, 208*(3), 519-533.

Cagnoli, C., Stevanin, G., Brussino, A., Barberis, M., Mancini, C., Margolis, R. L., Holmes, S. E., Nobili, M., Forlani, S., Padovan, S., Pappi, P., Zaros, C., Leber, I., Ribai, P., Pugliese, L., Assalto, C., Brice, A., Migone, N., Dürr, A.& Brusco, A. (2010). Missense mutations in the AFG3L2 proteolytic domain account for ~1.5% of European autosomal dominant cerebellar ataxias. *Human Mutation, 31*(10), 1117-1124.

Calvo, S. E., Clauser, K. R.& Mootha, V. K. (2016). MitoCarta2.0: an updated inventory of mammalian mitochondrial proteins. *Nucleic Acids Research, 44*(D1), D1251-D1257.

Calvo, S. E.& Mootha, V. K. (2010). The Mitochondrial Proteome and Human Disease. *Annual Review of Genomics and Human Genetics, 11*, 25-44.

Camberg, J. L., Hoskins, J. R.& Wickner, S. (2009). ClpXP protease degrades the cytoskeletal protein, FtsZ, and modulates FtsZ polymer dynamics. *Proceedings of the National Academy of Sciences, 106*(26), 10614-10619.

Campuzano, V., Montermini, L., Lutz, Y., Cova, L., Hindelang, C., Jiralerspong, S., Trottier, Y., Kish, S. J., Faucheux, B., Trouillas, P., Authier, F. J., Dürr, A., Mandel, J.-L., Vescovi, A., Pandolfo, M.& Koenig, M. (1997). Frataxin is Reduced in Friedreich Ataxia Patients and is Associated with Mitochondrial Membranes. *Human Molecular Genetics, 6*(11), 1771-1780.

Campuzano, V., Montermini, L., Moltò, M. D., Pianese, L., Cossée, M., Cavalcanti, F., Monros, E., Rodius, F., Duclos, F., Monticelli, A., Zara, F., Cañizares, J., Koutnikova, H., Bidichandani, S. I., Gellera, C., Brice, A., Trouillas, P., De Michele, G., Filla, A., De Frutos, R., Palau, F., Patel, P. I., Di Donato, S., Mandel, J.-L., Cocozza, S., Koenig, M.& Pandolfo, M. (1996). Friedreich's Ataxia: Autosomal Recessive Disease Caused by an Intronic GAA Triplet Repeat Expansion. *Science, 271*(5254), 1423-1427.

Cao, S. S., Zimmermann, E. M., Chuang, B. M., Song, B., Nwokoye, A., Wilkinson, J. E., Eaton, K. A.& Kaufman, R. J. (2013). The Unfolded Protein Response and Chemical Chaperones Reduce Protein Misfolding and Colitis in Mice. *Gastroenterology, 144*(5), 989-1000.e1006.

Casari, G., De Fusco, M., Ciarmatori, S., Zeviani, M., Mora, M., Fernandez, P., De Michele, G., Filla, A., Cocozza, S., Marconi, R., Dürr, A., Fontaine, B.& Ballabio, A. (1998). Spastic Paraplegia and OXPHOS Impairment Caused by Mutations in Paraplegin, a Nuclear-Encoded Mitochondrial Metalloprotease. *Cell, 93*(6), 973-983.

Castelli, J. C., Hassel, B. A., Wood, K. A., Li, X.-L., Amemiya, K., Dalakas, M. C., Torrence, P. F.& Youle, R. J. (1997). A Study of the Interferon Antiviral Mechanism: Apoptosis Activation by the 2–5A System. *The Journal of Experimental Medicine, 186*(6), 967-972.

Catanzariti, A.-M., Soboleva, T. A., Jans, D. A., Board, P. G.& Baker, R. T. (2004). An efficient system for high-level expression and easy purification of authentic recombinant proteins. *Protein Science : A Publication of the Protein Society, 13*(5), 1331-1339.

Cavadini, P., Gellera, C., Patel, P. I.& Isaya, G. (2000). Human frataxin maintains mitochondrial iron homeostasis in Saccharomyces cerevisiae. *Human Molecular Genetics, 9*(17), 2523-2530.

Cha, S. S., An, Y. J., Lee, C. R., Lee, H. S., Kim, Y. G., Kim, S. J., Kwon, K. K., De Donatis, G. M., Lee, J. H., Maurizi, M. R.& Kang, S. G. (2010). Crystal structure of Lon protease: molecular architecture of gated entry to a sequestered degradation chamber. *The EMBO Journal, 29*(20), 3520-3530.

Chacinska, A., Koehler, C. M., Milenkovic, D., Lithgow, T.& Pfanner, N. (2009). Importing Mitochondrial Proteins: Machineries and Mechanisms. *Cell, 138*(4), 628-644.

Chen, H., Chomyn, A.& Chan, D. C. (2005). Disruption of Fusion Results in Mitochondrial Heterogeneity and Dysfunction. *Journal of Biological Chemistry, 280*(28), 26185-26192.

Chen, H., Detmer, S. A., Ewald, A. J., Griffin, E. E., Fraser, S. E.& Chan, D. C. (2003). Mitofusins Mfn1 and Mfn2 coordinately regulate mitochondrial fusion and are essential for embryonic development. *The Journal of Cell Biology, 160*(2), 189-200.

Cheng, C. W., Kuo, C. Y., Fan, C. C., Fang, W. C., Jiang, S. S., Lo, Y. K., Wang, T. Y., Kao, M. C.& Lee, A. Y. L. (2013). Overexpression of Lon contributes to survival and aggressive phenotype of cancer cells through mitochondrial complex I-mediated generation of reactive oxygen species. *Cell Death and Disease, 4*, e681.

Chinnery, P. F. (2014). Mitochondrial Disorders Overview. In R. A. Pagon, M. P. Adam, H. H. Ardinger, S. E. Wallace, A. Amemiya, L. J. H. Bean, T. D. Bird, C. T. Fong, H. C. Mefford, R. J. H. Smith, & K. Stephens (Eds.), *GeneReviews(R)* (Updated August 14 2014 ed.). Seattle (WA).

Choi, K.-H.& Licht, S. (2005). Control of Peptide Product Sizes by the Energy-Dependent Protease ClpAP. *Biochemistry, 44*(42), 13921-13931.

Christensen, K., Bose, H. S., Harris, F. M., Miller, W. L.& Bell, J. D. (2001). Binding of Steroidogenic Acute Regulatory Protein to Synthetic Membranes Suggests an Active Molten Globule. *Journal of Biological Chemistry, 276*(20), 17044-17051.

Clark, B. J., Wells, J., King, S. R.& Stocco, D. M. (1994). The purification, cloning, and expression of a novel luteinizing hormone-induced mitochondrial protein in MA-10 mouse Leydig tumor cells. Characterization of the steroidogenic acute regulatory protein (StAR). *Journal of Biological Chemistry, 269*(45), 28314-28322.

Clarke, K. J., Adams, A. E., Manzke, L. H., Pearson, T. W., Borchers, C. H.& Porter, R. K. (2012). A role for ubiquitinylation and the cytosolic proteasome in turnover of mitochondrial uncoupling protein 1 (UCP1). *Biochimica et Biophysica Acta (BBA) - Bioenergetics, 1817*(10), 1759-1767.

Claros, M. G.& Vincens, P. (1996). Computational Method to Predict Mitochondrially Imported Proteins and their Targeting Sequences. *European Journal of Biochemistry, 241*(3), 779-786.

Cohen, M. M. J., Leboucher, G. P., Livnat-Levanon, N., Glickman, M. H.& Weissman, A. M. (2008). Ubiquitin–Proteasome-dependent Degradation of a Mitofusin, a Critical Regulator of Mitochondrial Fusion. *Molecular Biology of the Cell, 19*(6), 2457-2464.

Cole, A., Wang, Z., Coyaud, E., Voisin, V., Gronda, M., Jitkova, Y., Mattson, R., Hurren, R., Babovic, S., Maclean, N., Restall, I., Wang, X., Jeyaraju, Danny V., Sukhai, Mahadeo A., Prabha, S., Bashir, S., Ramakrishnan, A., Leung, E., Qia, Yi H., Zhang, N., Combes, Kevin R., Ketela, T., Lin, F., Houry, Walid A., Aman, A., Al-awar, R., Zheng, W., Wienholds, E., Xu, Chang J., Dick, J., Wang, Jean C. Y., Moffat, J., Minden, Mark D., Eaves, Connie J., Bader, Gary D., Hao, Z., Kornblau, Steven M., Raught, B.& Schimmer, Aaron D. (2015). Inhibition of the Mitochondrial Protease ClpP as a Therapeutic Strategy for Human Acute Myeloid Leukemia. *Cancer Cell, 27*(6), 864-876.

Correia, Ana R., Adinolfi, S., Pastore, A.& Gomes, Cláudio M. (2006). Conformational stability of human frataxin and effect of Friedreich's ataxia-related mutations on protein folding. *Biochemical Journal, 398*(3), 605-611.

Correia, A. R., Pastore, C., Adinolfi, S., Pastore, A.& Gomes, C. M. (2008). Dynamics, stability and iron-binding activity of frataxin clinical mutants. *FEBS Journal, 275*(14), 3680-3690.

Corydon, J. T., Wilsbech, M., Jespersgaard, C., Andresen, S. B., Børglum, D. A., Pedersen, S., Bolund, L., Gregersen, N.& Bross, P. (2000). Human and mouse mitochondrial orthologs of bacterial ClpX. *Mammalian Genome, 11*(10), 899-905.

Corydon, T. J., Bross, P., Holst, H. U., Neve, S., Kristiansen, K., Gregersen, N.& Bolund, L. (1998). A human homologue of *Escherichia coli* ClpP caseinolytic protease: recombinant expression, intracellular processing and subcellular localization. *Biochemical Journal, 331*(Pt 1), 309-316.

Cossée, M., Dürr, A., Schmitt, M., Dahl, N., Trouillas, P., Allinson, P., Kostrzewa, M., Nivelon-Chevallier, A., Gustavson, K.-H., Kohlschütter, A., Müller, U., Mandel, J.-L., Brice, A., Koenig, M., Cavalcanti, F., Tammaro, A., De Michele, G., Filla, A., Cocozza, S., Labuda, M., Montermini, L., Poirier, J.& Pandolfo, M. (1999). Friedreich's ataxia: Point mutations and clinical presentation of compound heterozygotes. *Annals of Neurology, 45*(2), 200-206.

Crampton, D. J., Mukherjee, S.& Richardson, C. C. (2006). DNA-Induced Switch from Independent to Sequential dTTP Hydrolysis in the Bacteriophage T7 DNA Helicase. *Molecular Cell, 21*(2), 165-174.

Cruciat, C. M., Hell, K., Folsch, H., Neupert, W.& Stuart, R. A. (1999). Bcs1p, an AAA-family member, is a chaperone for the assembly of the cytochrome bc(1) complex. *The EMBO Journal, 18*, 5226-5233.

De Castro, R. E., Maupin-Furlow, J. A., Giménez, M. I., Herrera Seitz, M. K.& Sánchez, J. J. (2006). Haloarchaeal proteases and proteolytic systems. *FEMS Microbiology Reviews, 30*(1), 17-35.

de Lonlay, P., Valnot, I., Barrientos, A., Gorbatyuk, M., Tzagoloff, A., Taanman, J.-W., Benayoun, E., Chretien, D., Kadhom, N., Lombes, A., de Baulny, H. O., Niaudet, P., Munnich, A., Rustin, P.& Rotig, A. (2001). A mutant mitochondrial respiratory chain assembly protein causes complex III deficiency in patients with tubulopathy, encephalopathy and liver failure. *Nature Genetics, 29*(1), 57-60.

Deepa, S. S., Bhaskaran, S., Ranjit, R., Qaisar, R., Nair, B. C., Liu, Y., Walsh, M. E., Fok, W. C.& Van Remmen, H. (2015). Down-regulation of the mitochondrial matrix peptidase ClpP in muscle cells causes mitochondrial dysfunction and decreases cell proliferation. *Free Radical Biology and Medicine*.

Delettre, C., Lenaers, G., Griffoin, J.-M., Gigarel, N., Lorenzo, C., Belenguer, P., Pelloquin, L., Grosgeorge, J., Turc-Carel, C., Perret, E., Astarie-Dequeker, C., Lasquellec, L., Arnaud, B., Ducommun, B., Kaplan, J.& Hamel, C. P. (2000). Nuclear gene OPA1, encoding a mitochondrial dynamin-related protein, is mutated in dominant optic atrophy. *Nature Genetics, 26*(2), 207-210.

Detmer, S. A.& Chan, D. C. (2007). Functions and dysfunctions of mitochondrial dynamics. *Nature Reviews Molecular Cell Biology, 8*(11), 870-879.

Di Bella, D., Lazzaro, F., Brusco, A., Plumari, M., Battaglia, G., Pastore, A., Finardi, A., Cagnoli, C., Tempia, F., Frontali, M., Veneziano, L., Sacco, T., Boda, E., Brussino, A., Bonn, F., Castellotti, B., Baratta, S., Mariotti, C., Gellera, C., Fracasso, V., Magri, S., Langer, T., Plevani, P., Di Donato, S., Muzi-Falconi, M.& Taroni, F. (2010). Mutations in the mitochondrial protease gene AFG3L2 cause dominant hereditary ataxia SCA28. *Nature Genetics, 42*(4), 313-321.

Díaz-Guerra, M., Rivas, C.& Esteban, M. (1997). Activation of the IFN-Inducible Enzyme RNase L Causes Apoptosis of Animal Cells. *Virology, 236*(2), 354-363.

Dougan, D. A., Reid, B. G., Horwich, A. L.& Bukau, B. (2002). ClpS, a Substrate Modulator of the ClpAP Machine. *Molecular Cell, 9*(3), 673-683.

Dougan, D. A., Weber-Ban, E.& Bukau, B. (2003). Targeted Delivery of an ssrA-Tagged Substrate by the Adaptor Protein SspB to Its Cognate AAA+ Protein ClpX. *Molecular Cell, 12*(2), 373-380.

Dröge, W. (2002). Free Radicals in the Physiological Control of Cell Function. *Physiological Reviews, 82*(1), 47-95.

Drozdetskiy, A., Cole, C., Procter, J.& Barton, G. J. (2015). JPred4: a protein secondary structure prediction server. *Nucleic Acids Research, 43*(W1), W389-W394.

Ebel, W., Skinner, M. M., Dierksen, K. P., Scott, J. M.& Trempy, J. E. (1999). A Conserved Domain in *Escherichia coli* Lon Protease Is Involved in Substrate Discriminator Activity. *Journal of Bacteriology, 181*(7), 2236-2243.

Edmunds, T.& Goldberg, A. L. (1986). Role of ATP hydrolysis in the degradation of proteins by protease la from *Escherichia coli*. *Journal of Cellular Biochemistry, 32*(3), 187-191.

Eilers, M.& Schatz, G. (1986). Binding of a specific ligand inhibits import of a purified precursor protein into mitochondria. *Nature, 322*(6076), 228-232.

Elmore, S. P., Qian, T., Grissom, S. F.& Lemasters, J. J. (2001). The mitochondrial permeability transition initiates autophagy in rat hepatocytes. *The FASEB Journal, 15*(12), 2286-2287.

Emanuelsson, O., Nielsen, H., Brunak, S.& von Heijne, G. (2000). Predicting Subcellular Localization of Proteins Based on their N-terminal Amino Acid Sequence. *Journal of Molecular Biology, 300*(4), 1005-1016.

Erbse, A., Schmidt, R., Bornemann, T., Schneider-Mergener, J., Mogk, A., Zahn, R., Dougan, D. A.& Bukau, B. (2006). ClpS is an essential component of the N-end rule pathway in *Escherichia coli*. *Nature, 439*(7077), 753-756.

Erjavec, N., Bayot, A., Gareil, M., Camougrand, N., Nystrom, T., Friguet, B.& Bulteau, A.-L. (2013). Deletion of the mitochondrial Pim1/Lon protease in yeast results in accelerated aging and impairment of the proteasome. *Free Radical Biology and Medicine, 56*, 9-16.

Erzberger, J. P.& Berger, J. M. (2006). EVOLUTIONARY RELATIONSHIPS AND STRUCTURAL MECHANISMS OF AAA+ PROTEINS. *Annual Review of Biophysics and Biomolecular Structure, 35*(1), 93-114.

Esser, K., Tursun, B., Ingenhoven, M., Michaelis, G.& Pratje, E. (2002). A Novel Two-step Mechanism for Removal of a Mitochondrial Signal Sequence Involves the mAAA Complex and the Putative Rhomboid Protease Pcp1. *Journal of Molecular Biology, 323*(5), 835-843.

Fan, J.-Q., Ishii, S., Asano, N.& Suzuki, Y. (1999). Accelerated transport and maturation of lysosomal [alpha]-galactosidase A in Fabry lymphoblasts by an enzyme inhibitor. *Nature Medicine, 5*(1), 112-115.

Farrell, C. M., Baker, T. A.& Sauer, R. T. (2007). Altered specificity of a AAA+ protease. *Molecular cell, 25*(1), 161-166.

Farrell, C. M., Grossman, A. D.& Sauer, R. T. (2005). Cytoplasmic degradation of ssrA-tagged proteins. *Molecular Microbiology, 57*(6), 1750-1761.

Ferreirinha, F., Quattrini, A., Pirozzi, M., Valsecchi, V., Dina, G., Broccoli, V., Auricchio, A., Piemonte, F., Tozzi, G., Gaeta, L., Casari, G., Ballabio, A.& Rugarli, E. I. (2004). Axonal degeneration in paraplegin-deficient mice is associated with abnormal mitochondria and impairment of axonal transport. *The Journal of Clinical Investigation, 113*(2), 231-242.

Figge, M. T., Reichert, A. S., Meyer-Hermann, M.& Osiewacz, H. D. (2012). Deceleration of Fusion–Fission Cycles Improves Mitochondrial Quality Control during Aging. *PLoS Computational Biology, 8*(6), e1002576.

Finkel, T. (2012). Signal Transduction by Mitochondrial Oxidants. *The Journal of Biological Chemistry, 287*(7), 4434-4440.

Fischer, F., Langer, J. D.& Osiewacz, H. D. (2015). Identification of potential mitochondrial CLPXP protease interactors and substrates suggests its central role in energy metabolism. *Scientific Reports, 5*, 18375.

Flanagan, J. M., Wall, J. S., Capel, M. S., Schneider, D. K.& Shanklin, J. (1995). Scanning Transmission Electron Microscopy and Small-Angle Scattering Provide Evidence that Native *Escherichia coli* ClpP is a Tetradecamer with an Axial Pore. *Biochemistry, 34*(34), 10910-10917.

Flynn, J. M., Levchenko, I., Seidel, M., Wickner, S. H., Sauer, R. T.& Baker, T. A. (2001). Overlapping recognition determinants within the ssrA degradation tag allow modulation of proteolysis. *Proceedings of the National Academy of Sciences, 98*(19), 10584-10589.

Flynn, J. M., Neher, S. B., Kim, Y.-I., Sauer, R. T.& Baker, T. A. (2003). Proteomic Discovery of Cellular Substrates of the ClpXP Protease Reveals Five Classes of ClpX-Recognition Signals. *Molecular Cell, 11*(3), 671-683.

Fu, G. K., Smith, M. J.& Markovitz, D. M. (1997). Bacterial Protease Lon Is a Site-specific DNA-binding Protein. *Journal of Biological Chemistry, 272*(1), 534-538.

Fukasawa, Y., Tsuji, J., Fu, S.-C., Tomii, K., Horton, P.& Imai, K. (2015). MitoFates: Improved Prediction of Mitochondrial Targeting Sequences and Their Cleavage Sites. *Molecular & Cellular Proteomics, 14*(4), 1113-1126.

Fukuda, R., Zhang, H., Kim, J.-w., Shimoda, L., Dang, C. V.& Semenza, Gregg L. (2007). HIF-1 Regulates Cytochrome Oxidase Subunits to Optimize Efficiency of Respiration in Hypoxic Cells. *Cell, 129*(1), 111-122.

Fukui, T., Eguchi, T., Atomi, H.& Imanaka, T. (2002). A Membrane-Bound Archaeal Lon Protease Displays ATP-Independent Proteolytic Activity towards Unfolded Proteins and ATP-Dependent Activity for Folded Proteins. *Journal of Bacteriology, 184*(13), 3689-3698.

Gai, D., Zhao, R., Li, D., Finkielstein, C. V.& Chen, X. S. (2004). Mechanisms of Conformational Change for a Replicative Hexameric Helicase of SV40 Large Tumor Antigen. *Cell, 119*(1), 47-60.

Gakh, O., Cavadini, P.& Isaya, G. (2002). Mitochondrial processing peptidases. *Biochimica et Biophysica Acta (BBA) - Molecular Cell Research, 1592*(1), 63-77.

Galea, C. A., Huq, A., Lockhart, P. J., Tai, G., Corben, L. A., Yiu, E. M., Gurrin, L. C., Lynch, D. R., Gelbard, S., Durr, A., Pousset, F., Parkinson, M., Labrum, R., Giunti, P., Perlman, S. L., Delatycki, M. B.& Evans-Galea, M. V. (2016). Compound heterozygous FXN mutations and clinical outcome in friedreich ataxia. *Annals of Neurology, 79*(3), 485-495.

García-Nafría, J., Ondrovičová, G., Blagova, E., Levdikov, V. M., Bauer, J. A., Suzuki, C. K., Kutejová, E., Wilkinson, A. J.& Wilson, K. S. (2010). Structure of the catalytic domain of the human mitochondrial Lon protease: Proposed relation of oligomer formation and activity. *Protein Science, 19*(5), 987-999.

Gersch, M., Stahl, M., Poreba, M., Dahmen, M., Dziedzic, A., Drag, M.& Sieber, S. A. (2015). Barrel-shaped ClpP Proteases Display Attenuated Cleavage Specificities. *ACS Chemical Biology*.

Ghezzi, D.& Zeviani, M. (2012). Assembly Factors of Human Mitochondrial Respiratory Chain Complexes: Physiology and Pathophysiology. In B. Kadenbach (Ed.), *Mitochondrial Oxidative Phosphorylation: Nuclear-Encoded Genes, Enzyme Regulation, and Pathophysiology* (pp. 65-106). New York, NY: Springer New York.

Gibellini, L., Pinti, M., Bartolomeo, R., Biasi, S. D., Cormio, A., Musicco, C., Carnevale, G., Pecorini, S., Nasi, M., Pol, A. D.& Cossarizza, A. (2015). Inhibition of Lon protease by triterpenoids alters mitochondria and is associated to cell death in human cancer cells. *Oncotarget, 6*(28), 25466-25483.

Gibellini, L., Pinti, M., Boraldi, F., Giorgio, V., Bernardi, P., Bartolomeo, R., Nasi, M., De Biasi, S., Missiroli, S., Carnevale, G., Losi, L., Tesei, A., Pinton, P., Quaglino, D.& Cossarizza, A. (2014). Silencing of mitochondrial Lon protease deeply impairs mitochondrial

proteome and function in colon cancer cells. *The FASEB Journal, 28*(12), 5122-5135.

Gispert, S., Parganlija, D., Klinkenberg, M., Dröse, S., Wittig, I., Mittelbronn, M., Grzmil, P., Koob, S., Hamann, A., Walter, M., Büchel, F., Adler, T., Hrabé de Angelis, M., Busch, D. H., Zell, A., Reichert, A. S., Brandt, U., Osiewacz, H. D., Jendrach, M.& Auburger, G. (2013). Loss of mitochondrial peptidase Clpp leads to infertility, hearing loss plus growth retardation via accumulation of CLPX, mtDNA and inflammatory factors. *Human Molecular Genetics, 22*(24), 4871-4887.

Glynn, S. E., Martin, A., Nager, A. R., Baker, T. A.& Sauer, R. T. (2009). Crystal structures of asymmetric ClpX hexamers reveal nucleotide-dependent motions in a AAA+ protein-unfolding machine. *Cell, 139*(4), 744-756.

Glynn, S. E., Nager, A. R., Baker, T. A.& Sauer, R. T. (2012). Dynamic and static components power unfolding in topologically closed rings of a AAA+ proteolytic machine. *Nature Structural & Molecular Biology, 19*(6), 616-622.

Goldberg, A. L., Moerschell, R. P., Hachung, C.& Maurizi, M. R. (1994). ATP-dependent protease La (Lon) from *Escherichia coli. Methods in Enzymology* (Vol. 244, pp. 350-375): Academic Press.

Gonzalez, M., Frank, E. G., Levine, A. S.& Woodgate, R. (1998). Lon-mediated proteolysis of the *Escherichia coli* UmuD mutagenesis protein: in vitro degradation and identification of residues required for proteolysis. *Genes & Development, 12*(24), 3889-3899.

Gonzalez, M., Rasulova, F., Maurizi, M. R.& Woodgate, R. (2000). Subunit-specific degradation of the UmuD/D′ heterodimer by the ClpXP protease: the role of trans recognition in UmuD′ stability. *The EMBO Journal, 19*(19), 5251-5258.

Gosslau, A., Ruoff, P., Mohsenzadeh, S., Hobohm, U.& Rensing, L. (2001). Heat Shock and Oxidative Stress-induced Exposure of Hydrophobic Protein Domains as Common Signal in the Induction of Hsp68. *Journal of Biological Chemistry, 276*(3), 1814-1821.

Goto-Yamada, S., Mano, S., Nakamori, C., Kondo, M., Yamawaki, R., Kato, A.& Nishimura, M. (2014). Chaperone and Protease Functions of LON Protease 2 Modulate the Peroxisomal Transition and Degradation with Autophagy. *Plant and Cell Physiology, 55*(3), 482-496.

Gottesman, S., Roche, E., Zhou, Y.& Sauer, R. T. (1998). The ClpXP and ClpAP proteases degrade proteins with carboxy-terminal peptide tails added by the SsrA-tagging system. *Genes & Development, 12*(9), 1338-1347.

Granot, Z., Geiss-Friedlander, R., Melamed-Book, N., Eimerl, S., Timberg, R., Weiss, A. M., Hales, K. H., Hales, D. B., Stocco, D. M.& Orly, J. (2003). Proteolysis of Normal and Mutated Steroidogenic Acute Regulatory Proteins in the Mitochondria: the Fate of Unwanted Proteins. *Molecular Endocrinology, 17*(12), 2461-2476.

Granot, Z., Kobiler, O., Melamed-Book, N., Eimerl, S., Bahat, A., Lu, B., Braun, S., Maurizi, M. R., Suzuki, C. K., Oppenheim, A. B.& Orly, J. (2007a). Turnover of Mitochondrial Steroidogenic Acute Regulatory (StAR) Protein by Lon Protease: The Unexpected Effect of Proteasome Inhibitors. *Molecular Endocrinology, 21*(9), 2164-2177.

Granot, Z., Melamed-Book, N., Bahat, A.& Orly, J. (2007b). Turnover of StAR protein: Roles for the proteasome and mitochondrial proteases. *Molecular and Cellular Endocrinology, 265–266*, 51-58.

Granot, Z., Silverman, E., Friedlander, R., Melamed-Book, N., Eimerl, S., Timberg, R., Hales, K. H., Hales, D. B., Stocco, D. M.& Orly, J. (2002). The life cycle of the steroidogenic acute regulatory protein (StAR): From transcription through proteolysis. *Endocrine Research, 28*(4), 375-386.

Greene, A. W., Grenier, K., Aguileta, M. A., Muise, S., Farazifard, R., Haque, M. E., McBride, H. M., Park, D. S.& Fon, E. A. (2012). Mitochondrial processing peptidase regulates PINK1 processing, import and Parkin recruitment. *EMBO reports, 13*(4), 378-385.

Gribun, A., Kimber, M. S., Ching, R., Sprangers, R., Fiebig, K. M.& Houry, W. A. (2005). The ClpP Double Ring Tetradecameric Protease Exhibits Plastic Ring-Ring Interactions, and the N Termini of Its Subunits Form Flexible Loops That Are Essential for ClpXP and ClpAP Complex Formation. *Journal of Biological Chemistry, 280*(16), 16185-16196.

Grimaud, R., Kessel, M., Beuron, F., Steven, A. C.& Maurizi, M. R. (1998). Enzymatic and Structural Similarities between the *Escherichia coli* ATP-dependent Proteases, ClpXP and ClpAP. *Journal of Biological Chemistry, 273*(20), 12476-12481.

Gu, Z. T., Wang, H., Li, L., Liu, Y. S., Deng, X. B., Huo, S. F., Yuan, F. F., Liu, Z. F., Tong, H. S.& Su, L. (2014). Heat stress induces apoptosis through transcription-independent p53-mediated mitochondrial pathways in human umbilical vein endothelial cell. *Scientific Reports, 4*, 4469.

Guillon, B., Bulteau, A.-L., Wattenhofer-Donzé, M., Schmucker, S., Friguet, B., Puccio, H., Drapier, J.-C.& Bouton, C. (2009). Frataxin deficiency causes upregulation of mitochondrial Lon and ClpP proteases and severe loss of mitochondrial Fe–S proteins. *FEBS Journal, 276*(4), 1036-1047.

Gur, E. (2013). The Lon AAA+ Protease. In D. A. Dougan (Ed.), *Regulated Proteolysis in Microorganisms*. Dordrecht: Springer Netherlands.

Gur, E., Ottofueling, R.& Dougan, D. A. (2013). Machines of Destruction – AAA+ Proteases and the Adaptors That Control Them. In A. D. Dougan (Ed.), *Regulated Proteolysis in Microorganisms* (pp. 3-33). Dordrecht: Springer Netherlands.

Gur, E.& Sauer, R. T. (2008). Recognition of misfolded proteins by Lon, a AAA+ protease. *Genes & Development, 22*(16), 2267-2277.

Gur, E.& Sauer, R. T. (2009). Degrons in protein substrates program the speed and operating efficiency of the AAA+ Lon proteolytic machine. *Proceedings of the National Academy of Sciences, 106*(44), 18503-18508.

Gur, E., Vishkautzan, M.& Sauer, R. T. (2012). Protein unfolding and degradation by the AAA+ Lon protease. *Protein Science : A Publication of the Protein Society, 21*(2), 268-278.

Habib, S. J., Neupert, W.& Rapaport, D. (2007). Analysis and Prediction of Mitochondrial Targeting Signals *Methods in Cell Biology* (Vol. 80, pp. 761-781): Academic Press.

Hanahan, D. (1983). Studies on transformation of *Escherichia coli* with plasmids. *Journal of Molecular Biology, 166*(4), 557-580.

Hansen, J., Corydon, T. J., Palmfeldt, J., Dürr, A., Fontaine, B., Nielsen, M. N., Christensen, J. H., Gregersen, N.& Bross, P. (2008). Decreased expression of the mitochondrial matrix proteases Lon and ClpP in cells from a patient with hereditary spastic paraplegia (SPG13). *Neuroscience, 153*(2), 474-482.

Hanson, P. I.& Whiteheart, S. W. (2005). AAA+ proteins: have engine, will work. *Nature Reviews Molecular Cell Biology, 6*(7), 519-529.

Hao, H.-X., Khalimonchuk, O., Schraders, M., Dephoure, N., Bayley, J.-P., Kunst, H., Devilee, P., Cremers, C. W. R. J., Schiffman, J. D., Bentz, B. G., Gygi, S. P., Winge, D. R., Kremer, H.& Rutter, J. (2009). SDH5, a Gene Required for Flavination of Succinate Dehydrogenase, Is Mutated in Paraganglioma. *Science, 325*(5944), 1139-1142.

Harbauer, Angelika B., Zahedi, René P., Sickmann, A., Pfanner, N.& Meisinger, C. (2014). The Protein Import Machinery of Mitochondria—A Regulatory Hub in Metabolism, Stress, and Disease. *Cell Metabolism, 19*(3), 357-372.

Harlow, E.& Lane, D. (1999). *Using Antibodies: A Laboratory Manual*. Cold Spring Harbour: Cold Spring Harbour Laboratory Press.

Harrison, J. F., Hollensworth, S. B., Spitz, D. R., Copeland, W. C., Wilson, G. L.& LeDoux, S. P. (2005). Oxidative stress-induced apoptosis in neurons correlates with mitochondrial DNA base excision repair pathway imbalance. *Nucleic Acids Research, 33*(14), 4660-4671.

Hartl, F. U., Bracher, A.& Hayer-Hartl, M. (2011). Molecular chaperones in protein folding and proteostasis. *Nature, 475*(7356), 324-332.

Haynes, C. M., Petrova, K., Benedetti, C., Yang, Y.& Ron, D. (2007). ClpP Mediates Activation of a Mitochondrial Unfolded Protein Response in C. elegans. *Developmental Cell, 13*(4), 467-480.

Herman, C., Prakash, S., Lu, C. Z., Matouschek, A.& Gross, C. A. (2003). Lack of a Robust Unfoldase Activity Confers a Unique Level of Substrate Specificity to the Universal AAA Protease FtsH. *Molecular Cell, 11*(3), 659-669.

Hersch, G. L., Burton, R. E., Bolon, D. N., Baker, T. A.& Sauer, R. T. (2005). Asymmetric Interactions of ATP with the AAA+ ClpX6 Unfoldase: Allosteric Control of a Protein Machine. *Cell, 121*(7), 1017-1027.

Hinnerwisch, J., Reid, B. G., Fenton, W. A.& Horwich, A. L. (2005). Roles of the N-domains of the ClpA Unfoldase in Binding Substrate Proteins and in Stable Complex Formation with the ClpP Protease. *Journal of Biological Chemistry, 280*(49), 40838-40844.

Hinson, J. T., Fantin, V. R., Schönberger, J., Breivik, N., Siem, G., McDonough, B., Sharma, P., Keogh, I., Godinho, R., Santos, F., Esparza, A., Nicolau, Y., Selvaag, E., Cohen, B. H., Hoppel, C. L., Tranebjærg, L., Eavey, R. D., Seidman, J. G.& Seidman, C. E. (2007). Missense Mutations in the BCS1L Gene as a Cause of the Björnstad Syndrome. *New England Journal of Medicine, 356*(8), 809-819.

Hipp, M. S., Park, S.-H.& Hartl, F. U. (2014). Proteostasis impairment in protein-misfolding and -aggregation diseases. *Trends in Cell Biology, 24*(9), 506-514.

Hori, O., Ichinoda, F., Tamatani, T., Yamaguchi, A., Sato, N., Ozawa, K., Kitao, Y., Miyazaki, M., Harding, H. P., Ron, D., Tohyama, M., M Stern, D.& Ogawa, S. (2002). Transmission of cell stress from endoplasmic reticulum to mitochondria: enhanced expression of Lon protease. *The Journal of Cell Biology, 157*(7), 1151-1160.

Hoskins, J. R., Yanagihara, K., Mizuuchi, K.& Wickner, S. (2002). ClpAP and ClpXP degrade proteins with tags located in the interior of the primary sequence. *Proceedings of the National Academy of Sciences, 99*(17), 11037-11042.

Hwang, C.-S., Shemorry, A.& Varshavsky, A. (2010). N-Terminal Acetylation of Cellular Proteins Creates Specific Degradation Signals. *Science, 327*(5968), 973-977.

Indio, V., Martelli, P. L., Savojardo, C., Fariselli, P.& Casadio, R. (2013). The prediction of organelle-targeting peptides in eukaryotic proteins with Grammatical-Restrained Hidden Conditional Random Fields. *Bioinformatics, 29*(8), 981-988.

Indran, I. R., Tufo, G., Pervaiz, S.& Brenner, C. (2011). Recent advances in apoptosis, mitochondria and drug resistance in cancer cells. *Biochimica et Biophysica Acta (BBA) - Bioenergetics, 1807*(6), 735-745.

Inobe, T., Fishbain, S., Prakash, S.& Matouschek, A. (2011). Defining the geometry of the two-component proteasome degron. *Nature Chemical Biology, 7*(3), 161-167.

Inoue, M., Kamada, H., Abe, Y., Higashisaka, K., Nagano, K., Mukai, Y., Yoshioka, Y., Tsutsumi, Y.& Tsunoda, S.-i. (2015). Aminopeptidase P3, a new member of the TNF–TNFR2 signaling complex, induces phosphorylation of JNK1 and JNK2. *Journal of Cell Science, 128*(4), 656-669.

Ishihara, N., Fujita, Y., Oka, T.& Mihara, K. (2006). Regulation of mitochondrial morphology through proteolytic cleavage of OPA1. *The EMBO Journal, 25*(13), 2966-2977.

Ishii, Y., Sonezaki, S., Iwasaki, Y., Miyata, Y., Akita, K., Kato, Y.& Amano, F. (2000). Regulatory Role of C-Terminal Residues of SulA in Its Degradation by Lon Protease in *Escherichia coli*. *Journal of Biochemistry, 127*(5), 837-844.

Iyer, L. M., Leipe, D. D., Koonin, E. V.& Aravind, L. (2004). Evolutionary history and higher order classification of AAA+ ATPases. *Journal of Structural Biology, 146*(1–2), 11-31.

Jayasekera, M. M. K., Foltin, S. K., Olson, E. R.& Holler, T. P. (2000). *Escherichia coli* Requires the Protease Activity of FtsH for Growth. *Archives of Biochemistry and Biophysics, 380*(1), 103-107.

Jenkinson, E. M., Clayton-Smith, J., Mehta, S., Bennett, C., Reardon, W., Green, A., Pearce, S. H. S., De Michele, G., Conway, G. S., Cilliers, D., Moreton, N., Davis, J. R. E., Trump, D.& Newman, W. G. (2012). Perrault syndrome: further evidence for genetic heterogeneity. *Journal of Neurology, 259*(5), 974-976.

Jenkinson, Emma M., Rehman, Atteeq U., Walsh, T., Clayton-Smith, J., Lee, K., Morell, Robert J., Drummond, Meghan C., Khan, Shaheen N., Naeem, Muhammad A., Rauf, B., Billington, N., Schultz, Julie M., Urquhart, Jill E., Lee, Ming K., Berry, A., Hanley, Neil A., Mehta, S., Cilliers, D., Clayton, Peter E., Kingston,

H., Smith, Miriam J., Warner, Thomas T., Black, Graeme C., Trump, D., Davis, Julian R. E., Ahmad, W., Leal, Suzanne M., Riazuddin, S., King, M.-C., Friedman, Thomas B.& Newman, William G. (2013). Perrault Syndrome Is Caused by Recessive Mutations in CLPP, Encoding a Mitochondrial ATP-Dependent Chambered Protease. *The American Journal of Human Genetics, 92*(4), 605-613.

Jeon, H. B., Choi, E. S., Yoon, J. H., Hwang, J. H., Chang, J. W., Lee, E. K., Choi, H. W., Park, Z.-Y.& Yoo, Y. J. (2007). A proteomics approach to identify the ubiquitinated proteins in mouse heart. *Biochemical and Biophysical Research Communications, 357*(3), 731-736.

Jin, S. M.& Youle, R. J. (2013). The accumulation of misfolded proteins in the mitochondrial matrix is sensed by PINK1 to induce PARK2/Parkin-mediated mitophagy of polarized mitochondria. *Autophagy, 9*(11), 1750-1757.

Johnston, A. J., Hoogenraad, J., Dougan, D. A., Truscott, K. N., Yano, M., Mori, M., Hoogenraad, N. J.& Ryan, M. T. (2002). Insertion and Assembly of Human Tom7 into the Preprotein Translocase Complex of the Outer Mitochondrial Membrane. *Journal of Biological Chemistry, 277*(44), 42197-42204.

Johri, A.& Beal, M. F. (2012). Mitochondrial Dysfunction in Neurodegenerative Diseases. *The Journal of Pharmacology and Experimental Therapeutics, 342*(3), 619-630.

Jonckheere, A. I., Smeitink, J. A. M.& Rodenburg, R. J. T. (2012). Mitochondrial ATP synthase: architecture, function and pathology. *Journal of Inherited Metabolic Disease, 35*(2), 211-225.

Joshi, S. A., Hersch, G. L., Baker, T. A.& Sauer, R. T. (2004). Communication between ClpX and ClpP during substrate processing and degradation. *Nature Structural & Molecular Biology, 11*(5), 404-411.

Jucker, M.& Walker, L. C. (2013). Self-propagation of pathogenic protein aggregates in neurodegenerative diseases. *Nature, 501*(7465), 45-51.

Justo, R., Oliver, J.& Gianotti, M. (2005). Brown adipose tissue mitochondrial subpopulations show different morphological and thermogenic characteristics. *Mitochondrion, 5*(1), 45-53.

Kadenbach, B.& Hüttemann, M. (2015). The subunit composition and function of mammalian cytochrome c oxidase. *Mitochondrion, 24*, 64-76.

Kang, P. J., Ostermann, J., Shilling, J., Neupert, W., Craig, E. A.& Pfanner, N. (1990). Requirement for hsp70 in the mitochondrial

matrix for translocation and folding of precursor proteins. *Nature, 348*(6297), 137-143.

Kang, S. G., Dimitrova, M. N., Ortega, J., Ginsburg, A.& Maurizi, M. R. (2005). Human Mitochondrial ClpP Is a Stable Heptamer That Assembles into a Tetradecamer in the Presence of ClpX. *Journal of Biological Chemistry, 280*(42), 35424-35432.

Kang, S. G., Maurizi, M. R., Thompson, M., Mueser, T.& Ahvazi, B. (2004). Crystallography and mutagenesis point to an essential role for the N-terminus of human mitochondrial ClpP. *Journal of Structural Biology, 148*(3), 338-352.

Kang, S. G., Ortega, J., Singh, S. K., Wang, N., Huang, N.-n., Steven, A. C.& Maurizi, M. R. (2002). Functional Proteolytic Complexes of the Human Mitochondrial ATP-dependent Protease, hClpXP. *Journal of Biological Chemistry, 277*(23), 21095-21102.

Kao, T. Y., Chiu, Y. C., Fang, W. C., Cheng, C. W., Kuo, C. Y., Juan, H. F., Wu, S. H.& Lee, A. Y. L. (2015). Mitochondrial Lon regulates apoptosis through the association with Hsp60-mtHsp70 complex. *Cell Death & Disease, 6*, e1642.

Karata, K., Inagawa, T., Wilkinson, A. J., Tatsuta, T.& Ogura, T. (1999). Dissecting the Role of a Conserved Motif (the Second Region of Homology) in the AAA Family of ATPases: SITE-DIRECTED MUTAGENESIS OF THE ATP-DEPENDENT PROTEASE FtsH. *Journal of Biological Chemistry, 274*(37), 26225-26232.

Karbowski, M.& Youle, R. J. (2011). Regulating mitochondrial outer membrane proteins by ubiquitination and proteasomal degradation. *Current Opinion in Cell Biology, 23*(4), 476-482.

Kardon, Julia R., Yien, Yvette Y., Huston, Nicholas C., Branco, Diana S., Hildick-Smith, Gordon J., Rhee, Kyu Y., Paw, Barry H.& Baker, Tania A. (2015). Mitochondrial ClpX Activates a Key Enzyme for Heme Biosynthesis and Erythropoiesis. *Cell, 161*(4), 858-867.

Kasashima, K., Sumitani, M.& Endo, H. (2012). Maintenance of mitochondrial genome distribution by mitochondrial AAA+ protein ClpX. *Experimental Cell Research, 318*(18), 2335-2343.

Kenniston, J. A., Baker, T. A., Fernandez, J. M.& Sauer, R. T. (2003). Linkage between ATP Consumption and Mechanical Unfolding during the Protein Processing Reactions of an AAA+ Degradation Machine. *Cell, 114*(4), 511-520.

Kikuchi, M., Hatano, N., Yokota, S., Shimozawa, N., Imanaka, T.& Taniguchi, H. (2004). Proteomic Analysis of Rat Liver Peroxisome: PRESENCE OF PEROXISOME-SPECIFIC ISOZYME OF LON PROTEASE. *Journal of Biological Chemistry, 279*(1), 421-428.

Kim, I., Rodriguez-Enriquez, S.& Lemasters, J. J. (2007). Selective degradation of mitochondria by mitophagy. *Archives of Biochemistry and Biophysics, 462*(2), 245-253.

Kim, Y.-I., Levchenko, I., Fraczkowska, K., Woodruff, R. V., Sauer, R. T.& Baker, T. A. (2001). Molecular determinants of complex formation between Clp/Hsp100 ATPases and the ClpP peptidase. *Nature Structural & Molecular Biology 8*(3), 230-233.

Kimber, M. S., Yu, A. Y. H., Borg, M., Leung, E., Chan, H. S.& Houry, W. A. (2010). Structural and Theoretical Studies Indicate that the Cylindrical Protease ClpP Samples Extended and Compact Conformations. *Structure, 18*(7), 798-808.

Kirstein, J., Hoffmann, A., Lilie, H., Schmidt, R., Rübsamen-Waigmann, H., Brötz-Oesterhelt, H., Mogk, A.& Turgay, K. (2009a). The antibiotic ADEP reprogrammes ClpP, switching it from a regulated to an uncontrolled protease. *EMBO Molecular Medicine, 1*(1), 37-49.

Kirstein, J., Moliere, N., Dougan, D. A.& Turgay, K. (2009b). Adapting the machine: adaptor proteins for Hsp100/Clp and AAA+ proteases. *Nature Reviews Microbiology, 7*(8), 589-599.

Kisselev, A. F., Akopian, T. N., Woo, K. M.& Goldberg, A. L. (1999). The Sizes of Peptides Generated from Protein by Mammalian 26 and 20 S Proteasomes: IMPLICATIONS FOR UNDERSTANDING THE DEGRADATIVE MECHANISM AND ANTIGEN PRESENTATION. *Journal of Biological Chemistry, 274*(6), 3363-3371.

Kita, K., Suzuki, T.& Ochi, T. (2012). Diphenylarsinic Acid Promotes Degradation of Glutaminase C by Mitochondrial Lon Protease. *Journal of Biological Chemistry, 287*(22), 18163-18172.

Kondadi, A. K., Wang, S., Montagner, S., Kladt, N., Korwitz, A., Martinelli, P., Herholz, D., Baker, M. J., Schauss, A. C., Langer, T.& Rugarli, E. I. (2014). Loss of the m-AAA protease subunit AFG3L2 causes mitochondrial transport defects and tau hyperphosphorylation. *The EMBO Journal, 33*(9), 1011-1026.

Koodathingal, P., Jaffe, N. E., Kraut, D. A., Prakash, S., Fishbain, S., Herman, C.& Matouschek, A. (2009). ATP-dependent Proteases Differ Substantially in Their Ability to Unfold Globular Proteins. *Journal of Biological Chemistry, 284*(28), 18674-18684.

Koppen, M., Bonn, F., Ehses, S.& Langer, T. (2009). Autocatalytic Processing of m-AAA Protease Subunits in Mitochondria. *Molecular Biology of the Cell, 20*(19), 4216-4224.

Koppen, M.& Langer, T. (2007). Protein Degradation within Mitochondria: Versatile Activities of AAA Proteases and Other Peptidases. *Critical Reviews in Biochemistry and Molecular Biology, 42*(3), 221-242.

Kowarsch, A., Fuchs, A., Frishman, D.& Pagel, P. (2010). Correlated Mutations: A Hallmark of Phenotypic Amino Acid Substitutions. *PLOS Computational Biology, 6*(9), e1000923.

Krzywda, S., Brzozowski, A. M., Verma, C., Karata, K., Ogura, T.& Wilkinson, A. J. (2002). The Crystal Structure of the AAA Domain of the ATP-Dependent Protease FtsH of *Escherichia coli* at 1.5 Å Resolution. *Structure, 10*(8), 1073-1083.

Kundu, M., Lindsten, T., Yang, C.-Y., Wu, J., Zhao, F., Zhang, J., Selak, M. A., Ney, P. A.& Thompson, C. B. (2008). Ulk1 plays a critical role in the autophagic clearance of mitochondria and ribosomes during reticulocyte maturation. *Blood, 112*(4), 1493-1502.

Kutejová, E., DurčovÁ, G., SurovkovÁ, E.& Kužela, Š. (1993). Yeast mitochondrial ATP-dependent protease: purification and comparison with the homologous rat enzyme and the bacterial ATP-dependent protease La. *FEBS Letters, 329*(1-2), 47-50.

Laemmli, U. K. (1970). Cleavage of Structural Proteins during the Assembly of the Head of Bacteriophage T4. *Nature, 227*(5259), 680-685.

Lanzetta, P. A., Alvarez, L. J., Reinach, P. S.& Candia, O. A. (1979). An improved assay for nanomole amounts of inorganic phosphate. *Analytical Biochemistry, 100*(1), 95-97.

Lau, E., Wang, D., Zhang, J., Yu, H., Lam, M. P. Y., Liang, X., Zong, N., Kim, T.-Y.& Ping, P. (2012). Substrate- and Isoform-Specific Proteome Stability in Normal and Stressed Cardiac Mitochondria. *Circulation Research, 110*(9), 1174-1178.

Laue, T. M., Shah, B. D., Ridgeway, T. M.& Pelletier, S. L. (1992). Computer-aided interpretation of analytical sedimentation data for proteins. In S. E. Harding, A. J. Rowe, & J. C. Horton (Eds.), *Analytical Ultracentrifugation in Biochemistry and Polymer Science* (pp. 90–125). Cambridge: Royal Society of Chemistry.

Lavigne, P., Najmanivich, R.& LeHoux, J.-G. (2010). Mammalian StAR-Related Lipid Transfer (START) Domains with Specificity for Cholesterol: Structural Conservation and Mechanism of Reversible Binding. In R. J. Harris (Ed.), *Cholesterol Binding and Cholesterol Transport Proteins: Structure and Function in Health and Disease* (pp. 425-437). Dordrecht: Springer Netherlands.

Lecker, S. H., Goldberg, A. L.& Mitch, W. E. (2006). Protein Degradation by the Ubiquitin–Proteasome Pathway in Normal and Disease States. *Journal of the American Society of Nephrology, 17*(7), 1807-1819.

Lee, C., Schwartz, M. P., Prakash, S., Iwakura, M.& Matouschek, A. (2001). ATP-Dependent Proteases Degrade Their Substrates by

Processively Unraveling Them from the Degradation Signal. *Molecular Cell, 7*(3), 627-637.

Lee, D. H.& Goldberg, A. L. (1998). Proteasome inhibitors: valuable new tools for cell biologists. *Trends in Cell Biology, 8*(10), 397-403.

Lee, M. E., Baker, T. A.& Sauer, R. T. (2010). Control of substrate gating and translocation into ClpP by channel residues and ClpX binding. *Journal of Molecular Biology, 399*(5), 707-718.

Lee, Y. J., Jeong, S.-Y., Karbowski, M., Smith, C. L.& Youle, R. J. (2004a). Roles of the Mammalian Mitochondrial Fission and Fusion Mediators Fis1, Drp1, and Opa1 in Apoptosis. *Molecular Biology of the Cell, 15*(11), 5001-5011.

Lee, Y. L., Hsu, C.-H.& Wu, S.-H. (2004b). Functional Domains of Brevibacillus thermoruber Lon Protease for Oligomerization and DNA Binding: ROLE OF N-TERMINAL AND SENSOR AND SUBSTRATE DISCRIMINATION DOMAINS. *Journal of Biological Chemistry, 279*(33), 34903-34912.

Lemasters, J. J., Nieminen, A.-L., Qian, T., Trost, L. C., Elmore, S. P., Nishimura, Y., Crowe, R. A., Cascio, W. E., Bradham, C. A., Brenner, D. A.& Herman, B. (1998). The mitochondrial permeability transition in cell death: a common mechanism in necrosis, apoptosis and autophagy. *Biochimica et Biophysica Acta (BBA) - Bioenergetics, 1366*(1–2), 177-196.

Leonhard, K., Herrmann, J. M., Stuart, R. A., Mannhaupt, G., Neupert, W.& Langer, T. (1996). AAA proteases with catalytic sites on opposite membrane surfaces comprise a proteolytic system for the ATP-dependent degradation of inner membrane proteins in mitochondria. *The EMBO Journal, 15*(16), 4218-4229.

Levchenko, I., Seidel, M., Sauer, R. T.& Baker, T. A. (2000). A Specificity-Enhancing Factor for the ClpXP Degradation Machine. *Science, 289*(5488), 2354-2356.

Li, D. H. S., Chung, Y. S., Gloyd, M., Joseph, E., Ghirlando, R., Wright, G. D., Cheng, Y.-Q., Maurizi, M. R., Guarné, A.& Ortega, J. (2010). Acyldepsipeptide Antibiotics Induce the Formation of a Structured Axial Channel in ClpP: A Model for the ClpX/ClpA-Bound State of ClpP. *Chemistry & Biology, 17*(9), 959-969.

Li, S., Chien, S.& Brånemark, P.-I. (1999). Heat shock-induced necrosis and apoptosis in osteoblasts. *Journal of Orthopaedic Research, 17*(6), 891-899.

Li, X., Fang, P., Mai, J., Choi, E. T., Wang, H.& Yang, X.-f. (2013). Targeting mitochondrial reactive oxygen species as novel therapy for inflammatory diseases and cancers. *Journal of Hematology & Oncology, 6*, 19-19.

Lin, M. T.& Beal, M. F. (2006). Mitochondrial dysfunction and oxidative stress in neurodegenerative diseases. *Nature, 443*(7113), 787-795.

Liu, J., Rone, M. B.& Papadopoulos, V. (2006). Protein-Protein Interactions Mediate Mitochondrial Cholesterol Transport and Steroid Biosynthesis. *Journal of Biological Chemistry, 281*(50), 38879-38893.

Liu, T., Lu, B., Lee, I., Ondrovičová, G., Kutejová, E.& Suzuki, C. K. (2004). DNA and RNA Binding by the Mitochondrial Lon Protease Is Regulated by Nucleotide and Protein Substrate. *Journal of Biological Chemistry, 279*(14), 13902-13910.

Liu, Y., Lan, L., Huang, K., Wang, R., Xu, C., Shi, Y., Wu, X., Wu, Z., Zhang, J., Chen, L., Wang, L., Yu, X., Zhu, H.& Lu, B. (2014). Inhibition of Lon blocks cell proliferation, enhances chemosensitivity by promoting apoptosis and decreases cellular bioenergetics of bladder cancer: potential roles of Lon as a prognostic marker and therapeutic target in baldder cancer. *Oncotarget, 5*(22), 11209-11224.

Lowth, B. R., Kirstein-Miles, J., Saiyed, T., Brötz-Oesterhelt, H., Morimoto, R. I., Truscott, K. N.& Dougan, D. A. (2012). Substrate recognition and processing by a Walker B mutant of the human mitochondrial AAA+ protein CLPX. *Journal of Structural Biology, 179*(2), 193-201.

Lu, B., Lee, J., Nie, X., Li, M., Morozov, Y. I., Venkatesh, S., Bogenhagen, D. F., Temiakov, D.& Suzuki, C. K. (2013). Phosphorylation of human TFAM in mitochondria impairs DNA binding and promotes degradation by the AAA(+) Lon protease. *Molecular cell, 49*(1), 121-132.

Lu, B., Yadav, S., Shah, P. G., Liu, T., Tian, B., Pukszta, S., Villaluna, N., Kutejová, E., Newlon, C. S., Santos, J. H.& Suzuki, C. K. (2007). Roles for the Human ATP-dependent Lon Protease in Mitochondrial DNA Maintenance. *Journal of Biological Chemistry, 282*(24), 17363-17374.

Luciakova, K., Sokolikova, B., Chloupkova, M.& Nelson, B. D. (1999). Enhanced mitochondrial biogenesis is associated with increased expression of the mitochondrial ATP-dependent Lon protease. *FEBS Letters, 444*(2-3), 186-188.

Lutsenko, S.& Cooper, M. J. (1998). Localization of the Wilson's disease protein product to mitochondria. *Proceedings of the National Academy of Sciences, 95*(11), 6004-6009.

MacArthur, D. G., Balasubramanian, S., Frankish, A., Huang, N., Morris, J., Walter, K., Jostins, L., Habegger, L., Pickrell, J. K., Montgomery, S. B., Albers, C. A., Zhang, Z. D., Conrad, D. F., Lunter, G., Zheng, H., Ayub, Q., DePristo, M. A., Banks, E., Hu,

M., Handsaker, R. E., Rosenfeld, J. A., Fromer, M., Jin, M., Mu, X. J., Khurana, E., Ye, K., Kay, M., Saunders, G. I., Suner, M.-M., Hunt, T., Barnes, I. H. A., Amid, C., Carvalho-Silva, D. R., Bignell, A. H., Snow, C., Yngvadottir, B., Bumpstead, S., Cooper, D. N., Xue, Y., Romero, I. G., Wang, J., Li, Y., Gibbs, R. A., McCarroll, S. A., Dermitzakis, E. T., Pritchard, J. K., Barrett, J. C., Harrow, J., Hurles, M. E., Gerstein, M. B.& Tyler-Smith, C. (2012). A Systematic Survey of Loss-of-Function Variants in Human Protein-Coding Genes. *Science, 335*(6070), 823-828.

MacKenzie, J. A.& Payne, R. M. (2007). Mitochondrial Protein Import and Human Health and Disease. *Biochimica et Biophysica Acta, 1772*(5), 509-523.

Major, T., von Janowsky, B., Ruppert, T., Mogk, A.& Voos, W. (2006). Proteomic Analysis of Mitochondrial Protein Turnover: Identification of Novel Substrate Proteins of the Matrix Protease Pim1. *Molecular and Cellular Biology, 26*(3), 762-776.

Marlin, S., Lacombe, D., Jonard, L., Leboulanger, N., Bonneau, D., Goizet, C., Billette de Villemeur, T., Cabrol, S., Houang, M., Moatti, L., Feldmann, D.& Denoyelle, F. (2008). Perrault syndrome: Report of four new cases, review and exclusion of candidate genes. *American Journal of Medical Genetics Part A, 146A*(5), 661-664.

Martin, A., Baker, T. A.& Sauer, R. T. (2007). Distinct Static and Dynamic Interactions Control ATPase-Peptidase Communication in a AAA+ Protease. *Molecular Cell, 27*(1), 41-52.

Martin, A., Baker, T. A.& Sauer, R. T. (2008). Diverse Pore Loops of the AAA+ ClpX Machine Mediate Unassisted and Adaptor-Dependent Recognition of ssrA-Tagged Substrates. *Molecular Cell, 29*(4), 441-450.

Martin, W.& Schnarrenberger, C. (1997). The evolution of the Calvin cycle from prokaryotic to eukaryotic chromosomes: a case study of functional redundancy in ancient pathways through endosymbiosis. *Current Genetics, 32*(1), 1-18.

Mathieu, A., Fleury, A., Ducharme, L., Lavigne, P.& LeHoux, J. (2002). Insights into steroidogenic acute regulatory protein (StAR)-dependent cholesterol transfer in mitochondria: evidence from molecular modeling and structure-based thermodynamics supporting the existence of partially unfolded states of StAR. *Journal of Molecular Endocrinology, 29*(3), 327-345.

Matsushima, Y., Goto, Y.-i.& Kaguni, L. S. (2010). Mitochondrial Lon protease regulates mitochondrial DNA copy number and transcription by selective degradation of mitochondrial transcription factor A (TFAM). *Proceedings of the National Academy of Sciences, 107*(43), 18410-18415.

Matyskiela, M. E., Lander, G. C.& Martin, A. (2013). Conformational switching of the 26S proteasome enables substrate degradation. *Nature Structural & Molecular Biology, 20*(7), 781-788.

Matyskiela, M. E.& Martin, A. (2013). Design Principles of a Universal Protein Degradation Machine. *Journal of Molecular Biology, 425*(2), 199-213.

Maurizi, M. R. (1987). Degradation in vitro of bacteriophage lambda N protein by Lon protease from *Escherichia coli*. *Journal of Biological Chemistry, 262*(6), 2696-2703.

Maurizi, M. R., Clark, W. P., Katayama, Y., Rudikoff, S., Pumphrey, J., Bowers, B.& Gottesman, S. (1990a). Sequence and structure of Clp P, the proteolytic component of the ATP-dependent Clp protease of *Escherichia coli*. *Journal of Biological Chemistry, 265*(21), 12536-12545.

Maurizi, M. R., Clark, W. P., Kim, S. H.& Gottesman, S. (1990b). Clp P represents a unique family of serine proteases. *Journal of Biological Chemistry, 265*(21), 12546-12552.

McCarron, J. G., Wilson, C., Sandison, M. E., Olson, M. L., Girkin, J. M., Saunter, C.& Chalmers, S. (2013). From Structure to Function: Mitochondrial Morphology, Motion and Shaping in Vascular Smooth Muscle. *Journal of Vascular Research, 50*(5), 357-371.

McMillan, H. J., Worthylake, T., Schwartzentruber, J., Gottlieb, C. C., Lawrence, S. E., MacKenzie, A., Beaulieu, C. L., Mooyer, P. A. W., Wanders, R. J. A., Majewski, J., Bulman, D. E., Geraghty, M. T., Ferdinandusse, S.& Boycott, K. M. (2012). Specific combination of compound heterozygous mutations in 17β-hydroxysteroid dehydrogenase type 4 (HSD17B4) defines a new subtype of D-bifunctional protein deficiency. *Orphanet Journal of Rare Diseases, 7*(1), 1-9.

Meisinger, C., Pfanner, N.& Truscott, K. N. (2006). Isolation of Yeast Mitochondria. In W. Xiao (Ed.), *Yeast Protocol* (pp. 33-39). Totowa, NJ: Humana Press.

Mercille, S.& Massie, B. (1994). Induction of apoptosis in nutrient-deprived cultures of hybridoma and myeloma cells. *Biotechnology and Bioengineering, 44*(9), 1140-1154.

Morino, H., Pierce, S. B., Matsuda, Y., Walsh, T., Ohsawa, R., Newby, M., Hiraki-Kamon, K., Kuramochi, M., Lee, M. K., Klevit, R. E., Martin, A., Maruyama, H., King, M.-C.& Kawakami, H. (2014). Mutations in Twinkle primase-helicase cause Perrault syndrome with neurologic features. *Neurology, 83*(22), 2054-2061.

Motohashi, M., Wempe, M. F., Mutou, T., Takahashi, H., Kansaku, N., Ikegami, M., Inomata, T., Asari, M.& Wakui, S. (2016). Male rats

exposed in utero to di(n-butyl) phthalate: Age-related changes in Leydig cell smooth endoplasmic reticulum and testicular testosterone-biosynthesis enzymes/proteins. *Reproductive Toxicology, 59*, 139-146.

Murcia, M., Faráldo-Gómez, J. D., Maxfield, F. R.& Roux, B. (2006). Modeling the structure of the StART domains of MLN64 and StAR proteins in complex with cholesterol. *Journal of Lipid Research, 47*(12), 2614-2630.

Narendra, D., Tanaka, A., Suen, D.-F.& Youle, R. J. (2008). Parkin is recruited selectively to impaired mitochondria and promotes their autophagy. *The Journal of Cell Biology, 183*(5), 795-803.

Neher, S. B., Flynn, J. M., Sauer, R. T.& Baker, T. A. (2003a). Latent ClpX-recognition signals ensure LexA destruction after DNA damage. *Genes & Development, 17*(9), 1084-1089.

Neher, S. B., Sauer, R. T.& Baker, T. A. (2003b). Distinct peptide signals in the UmuD and UmuD′ subunits of UmuD/D′ mediate tethering and substrate processing by the ClpXP protease. *Proceedings of the National Academy of Sciences, 100*(23), 13219-13224.

Neupert, W.& Herrmann, J. M. (2007). Translocation of Proteins into Mitochondria. *Annual Review of Biochemistry, 76*(1), 723-749.

Ng, P. C.& Henikoff, S. (2006). Predicting the Effects of Amino Acid Substitutions on Protein Function. *Annual Review of Genomics and Human Genetics, 7*(1), 61-80.

Ngo, J. K.& Davies, K. J. A. (2009). Mitochondrial Lon protease is a human stress protein. *Free Radical Biology and Medicine, 46*(8), 1042-1048.

Ngo, J. K., Pomatto, L. C. D., Bota, D. A., Koop, A. L.& Davies, K. J. A. (2011). Impairment of Lon-Induced Protection Against the Accumulation of Oxidized Proteins in Senescent Wi-38 Fibroblasts. *The Journals of Gerontology Series A: Biological Sciences and Medical Sciences, 66A*(11), 1178-1185.

Nie, X., Li, M., Lu, B., Zhang, Y., Lan, L., Chen, L.& Lu, J. (2013). Down-Regulating Overexpressed Human Lon in Cervical Cancer Suppresses Cell Proliferation and Bioenergetics. *PLoS ONE, 8*(11), e81084.

Nishii, W., Maruyama, T., Matsuoka, R., Muramatsu, T.& Takahashi, K. (2002). The unique sites in SulA protein preferentially cleaved by ATP-dependent Lon protease from *Escherichia coli*. *European Journal of Biochemistry, 269*(2), 451-457.

Nishii, W., Suzuki, T., Nakada, M., Kim, Y.-T., Muramatsu, T.& Takahashi, K. (2005). Cleavage mechanism of ATP-dependent Lon

protease toward ribosomal S2 protein. *FEBS Letters, 579*(30), 6846-6850.

Nolden, M., Ehses, S., Koppen, M., Bernacchia, A., Rugarli, E. I.& Langer, T. (2005). The m-AAA Protease Defective in Hereditary Spastic Paraplegia Controls Ribosome Assembly in Mitochondria. *Cell, 123*(2), 277-289.

Nunnari, J.& Suomalainen, A. (2012). Mitochondria: In Sickness and in Health. *Cell, 148*(6), 1145-1159.

Nyquist, K.& Martin, A. (2014). Marching to the beat of the ring: polypeptide translocation by AAA+ proteases. *Trends in biochemical sciences, 39*(2), 53-60.

Ogura, T., Inoue, K., Tatsuta, T., Suzaki, T., Karata, K., Young, K., Su, L.-H., Fierke, C. A., Jackman, J. E., Raetz, C. R. H., Coleman, J., Tomoyasu, T.& Matsuzawa, H. (1999). Balanced biosynthesis of major membrane components through regulated degradation of the committed enzyme of lipid A biosynthesis by the AAA protease FtsH (HflB) in *Escherichia coli*. *Molecular Microbiology, 31*(3), 833-844.

Ogura, T.& Wilkinson, A. J. (2001). AAA+ superfamily ATPases: common structure–diverse function. *Genes to Cells, 6*(7), 575-597.

Okumoto, K., Kametani, Y.& Fujiki, Y. (2011). Two Proteases, Trypsin Domain-containing 1 (Tysnd1) and Peroxisomal Lon Protease (PsLon), Cooperatively Regulate Fatty Acid β-Oxidation in Peroxisomal Matrix. *Journal of Biological Chemistry, 286*(52), 44367-44379.

Olichon, A., Baricault, L., Gas, N., Guillou, E., Valette, A., Belenguer, P.& Lenaers, G. (2003). Loss of OPA1 Perturbates the Mitochondrial Inner Membrane Structure and Integrity, Leading to Cytochrome c Release and Apoptosis. *Journal of Biological Chemistry, 278*(10), 7743-7746.

Olivares, A. O., Baker, T. A.& Sauer, R. T. (2016). Mechanistic insights into bacterial AAA+ proteases and protein-remodelling machines. *Nature Reviews Microbiology, 14*(1), 33-44.

Ondrovičová, G., Liu, T., Singh, K., Tian, B., Li, H., Gakh, O., Perečko, D., Janata, J., Granot, Z., Orly, J., Kutejová, E.& Suzuki, C. K. (2005). Cleavage Site Selection within a Folded Substrate by the ATP-dependent Lon Protease. *Journal of Biological Chemistry, 280*(26), 25103-25110.

Ostersetzer, O., Kato, Y., Adam, Z.& Sakamoto, W. (2007). Multiple Intracellular Locations of Lon Protease in Arabidopsis: Evidence for the Localization of AtLon4 to Chloroplasts. *Plant and Cell Physiology, 48*(6), 881-885.

Özcan, U., Yilmaz, E., Özcan, L., Furuhashi, M., Vaillancourt, E., Smith, R. O., Görgün, C. Z.& Hotamisligil, G. S. (2006). Chemical Chaperones Reduce ER Stress and Restore Glucose Homeostasis in a Mouse Model of Type 2 Diabetes. *Science, 313*(5790), 1137-1140.

Page, C. C., Moser, C. C.& Dutton, P. L. (2003). Mechanism for electron transfer within and between proteins. *Current Opinion in Chemical Biology, 7*(5), 551-556.

Panov, A. V., Gutekunst, C.-A., Leavitt, B. R., Hayden, M. R., Burke, J. R., Strittmatter, W. J.& Greenamyre, J. T. (2002). Early mitochondrial calcium defects in Huntington's disease are a direct effect of polyglutamines. *Nature Neuroscience, 5*(8), 731-736.

Papadopoulos, V., Baraldi, M., Guilarte, T. R., Knudsen, T. B., Lacapère, J.-J., Lindemann, P., Norenberg, M. D., Nutt, D., Weizman, A., Zhang, M.-R.& Gavish, M. (2006). Translocator protein (18 kDa): new nomenclature for the peripheral-type benzodiazepine receptor based on its structure and molecular function. *Trends in Pharmacological Sciences, 27*(8), 402-409.

Park, E., Rho, Y. M., Koh, O.-j., Ahn, S. W., Seong, I. S., Song, J.-J., Bang, O., Seol, J. H., Wang, J., Eom, S. H.& Chung, C. H. (2005). Role of the GYVG Pore Motif of HslU ATPase in Protein Unfolding and Translocation for Degradation by HslV Peptidase. *Journal of Biological Chemistry, 280*(24), 22892-22898.

Parsell, D.& Lindquist, S. (1993). The function of heat-shock proteins in stress tolerance: degradation and reactivation of damaged proteins. *Annual Review of Genetics, 27*(1), 437-496.

Patterson-Ward, J., Tedesco, J., Hudak, J., Fishovitz, J., Becker, J., Frase, H., McNamara, K.& Lee, I. (2009). UTILIZATION OF SYNTHETIC PEPTIDES TO EVALUATE THE IMPORTANCE OF SUBSTRATE INTERACTION AT THE PROTEOLYTIC SITE OF ESCHERICHIA COLI LON PROTEASE. *Biochimica et Biophysica Acta, 1794*(9), 1355-1363.

Patti, M.-E.& Corvera, S. (2010). The Role of Mitochondria in the Pathogenesis of Type 2 Diabetes. *Endocrine Reviews, 31*(3), 364-395.

Payne, B. A. I.& Chinnery, P. F. (2015). Mitochondrial dysfunction in aging: Much progress but many unresolved questions. *Biochimica et Biophysica Acta (BBA) - Bioenergetics, 1847*(11), 1347-1353.

Perugini, M. A., Schuck, P.& Howlett, G. J. (2000). Self-association of Human Apolipoprotein E3 and E4 in the Presence and Absence of Phospholipid. *Journal of Biological Chemistry, 275*(47), 36758-36765.

Peth, A., Nathan, J. A.& Goldberg, A. L. (2013). The ATP Costs and Time Required to Degrade Ubiquitinated Proteins by the 26 S Proteasome. *The Journal of Biological Chemistry, 288*(40), 29215-29222.

Petrescu, A. D., Gallegos, A. M., Okamura, Y., Strauss, J. F.& Schroeder, F. (2001). Steroidogenic Acute Regulatory Protein Binds Cholesterol and Modulates Mitochondrial Membrane Sterol Domain Dynamics. *Journal of Biological Chemistry, 276*(40), 36970-36982.

Phillips, T. A., VanBogelen, R. A.& Neidhardt, F. C. (1984). lon gene product of *Escherichia coli* is a heat-shock protein. *Journal of Bacteriology, 159*(1), 283-287.

Pierce, S. B., Chisholm, K. M., Lynch, E. D., Lee, M. K., Walsh, T., Opitz, J. M., Li, W., Klevit, R. E.& King, M.-C. (2011). Mutations in mitochondrial histidyl tRNA synthetase HARS2 cause ovarian dysgenesis and sensorineural hearing loss of Perrault syndrome. *Proceedings of the National Academy of Sciences, 108*(16), 6543-6548.

Pierce, Sarah B., Gersak, K., Michaelson-Cohen, R., Walsh, T., Lee, Ming K., Malach, D., Klevit, Rachel E., King, M.-C.& Levy-Lahad, E. (2013). Mutations in LARS2, Encoding Mitochondrial Leucyl-tRNA Synthetase, Lead to Premature Ovarian Failure and Hearing Loss in Perrault Syndrome. *The American Journal of Human Genetics, 92*(4), 614-620.

Pierce, S. B., Walsh, T., Chisholm, K. M., Lee, M. K., Thornton, A. M., Fiumara, A., Opitz, J. M., Levy-Lahad, E., Klevit, R. E.& King, M.-C. (2010). Mutations in the DBP-Deficiency Protein HSD17B4 Cause Ovarian Dysgenesis, Hearing Loss, and Ataxia of Perrault Syndrome. *The American Journal of Human Genetics, 87*(2), 282-288.

Pierson, T. M., Adams, D., Bonn, F., Martinelli, P., Cherukuri, P. F., Teer, J. K., Hansen, N. F., Cruz, P., Mullikin for the Nisc Comparative Sequencing Program, J. C., Blakesley, R. W., Golas, G., Kwan, J., Sandler, A., Fuentes Fajardo, K., Markello, T., Tifft, C., Blackstone, C., Rugarli, E. I., Langer, T., Gahl, W. A.& Toro, C. (2011). Whole-Exome Sequencing Identifies Homozygous *AFG3L2* Mutations in a Spastic Ataxia-Neuropathy Syndrome Linked to Mitochondrial *m*-AAA Proteases. *PLoS Genetics, 7*(10), e1002325.

Pinti, M., Gibellini, L., De Biasi, S., Nasi, M., Roat, E., O'Connor, J.-E.& Cossarizza, A. (2011). Functional characterization of the promoter of the human Lon protease gene. *Mitochondrion, 11*(1), 200-206.

Pinti, M., Gibellini, L., Liu, Y., Xu, S., Lu, B.& Cossarizza, A. (2015). Mitochondrial Lon protease at the crossroads of oxidative stress,

ageing and cancer. *Cellular and Molecular Life Sciences, 72*(24), 4807-4824.

Porto, C., Cardone, M., Fontana, F., Rossi, B., Tuzzi, M. R., Tarallo, A., Barone, M. V., Andria, G.& Parenti, G. (2009). The Pharmacological Chaperone N-butyldeoxynojirimycin Enhances Enzyme Replacement Therapy in Pompe Disease Fibroblasts. *Molecular Therapy: the Journal of the American Society of Gene Therapy, 17*(6), 964-971.

Powers, E. T., Morimoto, R. I., Dillin, A., Kelly, J. W.& Balch, W. E. (2009). Biological and Chemical Approaches to Diseases of Proteostasis Deficiency. *Annual Review of Biochemistry, 78*(1), 959-991.

Prakash, S., Inobe, T., Hatch, A. J.& Matouschek, A. (2009). Substrate selection by the proteasome during degradation of protein complexes. *Nature Chemical Biology, 5*(1), 29-36.

Prakash, S., Tian, L., Ratliff, K. S., Lehotzky, R. E.& Matouschek, A. (2004). An unstructured initiation site is required for efficient proteasome-mediated degradation. *Nature Structural & Molecular Biology, 11*(9), 830-837.

Prasad, M., Kaur, J., Pawlak, K. J., Bose, M., Whittal, R. M.& Bose, H. S. (2015). Mitochondria-associated Endoplasmic Reticulum Membrane (MAM) Regulates Steroidogenic Activity via Steroidogenic Acute Regulatory Protein (StAR)-Voltage-dependent Anion Channel 2 (VDAC2) Interaction. *Journal of Biological Chemistry, 290*(5), 2604-2616.

Privalle, C. T., Crivello, J. F.& Jefcoate, C. R. (1983). Regulation of intramitochondrial cholesterol transfer to side-chain cleavage cytochrome P-450 in rat adrenal gland. *Proceedings of the National Academy of Sciences, 80*(3), 702-706.

Quirós, Pedro M., Español, Y., Acín-Pérez, R., Rodríguez, F., Bárcena, C., Watanabe, K., Calvo, E., Loureiro, M., Fernández-García, M. S., Fueyo, A., Vázquez, J., Enríquez, José A.& López-Otín, C. (2014). ATP-Dependent Lon Protease Controls Tumor Bioenergetics by Reprogramming Mitochondrial Activity. *Cell Reports, 8*(2), 542-556.

Radke, S., Chander, H., Schäfer, P., Meiss, G., Krüger, R., Schulz, J. B.& Germain, D. (2008). Mitochondrial Protein Quality Control by the Proteasome Involves Ubiquitination and the Protease Omi. *The Journal of Biological Chemistry, 283*(19), 12681-12685.

Raimundo, N., Song, L., Shutt, Timothy E., McKay, Sharen E., Cotney, J., Guan, M.-X., Gilliland, Thomas C., Hohuan, D., Santos-Sacchi, J.& Shadel, Gerald S. (2012). Mitochondrial Stress Engages E2F1 Apoptotic Signaling to Cause Deafness. *Cell, 148*(4), 716-726.

Ratelade, J., Miot, M.-C., Johnson, E., Betton, J.-M., Mazodier, P.& Benaroudj, N. (2009). Production of Recombinant Proteins in the lon-Deficient BL21(DE3) Strain of *Escherichia coli* in the Absence of the DnaK Chaperone. *Applied and Environmental Microbiology, 75*(11), 3803-3807.

Ravid, T.& Hochstrasser, M. (2008). Diversity of degradation signals in the ubiquitin-proteasome system. *Nature Reviews Molecular Cell Biology, 9*(9), 679-689.

Rawlings, N. D., Waller, M., Barrett, A. J.& Bateman, A. (2014). MEROPS: the database of proteolytic enzymes, their substrates and inhibitors. *Nucleic Acids Research, 42*(Database issue), D503-D509.

Reinstein, E.& Ciechanover, A. (2006). Narrative Review: Protein Degradation and Human Diseases: The Ubiquitin Connection. *Annals of Internal Medicine, 145*(9), 676-684.

Rodriguez-Enriquez, S., Kai, Y., Maldonado, E., Currin, R. T.& Lemasters, J. J. (2009). Roles of mitophagy and the mitochondrial permeability transition in remodeling of cultured rat hepatocytes. *Autophagy, 5*(8), 1099-1106.

Ronen-Fuhrmann, T., Timberg, R., King, S. R., Hales, K. H., Hales, D. B., Stocco, D. M.& Orly, J. (1998). Spatio-Temporal Expression Patterns of Steroidogenic Acute Regulatory Protein (StAR) During Follicular Development in the Rat Ovary. *Endocrinology, 139*(1), 303-315.

Roostaee, A., Barbar, É., LeHoux, J.-G.& Lavigne, P. (2008). Cholesterol binding is a prerequisite for the activity of the steroidogenic acute regulatory protein (StAR). *Biochemical Journal, 412*(3), 553-562.

Rospert, S., Looser, R., Dubaquie, Y., Matouschek, A., Glick, B. S.& Schatz, G. (1996). Hsp60-independent protein folding in the matrix of yeast mitochondria. *The EMBO Journal, 15*(4), 764-774.

Rotanova, T. V., Botos, I., Melnikov, E. E., Rasulova, F., Gustchina, A., Maurizi, M. R.& Wlodawer, A. (2006). Slicing a protease: Structural features of the ATP-dependent Lon proteases gleaned from investigations of isolated domains. *Protein Science : A Publication of the Protein Society, 15*(8), 1815-1828.

Rötig, A. (2011). Human diseases with impaired mitochondrial protein synthesis. *Biochimica et Biophysica Acta (BBA) - Bioenergetics, 1807*(9), 1198-1205.

Rotig, A., de Lonlay, P., Chretien, D., Foury, F., Koenig, M., Sidi, D., Munnich, A.& Rustin, P. (1997). Aconitase and mitochondrial iron-sulphur protein deficiency in Friedreich ataxia. *Nature Genetics, 17*(2), 215-217.

Sambrook, J.& Russell, D. W. (2006). The Inoue Method for Preparation and Transformation of Competent *E. coli*: "Ultra-Competent" Cells. *Cold Spring Harbor Protocols, 2006*(1), pdb.prot3944.

Sánchez-Caballero, L., Guerrero-Castillo, S.& Nijtmans, L. (2016). Unraveling the complexity of mitochondrial complex I assembly: A dynamic process. *Biochimica et Biophysica Acta (BBA) - Bioenergetics, 1857*(7), 980-990.

Sass, P., Josten, M., Famulla, K., Schiffer, G., Sahl, H.-G., Hamoen, L.& Brötz-Oesterhelt, H. (2011). Antibiotic acyldepsipeptides activate ClpP peptidase to degrade the cell division protein FtsZ. *Proceedings of the National Academy of Sciences, 108*(42), 17474-17479.

Sauer, R. T.& Baker, T. A. (2011). AAA+ Proteases: ATP-Fueled Machines of Protein Destruction. *Annual Review of Biochemistry, 80*(1), 587-612.

Sauer, R. T., Bolon, D. N., Burton, B. M., Burton, R. E., Flynn, J. M., Grant, R. A., Hersch, G. L., Joshi, S. A., Kenniston, J. A., Levchenko, I., Neher, S. B., Oakes, E. S. C., Siddiqui, S. M., Wah, D. A.& Baker, T. A. (2004). Sculpting the Proteome with AAA+ Proteases and Disassembly Machines. *Cell, 119*(1), 9-18.

Savopoulos, J. W., Carter, P. S., Turconi, S., Pettman, G. R., Karran, E. H., Gray, C. W., Ward, R. V., Jenkins, O.& Creasy, C. L. (2000). Expression, Purification, and Functional Analysis of the Human Serine Protease HtrA2. *Protein Expression and Purification, 19*(2), 227-234.

Schagger, H.& von Jagow, G. (1991). Blue native electrophoresis for isolation of membrane protein complexes in enzymatically active form. *Analytical Biochemistry, 199*(2), 223-231.

Schägger, H.& von Jagow, G. (1987). Tricine-sodium dodecyl sulfate-polyacrylamide gel electrophoresis for the separation of proteins in the range from 1 to 100 kDa. *Analytical Biochemistry, 166*(2), 368-379.

Scherz-Shouval, R., Shvets, E., Fass, E., Shorer, H., Gil, L.& Elazar, Z. (2007). Reactive oxygen species are essential for autophagy and specifically regulate the activity of Atg4. *The EMBO Journal, 26*(7), 1749-1760.

Schoemaker, J. M., Gayda, R. C.& Markovitz, A. (1984). Regulation of cell division in *Escherichia coli*: SOS induction and cellular location of the sulA protein, a key to lon-associated filamentation and death. *Journal of Bacteriology, 158*(2), 551-561.

Schuck, P. (2000). Size-Distribution Analysis of Macromolecules by Sedimentation Velocity Ultracentrifugation and Lamm Equation Modeling. *Biophysical Journal, 78*(3), 1606-1619.

Schuck, P., Perugini, M. A., Gonzales, N. R., Howlett, G. J.& Schubert, D. (2002). Size-Distribution Analysis of Proteins by Analytical Ultracentrifugation: Strategies and Application to Model Systems. *Biophysical Journal, 82*(2), 1096-1111.

Schweder, T., Lee, K. H., Lomovskaya, O.& Matin, A. (1996). Regulation of *Escherichia coli* starvation sigma factor (sigma s) by ClpXP protease. *Journal of Bacteriology, 178*(2), 470-476.

Sen, M., Maillard, Rodrigo A., Nyquist, K., Rodriguez-Aliaga, P., Pressé, S., Martin, A.& Bustamante, C. (2013). The ClpXP Protease Unfolds Substrates Using a Constant Rate of Pulling but Different Gears. *Cell, 155*(3), 636-646.

Seong-Cheol, P., Baolei, J., Jae-Kyung, Y., Duyet Le, V., Yong Gi, S., Sang Woo, H., Young-Joo, J., Chin Ha, C.& Gang-Won, C. (2006). Oligomeric Structure of the ATP-dependent Protease La (Lon) of *Escherichia coli*. *Mol. Cells, 21*(1), 129-134.

Shimokata, K., Kitada, S., Ogishima, T.& Ito, A. (1998). Role of α-Subunit of Mitochondrial Processing Peptidase in Substrate Recognition. *Journal of Biological Chemistry, 273*(39), 25158-25163.

Shirai, Y., Akiyama, Y.& Ito, K. (1996). Suppression of ftsH mutant phenotypes by overproduction of molecular chaperones. *Journal of Bacteriology, 178*(4), 1141-1145.

Shotland, Y., Koby, S., Teff, D., Mansur, N., Oren, D. A., Tatematsu, K., Tomoyasu, T., Kessel, M., Bukau, B., Ogura, T.& Oppenheim, A. B. (1997). Proteolysis of the phage λ CII regulatory protein by FtsH (HflB) of *Escherichia coli*. *Molecular Microbiology, 24*(6), 1303-1310.

Shotland, Y., Teff, D., Koby, S., Kobiler, O.& Oppenheim, A. B. (2000). Characterization of a conserved α-helical, coiled-coil motif at the C-terminal domain of the ATP-dependent FtsH (HflB) protease of *Escherichia coli*. *Journal of Molecular Biology, 299*(4), 953-964.

Song, M., Shao, H., Mujeeb, A., James, T. L.& Miller, W. L. (2001). Molten-globule structure and membrane binding of the N-terminal protease-resistant domain (63-193) of the steroidogenic acute regulatory protein (StAR). *Biochemical Journal, 356*(Pt 1), 151-158.

Stahlberg, H., Kutejová, E., Suda, K., Wolpensinger, B., Lustig, A., Schatz, G., Engel, A.& Suzuki, C. K. (1999). Mitochondrial Lon of Saccharomyces cerevisiae is a ring-shaped protease with seven flexible subunits. *Proceedings of the National Academy of Sciences, 96*(12), 6787-6790.

Stehling, O., Elsässer, H.-P., Brückel, B., Mühlenhoff, U.& Lill, R. (2004). Iron–sulfur protein maturation in human cells: evidence for a function of frataxin. *Human Molecular Genetics, 13*(23), 3007-3015.

Stinson, Benjamin M., Nager, Andrew R., Glynn, Steven E., Schmitz, Karl R., Baker, Tania A.& Sauer, Robert T. (2013). Nucleotide Binding and Conformational Switching in the Hexameric Ring of a AAA+ Machine. *Cell, 153*(3), 628-639.

Stocco, D. M.& Sodeman, T. C. (1991). The 30-kDa mitochondrial proteins induced by hormone stimulation in MA-10 mouse Leydig tumor cells are processed from larger precursors. *Journal of Biological Chemistry, 266*(29), 19731-19738.

Stowe, D. F.& Camara, A. K. S. (2009). Mitochondrial Reactive Oxygen Species Production in Excitable Cells: Modulators of Mitochondrial and Cell Function. *Antioxidants & Redox Signaling, 11*(6), 1373-1414.

Strauss III, J. F., Kishida, T., Christenson, L. K., Fujimoto, T.& Hiroi, H. (2003). START domain proteins and the intracellular trafficking of cholesterol in steroidogenic cells. *Molecular and Cellular Endocrinology, 202*(1–2), 59-65.

Strauss, Kevin A., Jinks, Robert N., Puffenberger, Erik G., Venkatesh, S., Singh, K., Cheng, I., Mikita, N., Thilagavathi, J., Lee, J., Sarafianos, S., Benkert, A., Koehler, A., Zhu, A., Trovillion, V., McGlincy, M., Morlet, T., Deardorff, M., Innes, A. M., Prasad, C., Chudley, Albert E., Lee, Irene Nga W.& Suzuki, Carolyn K. (2015). CODAS Syndrome Is Associated with Mutations of LONP1, Encoding Mitochondrial AAA+ Lon Protease. *The American Journal of Human Genetics, 96*(1), 121-135.

Suen, D.-F., Narendra, D. P., Tanaka, A., Manfredi, G.& Youle, R. J. (2010). Parkin overexpression selects against a deleterious mtDNA mutation in heteroplasmic cybrid cells. *Proceedings of the National Academy of Sciences, 107*(26), 11835-11840.

Sundar, S., McGinness, K. E., Baker, T. A.& Sauer, R. T. (2010). Multiple sequence signals direct recognition and degradation of protein substrates by the AAA+ protease HslUV. *Journal of Molecular Biology, 403*(3), 420-429.

Suzuki, S. W., Onodera, J.& Ohsumi, Y. (2011). Starvation Induced Cell Death in Autophagy-Defective Yeast Mutants Is Caused by Mitochondria Dysfunction. *PLoS ONE, 6*(2), e17412.

Sysoeva, T. A., Chowdhury, S., Guo, L.& Nixon, B. T. (2013). Nucleotide-induced asymmetry within ATPase activator ring drives σ54–RNAP interaction and ATP hydrolysis. *Genes & Development, 27*(22), 2500-2511.

Szklarczyk, R., Nooteboom, M.& Osiewacz, H. D. (2014). Control of mitochondrial integrity in ageing and disease. *Philosophical Transactions of the Royal Society B: Biological Sciences, 369*(1646), 20130439.

Takahashi, A., Masuda, A., Sun, M., Centonze, V. E.& Herman, B. (2004). Oxidative stress-induced apoptosis is associated with alterations in mitochondrial caspase activity and Bcl-2-dependent alterations in mitochondrial pH (pHm). *Brain Research Bulletin, 62*(6), 497-504.

Teng, H., Wu, B., Zhao, K., Yang, G., Wu, L.& Wang, R. (2013). Oxygen-sensitive mitochondrial accumulation of cystathionine β-synthase mediated by Lon protease. *Proceedings of the National Academy of Sciences, 110*(31), 12679-12684.

Thompson, M. W., Singh, S. K.& Maurizi, M. R. (1994). Processive degradation of proteins by the ATP-dependent Clp protease from *Escherichia coli*. Requirement for the multiple array of active sites in ClpP but not ATP hydrolysis. *Journal of Biological Chemistry, 269*(27), 18209-18215.

Thorsell, A.-G., Lee, W. H., Persson, C., Siponen, M. I., Nilsson, M., Busam, R. D., Kotenyova, T., Schüler, H.& Lehtiö, L. (2011). Comparative Structural Analysis of Lipid Binding START Domains. *PLoS ONE, 6*(6), e19521.

Tian, Q., Li, T., Hou, W., Zheng, J., Schrum, L. W.& Bonkovsky, H. L. (2011). Lon Peptidase 1 (LONP1)-dependent Breakdown of Mitochondrial 5-Aminolevulinic Acid Synthase Protein by Heme in Human Liver Cells. *Journal of Biological Chemistry, 286*(30), 26424-26430.

Timmis, J. N., Ayliffe, M. A., Huang, C. Y.& Martin, W. (2004). Endosymbiotic gene transfer: organelle genomes forge eukaryotic chromosomes. *Nature Reviews Genetics, 5*(2), 123-135.

Tomoyasu, T., Gamer, J., Bukau, B., Kanemori, M., Mori, H., Rutman, A. J., Oppenheim, A. B., Yura, T., Yamanaka, K.& Niki, H. (1995). *Escherichia coli* FtsH is a membrane-bound, ATP-dependent protease which degrades the heat-shock transcription factor sigma 32. *The EMBO Journal, 14*(11), 2551-2560.

Tomoyasu, T., Yamanaka, K., Murata, K., Suzaki, T., Bouloc, P., Kato, A., Niki, H., Hiraga, S.& Ogura, T. (1993a). Topology and subcellular localization of FtsH protein in *Escherichia coli*. *Journal of Bacteriology, 175*(5), 1352-1357.

Tomoyasu, T., Yuki, T., Morimura, S., Mori, H., Yamanaka, K., Niki, H., Hiraga, S.& Ogura, T. (1993b). The *Escherichia coli* FtsH protein is a prokaryotic member of a protein family of putative ATPases

involved in membrane functions, cell cycle control, and gene expression. *Journal of Bacteriology, 175*(5), 1344-1351.

Truscott, K. N., Bezawork-Geleta, A.& Dougan, D. A. (2011). Unfolded protein responses in bacteria and mitochondria: A central role for the ClpXP machine. *IUBMB Life, 63*(11), 955-963.

Truscott, K. N., Lowth, B. R., Strack, P. R.& Dougan, D. A. (2010). Diverse functions of mitochondrial AAA+ proteins: protein activation, disaggregation, and degradation. *Biochemistry and Cell Biology, 88*(1), 97-108.

Tsujishita, Y.& Hurley, J. H. (2000). Structure and lipid transport mechanism of a StAR-related domain. *Nature Structural & Molecular Biology, 7*(5), 408-414.

Tuppen, H. A. L., Blakely, E. L., Turnbull, D. M.& Taylor, R. W. (2010). Mitochondrial DNA mutations and human disease. *Biochimica et Biophysica Acta (BBA) - Bioenergetics, 1797*(2), 113-128.

Twig, G., Elorza, A., Molina, A. J. A., Mohamed, H., Wikstrom, J. D., Walzer, G., Stiles, L., Haigh, S. E., Katz, S., Las, G., Alroy, J., Wu, M., Py, B. F., Yuan, J., Deeney, J. T., Corkey, B. E.& Shirihai, O. S. (2008). Fission and selective fusion govern mitochondrial segregation and elimination by autophagy. *The EMBO Journal, 27*(2), 433-446.

Vaca Jacome, A. S., Rabilloud, T., Schaeffer-Reiss, C., Rompais, M., Ayoub, D., Lane, L., Bairoch, A., Van Dorsselaer, A.& Carapito, C. (2015). N-terminome analysis of the human mitochondrial proteome. *PROTEOMICS, 15*(14), 2519-2524.

van der Giezen, M. (2011). Mitochondria and the Rise of Eukaryotes. *BioScience, 61*(8), 594-601.

van Dyck, L., Dembowski, M., Neupert, W.& Langer, T. (1998). Mcx1p, a ClpX homologue in mitochondria of Saccharomyces cerevisiae. *FEBS Letters, 438*(3), 250-254.

Van Dyck, L., Pearce, D. A.& Sherman, F. (1994). PIM1 encodes a mitochondrial ATP-dependent protease that is required for mitochondrial function in the yeast Saccharomyces cerevisiae. *Journal of Biological Chemistry, 269*(1), 238-242.

Van Melderen, L., Thi, M. H. D., Lecchi, P., Gottesman, S., Couturier, M.& Maurizi, M. R. (1996). ATP-dependent Degradation of CcdA by Lon Protease: EFFECTS OF SECONDARY STRUCTURE AND HETEROLOGOUS SUBUNIT INTERACTIONS. *Journal of Biological Chemistry, 271*(44), 27730-27738.

Varshavsky, A. (2011). The N-end rule pathway and regulation by proteolysis. *Protein Science, 20*(8), 1298-1345.

Venkatesh, S., Lee, J., Singh, K., Lee, I.& Suzuki, C. K. (2012). Multitasking in the mitochondrion by the ATP-dependent Lon protease. *Biochimica et Biophysica Acta (BBA) - Molecular Cell Research, 1823*(1), 56-66.

Vineyard, D., Patterson-Ward, J., Berdis, A. J.& Lee, I. (2005). Monitoring the Timing of ATP Hydrolysis with Activation of Peptide Cleavage in *Escherichia coli* Lon by Transient Kinetics. *Biochemistry, 44*(5), 1671-1682.

Visapää, I., Fellman, V., Vesa, J., Dasvarma, A., Hutton, J. L., Kumar, V., Payne, G. S., Makarow, M., Van Coster, R., Taylor, R. W., Turnbull, D. M., Suomalainen, A.& Peltonen, L. (2002). GRACILE Syndrome, a Lethal Metabolic Disorder with Iron Overload, Is Caused by a Point Mutation in BCS1L. *The American Journal of Human Genetics, 71*(4), 863-876.

Vögtle, F. N., Prinz, C., Kellermann, J., Lottspeich, F., Pfanner, N.& Meisinger, C. (2011). Mitochondrial protein turnover: role of the precursor intermediate peptidase Oct1 in protein stabilization. *Molecular Biology of the Cell, 22*(13), 2135-2143.

Vögtle, F. N., Wortelkamp, S., Zahedi, R. P., Becker, D., Leidhold, C., Gevaert, K., Kellermann, J., Voos, W., Sickmann, A., Pfanner, N.& Meisinger, C. (2009). Global Analysis of the Mitochondrial N-Proteome Identifies a Processing Peptidase Critical for Protein Stability. *Cell, 139*(2), 428-439.

von Janowsky, B., Knapp, K., Major, T., Krayl, M., Guiard, B.& Voos, W. (2005). Structural properties of substrate proteins determine their proteolysis by the mitochondrial AAA+ protease Pim1. *Biol Chem, 386*(12), 1307-1317.

Voos, W. (2013). Chaperone–protease networks in mitochondrial protein homeostasis. *Biochimica et Biophysica Acta (BBA) - Molecular Cell Research, 1833*(2), 388-399.

Voos, W., Ward, L. A.& Truscott, K. N. (2013). The Role of AAA+ Proteases in Mitochondrial Protein Biogenesis, Homeostasis and Activity Control. In A. D. Dougan (Ed.), *Regulated Proteolysis in Microorganisms* (pp. 223-263). Dordrecht: Springer Netherlands.

Wah, D. A., Levchenko, I., Rieckhof, G. E., Bolon, D. N., Baker, T. A.& Sauer, R. T. (2003). Flexible Linkers Leash the Substrate Binding Domain of SspB to a Peptide Module that Stabilizes Delivery Complexes with the AAA+ ClpXP Protease. *Molecular Cell, 12*(2), 355-363.

Wang, C.& Youle, R. J. (2009). The Role of Mitochondria in Apoptosis. *Annual Review of Genetics, 43*(1), 95-118.

Wang, H.-M., Cheng, K.-C., Lin, C.-J., Hsu, S.-W., Fang, W.-C., Hsu, T.-F., Chiu, C.-C., Chang, H.-W., Hsu, C.-H.& Lee, A. Y.-L. (2010). Obtusilactone A and (−)-sesamin induce apoptosis in human lung cancer cells by inhibiting mitochondrial Lon protease and activating DNA damage checkpoints. *Cancer Science, 101*(12), 2612-2620.

Wang, J., Hartling, J. A.& Flanagan, J. M. (1997). The Structure of ClpP at 2.3 Å Resolution Suggests a Model for ATP-Dependent Proteolysis. *Cell, 91*(4), 447-456.

Wang, J. D., Herman, C., Tipton, K. A., Gross, C. A.& Weissman, J. S. (2002). Directed Evolution of Substrate-Optimized GroEL/S Chaperonins. *Cell, 111*(7), 1027-1039.

Wang, L., Azad, N., Kongkaneramit, L., Chen, F., Lu, Y., Jiang, B.-H.& Rojanasakul, Y. (2008). The Fas Death Signaling Pathway Connecting Reactive Oxygen Species Generation and FLICE Inhibitory Protein Down-Regulation. *The Journal of Immunology, 180*(5), 3072-3080.

Wang, N., Gottesman, S., Willingham, M. C., Gottesman, M. M.& Maurizi, M. R. (1993). A human mitochondrial ATP-dependent protease that is highly homologous to bacterial Lon protease. *Proceedings of the National Academy of Sciences, 90*(23), 11247-11251.

Wang, N., Maurizi, M. R., Emmert-Buck, L.& Gottesman, M. M. (1994). Synthesis, processing, and localization of human Lon protease. *Journal of Biological Chemistry, 269*(46), 29308-29313.

Wang, Y.& Bogenhagen, D. F. (2006). Human Mitochondrial DNA Nucleoids Are Linked to Protein Folding Machinery and Metabolic Enzymes at the Mitochondrial Inner Membrane. *Journal of Biological Chemistry, 281*(35), 25791-25802.

Watters, D. (1999). Molecular mechanisms of ionizing radiation-induced apoptosis. *Immunology & Cell Biology, 77*(3), 263-271.

Wawrzynow, A., Wojtkowiak, D., Marszalek, J., Banecki, B., Jonsen, M., Graves, B., Georgopoulos, C.& Zylicz, M. (1995). The ClpX heat-shock protein of *Escherichia coli*, the ATP-dependent substrate specificity component of the ClpP-ClpX protease, is a novel molecular chaperone. *The EMBO Journal, 14*(9), 1867-1877.

Waxman, L.& Goldberg, A. (1986). Selectivity of intracellular proteolysis: protein substrates activate the ATP-dependent protease (La). *Science, 232*(4749), 500-503.

Waxman, L.& Goldberg, A. L. (1985). Protease La, the lon gene product, cleaves specific fluorogenic peptides in an ATP-dependent reaction. *Journal of Biological Chemistry, 260*(22), 12022-12028.

Wendler, P., Ciniawsky, S., Kock, M.& Kube, S. (2012). Structure and function of the AAA+ nucleotide binding pocket. *Biochimica et Biophysica Acta (BBA) - Molecular Cell Research, 1823*(1), 2-14.

Westermann, B. (2010). Mitochondrial fusion and fission in cell life and death. *Nature Reviews Molecular Cell Biology, 11*(12), 872-884.

Wohlever, M. L., Baker, T. A.& Sauer, R. T. (2014). Roles of the N domain of the AAA+ Lon protease in substrate recognition, allosteric regulation and chaperone activity. *Molecular Microbiology, 91*(1), 66-78.

Wojtkowiak, D., Georgopoulos, C.& Zylicz, M. (1993). Isolation and characterization of ClpX, a new ATP-dependent specificity component of the Clp protease of *Escherichia coli*. *Journal of Biological Chemistry, 268*(30), 22609-22617.

Wojtyra, U. A., Thibault, G., Tuite, A.& Houry, W. A. (2003). The N-terminal Zinc Binding Domain of ClpX Is a Dimerization Domain That Modulates the Chaperone Function. *Journal of Biological Chemistry, 278*(49), 48981-48990.

Wright, G., Terada, K., Yano, M., Sergeev, I.& Mori, M. (2001). Oxidative Stress Inhibits the Mitochondrial Import of Preproteins and Leads to Their Degradation. *Experimental Cell Research, 263*(1), 107-117.

Wrobel, L., Topf, U., Bragoszewski, P., Wiese, S., Sztolsztener, M. E., Oeljeklaus, S., Varabyova, A., Lirski, M., Chroscicki, P., Mroczek, S., Januszewicz, E., Dziembowski, A., Koblowska, M., Warscheid, B.& Chacinska, A. (2015). Mistargeted mitochondrial proteins activate a proteostatic response in the cytosol. *Nature, 524*(7566), 485-488.

Yakamavich, J. A., Baker, T. A.& Sauer, R. T. (2008). Asymmetric nucleotide transactions of the HslUV protease. *Journal of Molecular Biology, 380*(5), 946-957.

Yano, T., Nishio, S.-y.& Usami, S.-i. (2014). Frequency of mitochondrial mutations in non-syndromic hearing loss as well as possibly responsible variants found by whole mitochondrial genome screening. *Journal of Human Genetics, 59*(2), 100-106.

Yaworsky, D. C., Baker, B. Y., Bose, H. S., Best, K. B., Jensen, L. B., Bell, J. D., Baldwin, M. A.& Miller, W. L. (2005). pH-dependent Interactions of the Carboxyl-terminal Helix of Steroidogenic Acute Regulatory Protein with Synthetic Membranes. *Journal of Biological Chemistry, 280*(3), 2045-2054.

Yoneda, T., Benedetti, C., Urano, F., Clark, S. G., Harding, H. P.& Ron, D. (2004). Compartment-specific perturbation of protein handling activates genes encoding mitochondrial chaperones. *Journal of Cell Science, 117*(18), 4055-4066.

Youle, R. J.& van der Bliek, A. M. (2012). Mitochondrial Fission, Fusion, and Stress. *Science, 337*(6098), 1062-1065.

Zardecki, C., Dutta, S., Goodsell, D. S., Voigt, M.& Burley, S. K. (2016). RCSB Protein Data Bank: A Resource for Chemical, Biochemical, and Structural Explorations of Large and Small Biomolecules. *Journal of Chemical Education, 93*(3), 569-575.

Zhang, H., Bosch-Marce, M., Shimoda, L. A., Tan, Y. S., Baek, J. H., Wesley, J. B., Gonzalez, F. J.& Semenza, G. L. (2008). Mitochondrial Autophagy Is an HIF-1-dependent Adaptive Metabolic Response to Hypoxia. *Journal of Biological Chemistry, 283*(16), 10892-10903.

Zhang, X., Zheng, Y., Fried, L. E., Du, Y., Montano, S. J., Sohn, A., Lefkove, B., Holmgren, L., Arbiser, J. L., Holmgren, A.& Lu, J. (2011). Disruption of the mitochondrial thioredoxin system as a cell death mechanism of cationic triphenylmethanes. *Free Radical Biology and Medicine, 50*(7), 811-820.

Zhang, Y., Goldman, S., Baerga, R., Zhao, Y., Komatsu, M.& Jin, S. (2009). Adipose-specific deletion of autophagy-related gene 7 (atg7) in mice reveals a role in adipogenesis. *Proceedings of the National Academy of Sciences, 106*(47), 19860-19865.

Zhang, Y.& Maurizi, M. R. (2016). Mitochondrial ClpP activity is required for cisplatin resistance in human cells. *Biochimica et Biophysica Acta (BBA) - Molecular Basis of Disease, 1862*(2), 252-264.

Zhao, Q., Wang, J., Levichkin, I. V., Stasinopoulos, S., Ryan, M. T.& Hoogenraad, N. J. (2002). A mitochondrial specific stress response in mammalian cells. *The EMBO Journal, 21*(17), 4411-4419.

Zheng, L., Baumann, U.& Reymond, J.-L. (2004). An efficient one-step site-directed and site-saturation mutagenesis protocol. *Nucleic Acids Research, 32*(14), e115-e115.

Zhou, Y., Gottesman, S., Hoskins, J. R., Maurizi, M. R.& Wickner, S. (2001). The RssB response regulator directly targets ςS for degradation by ClpXP. *Genes & Development, 15*(5), 627-637.

Zuchner, S., Mersiyanova, I. V., Muglia, M., Bissar-Tadmouri, N., Rochelle, J., Dadali, E. L., Zappia, M., Nelis, E., Patitucci, A., Senderek, J., Parman, Y., Evgrafov, O., Jonghe, P. D., Takahashi, Y., Tsuji, S., Pericak-Vance, M. A., Quattrone, A., Battologlu, E., Polyakov, A. V., Timmerman, V., Schroder, J. M.& Vance, J. M. (2004). Mutations in the mitochondrial GTPase mitofusin 2 cause Charcot-Marie-Tooth neuropathy type 2A. *Nature Genetics, 36*(5), 449-451.